universität wien

DISSERTATION

Titel der Dissertation

Elemental Imaging and Biological Activity of Tumor-Inhibiting Platinum Compounds

Verfasser

Anton Legin, MSc

angestrebter akademischer Grad

Doktor der Naturwissenschaften (Dr. rer. nat.)

Wien, 2014

Studienkennzahl lt. Studienblatt:	A 791 419
Dissertationsgebiet lt. Studienblatt:	Chemie
Betreuerin / Betreuer:	O. Univ.-Prof. Dr. Dr. Bernhard K. Keppler

Acknowledgements

The author is sincerely grateful to all those people who directly or indirectly were involved or contributed to this work.

I would like to acknowledge O. Univ.-Prof. Dr. Dr. Bernhard K. Keppler for giving me the unique opportunity to carry out my doctoral research in his multidisciplinary and perfectly equipped group as well as for financial support.

I am deeply grateful for the assistance of Dr. Michael Jakupec with careful and critical supervision of the work at all stages, discussion of results and dissertation editing; for his encouragement and overall support.

The author is warmly grateful to the members of the cell culture facility (Robert, Simone, Gerhard, Caroline, Erik, Conny, Michaela, Lea and Kati) for their continuous support and participation in the discussion of the results as well as for the unforgettable working atmosphere. I would like to acknowledge all members of the Bioinorganic Chemistry research group, especially Michael Malarek, Alexander Egger, Alexander Roller and Sarah Theiner for their constant support, collaboration and fellowship.

I would like to acknowledge our collaboration partners – Mag. Arno Schintlmeister and O. Univ.-Prof. Dr. Michael Wagner – who contributed significantly to the main topic of the dissertation.

I would like to express the deepest gratitude to the people who helped me to overcome the administrative and bureaucratic issues on all stages, especially to Elfriede Limberger, who kindly guided me throughout the working process.

The author is heartily grateful to Maria Novak for her everyday backing, moral support and endless patience in the time of doctoral study and dissertation preparation. For the encouragement and listening that have helped me to progress for the last years.

Besides the people whom I worked with at the University of Vienna, I want to genuinely thank my parents and grandparents, my brothers, my nieces and friends for supporting me throughout the period of my study.

Abstract

Platinum-based drugs play an important role in cancer therapy mainly due to their high curative potential in certain malignancies. The mechanisms underlying the efficacy, selectivity and side effects of platinum and other metal-based drugs are not sufficiently well understood, though. Interactions with different cell organelles may contribute to these mechanisms. The elucidation of the cellular targets and mechanisms of different platinum drugs may aid in the design of new classes of active antitumor agents with improved therapeutic index.

Multi-elemental, isotope-selective imaging by means of NanoSIMS combined with different visualization methods has recently been shown to be a highly sensitive technique for the detection of isotopically labeled compounds in cell biology. A main scope of the first project was the establishment of a reliable combinatory technique for mapping of the subcellular distribution of anticancer compounds, including the identification of structures accumulating the drugs. The subcellular distribution of ^{15}N-labeled cisplatin in human colon cancer cells was consistently characterized by means of NanoSIMS elemental imaging correlated with confocal laser scanning microscopy (CLSM). Platinum was demonstrated to accumulate both in cytoplasmic and nuclear structures. The combinatory approach revealed platinum colocalization with sulfur-rich organelles which were further proven to be of a lysosomal origin. Additionally, statistical analyses confirmed the colocalization of platinum with phosphorus-rich chromatin structures, supporting the important role of DNA binding in the mechanism of action of the drug. The parallel investigation of the distribution of the metal and the ammonia ligands of cisplatin suggested partial dissociation of Pt-N bonds during the accumulation process, in particular within nucleoli at elevated cisplatin concentrations. The unexpected change in stoichiometry of cisplatin and its implications on the mechanisms of action of the drug need to be further evaluated. We showed that the synopsis of high-resolution drug distribution patterns (elemental imaging) and cell morphology (confocal microscopy) holds much promise for resolving questions concerning cellular targets that might be involved in mode of action of clinically relevant and novel anticancer drugs.

Beside the establishment of the combinatory imaging studies an in vitro anticancer properties of several classes of classic and non-classic platinum compounds were investigated. Antiproliferative effects of pH-sensitive acetoxime platinum(II) complexes were evaluated in cancer cells of different origin under slightly acidic conditions. In this project relatively inert platinum species were demonstrated *in vitro* to be capable of activation in the slightly acidic microenvironment of solid tumors. In another project the activation of the *trans*-geometry was tested on a group of novel oximato-bridged platinum(II) di- and trimer(s) confirming the high antiproliferative activity and the potency of apoptosis induction of *trans*-configured platinum(II) complexes. Several complexes were

proven to be strong apoptotic agents, which could induce cell death even in the cisplatin-resistant SW480 cell line. Further, the cytotoxity of ferrocenyl platinum(IV)-based complexes and the induction of apoptosis and necrosis by bis(carboxylato)dichloridobis(ethylamine) platinum(IV)-compounds were tested in a set of human cancer cell lines, showing the promising potential to overcome the intrinsic resistance to cisplatin in SW480 cells.

Zusammenfassung

Platin-basierte Substanzen spielen eine wichtige Rolle in der Krebstherapie aufgrund ihres hohen kurativen Potentials bei bestimmten bösartigen Erkrankungen. Die Mechanismen, welche der Wirksamkeit, der Selektivität und den Nebenwirkungen zu Grunde liegen, sind allerdings nicht ausreichend verstanden. Wechselwirkungen mit verschiedenen Zellorganellen können zu diesen Mechanismen beitragen. Die Aufklärung der zellulären Zielstrukturen und Mechanismen verschiedener platin-basierter Substanzen könnte helfen, neue antitumorale Substanzen zu finden, welche einen verbesserten therapeutischen Index aufweisen.

Es wurde gezeigt, dass isotopen-selektives Multielement-Imaging mittels einer Kombination von NanoSIMS mit verschiedenen Visualisierungsmethoden eine hoch sensitive Methode darstellt, um isotopen-markierte Substanzen in zellbiologischen Proben zu detektieren. Gegenstand des ersten Teils der Arbeit war es, mittels der genannten Kombination von Techniken eine zuverlässige Methode für die Darstellung der subzellulären Verteilung antitumoraler Substanzen und die Identifizierung jener Organellen, in welchen die Substanzen angereichert werden, zu etablieren. Die subzelluläre Verteilung von ^{15}N-markiertem Cisplatin in menschlichen Darmkrebszellen wurde charakterisiert, indem die Element-Verteilungen in den NanoSIMS-Bildern mit konfokaler Laser-Scanning-Mikroskopie (CLSM) in Beziehung gesetzt wurden. Es wurde gezeigt, dass sich Platin sowohl in cytoplasmatischen als auch in nukleären Strukturen anreichert. Die Kombination der Techniken ergab, dass Platin in schwefelreichen Organellen akkumuliert wird, welche als von lysosomalem Ursprung identifiziert wurden. Darüber hinaus bestätigten statistische Analysen eine Kolokalisation von Platin mit phosphorreichen Chromatinstrukturen, was die wichtige Rolle der DNA-Bindung im Wirkmechanismus der Substanz untermauert. Die gleichzeitige Untersuchung der Verteilung des Metalls und jener der Ammin-Liganden legt eine teilweise Dissoziation der Pt-N Bindungen während des Akkumulations-Vorgangs nahe, insbesondere in den Nucleoli bei höheren Cisplatin-Konzentrationen. Die unerwartete Veränderung der Stöchiometrie von Cisplatin und deren Bedeutung für den Wirkmechanismus der Substanz bedürfen weiterer Untersuchungen. Wir konnten zeigen, dass die Zusammenschau von hochaufgelösten Substanz-Verteilungsmustern (Element-Imaging) und Zellmorphologie (konfokale Mikroskopie) ein viel versprechender Ansatz ist, um Fragen der zellulären Zielstrukturen, welche eine Rolle im Wirkmechanismus klinisch relevanter und neuartiger antitumoraler Substanzen spielen, zu klären.

Neben der Etablierung dieser kombinations-basierten Imaging-Studien wurde eine Reihe von In-vitro-Untersuchungen zu den antitumoralen Wirkungen verschiedener Klassen von klassischen- und nicht-klassischen Platinverbindungen durchgeführt. Die pH-abhängigen antiproliferativen Effekte von Acetoxim-Platin(II)-Komplexen wurden unter schwach sauren Bedingungen an Krebszellen

unterschiedlichen Ursprungs untersucht. In diesem Projekt konnte in vitro gezeigt werden, dass relativ inerte Platinspezies im leicht sauren Mikromilieu solider Tumore aktivierbar sind. In einem anderen Projekt wurde die Aktivierung der *Trans*-Geometrie an neuartigen oximato-verbrückten Platin(II)-Dimeren und -Trimeren untersucht, wobei die hohe antiproliferative Aktivität der *trans*-konfigurierten Platin(II)-Komplexe und deren Vermögen, Apoptose zu induzieren, bestätigt wurden. Es wurde bewiesen, dass einige dieser Komplexe starke Apoptose auslösende Eigenschaften aufweisen, welche den Zelltod sogar in der cisplatin-resistenten Darmkrebs-Zelllinie SW480 induzieren konnten. Weiters wurden die Zytotoxizität von Ferrocenyl enthaltenden Platin(IV)-Komplexen und die Induktion von Apoptose und Nekrose durch Bis(carboxylato)dichloridobis(ethylamin)platin(IV)-Verbindungen in einer Reihe humaner Krebszelllinien untersucht und gezeigt, dass diese ein viel versprechendes Vermögen aufweisen, die intrinsische Cisplatin-Resistenz in SW480-Zellen zu überwinden.

Table of Contents

Index of Figures

1. Introduction

1.1 Epidemiology of Cancer

Rising living standards, improved lifestyle, better nutrition, sanitation and housing, as well as easier access to quality health services – all these factors contribute to the increase of life expectancy in European countries. Across the 27 member states of the European Union, the average life expectancy at birth reached 75.3 years for men and 81.7 years for women in 2010. The long-term prognosis anticipates that life span will continue to increase in the European Union in the future, to reach 84.6 years for males and 89.1 for females in the year 2060[1]. The life expectancy is strongly dependent on the incidence of age-specific disorders, such as cardiovascular disease or cancer.

Cancer is a general term encompassing a broad spectrum of malignant neoplasms that can affect almost any part of the body with more than hundred different types of disease known. Cancer is associated with abnormal cell behavior leading to uncontrolled growth of the tumorous tissue. In the dissemination stage, cancer cells are capable of spreading to tissues in different parts of the body resulting in metastasis formation.

In general there were over 3.5 million new cases of cancer with an average mortality of up to 50% registered in Europe in the year 2012. The most common types of cancer are breast cancer (464,000 cases; 13.5% of the total), colorectal cancer (447,000; 13.0%), prostate cancer (417,000; 12.1%) and lung cancer (410,000; 11.9%). The most frequent cause of death from malignant neoplasms is lung cancer (353,000 deaths; 20% of the total), followed by colorectal (215,000 deaths; 12.2%), breast (131,000; 7.5%) and stomach cancer (107,000; 6.1%)[2]. These cancers are among the most difficult to deal with together with the malignancies with a generally poor prognosis (e.g. pancreas, liver, brain tumors).

Cancer appears to be the second most prevailing cause of death in Austria, being outnumbered only by cardiovascular diseases. The number of heart and circulatory system associated mortalities (42.7% of total death cases in the year 2012) is followed by the mortality from malignant neoplasms with about a quarter of all death cases (25.5% in 2012). Due to the significant improvement in early cancer diagnostics and cure the cancer mortality rate among men and women decreased in about 11% in the first decade of the century (2001 to 2011). However, the cancer incidence might fluctuate and is not easy to predict, for example, in recent years a decreasing trend in lung cancer incidence and mortality (-18.7%) was observed in men; however, an increasing trend was observed in women (+25.2%)[3].

Estimated over 50,000 people were diagnosed with cancer in 2012 in Austria, with around half of male patients diagnosed with prostate, lung or colorectal cancer and half of female patients diagnosed with

breast, lung or colorectal cancer (Fig.1). The most common cancer site in women is breast, whereas it is prostate in men[2]. The tumor site causing the highest number of fatalities in all patients, continues to be lung. Although in women the mortality from lung cancer is lower than that from breast cancer, the continuously increasing trend of incidence should be taken into account. Recently the long-term prognosis for several cancer types diagnosed prior to late stages of disease continues to improve, in particular for prostate, ovarian and breast cancers. However, there is an enduring necessity in discovering effective treatments for hardly curable cancer types such as pancreas, lung and liver malignancies.

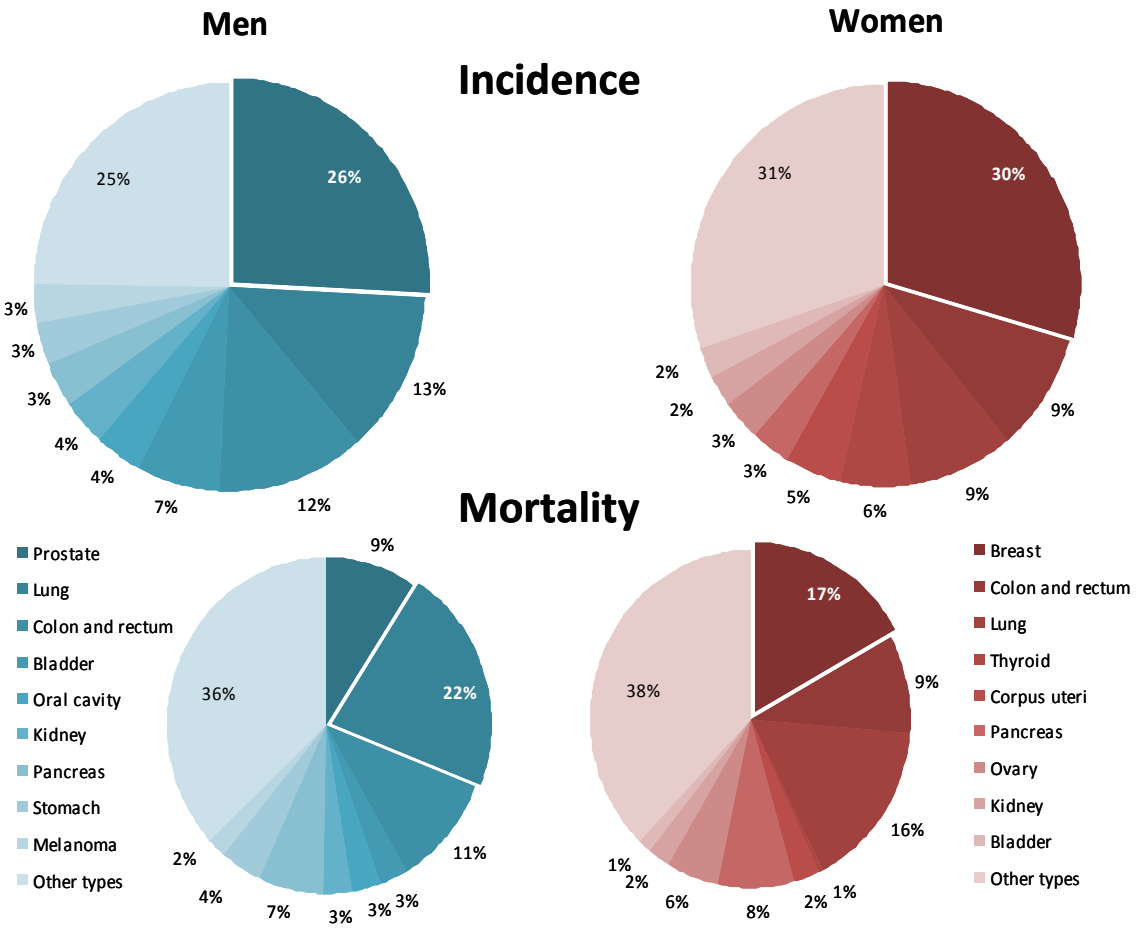

Figure 1. The estimated incidence and mortality of the 10 most common cancers in Austria in the year 2012. The segments of the pie chart reflect the percentages of total number of cases.

1.2 Metal-based Anticancer Drugs

1.2.1 Cisplatin in Cancer Therapy and its Mode of Action

The knowledge about the cytostatic activity of platinum-based compounds emerged from electrophysiological experiments on bacteria *Escherichia coli* conducted by Barnet Rosenberg and co-workers back in 1965[4]. Soluble complexes generated by platinum electrodes in ammonium-containing medium were shown to arrest bacterial cell division while sustaining the longitudinal growth of the bacteria. Further on the square-planar Pt(II) complex $[Pt^{II}Cl_2(NH_3)_2]$ (*cis*-diamminedichloridoplatinum(II), or cisplatin) was found to effectively reduce the mass of sarcomas in rats[5]. Ten more years were needed before cisplatin became established in clinical therapy of cancer patients[6]. The discovery of cisplatin gave rise to multiple investigations in the area of metal-based chemotherapeutics. Thousands of putative anticancer compounds were synthesized and characterized in the last decades however, only few of them reached clinical trials.

Cisplatin is applied as a first-line treatment for various carcinomas and sarcomas and was found to improve the survival and quality of life of patients in clinical trials with testicular, ovarian, cervical, bladder, head and neck, esophageal and non-small cell lung cancer, alone or in systemic therapies.[6-11] Though cisplatin is widely and long used in chemotherapy, there are several major drawbacks associated with its application, namely, acquisition of resistance and diverse side effects. A variety of resistance mechanisms are supposed to play an important role in the fate of cisplatin, such as decreased cellular uptake, increased drug efflux and detoxification, escape from apoptosis by cisplatin tolerance and enhancement of DNA repair[12]. Since the establishment of cisplatin in the clinics the most pronounced side effects were usually associated with dose-limiting nephrotoxicity, ototoxicity, and/or peripheral neurotoxicity[13-15]. In case of nephrotoxicity the introduction of the combinatorial strategies implementing chemotherapeutic and diuretic agents helped to overcome the dose-limiting nephrotoxicity. However the renoprotective effects are mostly partial and it stays unclear whether these approaches would limit the anticancer effects of cisplatin in tumors[16]. Today, a lot of efforts are undertaken to better understand the biochemical pathways altered by cisplatin in tumor cells that in turn may help to develop new therapeutic strategies, to overcome the drug resistance and to reduce side effects by synthesis of novel target-specific platinum drugs.

Following the intravenous administration of cisplatin as short-term infusion in physiological saline (rich in chloride ions) the chloride ligands are slowly displaced by water resulting in aquated or hydroxo species (Fig. 2). The aquation is supposed to occur more rapidly in the cells rather than in the blood stream due to the pronounced decrease in concentration of chloride ions from the body liquids (higher than 100 mM) to the cells (lower than 20 mM). In aqueous solution at neutral pH, the chloride ligands of cisplatin are replaced stepwise by water.

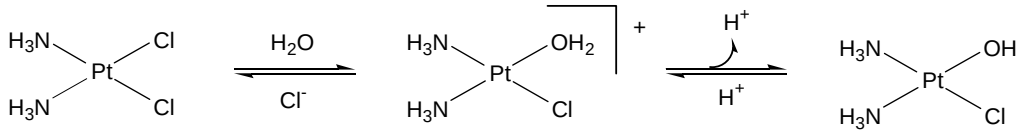

Figure 2. Behavior of cisplatin in aqueous solution. In a sufficiently long time span both leaving groups (chlorides) can be exchanged.

The accumulation of cisplatin in the cells is mainly canoed by the passive diffusion; however, several membrane transporters associated mainly with copper influx and efflux, such as copper transporters 1 and 2 (Ctr1, Ctr2), P-type copper-transporting ATPases (ATP7A and ATP7B), contribute by active transport (Fig. 3). Together with the organic cation transporter-2 (OCT2), and the multidrug and toxin extrusion transporter-1 (MATE1) these membrane channels are supposed to take part in the regulation of cellular accumulation of cisplatin[17-19].

When inside the cells, aquated cisplatin is prone to reacting with different N- and S-donor containing molecules[20, 21]. Although DNA is strongly considered as a critical target of cisplatin, it is still unclear how the drug reaches the DNA in the presence of multiple possible targets in membranes, cytoplasm and organelles[22]. The binding of cisplatin to proteins and peptides may modulate its biochemical properties and therefore diversify the putative cellular targets. The ability of platinum-based chemotherapeutics to inhibit cancer cell growth is strongly dependent on the balance between target efficiency (DNA binding) and biotransformation by sulfur nucleophiles. The principle of hard and soft acids and bases would predict cisplatin binding to S-donor ligands such as thiols preferentially over reactions with other nucleophiles[20, 22]. Consistently, intracellular sulfur-containing molecules such as glutathione, metallothioneines and thioredoxins have been reported to compete with DNA for metallodrug binding[23-25]. Additionally, the cisplatin molecules were shown to undergo specific modifications upon reaction with sulfur-rich binding sites on proteins[18, 26, 27]. Cytosolic thiol-rich scavenging proteins (metallothioneins), playing an important role in sequestration and detoxification of heavy metals, were also shown to provoke the loss of amine ligands in cisplatin[23, 28]. Binding to S-donors results in a *trans*-labilization of ligands that might facilitate the dissociation of the (otherwise inert) ammine ligands[22, 29].

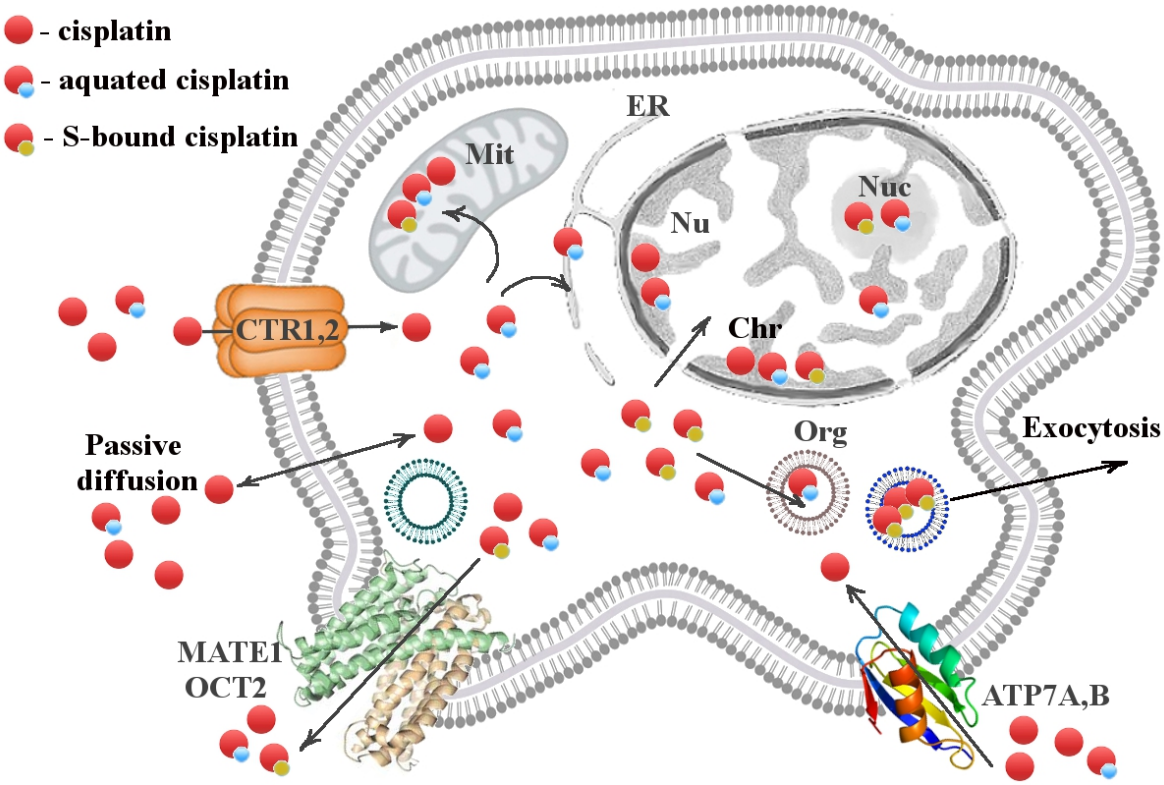

Figure 3. Accumulation of cisplatin in the cell and its major cellular targets. Chr – chromatin, ER – endoplasmic reticulum, Mit – mitochondria, Nu – nucleus, Nuc – nucleolus, Org – tissue specific cytoplasmic organelles (e.g. lysosomes, microsomes, melanosomes).

The primary target of cisplatin is generally accepted to be the nuclear DNA[30]. The aquated active forms of cisplatin induce cross-linking between the purine bases of DNA molecules leading to conformational changes in DNA secondary and tertiary structure (bending, unwinding). Nearly half of interactions of the drug with DNA are reported to be 1,2-intrastrand d(GpG) adducts between the N7 of the imidazole rings of adjacent guanine bases[31]. To a much lower extent the adenine bases may be involved with 1,2-intrastrand d(ApG) cross-links comprising about a quarter of all adducts. Additionally, 1,3-intrastrand and several types of interstrand adducts as well as a small fraction of monofunctional adducts occur (comprising less than 15% of all interactions, Fig. 4). The most common interaction between the N7 atoms of the purine bases is strongly considered to be the major adduct type that contributes to the cytotoxic activity of cisplatin[32, 33]. The DNA binding of cisplatin disturbs DNA functionality by inhibiting replication and transcription processes, leading to cell cycle arrest and ultimately to apoptosis[34]. Nucleotide excision repair (NER) is supposed to play a major role in removing the monofunctional DNA adducts, while the bifunctional adducts, including the most common d(GpG) adducts, are repaired the least effectively[34]. The mitochondrial DNA (mtDNA) and RNA were also reported as putative pharmacological targets for cisplatin[35, 36]. It is to be mentioned that the mtDNA is prone to cisplatin damage due to the absence of the NER pathway in mitochondria.

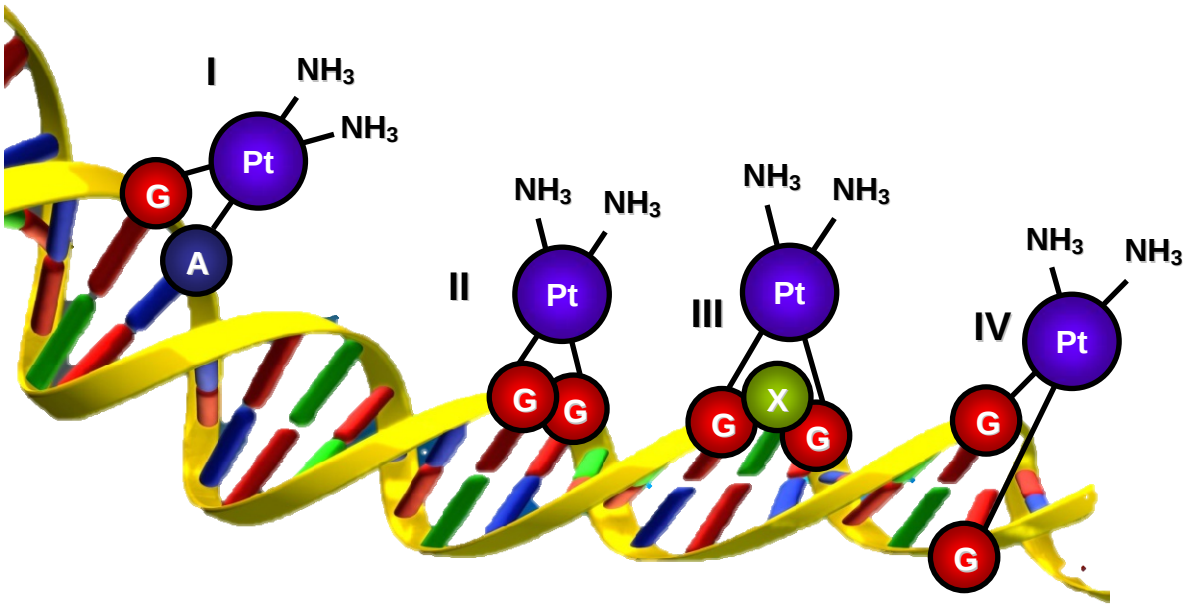

Figure 4. Most common cisplatin and DNA adduct formation[31, 32]. I – 1,2 intrastrand d(GpA) adducts (0-25%); II – 1,2 intrastrand d(GpG) adducts (50-65%), III – 1,3 intrastrand d(GpG) adducts (less than 10%); IV – interstrand d(GpG) adducts (less than 5%).

Multiple side effects as well as acquired and intrinsic resistance in different cancers are the main factors that provoke the search for novel drug candidates. The resistance to platinum-based drugs is a systemic process that simultaneously involves several protective mechanisms of the cells such as decreased platinum drug influx and increased drug efflux, drug inactivation by S-containing molecules, evasion of apoptosis and enhancement of DNA repair[37, 38]. Repair of platinum-DNA cross-links is known to involve well described repair mechanisms such as NER, homologous recombinational repair (HRR) and base excision repair (BER). The elucidation of the molecular mechanisms lying behind the mode of action, selectivity and side effects of platinum drugs will provide the background necessary for the synthetic design of novel platinum compounds with improved toxicity profile, circumvention of resistance and expansions of tumor indications[32].

1.2.2 Classic Platinum-based Chemotherapeutics

Thirty years after cisplatin has been introduced into clinical cancer therapy with resounding success, the development of new tumor-inhibiting platinum compounds continues to be a prolific field of research. Although recent years have seen the emergence of targeted cancer therapeutics, cisplatin still remains the only anticancer drug having turned a non-hematological malignancy (testicular cancer) in the disseminated stage into a mostly curable disease. The clinical success of cisplatin anticipated the discovery of second and third generation platinum(II)-based drugs, namely carboplatin and oxaliplatin (Fig. 5). All three compounds are indispensible in cancer therapy worldwide mainly due to their high curative potential in certain malignancies. These platinum(II) complexes are applied in various

combination therapies with partially different indications.[39] Cisplatin and carboplatin are applied in several genitourinary cancers, head/neck and lung cancer, while oxaliplatin is firmly established in combination therapy of advanced and metastasized colorectal tumors[40].

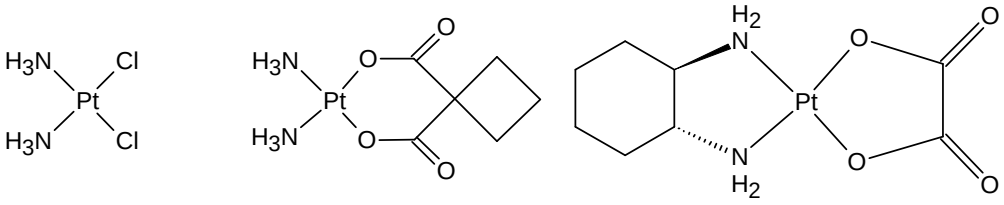

Figure 5. Structures of cisplatin, carboplatin and oxaliplatin.

Several platinum(II)-based drugs received regionally limited approval for clinical therapy *e.g.*, heptaplatin (in Korea), lobaplatin (in China) and nedaplatin (in Japan) (Fig. 6). These complexes either have shown enhanced anticancer effect in certain malignancies or proved to have less toxic side effects as compared to cisplatin and its analogues[40-42].

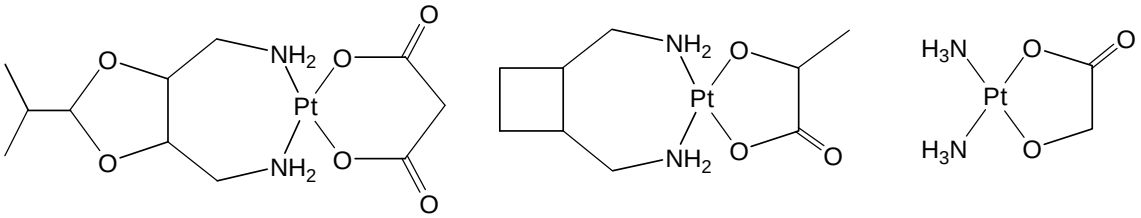

Figure 6. Structures of regionally approved platinum(II)-based anticancer drugs.

DNA is generally accepted as the critical target of cisplatin and its clinically approved analogues[31]. Their capacity of forming intrastrand and interstrand cross-links, with their consequences for DNA secondary structure and functions such as replication and transcription, as well as the mechanisms of recognition and repair of these DNA adducts are well known[43]. The same applies to the downstream effects, including cell cycle perturbations and cell death[30, 34]. Although the interaction of widely used platinum(II) drugs with tumor cells has been investigated in great detail, the mechanisms of selectivity, resistance, and toxicity are not completely understood (e.g. activity in enucleated cells[44, 45], interactions with cytoplasmic organelles[13-15]). Therefore, the investigation of the cellular targets of metal-based compounds in different model systems in order to improve the effectiveness of currently applied chemotherapies is indispensable.

1.2.3 Non-Classic Platinum(II)-based Complexes

Apart from attempts to modify platinum compounds for targeted therapy primarily aiming at increasing tumor selectivity rather than altering the basic mechanism of action, efforts have gradually shifted from the extensively investigated cisplatin analogues to *non-classic* platinum agents, which interact with their molecular targets in a different manner[46]. Especially the latter class, which contains

a continuously growing number of compounds with proven activity *in vitro* and *in vivo*, probably includes complexes that differ substantially from established platinum drugs in their mechanism of action and might display activity profiles extending to cisplatin-resistant tumors.

The success of cisplatin in comparison to its almost inactive *trans*-configured analogue transplatin has shaded the investigation of *trans*-configured complexes for several decades. The classic structure-activity relationships formulated for platinum-based chemotherapeutic agents were predicting the higher activity of the *cis*-configured complexes over their *trans*-analogues[47]. The general prerequisites for anticancer activity of platinum-based compounds were postulated by Cleare and Hoeschele: (i) the compound should be *cis*-configured; (ii) the species should bear no charge; (iii) the leaving groups should possess enough lability to enable the complex to interact with critical targets[47]. However, in the last decade there were plenty of examples of *trans*-configured platinum-based drugs with a comparable or even higher effect than that of their *cis*-congeners. In contrast to classic *cis*-configured platinum drugs, *trans*-platinum complexes show a low capacity of forming intrastrand cross-links, which are the predominant adducts of cisplatin, but form higher ratios of interstrand cross-links and monofunctional adducts[43]. However, the monofunctional adducts of several non-classic compounds with DNA were reported to be either very stable or able to convert slowly to a bifunctional mode[48, 49].

Different classes of non-classic platinum-based compounds were proven to exhibit cytotoxicity comparable or even higher than that of their *cis*-analogues and similar to cisplatin, whereas being substantially more cytotoxic than transplatin[46, 50, 51]. Several strategies were proven to effectively increase the cytotoxicity of *trans*-configured complexes (Fig. 7). The exchange of the ammines for sterically hindering ligands such as planar amines (e.g. pyridine, quinoline, thiazole), non-planar amines (e.g. piperazine and piperidine) or sterically demanding branched amines (e.g. methylbutanamine, *sec*-butanamine) gave a rise to a number of active complexes featuring reduced hydrolysis rates that in turn help the drug to reach the pharmacological target without being deactivated in the blood serum. These groups were reported to have high cytotoxicity in broad spectrum of tumor cell lines. Some complexes were found to have cytotoxicity profile different to the clinically used agents[52-55]. However, besides the high cytotoxic activity of latter classes of *trans*-platinum complexes *in vitro*, they were reported to possess only moderate or no activity in *in vivo* tests[50].

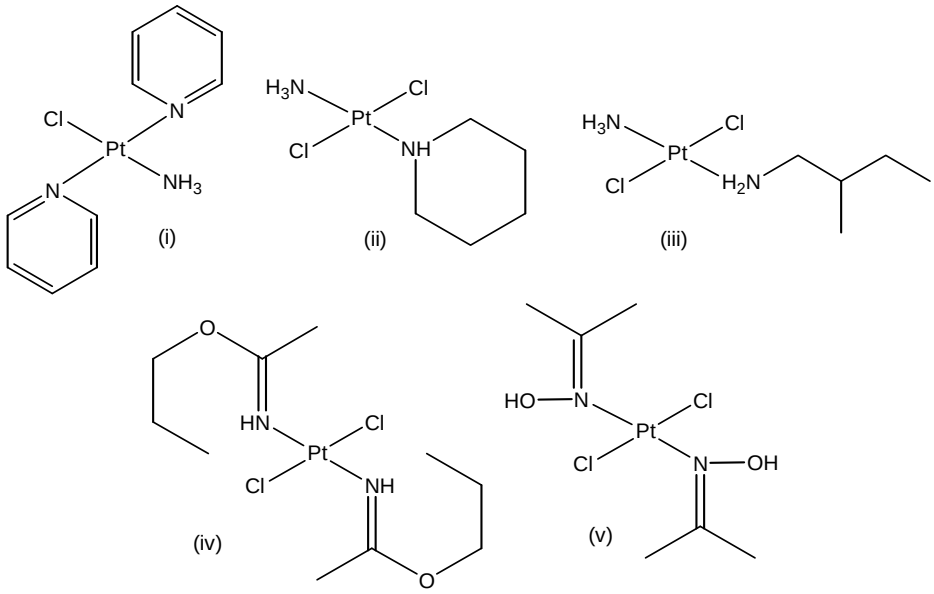

Figure 7. Examples of platinum(II)-based non-classic anticancer compounds. (i) *trans*-planar amine complexe with pyridine; (ii) non-planar platinum(II) complex with piperazine; (iii) platinum(II) complex with branched *sec*-butanamine; (iv) *trans*-platinum(II) complex bearing iminoether ligands; (v) platinum(II) complex with oxime ligands.

A clear evidence for the activation of the *trans*-geometry in platinum(II)-based complexes was previously demonstrated on species bearing iminoether, acetonimine and oxime ligands (Fig. 7)[56-58]. The *trans*-congeners often appeared to more effectively accumulate in the target cells, leading to apoptosis induction. Different cellular targets of these complexes were further investigated *in vitro*[59, 60]. A pH-dependent evaluation of antiproliferative effects of several acetoxime complexes at slightly acidic pH revealed an activation under possible "tumor site" conditions[61]. An acidic milieu as well as a reducing environment in solid tumor tissues have already been beneficially used to design new types of chemotherapeutics. The initially relatively inert platinum(II) species such as alkyldithiocarbonatoplatinum(II) and aminoalcoholatoplatinum(II) complexes were demonstrated to act as prodrugs that could be activated at the tumor site either by reduction or protonation (Fig. 8), resulting in the formation of biologically active drugs prone to interactions with surrounding cancer cells[62-64].

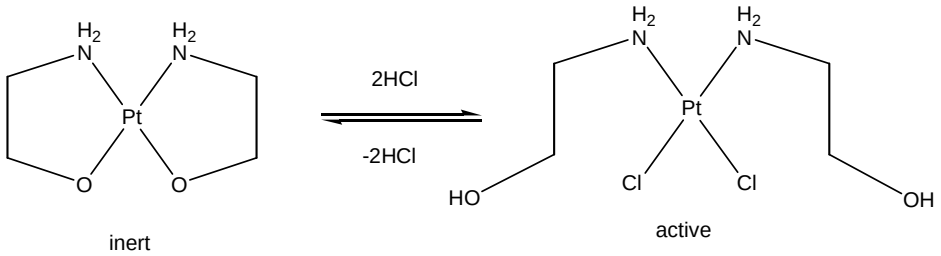

Figure 8. The activation of a bis(aminoalcoholato)platinum(II) complex in acidic environment.

The rapid and uncontrolled growth of the malignant tissue prevents the formation of a regular vasculature in solid tumors. The hypoxic environment, when cells are not sufficiently supplied with oxygen from the blood, favors an upregulated anaerobic pathway of energy production – glycolysis – instead of mitrochondrial oxidative phosphorylation that is normally employed downstream. The glycolytic switch of energy production was discovered also in the presence of oxygen and was termed "aerobic glycolysis"[65, 66]. As a result the lactic acid production is increased, leading to the acidification of the extracellular space. In the tumor site the tissue pH was reported to range between 5.5 and 7.3, while the normal tissue pH level is close to 7.4[67, 68]. Reprogramming of the energy metabolism resulting in hypoxia and acidic pH are well known hallmarks of solid tumors that could be effectively used to develop new classes of triggered pH sensitive platinum-based chemotherapeutics[69].

1.2.4 Platinum(IV)-based Compounds

Efforts were also made to develop platinum(IV) compounds for targeted therapy primarily aiming at site-specific activation in the tumor region[70]. The reducing environment in solid tumors as well as their acidic milieu have inspired the design of platinum(IV) complexes which can be activated under these conditions. The platinum(IV) complexes are less reactive than platinum(II) species, with the following implications: (i) the compounds can be applied orally as they are stable enough to be absorbed in the gastro-intestinal tract, (ii) the low reactivity allows for the utilization of novel synthetic routes, and (iii) they show reduced systemic toxicity, as they act as prodrugs[70]. Several representatives of the class (tetraplatin[71], iproplatin[72], satraplatin) have already been studied in clinical trials (Fig. 9).

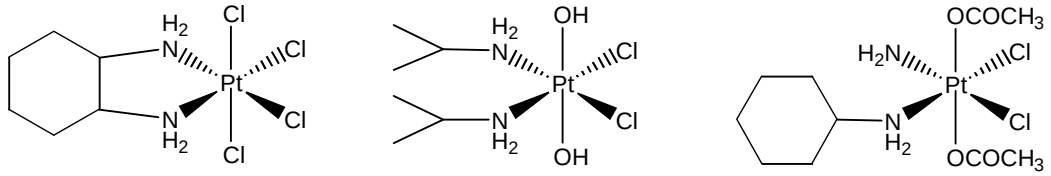

tetraplatin iproplatin satraplatin

Figure 9. Platinum(IV) complexes that entered clinical trials: tetraplatin, iproplatin, satraplatin.

The most potent of them – satraplatin – proved to be clinically active in combination with prednisone in refractory prostate cancer in a clinical III trial[73] and in radiation-based therapy[74] where it showed the ability to sensitize non-small cell lung cancer to radiation. The inert octahedral platinum(IV) complexes are supposed to require reduction with the release of the axial ligands (Fig. 10) by reducing agents such as ascorbic acid, glutathione, or high molecular weight biomolecules to result in the active square-planar platinum(II) metabolites[75, 76]. A wide variation of axial ligands from chloro to hydroxo to carboxylato moieties is a key for a broad span of both lipophilicity as well as reduction potential and gives an additional opportunity to label the compounds.

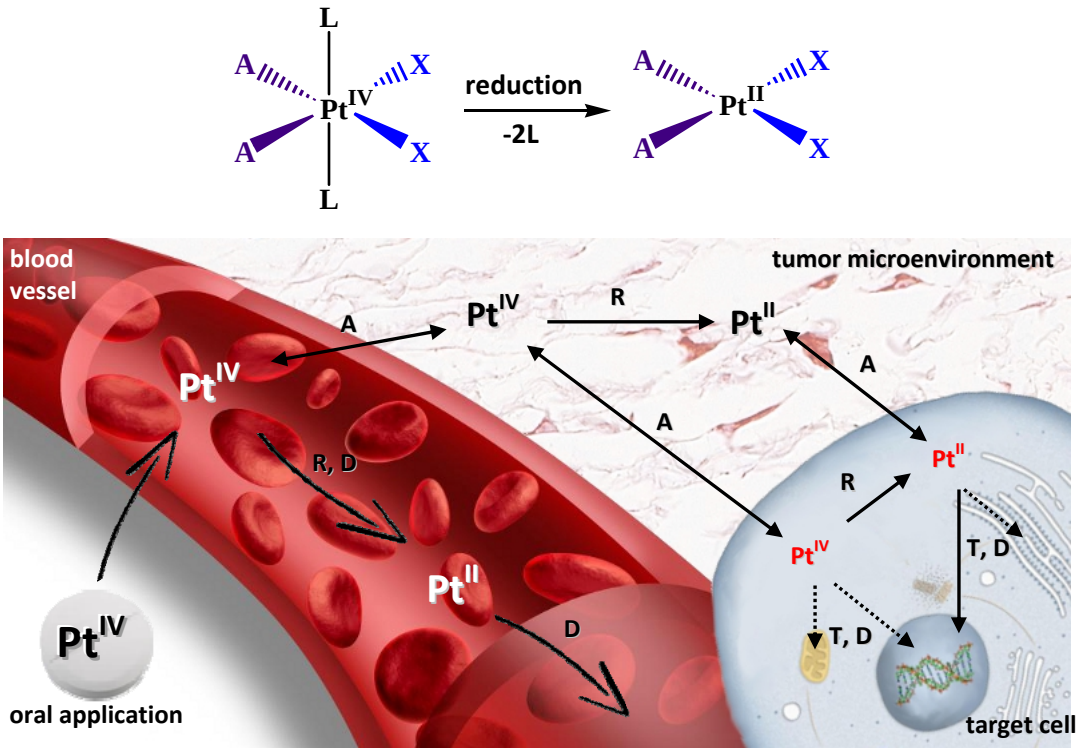

Figure 10. Activation by reduction with release of the axial ligands from the platinum(IV) compound and major transformations of platinum(IV) compounds *in vivo*: R – reduction; D – deactivation (e.g. due to binding to plasma proteins or intracellular sequestration); A – accumulation; T – target binding (e.g. interactions with DNA). Dotted arrows point to targets that might be involved in drug processing (mitochondria, ER, lysosomes).

Notwithstanding that DNA is the accepted crucial target for platinum drugs[30, 77], information about the mechanisms responsible for activation and cytotoxicity of platinum(IV) complexes is insufficient so far[78, 79]. What we know of mechanisms of action and even targets of platinum drugs is scarce and derived from investigations in simplified model systems mainly, therefore leaving room for uncertainty with regard to their behavior in human patients.

1.3 Subcellular Imaging of Anticancer Drugs

1.3.1 Visualization Techniques

While the crucial role of DNA as the main target for clinically relevant platinum drugs is generally accepted, the variety of possible interactions with cellular targets other than DNA has not been investigated in detail. Furthermore, the mechanisms of cytotoxicity, selectivity and resistance of cancer cell models to multiple platinum and ruthenium complexes have not been fully explored, neither *in vitro* nor *in vivo*. One of the important steps in this direction is to study the subcellular drug distribution in cellular organelles that might contribute to these mechanisms. Currently there is a rise

in the field of novel powerful imaging techniques that allow the visualization of both the drug distribution and the ultrastructure within the same cell.

The visualization of the subcellular distribution of pharmaceutical agents can yield valuable information pointing to the sites relevant for their biological activity as well as for detoxification. The methods routinely used for the detection of metals in biological samples are summarized in figure 11. Initially the subcellular distribution of platinum-based drugs was studied by cellular fractionation-based methods followed by spectrometric analysis by means of atomic absorption spectroscopy (AAS) or inductively coupled plasma mass spectrometry (ICPMS), which allows an estimation of metal accumulation in certain compartments or set of compartments (cytoplasmic, nuclear fractions)[80-82]. However, the fractionation methods are imperfect due to the risk of cross-contamination of fractions and partial loss of the analyte during sample preparation; they were continuously supplemented with methods applicable on the intact cells. The radioactive labeling and registration techniques developed in the last decades enabling not only distribution, but also pharmacokinetic studies[83, 84]; however, the application of this approach *in vivo* is restricted, partially due to the possible negative effect of the radioactively labeled molecules on the host tissues. The subcellular distribution of fluorescently-labeled platinum complexes by means of fluorescence microscopy was studied in different cell models[85-88]. The resolution of light microscopy-based techniques is constantly evolving and various fluorescent moieties might be used to follow the subcellular drug distribution. Moreover, the application of light microscopy for the detection of the drug inside the intact cells allows such approaches as live distribution imaging in the living cells. It should be mentioned; however, that the additional bulky ligands may affect the (sub)cellular transport and/or may be cleaved off by metabolic activity of the cell, resulting in a different fate than in the native compound.

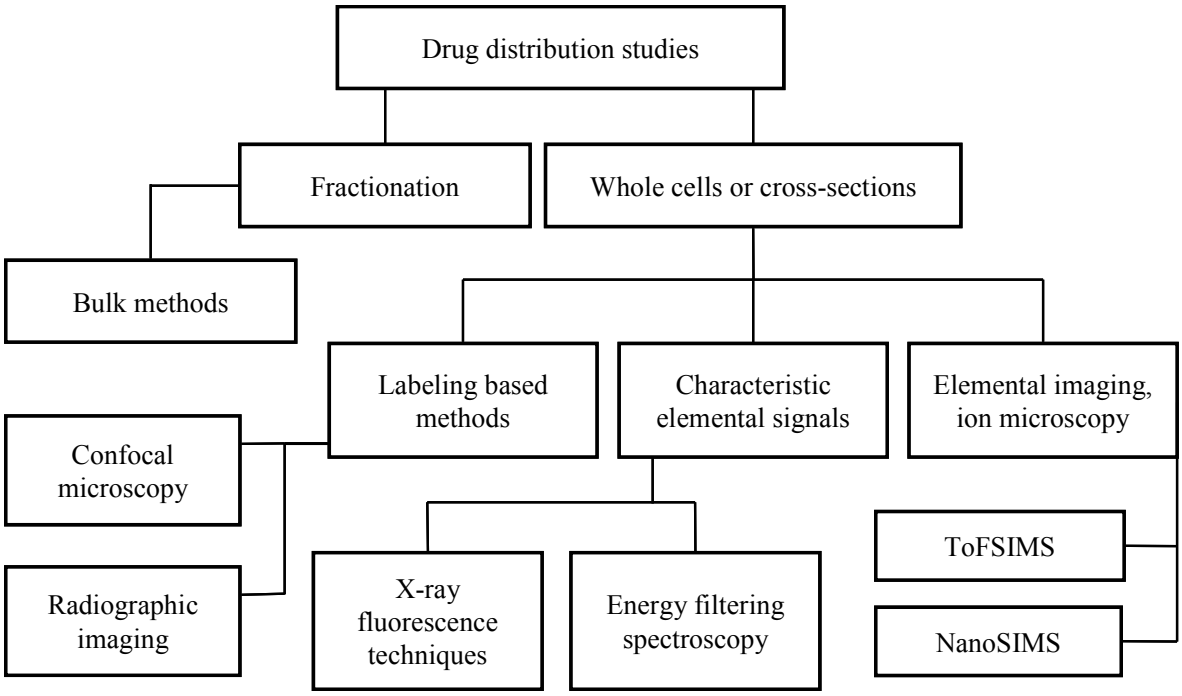

Figure 11. The methods used for the detection of anticancer drugs in biological samples.

The element specific imaging techniques, such as synchrotron based X-ray fluorescence microscopy, are suitable for highly sensitive, quantitative and oxidation state specific mapping of elements with Z>11[89, 90]. Thanks to the continuous improvement of X-ray beam focusing optics and high-sensitivity fluorescence detection systems X-ray fluorescence imaging has significantly evolved in the last decade[91-93]. Several studies of the subcellular distribution of platinum-based anticancer drugs by means of X-ray fluorescence microscopy show impressive sensitivity, though remain limited in spatial resolution that allows distinguishing the cytoplasmic and nuclear compartments so far[94, 95]. Transmission electron microscopy with energy dispersive X-ray (EDX) spectroscopy or energy filtering (EFTEM) enables, e. g., the gold subcellular imaging and offers unparalleled lateral resolution[96]. The capabilities of EFTEM and EDX for the investigation of trace amounts of platinum-based drugs inside the cells are limited due to the low sensitivity for platinum.

Multi-elemental imaging by means of secondary ion mass spectrometry (SIMS) combined with different visualization methods has recently been shown to be a highly sensitive technique for the detection of isotopically labeled compounds in plants, animals and microorganisms[97-99]. SIMS-based ion microscopy enables trace element and isotope-selective analysis with high spatial resolution. This unique capability of SIMS has recently been exploited in a few pioneering studies analyzing the subcellular distribution of Au and Pt in eukaryotic cells[96, 100-102].

1.3.2 Molecular and Elemental Imaging

The implementation of SIMS for imaging purposes has created indispensable research opportunities in the fields of cosmochemistry, environmental microbiology, cell biology, plant and soil science, materials science and geochemistry, because of its unique ability to acquire information about molecule- and element-specific composition of the sample with a submicrometer spatial resolution[103].

The ion microprobe concept is based on imaging by rastering a focused ion beam across the target surface. The principle of the SIMS imaging is briefly shown in figure 12. The primary ion beam (either positively or negatively charged ions, e.g. Cs^+, O_2^-) emitted from the ion source can be focused onto the surface of a sample with a diameter of 50-100 nm, eroding the target and producing secondary ions that can be mass analyzed. This approach enables high sensitivity, high mass resolving power and high lateral resolution of the resulting molecular- or element-specific images[104]. Depending on the ionization type and the mass spectrometer that is used to determine the secondary ions, there are two main techniques applied in imaging mass spectrometry: static and dynamic SIMS. The static SIMS is based on pulsed primary ion beam emission and time-of-flight mass spectrometry and provides a unique possibility to follow the molecular composition of the target. The dynamic SIMS is based on continuous primary ion beam emission and a magnetic sector mass analyzer with the emphasis on elemental- and isotopic-specific composition of the sample. There are certain requirements to the sample preparation due to the necessity of surface smoothness and introduction into an ultra-high-vacuum for the measurement (discussed in section 1.3.4).

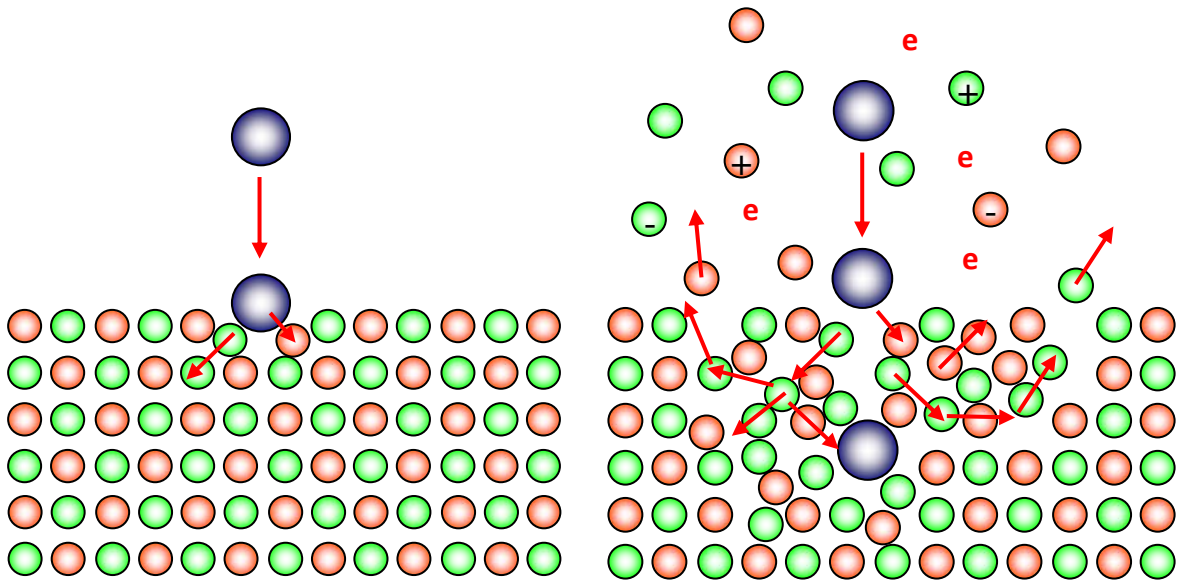

Figure 12. Principle of SIMS. The energetic primary ion beam (blue spheres) hits the sample surface (red and green spheres) and initiates a cascade of collisions between the atoms, resulting in the sputtering and partial ionization (positive or negative) of the uppermost atomic layers. The eroded

secondary ions of the polarity opposite to the primary beam continue to the mass analyzer where they are determined according to their mass to charge ratios. Additional information, reflecting the topography of the sample surface, can be obtained from analyses of the secondary electrons sputtered from the surface. (Courtesy of Arno Schintlmeister).

Multi-elemental, isotope-selective nano-scale secondary ion mass spectrometry (NanoSIMS) proved to be a suitable technique for mapping of isotopically labeled compounds[91, 97, 105] as well as rare elements (e.g. noble metals[96, 106, 107]) in samples with complex chemical composition. The dynamic NanoSIMS instruments (Cameca, France) are characterized by superior spatial resolution, high sensitivity and multi-collection capability that comes from a switch from a conventional 45° to a co-linear probe forming system, which allows the NanoSIMS instrument to accommodate two crucial features: the probe forming optics (primary beam focusing) and the extraction optics (secondary ions collection) are situated as close as possible to the sample, which allows simultaneous high qualitative focusing of the primary ions and collecting most of the secondary ions (Fig. 13).

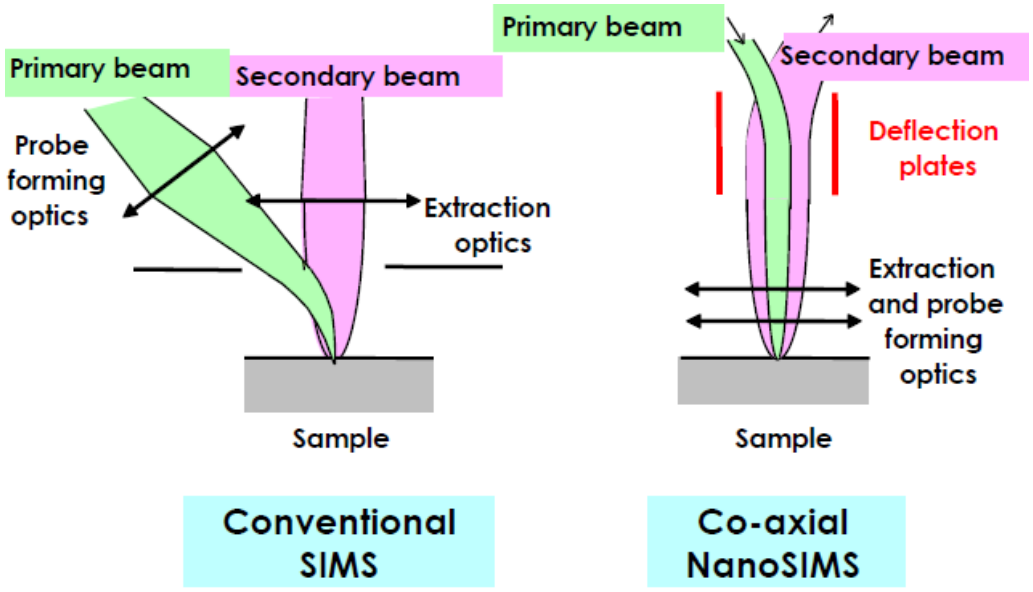

Figure 13. Conventional and co-axial configurations of the SIMS probe forming and extraction optics. Image is taken from the NanoSIMS instrumentation booklet (www.cameca.com).

1.3.3 Biological Applications of NanoSIMS

The application of SIMS for the elemental mapping of biological samples has made considerable progress in the last decade. Tracking the molecules across single cells and tissue samples became feasible with the evolution of SIMS instruments. Dynamic SIMS instruments utilizing energetic (several keV), chemically reactive primary ion beams (e.g. Cs^+, O^-) allow highly sensitive elemental and isotope-selective analyses, brought about through extensive ion bombardment induced fragmentation of sample molecules within the first layers of the sample surface. The combination of impressive spatial resolution, high sensitivity and high mass resolution renders NanoSIMS a cutting-

edge tool for elemental and isotopic studies in many fields from material sciences to biology and geo/cosmochemistry (see review by Hoppe et al.[103]). In the field of microbiology SIMS enables detailed insights into the functions of microorganisms in their natural environment[108]. Isotope-labeling techniques combined with molecular detection tools are a prerequisite for understanding the metabolic pathways between microorganisms and their hosts (e.g. intestinal ecosystem). Some novel approaches and findings in different areas of microbiology such as host-compound foraging by intestinal microbiota or the metabolic spectrum of ammonia oxidizing archaea were reported by M. Wagner and his group[98, 108, 109]. Fundamental examples of NanoSIMS-based multi-isotope mass spectrometry (MIMS) in cell biology, involving isotopic labeling (^{15}N, ^{13}C), were reported by the group of C. Lechene[110-112]. In the field of chemical pharmacology several successful attempts in detecting Au- and Pt-based anticancer drugs were reported[96, 100, 107], but the potential of NanoSIMS in this area is far from being fully exploited. NanoSIMS allows not only to qualitatively visualize fine-scale distribution of the target elements, but also to obtain quantitative data.

Apart from qualitative data (elemental imaging), SIMS enables quantitative elemental analysis that requires calibration standards that have to be highly similar in composition to the sample of interest. The signal intensities are strongly determined by instrumental parameters (e.g. primary ion beam intensity, spectrometer transmission), product of the sputter yield and ionization probability (the latter can vary over several orders of magnitude). Besides element-specific properties that play a decisive role in ion formation (i.e. ionization energy and electron affinity), the wide range of variation mainly comes from complex sample composition ('matrix effect') and the sample topography. As a consequence, quantitative results can only be obtained from the relative signal intensities when the signal intensity of the target element is normalized to the intensity of a closely related ion species. For elemental analysis, the analyte signal is preferably normalized to the intensity of a reference signal associated with an element that is abundant and homogeneously distributed within the sample matrix. The normalized signal intensity is proportional to the analyte concentration and may be quantified via calibration. The latter necessitates the preparation of standards which need to be as closely related to the sample properties as possible.

1.3.4 Combinatory Approaches

SIMS can simultaneously yield information both about the target element/isotope distribution (e.g. ^{13}C, ^{15}N and Pt) and that of abundant cellular elements/isotopes such as ^{12}C, ^{14}N, ^{31}P, $^{32/34}S$. The secondary ion signal intensity distribution images of the abundant elements can be readily used to distinguish some subcellular structures (e.g. cell borders, nucleus, nucleolus, cytoplasmic organelles, Fig. 14). However, the exact identification of small organelles is highly challenging (when judged only by morphological appearance and elemental composition) and thus requires the application of a

combinatory technique. Since SIMS is destructive, a stepwise and elaborated preparation technique allowing a consecutive analysis by different methods (e.g. microscopy/SIMS) is essential.

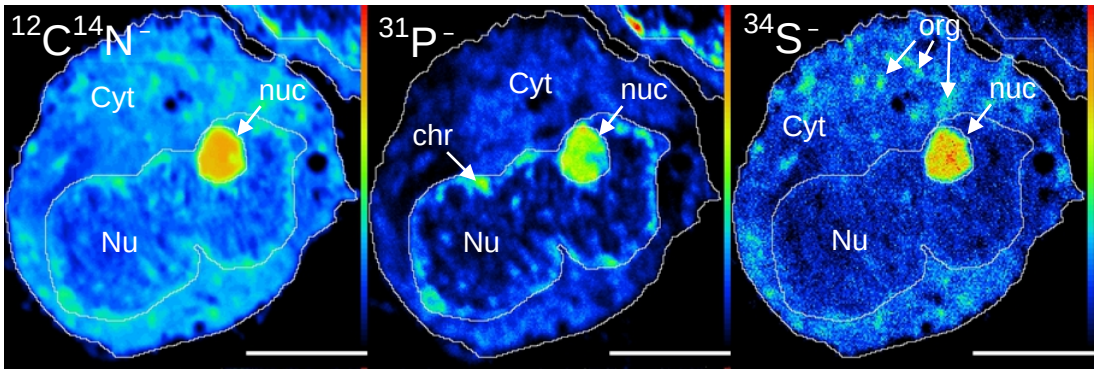

Figure 14. NanoSIMS $^{12}C^{14}N^-$, $^{31}P^-$ and $^{34}S^-$ and secondary ion signal intensity distribution maps of a semithin section of SW480 human colon cancer cells. Identifiable structures are: cytoplasm (Cyt), nucleus (Nu), nucleolus (nuc), chromatin (chr), cytoplasmic organelles (org). Intensities are displayed on a rainbow false-colour scale ranging from dark blue to red for low to high intensities, respectively. Scale bars = 5 µm. From Ref.[107]

Combinatory approaches involving SIMS have been reported with fluorescence *in-situ* hybridization (FISH), SEM/TEM, X-ray microscopy, or immuno-methodologies allowing simultaneous collection of functional, phylogenetic, and molecular information from individual cells, as thoroughly discussed in Ref.[113]. The application of fluorescence microscopy for oligonucleotide-probing in combination with NanoSIMS imaging proved to be a powerful tool capable of addressing many key questions in the animal and human microbiome[108, 114, 115]. Subcellular structures accumulating different compounds were successfully identified by confocal laser scanning microscopy coupled with SIMS analyses in samples treated with organelle trackers (Fig. 15) or in immuno-labeled samples[107, 116-118].

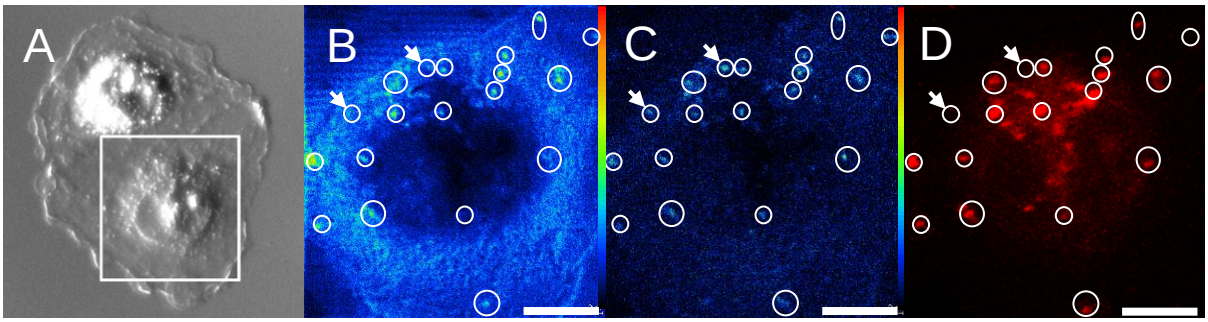

Figure 15. NanoSIMS secondary ion signal intensity distribution maps and confocal microscopy images of an adherent SW480 cell after 24 h exposure to 25 µM cisplatin, revealing cisplatin colocalization with acidic organelles. The screened region is marked with a frame in the differential interference contrast image (A). The confocal microscopy image of fluorine-containing LysoTracker Red (D) demonstrates a correlation with the $^{19}F^-$ secondary ion signal intensity distribution (B) and platinum distribution (C) patterns detected by NanoSIMS in the same cell. Arrows indicate a few

regions of platinum accumulation lacking fluorescence and $^{19}F^-$ signal intensity enhancement. Secondary ion signal intensities are displayed on a rainbow false-color scale ranging from dark blue to red for low to high intensities, respectively. Scale bars = 5 μm. From Ref.[107]

The best means for simultaneous identification of many organelles without additional labeling are electron microscopy techniques (TEM, SEM). There are several examples of electron microscopy combined with SIMS for applications in microbiology[110, 119, 120]. So far, the majority of the combinatory studies in cell biology were applied to conventional adherent cell cultures. Therefore, the development of a combined approach involving NanoSIMS, CLSM, and electron microscopy suitable for analyses of more complex systems such as multicellular spheroids and tissues would be valuable progress.

1.3.5 Sample Preparation

One of the major challenging tasks associated with (Nano)SIMS is sample preparation. The ideal would be a technique preserving both the structural and chemical integrity of the living cell. Even if this ideal could be fulfilled, SIMS remains destructive; therefore any complementary technique can be applied only prior to SIMS analyses on the very same region of interest. In addition, the measurement takes place under vacuum, necessitating resin-infiltrated or dried samples to avoid collapsing of the cells or soft tissues. To investigate diffusible ions (e.g. Na^+, K^+, Ca^{2+}) and water-soluble molecules (e.g. anticancer drugs), it is important to preserve the cells in their native state. There are two strategies to retain the chemical integrity during sample preparation for SIMS: conventional sample preparation and cryo-based techniques.

Conventional sample preparation methods (generally applied for TEM) require chemical fixation, dehydration with organic solvents, and resin embedding, usually in epoxy-based or acrylic polymers. The introduction of the resin matrix maintains a high structural integrity of the embedded samples that allows thin and ultrathin sectioning. Notably, such conventional techniques are prone to excessive extraction of molecules.

Rapid cryo-fixation is a reliable way for quick immobilization of any cellular material. Freeze-substitution helps to remove the frozen water from the cells at low temperatures (less than -80 °C to avoid ice crystal formation) and to reduce the possible diffusion of labile ions and molecules. Different protocols, for example the one outlined by Clode and Marshall[121], can be used to minimize movement of mobile ions such as Ca^{2+} and were successfully applied for investigations of the diffusible ion fraction in embedded samples by means of dynamic SIMS[122]. Some crucial advantages of resin-embedded samples, such as the flatness of sections and the infiltration with a relatively homogeneous matrix that reduces differential erosion rates, are discussed in a review by Guerquin-Kern et al.[123]

Additionally, the homogeneous matrix provides suitable reference signals for intensity normalization (e.g. C^- , C_2^- or O^-). Freeze substitution with subsequent embedding into epoxy-based resins should be regarded as the first choice for correlative TEM/SIMS analyses of trace elemental distribution. Epoxy embedding proved to have minimal analyte extraction effect if compared with methacrylates.

Sublimation-based cryo-preparation techniques allow preservation of the native cell matrix without embedding in resins. To expose the inside of cells, the cryofixed samples have to be freeze-dryed followed by dry fracturing at ambient temperature. Alternatively, freeze-fracturing might be performed on the frozen material prior to freeze drying. The applications of freeze-fracturing followed by freeze drying for the requirements of SIMS have been described in the works of Chandra et al[101, 124, 125]. These sublimation-based cryo-preparation methods may complicate quantitative SIMS analysis due to the lack of homogenously distributed matrix elements that can be used as reference signals (e.g. oxygen, carbon) and enhance the sample topography. Freeze-dried and dry fractured or freeze-fractured and dried samples, however, facilitate highly sensitive ^2H, ^{13}C and ^{18}O isotope measurements, which might be attenuated with resin embedding due to infiltration by hydrogen, carbon and oxygen with natural isotopic composition. Various preparation procedures enable different combinations of imaging techniques; the cryo-based sample preparations methods are briefly compared in figure 16.

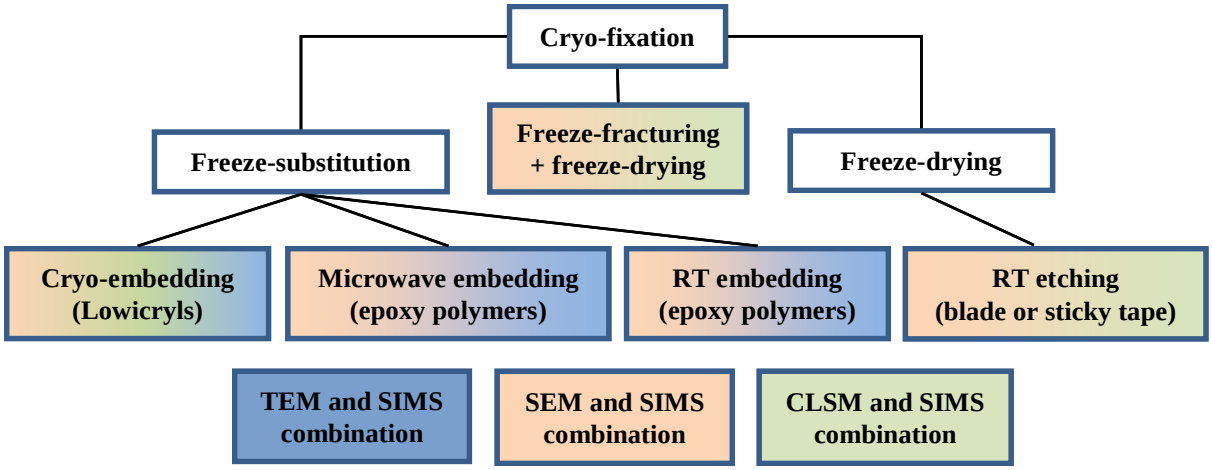

Figure 16. Sample preparation options and their possible application for combinatory analyses. Colors of the boxes correspond to method combinations (blue: TEM and SIMS, apricot: SEM and SIMS, green: CLSM and SIMS).

2. Results

This cumulative PhD dissertation is based on the following research articles from the fields of elemental imaging and the investigation of the cellular activity of platinum-based anticancer complexes.

NanoSIMS combined with fluorescence microscopy as a tool for subcellular imaging of isotopically labeled platinum-based anticancer drugs

Legin A. A., Schintlmeister A., Jakupec M. A., Galanski M., Lichtscheidl I., Wagner M., Keppler B. K.

Chemical Science 2014, **5**, 3135-3143. DOI: 10.1039/c3sc53426j

Multi-elemental, isotope selective nano-scale secondary ion mass spectrometry combined with confocal laser-scanning microscopy was successfully used to characterize the subcellular distribution of ^{15}N-labeled cisplatin in human colon cancer cells.

As the first author I contributed to every part of the project and coordinated the collaboration with the co-authors. I performed the correlative studies by means of confocal microscopy and NanoSIMS as well as the biological studies. I conducted the sample preparations that included both the resin embedded samples and LysoTracker labeled samples for combinatory analyses. I investigated the activity of cisplatin in the cell line SW480 with three different assays based on colorimetric MTT method and FACS analysis. I was involved in the cell study by means on confocal microscopy as well as secondary ion mass spectrometry. I performed the statistical analyses of the data as well as graphical representation and preparation of the images. I made a major contribution to the preparation of all chapters of the manuscript.

Synthesis, characterization, and cytotoxic activity of novel potentially pH-sensitive nonclassical platinum(II) complexes featuring 1,3-dihydroxyacetone oxime ligands

Scaffidi-Domianello Yu. Yu., Legin A. A., Jakupec M. A., Arion B. V., Kukushkin V. Yu. Galanski M., Keppler B. K.

Inorganic Chemistry 2011, **50**, 10673-10681. DOI: 10.1021/ic2010612

A group of novel nonclassic platinum(II) complexes were prepared and analytically characterized. The cytotoxicity of the investigated compounds in human cancer cells was found in the medium or even low micromolar range, which is remarkable for nonclassic platinum complexes with three coordinated N donor atoms. This research is an important contribution to the development of inert and unreactive complexes (prodrugs) which can be activated in the tumor tissue.

As the second author I contributed with the bioanalytical testing of the complexes and with the preparation of the respective chapters of the manuscript. I investigated the cytotoxicity of the compounds in a set-up of thee human cancer cell lines. Moreover, I performed the comparative study concerning the cytotoxic activity of the selected complexes under physiological and slightly acidic conditions.

Novel oximato-bridged platinum(II) di- and trimer(s): synthetic, structural, and in vitro anticancer activity studies

Scaffidi-Domianello Yu. Yu., Legin A. A., Jakupec M. A., Roller A., Kukushkin V. Yu. Galanski M., Keppler B. K.

Inorganic Chemistry 2012, **51**, 7153-7163. DOI: 0.1021/ic300148e

Novel platinum complexes of *trans* geometry were tested for antiproliferative activity and the potency of apoptosis induction. Several complexes were proven to be strong apoptotic agents, which could induce cell death even in the cisplatin-resistant cell line SW480.

I performed the cytotoxicity testing in various cancer cell lines by means of the colorimetric MTT assay and investigated the potency of the drugs to induce apoptosis/necrosis by means of FACS-based annexin V-FITC/propidium iodide assay. I also participated in the discussion and preparation of the manuscript (Methods, Results and Discussion chapters).

Synthesis and characterization of novel bis(carboxylato)dichloridobis(ethylamine) platinum(IV) complexes with higher cytotoxicity than cisplatin

Varbanov H., Valiahdi S. M., Legin A. A., Jakupec M. A., Roller A., Galanski M., Keppler B. K.

European Journal of Medical Chemistry 2011, **46**, 5456-5464. DOI: 10.1016/j.ejmech.2011.09.006

A series of six novel bis(carboxylato)dichloridobis(ethylamine)platinum(IV) complexes was synthesized and characterized in detail by elemental analysis, FT-IR, ESI-MS, HPLC, multinuclear NMR spectroscopy and bioanalytical MTT and FACS methods. We showed that the apoptosis-inducing potency of one compound is much higher than that of cisplatin in the intrinsically cisplatin-resistant SW480 (colon cancer) cells.

I studied the induction of apoptosis and necrosis, evaluated the results and took part in the manuscript preparation.

Platinum(IV) Complexes Featuring One or Two Axial Ferrocene Bearing Ligands - Synthesis, Characterization, and Cytotoxicity

Banfic J., Legin A. A., Jakupec M. A., Roller A., Galanski M., Keppler B. K.

European Journal of Inorganic Chemistry 2014, **2014**, 484-492. DOI: 10.1002/ejic.201301282

Cytotoxicity of novel ferrocenyl-containing platinum(IV) complexes was investigated in three human cancer cell lines deriving from ovarian carcinoma (CH1), colon carcinoma (SW480), and non-small-cell lung carcinoma (A549) by means of the colorimetric MTT assay. Promising IC50 values in the low micromolar range in CH1 and SW480 human cancer cells were found.

I contributed to the article by conduction of the cell biological experiments, evaluation and discussion of the data and participated in the manuscript preparation (Cytotoxicity, Experimental Section chapters).

All the listed articles are published in peer-reviewed international scientific journals and can be openly accessed online with the respective DOIs.

2.1 NanoSIMS combined with fluorescence microscopy as a tool for subcellular imaging of isotopically labeled platinum-based anticancer drugs

Legin A. A., Schintlmeister A., Jakupec M. A., Galanski M., Lichtscheidl I., Wagner M., Keppler B. K.

Chemical Science 2014, **5**, 3135-3143. DOI: 10.1039/c3sc53426j

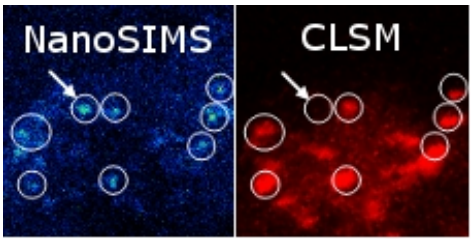

Chemical Science

EDGE ARTICLE

View Article Online
View Journal | View Issue

Cite this: *Chem. Sci.*, 2014, **5**, 3135

NanoSIMS combined with fluorescence microscopy as a tool for subcellular imaging of isotopically labeled platinum-based anticancer drugs†

Anton A. Legin,[ab] Arno Schintlmeister,[c] Michael A. Jakupec,[ab] Markus Galanski,[ab] Irene Lichtscheidl,[e] Michael Wagner[cd] and Bernhard K. Keppler*[ab]

Received 13th December 2013
Accepted 2nd April 2014

DOI: 10.1039/c3sc53426j

www.rsc.org/chemicalscience

Multi-elemental, isotope selective nano-scale secondary ion mass spectrometry (NanoSIMS) combined with confocal laser-scanning microscopy was used to characterize the subcellular distribution of ^{15}N-labeled cisplatin in human colon cancer cells. These analyses indicated predominant cisplatin colocalisation with sulfur-rich structures in both the nucleus and cytoplasm. Furthermore, colocalisation of platinum with phosphorus-rich chromatin regions was observed, which is consistent with its binding affinity to DNA as the generally accepted crucial target of the drug. Application of ^{15}N-labeled cisplatin and subsequent measurement of the nitrogen isotopic composition and determination of the relative intensities of platinum and nitrogen associated secondary ion signals in different cellular compartments with NanoSIMS suggested partial dissociation of Pt–N bonds during the accumulation process, in particular within nucleoli at elevated cisplatin concentrations. This finding raises the question as to whether the observed intracellular dissociation of the drug has implications for the mechanism of action of cisplatin. Within the cytoplasm, platinum mainly accumulated in acidic organelles, as demonstrated by a direct combination of specific fluorescent staining, confocal laser scanning microscopy and NanoSIMS. Different processing of platinum drugs in acidic organelles might be relevant for their detoxification, as well as for their mode of action.

Introduction

Platinum drugs play an important role in anticancer chemotherapy, predominantly due to their high curative potential in certain malignancies. In the past decades, the development of novel antitumour metal compounds was based mainly on experience gained from investigation of platinum drugs.[1–3] Whilst the limited spectrum of platinum-responsive tumours, severe side-effects and resistance induction prompted the development of metal-based complexes with central atoms other than platinum, cisplatin (*cis*-$PtCl_2[NH_3]_2$, CDDP) is still the most widely applied metal-based anticancer agent, showing pronounced efficacy most notably in testicular, head-and-neck and ovarian cancer treatment.

CDDP is generally believed to exert its antitumour effects by DNA adduct formation, thereby disturbing DNA functionality.[4,5] However, only 1–10% of cisplatin accumulated in the cell is supposed to reach the nuclear DNA.[2,6] In this context, it is interesting to note that cisplatin can also induce apoptosis in the absence of nuclear DNA, through caspase activation in HCT-116 colon cancer cytoplasts and in enucleated mouse kidney proximal tubule cells.[6,7]

Notwithstanding its high curative potential, cisplatin treatment is associated with undesirable side effects. Major adverse effects are neurotoxicity, ototoxicity and nephrotoxicity, which were shown to be highly dependent on the action of reactive oxygen and nitrogen species.[8,9] Cisplatin interactions with mitochondrial and lysosomal functions were reported to be involved in peripheral neuropathy.[10] Although the interaction of cisplatin with tumour cells has been investigated in great detail, the mechanisms of its selectivity, resistance, and toxicity are not completely understood.

Generally, visualisation of the subcellular distribution of pharmaceutical agents can yield valuable information on the

[a]*Institute of Inorganic Chemistry, University of Vienna, Waehringer Str. 42, A-1090, Vienna, Austria. E-mail: bernhard.keppler@univie.ac.at*

[b]*Research Platform "Translational Cancer Therapy Research", University of Vienna, Waehringer Str. 42, A-1090 Vienna, Austria*

[c]*Large-Instrument Facility for Advanced Isotope Research, University of Vienna, Althanstrasse 14, A-1090 Vienna, Austria*

[d]*Department of Microbiology and Ecosystem Research, Division of Microbial Ecology, University of Vienna, Althanstrasse 14, A-1090 Vienna, Austria*

[e]*Core Facility of Cell Imaging and Ultrastructure Research, University of Vienna, Althanstrasse 14, A-1090 Vienna, Austria*

† Electronic supplementary information (ESI) available: NanoSIMS data, cell viability experiments, materials and methods. See DOI: 10.1039/c3sc53426j

location of the sites relevant for biological activity, as well as for detoxification. The subcellular distribution of platinum-based drugs can be studied by carrying out cellular fractionation followed by spectrometric analysis, such as atomic absorption spectroscopy (AAS) or inductively coupled plasma mass spectrometry (ICPMS), which allows an estimation of platinum accumulation in certain compartments of the cell.[11–13] Due to the risk of cross-contamination of fractions and partial loss of the analyte during sample preparation, there is still an urgent need for methods which are applicable to intact single cells. Attempts have been made to study the subcellular distribution of fluorescently-labeled platinum complexes by fluorescence microscopy.[14–17] However, fluorescent moieties may affect the (sub)cellular transport, or may be cleaved off by the metabolic activity of the cell. Amongst the element specific imaging techniques, synchrotron based X-ray fluorescence microscopy shows great potential for highly sensitive, quantitative and oxidation state specific mapping of elements with $Z > 11$.[18,19] X-ray beam focusing optics and high-sensitivity fluorescence detection systems are being continuously improved.[20–22] However, studies addressing the subcellular distribution of platinum-based anticancer drugs using X-ray fluorescence microscopy remain limited thus far to the resolution of the cytoplasmic and nuclear compartments.[23,24] Transmission electron microscopy (TEM) with energy dispersive X-ray spectroscopy (EDS) or energy filtering (EFTEM) has been successfully used for gold subcellular imaging,[25] and offers unparalleled lateral resolution, but limited sensitivity in case of platinum.

NanoSIMS is an advanced type of dynamic secondary ion mass spectrometer, which was designed particularly for trace element and isotope analysis with high spatial resolution (down to 50 nm probe size).[26,27] The applicability of NanoSIMS for subcellular mapping of platinum deposited in eukaryotic cells was demonstrated by Usami *et al.*[28] and Eybe *et al.*[29] NanoSIMS is frequently combined with stable isotope probing (*e.g.* $^{13}C/^{12}C$ and/or $^{15}N/^{14}N$), which enables monitoring of the cellular uptake and distribution of isotopically labeled compounds.[30–35] Some of the advantages of NanoSIMS over different visualisation techniques for metal-based complexes have already been outlined by other authors.[25,36] In the case of platinum-based complexes, the capabilities of multi-elemental, isotope selective analysis allow information to be obtained about both the distribution of the metal and that of the isotopically labeled ligands, as recently shown for the cellular uptake of a polynuclear, ^{15}N-labeled Pt compound by Wedlock *et al.*[37] Moreover, NanoSIMS can be successfully combined with other techniques, such as electron microscopy, Raman microspectroscopy, confocal laser scanning microscopy and fluorescence *in situ* hybridization.[25,38–40]

In this paper, we report the combined application of NanoSIMS (for mapping the subcellular cisplatin distribution) and confocal laser-scanning microscopy (to identify the subcellular structures involved) in human cancer cells. The simultaneous detection of nitrogen-, phosphorus- and sulfur-containing secondary ions was utilized for correlation analysis of the distribution patterns of these biologically relevant elements with those of platinum. The excellent sensitivity of NanoSIMS for the detection of both platinum and ^{15}N isotopically labeled ligands is demonstrated, and we present a data evaluation procedure that enables monitoring of the ligand to central atom stoichiometry in different subcellular compartments.

Results and discussion

Semi-thin (300 nm) sections of resin-embedded human colon cancer cells (cell line SW480), obtained from adherent cell monolayers treated with ^{15}N-labeled cisplatin for 24 h, were examined using a NanoSIMS NS50L instrument from Cameca (Paris, France). The use of this rather (but not completely) cisplatin-insensitive cell line allowed for the application of cisplatin over a wide concentration range. Cell viability was confirmed with three different methods: an MTT-based cytotoxicity assay, as well as Annexin V-FITC/PI and JC-1 assays for apoptosis induction (see ESI† for details).

One of the major challenges associated with (Nano)SIMS is sample preparation. SIMS is destructive, which means that only post-mortem analysis can be accomplished. In addition, the measurement process takes place under ultra high vacuum (UHV), which leads to the collapse of cells during sample introduction. Resin embedding is efficient for the preservation of the cellular structure; however, fixation, treatment with an ethanol series, and the infiltration of acetone–resin mixtures can lead to the diffusible fraction of the drug being washed out. Consequently, it has to be assumed that the data acquired on the resin sections mainly refer to tightly bound cisplatin.

Fig. 1 displays elemental distribution maps obtained from a semi-thin resin section of cells treated with 25 μM CDDP. The cellular compartments were manually defined based on characteristic features which were identifiable in the secondary ion images, as follows: (1) cytoplasm, which includes all of the cell area outside the nucleus; (2) nucleus, demarcated by the chromatin rim (likely representing heterochromatin), but excluding the nucleolus (to avoid biasing); (3) nucleolus, a round shaped C-, N-, P- and S-rich structure inside the nucleus; and (4) chromatin, indicated by dense, phosphorus-rich (but not sulfur-rich), unevenly distributed regions along the inner membrane of the nucleus (see also Fig. S1† for an untreated control, and Fig. S2† for a sample of cells treated with 150 μM cisplatin). The $^{194}Pt^-$ signal intensity distribution revealed an accumulation of platinum in both the nucleic and cytoplasmic compartments. In the cytoplasm, platinum was accumulated in small aggregates, most of which were also rich in sulfur. In the nucleus, most of the platinum was associated with the nucleolus, which is rich in sulfur as well as phosphorus (Fig. 1 and S2†). The Pt distribution pattern was found to be similar for all samples exposed to ≥10 μM CDDP (for comparison, clinical peak plasma concentrations of cisplatin range between 8 and 64 μM, depending on the administration regimen);[41–43] at lower concentrations, the signals were more diffusely distributed (Fig. 2). However, even at CDDP concentrations as low as 2.5 μM, region of interest (ROI) specific analysis of the $^{12}C_2^-$ normalized $^{194}Pt^-$ signal intensities showed a significant enhancement of the average platinum signal intensity within treated cells, relative to the untreated control (Fig. S3;† Student's *t*-test, $p < 0.002$). ICPMS

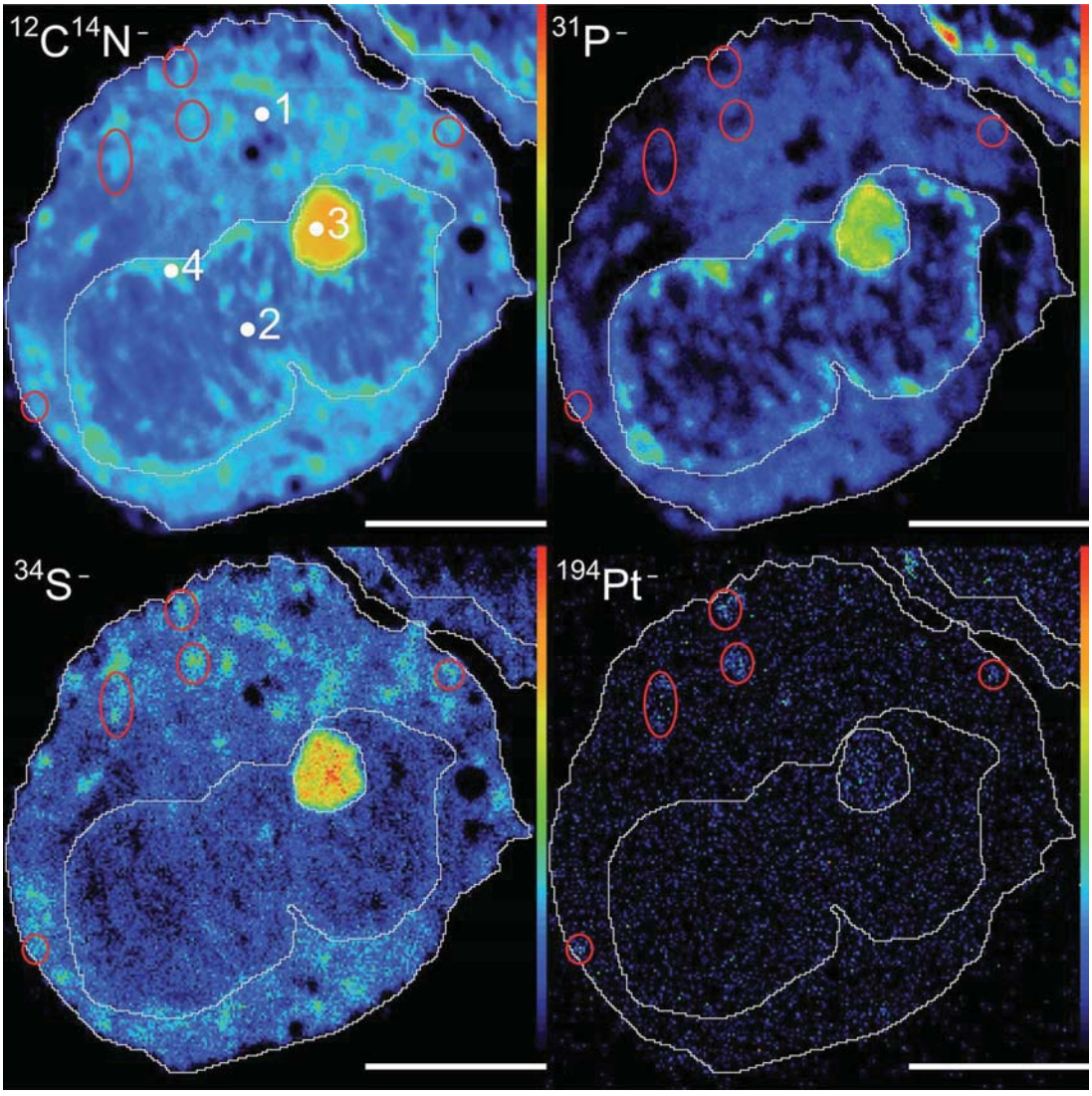

Fig. 1 Exemplary $^{12}C^{14}N^-$, $^{34}S^-$, $^{31}P^-$ and $^{194}Pt^-$ secondary ion signal intensity distribution maps acquired from semi-thin sections of SW480 cells treated with 25 μM of cisplatin. Regions of interest (ROIs) were manually defined within: (1) the cytoplasm; (2) the nucleus; (3) the nucleolus; and (4) the chromatin. According to the $^{194}Pt^-$ and $^{34}S^-$ signals, the drug is accumulated in small cytoplasmic, sulfur-rich aggregates (encircled in red), as well as in the nucleoli. Intensities are displayed on a rainbow false-color scale, ranging from dark blue to red for low to high intensities, respectively. The scale bars are 5 μm.

analyses of replicate samples revealed that the average platinum content in cells treated with 2.5 μM CDDP was <5 fg per cell (unpublished data). Taking into account that a 300 nm thick section of a cell which is 10 μm in diameter contains less than 5% of the total cell volume, the ICPMS results provide evidence of the impressive sensitivity of NanoSIMS for platinum detection in organic matrices. Among the subcellular compartments, the chromatin structures show a tendency for enhanced Pt accumulation compared to the average nucleus (without the nucleolus) and cytoplasm values, which becomes significant at exposure concentrations ≥100 μM (Fig. S3,† Student's *t*-test, $p < 0.022$). Moreover, the local accumulation of platinum within the nucleoli increased with increasing exposure concentrations, whereas the relative distribution in other compartments showed no significant changes, as evidenced by comparison of the $^{12}C_2^-$ normalized local $^{194}Pt^-$ signal intensities (Fig. S4†).

DNA is supposedly the crucial target for cisplatin, and this is consistent with our results, since phosphorus-rich regions (chromatin) yielded comparable or even elevated Pt signals with respect to other cellular compartments (*e.g.* the cytoplasm and nucleus without the nucleolus) (Fig. 1 and S2†). However, basic coordination chemistry (in particular, the principle of hard and soft acids and bases) would also predict Pt binding to S-donor ligands such as thiols.[44,45] It has been consistently postulated

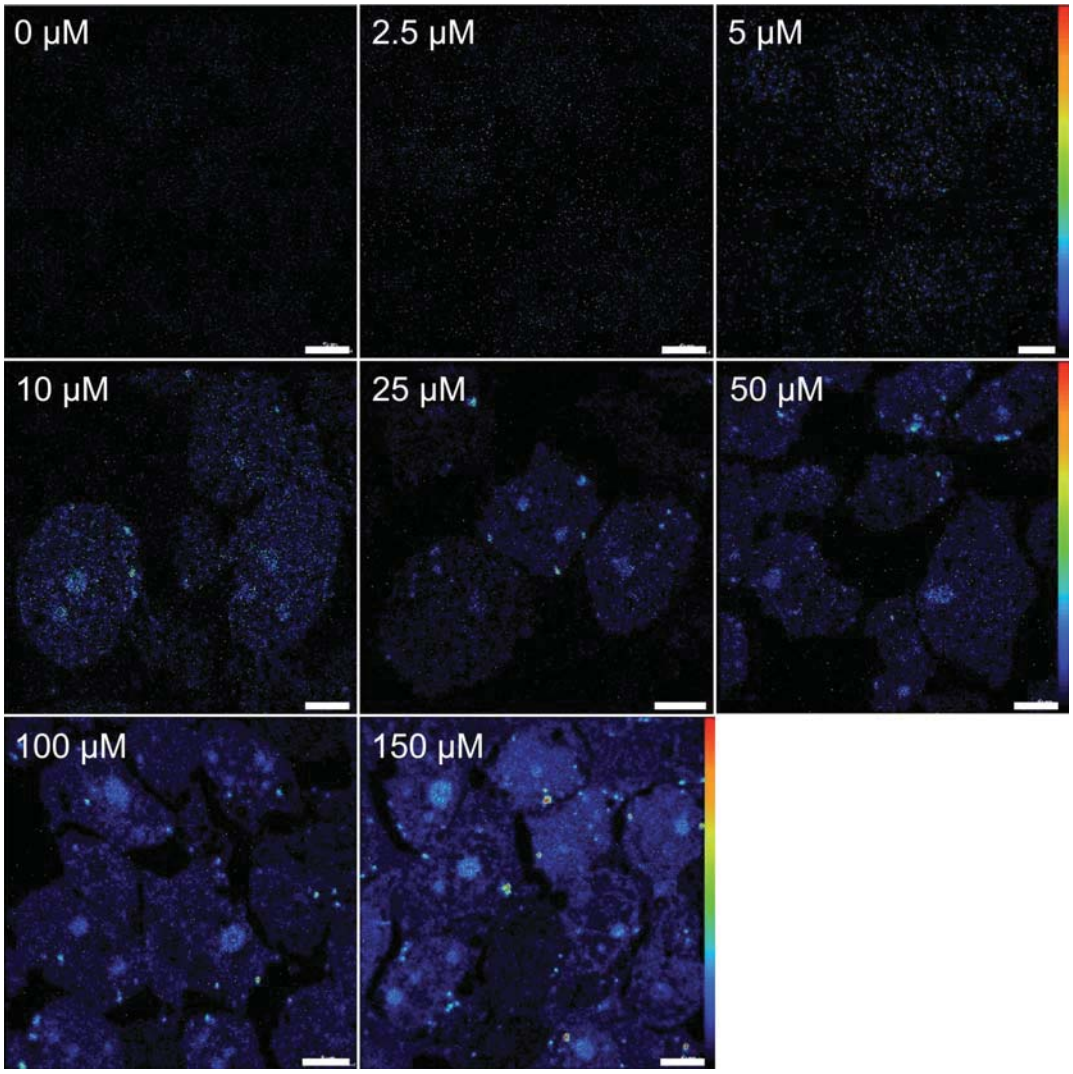

Fig. 2 NanoSIMS $^{194}Pt^-$ signal intensity distribution images obtained from semi-thin resin sections of SW480 cells treated with CDDP with various concentrations for 24 h. Signal intensities are displayed on a rainbow false-color scale, ranging from 0 counts per pixel (black) to max. 4 and 10 counts per pixel (red) for images from cells exposed to 0 to 10 μM and 25 to 150 μM CDDP, respectively. The primary ion beam was rastered over areas between 32 × 32 to 40 × 40 μm^2 at a resolution of 512 × 512 pixels for a total dwell time of 200 to 300 ms per pixel. Scale bars = 5 μm.

that intracellular sulfur-containing molecules such as glutathione, metallothioneines and thioredoxins compete with DNA for metallodrug binding.[46–48] This is also in accordance with our findings, as high amounts of Pt were co-localised with S-rich structures (nucleoli, cytoplasmic aggregates) in the cells (Fig. 1 and S2†). The anticancer efficacy of platinum-based agents depends on the balance between the target efficiency (DNA binding) and biotransformation by sulfur nucleophiles. Furthermore, methionines have been suspected to be favorable binding sites for cisplatin on proteins,[49] and, in particular, methionine-rich motifs (Met-motifs) of copper transporter 1 (Ctr1) were shown to effectively bind cisplatin,[50] with subsequent ammine ligand dissociation.[51] Metallothioneines – cytosolic thiol-rich scavenging proteins – were also shown to bind to cisplatin, hence provoking the loss of amine ligands, and playing an important role in the sequestration and detoxification of heavy metals.[46,52] Binding to S-donors results in the trans-labilization of ligands, facilitating the release of the (otherwise inert) ammine ligands.[45,53]

This effect might explain our finding that Pt-enriched nucleoli deviated from the other cellular compartments in their ligand to central atom stoichiometry of the accumulated CDDP, as displayed by the different slopes in the relative Pt to N uptake curves shown in Fig. 3. It has to be emphasized that the plotting of the ^{15}N isotope enrichment *versus* the platinum signal intensity, which is more intuitively appealing, fails to

indicate the compound stoichiometry, since the dependency of the isotopic enrichment level on the local nitrogen content is omitted. (In such a plot, nitrogen-rich compartments exhibit lower isotopic enrichment than nitrogen-poor areas, even if equal amounts of ^{15}N-labeled CDDP are accumulated, which may be misinterpreted as stoichiometric variations.) Accordingly, the secondary ion signals associated with the ligand(s) and the central atom need to be related to the total nitrogen content of the considered region. In fact, the fraction of nitrogen atoms which originate from the CDDP accumulation (N_{CDDP}/N_{tot}) can be obtained from the abundance of the isotopic label ($^{15}N/(^{14}N + {}^{15}N)$) contained in the administered compound ($a_{^{15}N,CDDP}$), the analysed sample ($a_{^{15}N,tot}$) and the untreated control ($a_{^{15}N,ctr}$) using an expression which reads:

$$\frac{N_{CDDP}}{N_{tot}} = \frac{a_{^{15}N,tot} - a_{^{15}N,ctr}}{a_{^{15}N,CDDP} - a_{^{15}N,ctr}} \quad (1)$$

It should be noted that the relationship is quantitative and does not require any further assumptions. Fig. 3 illustrates that the maximum amount of nitrogen originating from the ammine ligands was <0.4 per mil of the total nitrogen contained in the analysed cellular compartments, which, from an analytical point of view, corroborates the high performance of NanoSIMS in spatially resolved nitrogen isotope analysis. In contrast to the isotopically labeled ligands, the relative amount of accumulated platinum cannot be directly determined from the acquired data, since SIMS is only semi-quantitative for elemental analysis. What can be defined, however, is a quantity that is proportional to the concentration ratio (Pt/N_{tot}). Utilizing the $^{12}C_2^-$ secondary ion signal as a reference, this quantity can be formulated as a function of the measured $^{194}Pt^-$ and $^{12}CN^-$ signal intensities as follows:

$$\frac{Pt_{CDDP}}{N_{tot}} \propto \frac{^{194}Pt^-}{^{12}CN^-} = \left(\frac{^{194}Pt^-}{^{12}C_2^-}\right)_{Pt} \times \left(\frac{^{12}CN^-}{^{12}C_2^-}\right)_{avg}^{-1} \quad (2)$$

where the subscripts of the bracketed terms indicate values that were obtained from platinum measurements ('Pt') and averages from the platinum and ^{15}N measurements ('avg'), respectively. (Owing to instrumental constraints, the platinum distribution and nitrogen isotope composition had to be determined in sequential measurements; for details see the section 'NanoSIMS analysis' in the ESI.†) When considered together, the slope of the graph obtained from plotting (N_{CDDP}/N_{tot}) *vs.* (Pt_{CDDP}/N_{tot}) is proportional to the relative amounts of the accumulated ligands and central atoms. Fig. 3 shows that the nitrogen accumulation in nucleoli is disproportionally lower than that of Pt with increasing cisplatin concentrations, suggesting the cleavage of (ammine) ligands from the central atom. Moreover, the ROI analysis indicated an increase in the local sulfur content in the compartments (in particular in the nucleoli) of the cells treated with 100 μM and 150 μM CDDP (Fig. S5†), supporting the idea that N–Pt bond integrity might be affected by S-donors such as thiol-bearing molecules. In fact, we observed the colocalisation of Pt with S-rich structures; however, not all S-rich organelles are

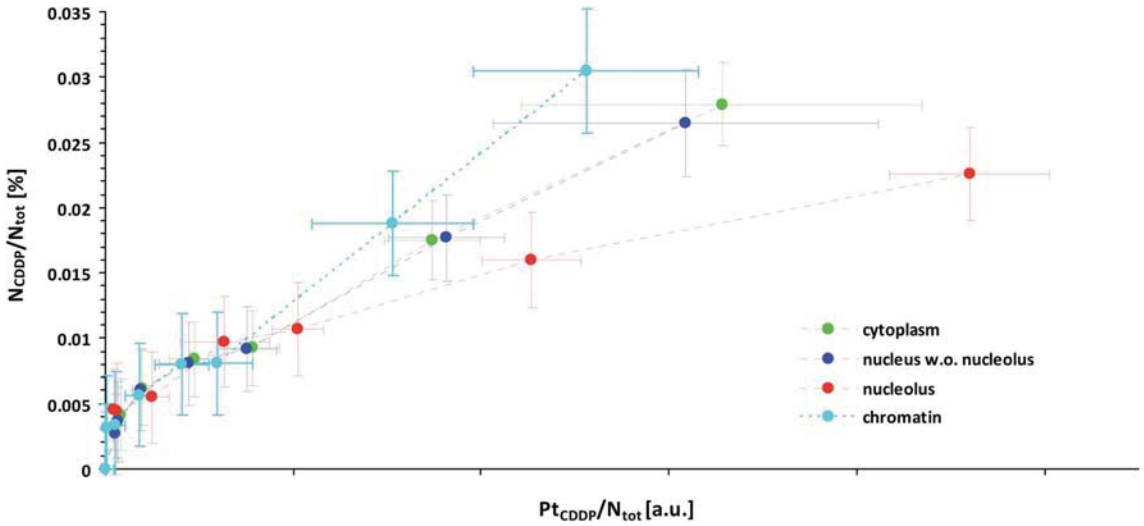

Fig. 3 Local subcellular ligand *vs.* central atom accumulation in SW480 cells upon 24 h exposure to ^{15}N-labeled cisplatin with eight different concentrations ranging from 0 μM (min. values, negative control) to 150 μM (max. values), as inferred from NanoSIMS Pt/N elemental mapping and determination of the local $^{15}N/^{14}N$ isotopic composition. Note that the slope of the curves is proportional to the N/Pt stoichiometry of the accumulated cisplatin. In particular, any flattening of the curves is indicative of cleavage and loss of ammine ligands. Symbols in green, blue, red and cyan refer to values obtained from ROIs defined within the cytoplasm, nucleus (excl. nucleolus), nucleoli and chromatin of individual cells, respectively. The error bars refer to one standard deviation calculated from the compartment specific ROI values. The mean counting error, which is an inverse measure of the analytical precision, was smaller than the dispersion of the individual ROI values (see also Fig. S7 and S8†). Further information about the calculation of the displayed quantities is provided in the text and in more detail in the ESI.†

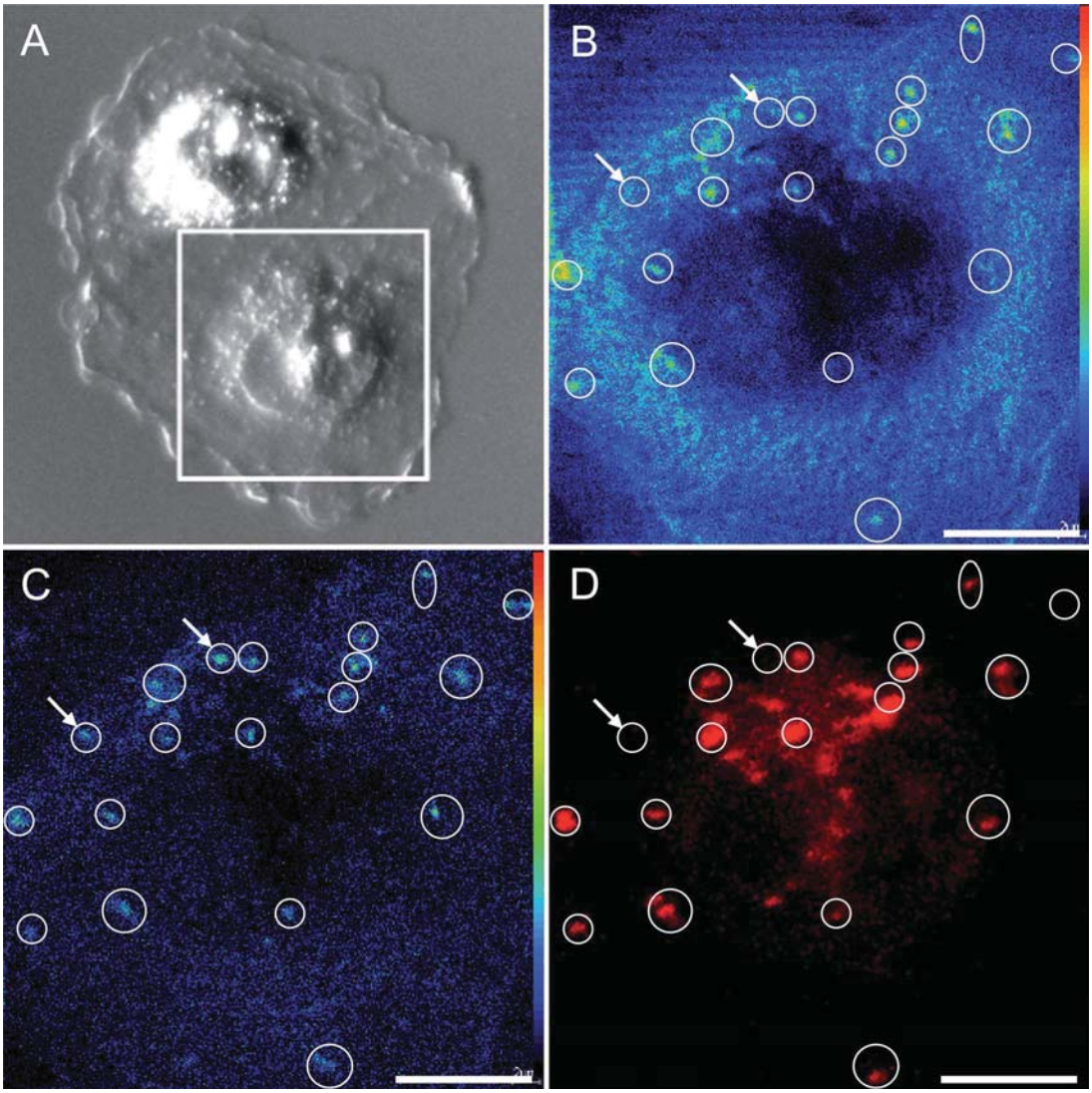

Fig. 4 NanoSIMS secondary ion signal intensity distribution maps and confocal microscopy images of an adherent SW480 cell after 24 h exposure to 25 μM cisplatin, revealing cisplatin colocalisation with acidic organelles in the cell. The screened region is marked with a frame in the differential interference contrast image of the cell (A). The confocal microscopy image of the (fluorine-containing) LysoTracker Red (D) demonstrates a correlation with the signal intensity patterns of both $^{19}F^-$ originating from LysoTracker Red (B) and $^{194}Pt^-$ originating from cisplatin (C) detected by NanoSIMS in the same cell. The arrows indicate a few regions of platinum accumulation without fluorescence and $^{19}F^-$ signal intensity enhancement (2 out of 20 labeled areas). Secondary ion signal intensities are displayed on a rainbow false-color scale ranging from dark blue to red for low to high intensities, respectively. The small misalignment between the fluorescence image and the secondary ion maps may originate from lens aberrations and/or cell shrinkage due to sample preparation. Scale bars = 5 μm.

subject to cisplatin accumulation (Fig. 1 and S2†). These data suggest platinum accumulation in specific organelles, rather than being sulfur-directed or randomly distributed.

Cisplatin may enter the cytoplasm in its native state *via* active transport (including endocytosis) and/or passive diffusion. The difference in chloride concentration between the cell culture medium, which is comparable to extracellular liquids (>100 mM), and the cytosol (<20 mM) is favourable for cisplatin aquation inside the cell. In aqueous solutions at neutral pH, the chlorido ligands of cisplatin are replaced stepwise by water. The bound water molecules are very labile, so cisplatin is capable of reacting preferably with the S- and N-donor ligands in the cell. Taking into account: (a) the affinity of cisplatin for thiol-containing molecules, (b) the possible affinity for acidic pH (cisplatin accumulation in acidic organelles was previously reported[24,54]), and (c) the morphological features of the organelles (small, vesicle-like structures), we hypothesised that cisplatin may co-localise in the cytoplasm with lysosomes.

The sensitivity and spatial resolution achieved with NanoSIMS multi-elemental mapping is high enough to distinguish platinum aggregation in the cytoplasm and the nucleolus without additional labeling. However, to reveal the nature of the cytoplasmic aggregates, we had to additionally apply confocal laser-scanning microscopy, which supported the co-localisation of the cytoplasmic platinum aggregates with acidic organelles (*e.g.* lysosomes) specifically marked with LysoTracker Red (Fig. 4). The hotspots in the $^{194}Pt^-$ intensity distribution image refer to the loci of Pt accumulation within the cytoplasm. The $^{19}F^-$ secondary ion signal intensity distribution pattern detected by NanoSIMS, together with the confocal microscopy image of the LysoTracker Red (LTR), demonstrate the correlated distribution of the fluorine-containing dye in acidic cytoplasmic organelles.

The organelles of the endocytotic and excretory pathways, *i.e.* the early and late endosomes, lysosomes and exosomes (secretory vesicles), are distributed throughout the cytoplasm; they undergo continuous maturation, transformation, fusion, and fission.[55,56] The acidification of lysosomal and late endosomal compartments was reported to reach pH 4.5 and pH 4.8, respectively,[57] and that of secretory vesicles reach approximately pH 5.5.[58] Therefore, several organelles originating from a *trans*-Golgi network (TGN) are possibly involved in cisplatin accumulation. Lysosomes were shown by other researchers to have a great impact on subcellular sequestration and the detoxification of heavy metals.[59,60] Melanosomes, with a lysosomal origin and acidic pH, were reported to trap Alexa Fluor conjugated CDDP (AF-CP) in cisplatin-insensitive MNT-1 melanotic melanoma cells, which was associated with low nuclear accumulation of the drug, whilst in the cisplatin-sensitive cell line KB-3, AF-CP was shown to accumulate in both the nucleus and cytoplasm.[24] A different line of research showed that cisplatin resistance in ovarian carcinoma cells is linked to elevated acidity of lysosomes.[17] A platinum-based drug bearing a fluorescent anthraquinone ligand was shown to reach the nucleus quickly (within the first 20 min to 2 h), followed by lysosomal sequestration after 24 h (whereby dissociation and different cellular trafficking of the ligands and platinum cannot be excluded). A defect in the endosomal/lysosomal acidification mechanism was shown to be a plausible contribution to cisplatin resistance in human epidermoid carcinoma cell lines.[61] Thus, the lysosomal trafficking of cisplatin may alter the sensitivity/resistance of the cells (*e.g.*, depending on lysosomal acidification capacity).

Cytoplasmic platinum aggregation with no nuclear localisation has been observed by other authors using SIMS to study the uptake and distribution of non-cytotoxic dichloroterpyridine platinum (PtTC) in Chinese Hamster Ovary (CHO) cells after treatment with 350 μM of the compound (no ligand distribution was investigated in this study).[28] Platinum signals correlated well with sulfur signals, which is in good agreement with our data. This supports the idea that S-rich molecules play an important role in the metabolisation of different platinum-based compounds. In contrast to our data, the study by Usami *et al.* showed for cisplatin, which was used as a control (30 μM, 5 h exposure), enhanced nuclear localisation with no pronounced cytoplasmic aggregation. Quite recently, the subcellular distribution of a ^{15}N-labeled, highly-charged polynuclear platinum compound (20 μM, 1–2 h exposure) was investigated using NanoSIMS in human MCF7 breast adenocarcinoma cells.[37] Both platinum aggregation in cytoplasmic vesicle-like structures and nucleolar enrichment were reported. However, no Pt signal was detected for cisplatin-treated samples (20 μM, 1–2 h exposure). The reason for the apparent discrepancy between these studies and our observations is most likely the different exposure time (1–2 h *vs.* 24 h exposure). Thus, the main difference between the behaviour of the polynuclear complex and that of cisplatin seems to lie in their different cellular pharmacokinetics, rather than fundamentally different subcellular distribution patterns.

Conclusions

NanoSIMS proved to be a highly sensitive technique for subcellular imaging of Pt in cell culture samples exposed to cisplatin. Application of the drug with ^{15}N isotopically labeled ammine ligands in a series of concentrations, and appropriate NanoSIMS data analysis, enabled monitoring of the N/Pt stoichiometry of the compound, which suggested partial dissociation of the Pt–N bonds, at least in nucleoli at elevated treatment concentrations. The colocalisation of platinum primarily with sulfur, but also with phosphorus-rich structures, is consistent with the known high affinity of platinum for sulfur donors, and binding to DNA as the generally accepted critical target. The indicated cleavage of ligands from platinum colocalising with S-rich nucleoli is consistent with the important role of thiol-bearing molecules (affecting Pt–N bond stability) in platinum processing. The partial dissociation of Pt–N bonds raises the question of possible implications for the mechanism of action with regard to nuclear targets. The accumulation of platinum within acidic organelles, as visualised by the combined application of NanoSIMS elemental mapping and fluorescence microscopy, might be relevant for the detoxification and/or mode of action of platinum drugs. In the case of the investigated SW480 cells, the cisplatin aggregation in S-rich acidic cytoplasmic organelles may contribute to their intrinsic resistance mechanisms. Additional experiments addressing possible parallels in Cu and Pt accumulation (due to the role of copper transporters in Pt uptake), and the use of ^{36}S-labeled thiols to study their involvement in platinum processing, should be considered.

Multi-elemental imaging by means of NanoSIMS might also reveal interactions/affinities of platinum with elements other than N, P and S. The methodological approach described here should also enable the investigation of antitumour compounds based on other metals (*e.g.* Ru, Os, Ga) and/or containing different isotopic labels (*e.g.* ^2H, ^{18}O, ^{13}C, ^{36}S), which renders NanoSIMS a powerful and widely applicable tool for subcellular drug imaging. Specifically, we have demonstrated the ability to obtain quantitative information about the distribution of the metal *vs.* ligand, shedding light on metal–ligand bond integrity. The combination of SIMS with complementary analytical and imaging techniques can aid in identifying and characterising subcellular structures highlighted in elemental distribution

patterns, as exemplified in our study by applying fluorescence confocal laser scanning microscopy with intracellular markers prior to NanoSIMS measurement of the same region of interest.

Acknowledgements

We gratefully acknowledge Mag. Daniela Gruber (Core Facility of Cell Imaging and Ultrastructure Research, University of Vienna, Austria) for instructions and assistance with sample preparation. We acknowledge Brigitte Marian (Institute of Cancer Research, Department of Medicine I, Medical University of Vienna, Austria) for providing SW480 cells. The authors are indebted to the Austrian Science Fund (FWF; project no. L567). The University of Vienna and its Faculties of Life Sciences and Chemistry are acknowledged for financial support of the NanoSIMS facility. M.W. was supported by ERC Advanced Grant 294343.

Notes and references

1 R. S. Go and A. A. Adjei, *J. Clin. Oncol.*, 1999, **17**, 409–422.
2 E. Raymond, S. Faivre, S. Chaney, J. Woynarowski and E. Cvitkovic, *Mol. Cancer Ther.*, 2002, **1**, 227–235.
3 T. Boulikas and M. Vougiouka, *Oncol. Rep.*, 2004, **11**, 559–595.
4 D. Wang and S. J. Lippard, *Nat. Rev. Drug Discovery*, 2005, **4**, 307–320.
5 A. M. Fichtinger-Schepman, J. L. van der Veer, J. H. den Hartog, P. H. Lohman and J. Reedijk, *Biochemistry*, 1985, **24**, 707–713.
6 F. Yu, J. Megyesi and P. M. Price, *Am. J. Physiol.: Renal, Fluid Electrolyte Physiol.*, 2008, **295**, F44–F52.
7 A. Mandic, J. Hansson, S. Linder and M. C. Shoshan, *J. Biol. Chem.*, 2003, **278**, 9100–9106.
8 J. Pourahmad, M. J. Hosseini, M. R. Eskandari, S. M. Shekarabi and B. Daraei, *Xenobiotica*, 2010, **40**, 763–771.
9 L. P. Rybak, C. A. Whitworth, D. Mukherjea and V. Ramkumar, *Proc. Natl. Acad. Sci. U. S. A.*, 2007, **226**, 157–167.
10 S. Quasthoff and H. P. Hartung, *J. Neurol.*, 2002, **249**, 9–17.
11 R. P. Sharma and I. R. Edwards, *Biochem. Pharmacol.*, 1983, **32**, 2665–2669.
12 M. Groessl, O. Zava and P. J. Dyson, *Metallomics*, 2011, **3**, 591–599.
13 D. Esteban-Fernandez, J. M. Verdaguer, R. Ramirez-Camacho, M. A. Palacios and M. M. Gomez-Gomez, *J. Anal. Toxicol.*, 2008, **32**, 140–146.
14 J. J. Wilson and S. J. Lippard, *Inorg. Chim. Acta*, 2012, **389**, 77–84.
15 J. Gao, Y. G. Liu and R. A. Zingaro, *Chem. Res. Toxicol.*, 2009, **22**, 1705–1712.
16 S. Wu, C. Zhu, C. Zhang, Z. Yu, W. He, Y. He, Y. Li, J. Wang and Z. Guo, *Inorg. Chem.*, 2011, **50**, 11847–11849.
17 G. V. Kalayda, B. A. Jansen, P. Wielaard, H. J. Tanke and J. Reedijk, *J. Biol. Inorg. Chem.*, 2005, **10**, 305–315.
18 S. Vogt and M. Ralle, *Anal. Bioanal. Chem.*, 2013, **405**, 1809–1820.
19 Z. Qin, J. A. Caruso, B. Lai, A. Matusch and J. S. Becker, *Metallomics*, 2011, **3**, 28–37.
20 K. L. Moore, E. Lombi, F. J. Zhao and C. R. Grovenor, *Anal. Bioanal. Chem.*, 2012, **402**, 3263–3273.
21 A. Carmona, P. Cloetens, G. Devès, S. Bohic and R. Ortega, *J. Anal. At. Spectrom.*, 2008, **23**, 1083.
22 S. Matsuyama, M. Shimura, H. Mimura, M. Fujii, H. Yumoto, Y. Sano, M. Yabashi, Y. Nishino, K. Tamasaku, T. Ishikawa and K. Yamauchi, *X-Ray Spectrom.*, 2009, **38**, 89–94.
23 M. D. Hall, C. T. Dillon, M. Zhang, P. Beale, Z. Cai, B. Lai, A. P. Stampfl and T. W. Hambley, *J. Biol. Inorg. Chem.*, 2003, **8**, 726–732.
24 K. G. Chen, J. C. Valencia, B. Lai, G. Zhang, J. K. Paterson, F. Rouzaud, W. Berens, S. M. Wincovitch, S. H. Garfield, R. D. Leapman, V. J. Hearing and M. M. Gottesman, *Proc. Natl. Acad. Sci. U. S. A.*, 2006, **103**, 9903–9907.
25 L. E. Wedlock, M. R. Kilburn, J. B. Cliff, L. Filgueira, M. Saunders and S. J. Berners-Price, *Metallomics*, 2011, **3**, 917–925.
26 G. Slodzian, B. Daigne, F. Girard, F. Boust and F. Hillion, *Biol. Cell*, 1992, **74**, 43–50.
27 C. Lechene, F. Hillion, G. McMahon, D. Benson, A. M. Kleinfeld, J. P. Kampf, D. Distel, Y. Luyten, J. Bonventre, D. Hentschel, K. M. Park, S. Ito, M. Schwartz, G. Benichou and G. Slodzian, *J. Biol.*, 2006, **5**, 20.
28 N. Usami, Y. Furusawa, K. Kobayashi, S. Lacombe, A. Reynaud-Angelin, E. Sage, T. D. Wu, A. Croisy, J. L. Guerquin-Kern and C. Le Sech, *Int. J. Radiat. Biol.*, 2008, **84**, 603–611.
29 T. Eybe, J. N. Audinot, T. Udelhoven, E. Lentzen, B. El Adib, J. Ziebel, L. Hoffmann and T. Bohn, *Chemosphere*, 2013, **90**, 1829–1838.
30 P. L. Clode, R. A. Stern and A. T. Marshall, *Microsc. Res. Tech.*, 2007, **70**, 220–229.
31 P. Hoppe, S. Cohen and A. Meibom, *Geostand. Geoanal. Res.*, 2013, **37**, 111–154.
32 R. Peteranderl and C. Lechene, *J. Am. Soc. Mass Spectrom.*, 2004, **15**, 478–485.
33 M. Tourna, M. Stieglmeier, A. Spang, M. Konneke, A. Schintlmeister, T. Urich, M. Engel, M. Schloter, M. Wagner, A. Richter and C. Schleper, *Proc. Natl. Acad. Sci. U. S. A.*, 2011, **108**, 8420–8425.
34 R. A. Foster, M. M. Kuypers, T. Vagner, R. W. Paerl, N. Musat and J. P. Zehr, *ISME J.*, 2011, **5**, 1484–1493.
35 H. Ploug, B. Adam, N. Musat, T. Kalvelage, G. Lavik, D. Wolf-Gladrow and M. M. M. Kuypers, *ISME J.*, 2011, **5**, 1549–1558.
36 A. C. Komor and J. K. Barton, *Chem. Commun.*, 2013, **49**, 3617–3630.
37 L. E. Wedlock, M. R. Kilburn, R. Liu, J. A. Shaw, S. J. Berners-Price and N. P. Farrell, *Chem. Commun.*, 2013, **49**, 6944–6946.
38 M. Wagner, *Annu. Rev. Microbiol.*, 2009, **63**, 411–429.
39 K. H. Lau, M. Christlieb, M. Schroder, H. Sheldon, A. L. Harris and C. R. Grovenor, *J. Microsc.*, 2010, **240**, 21–31.
40 D. Berry, B. Stecher, A. Schintlmeister, J. Reichert, S. Brugiroux, B. Wild, W. Wanek, A. Richter, I. Rauch,

T. Decker, A. Loy and M. Wagner, *Proc. Natl. Acad. Sci. U. S. A.*, 2013, **110**, 4720–4725.
41 S. Urien and F. Lokiec, *Br. J. Clin. Pharmacol.*, 2004, **57**, 756–763.
42 J. B. Vermorken, W. J. F. Vandervijgh, I. Klein, A. A. M. Hart, H. E. Gall and H. M. Pinedo, *Cancer Treat. Rep.*, 1984, **68**, 505–513.
43 J. J. Gullo, C. L. Litterst, P. J. Maguire, B. I. Sikic, D. F. Hoth and P. V. Woolley, *Cancer Chemother. Pharmacol.*, 1980, **5**, 21–26.
44 J. Reedijk, *Chem. Rev.*, 1999, **99**, 2499–2510.
45 D. Gibson, *Dalton Trans.*, 2009, 10681–10689.
46 G. Chu, *J. Biol. Chem.*, 1994, **269**, 787–790.
47 Y. Kasherman, S. Sturup and D. Gibson, *J. Med. Chem.*, 2009, **52**, 4319–4328.
48 M. Knipp, *Curr. Med. Chem.*, 2009, **16**, 522–537.
49 D. Wang and Z. Guo, *Anti-Cancer Agents Med. Chem.*, 2007, **7**, 19–34.
50 S. E. Crider, R. J. Holbrook and K. J. Franz, *Metallomics*, 2010, **2**, 74–83.
51 F. Arnesano, M. Losacco and G. Natile, *Dalton Trans.*, 2013, 2701–2711.
52 D. J. Smith, M. Jaggi, W. Zhang, A. Galich, C. Du, S. P. Sterrett, L. M. Smith and K. C. Balaji, *Urology*, 2006, **67**, 1341–1347.
53 S. J. Berners-Price, L. Ronconi and P. J. Sadler, *Prog. Nucl. Magn. Reson. Spectrosc.*, 2006, **49**, 65–98.
54 R. Safaei, B. J. Larson, T. C. Cheng, M. A. Gibson, S. Otani, W. Naerdemann and S. B. Howell, *Mol. Cancer Ther.*, 2005, **4**, 1595–1604.
55 J. Huotari and A. Helenius, *EMBO J.*, 2011, **30**, 3481–3500.
56 J. A. Pickett and J. M. Edwardson, *Traffic*, 2006, **7**, 109–116.
57 F. R. Maxfield and D. J. Yamashiro, *Adv. Exp. Med. Biol.*, 1987, **225**, 189–198.
58 C. G. Blackmore, A. Varro, R. Dimaline, L. Bishop, D. V. Gallacher and G. J. Dockray, *J. Physiol.*, 2001, **531**, 605–617.
59 M. M. Desouky, *Aquat. Toxicol.*, 2006, **77**, 143–152.
60 S. G. George, T. L. Coombs and B. J. S. Pirie, *Biochim. Biophys. Acta*, 1982, **716**, 61–71.
61 S. S. Chauhan, X. J. Liang, A. W. Su, A. Pai-Panandiker, D. W. Shen, J. A. Hanover and M. M. Gottesman, *Br. J. Cancer*, 2003, **88**, 1327–1334.

NanoSIMS combined with fluorescence microscopy as a tool for subcellular imaging of isotopically labeled platinum-based anticancer drugs

Anton A. Legin,[ab] Arno Schintlmeister,[c] Michael A. Jakupec,[ab] Markus Galanski,[ab] Irene Lichtscheidl,[e] Michael Wagner[cd] and Bernhard K. Keppler[ab]

[a] *Institute of Inorganic Chemistry, University of Vienna, Waehringer Str. 42, A-1090, Vienna, Austria*
[b] *Research Platform "Translational Cancer Therapy Research", University of Vienna, Waehringer Str. 42, A-1090 Vienna, Austria*
[c] *Large-Instrument Facility for Advanced Isotope Research, University of Vienna, Althanstrasse 14, A-1090 Vienna, Austria*
[d] *Department of Microbiology and Ecosystem Research, Division of Microbial Ecology, University of Vienna, Althanstrasse 14, A-1090 Vienna, Austria*
[e] *Core Facility of Cell Imaging and Ultrastructure Research, University of Vienna, Althanstrasse 14, A-1090 Vienna, Austria*

Electronic Supplementary Information (ESI†)

Contents

Experimental data

NanoSIMS data

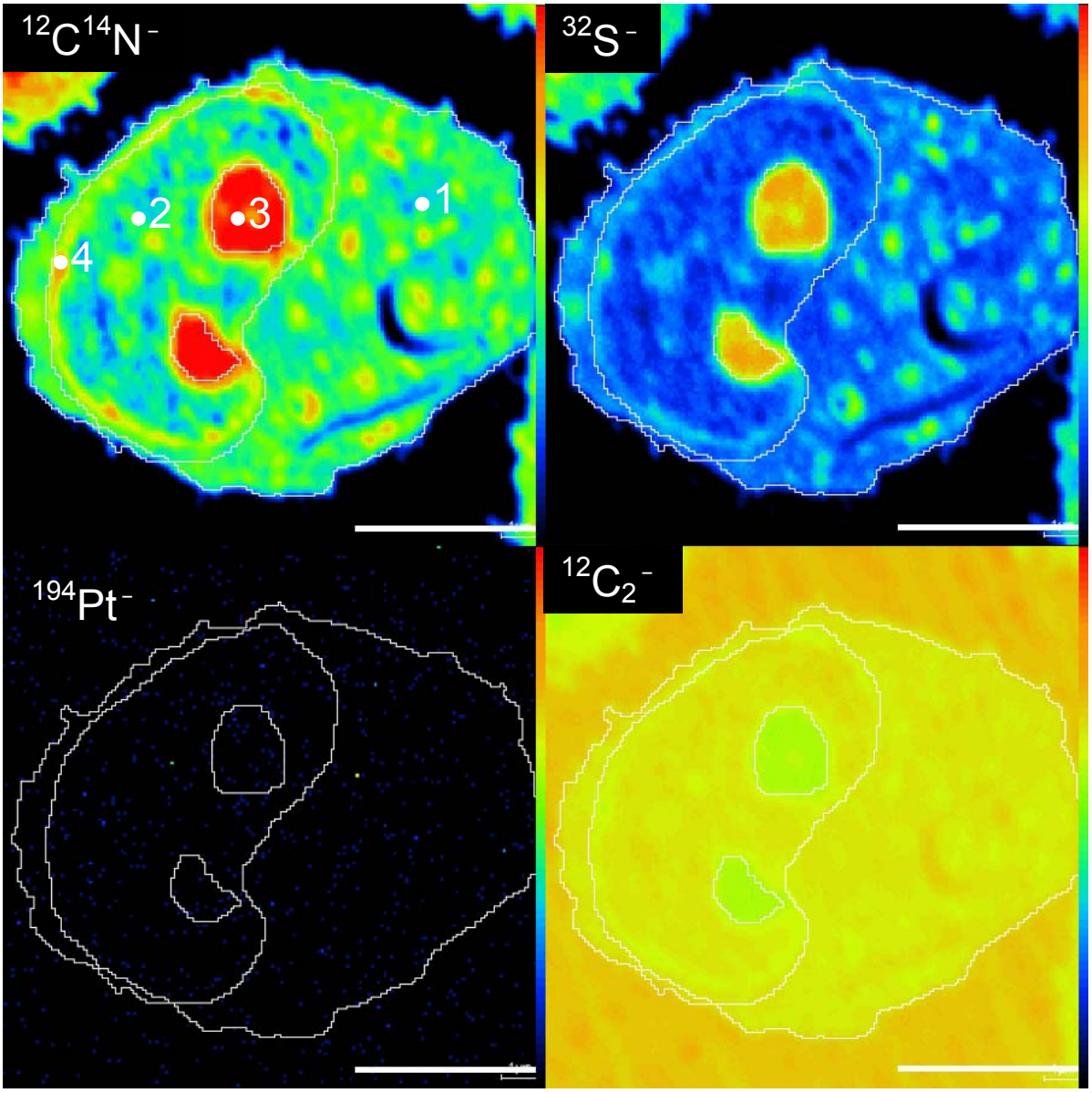

Fig. S1 NanoSIMS $^{32}S^-$, $^{194}Pt^-$, $^{12}C_2^-$ and $^{12}C^{14}N^-$ secondary ion signal intensity distribution maps of a semithin section of untreated SW480 human colon cancer cells. ROIs refer to (1) cytoplasm, (2) nucleus, (3) nucleolus, (4) chromatin. The few counts visble in the Pt channel originate from electronic noise and - to a minor degree - the detection of isobars. Intensities are displayed on a rainbow false-colour scale ranging from dark blue to red for low to high intensities, respectively. Scale bars = 5 µm.

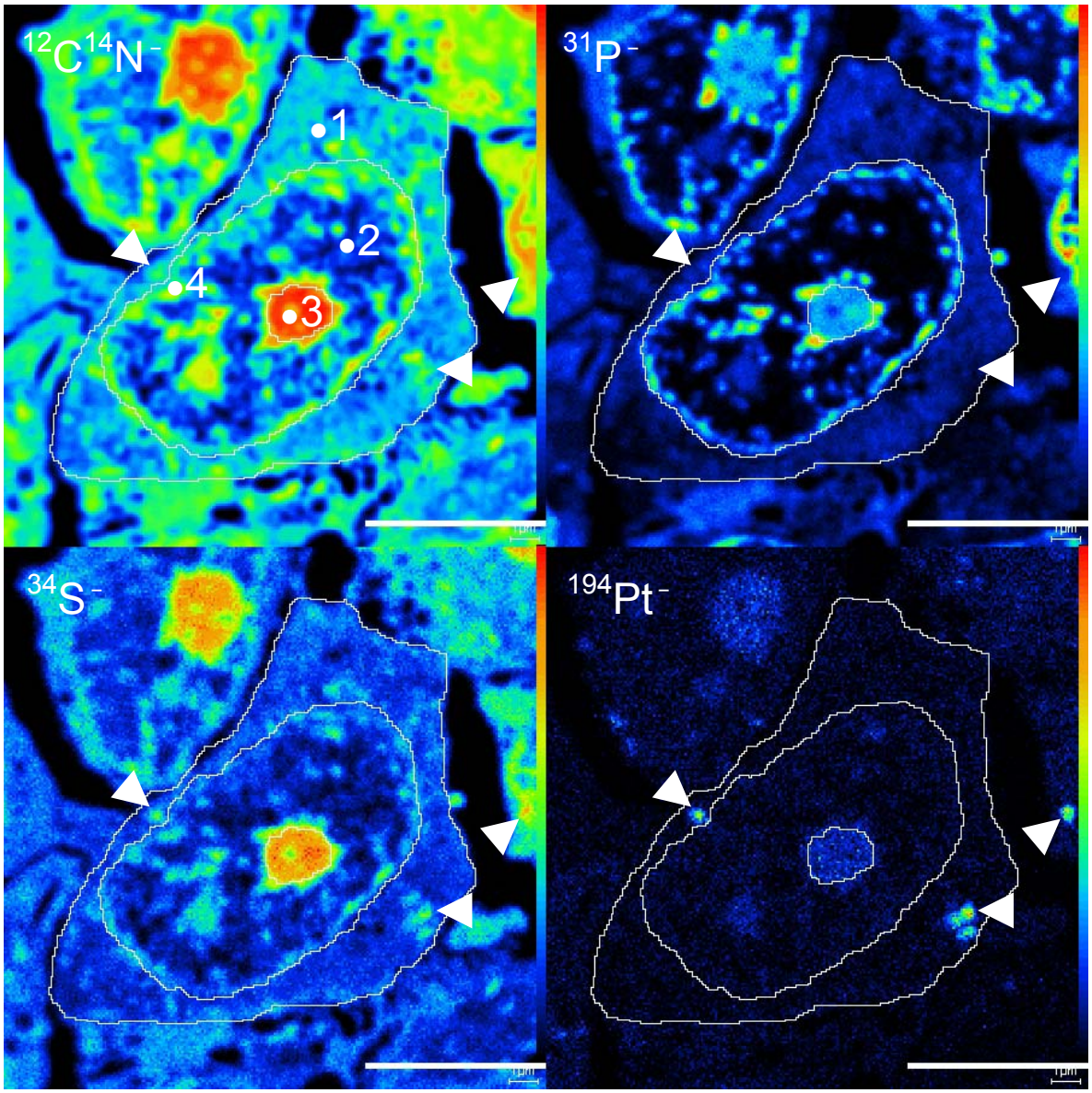

Fig. S2 NanoSIMS $^{12}C^{14}N^-$, $^{34}S^-$, $^{31}P^-$and $^{194}Pt^-$ secondary ion signal intensity distribution maps of a semithin section of SW480 human colon cancer cells upon treatment with 150 µM CDDP for 24 h. ROIs refer to (1) cytoplasm, (2) nucleus, (3) nucleolus, (4) chromatin. Note the cytoplasmic accumulation of platinum in sulfur-rich aggregates (white arrowheads). Intensities are displayed on a rainbow false-colour scale ranging from dark blue to red for low to high intensities, respectively. Scale bars = 5 µm.

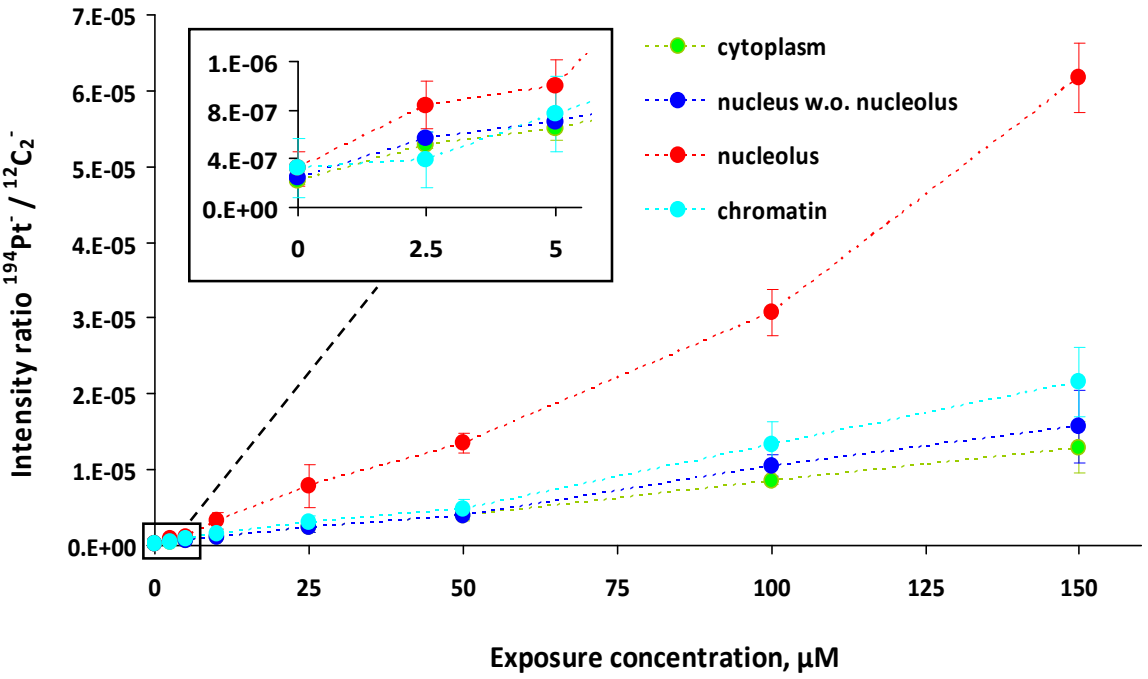

Fig. S3 Subcellular platinum distribution in SW480 cells upon 24 h CDDP exposure in the concentration range from 0 µM (min. values, control) to 150 µM (max. values), as inferred from the $^{12}C_2^-$ normalised $^{194}Pt^-$ signal intensities. The different colours of the symbols refer to values obtained from ROIs defined within the cytoplasm (green), nucleus (excl. neucleolus, dark blue), chromatin (cyan) and nucleoli (red) of individual cells. Error bars correspond to one standard deviation of the individual ROI values within each compartment. Note that the chromatin structures show a tendency of enhanced Pt accumulation in comparison to the averaged nucleus (w.o. nucleolus) and the cytoplasm, which becomes significant at exposure concentrations ≥ 100 µM (Student's t-test, $p < 0.022$).

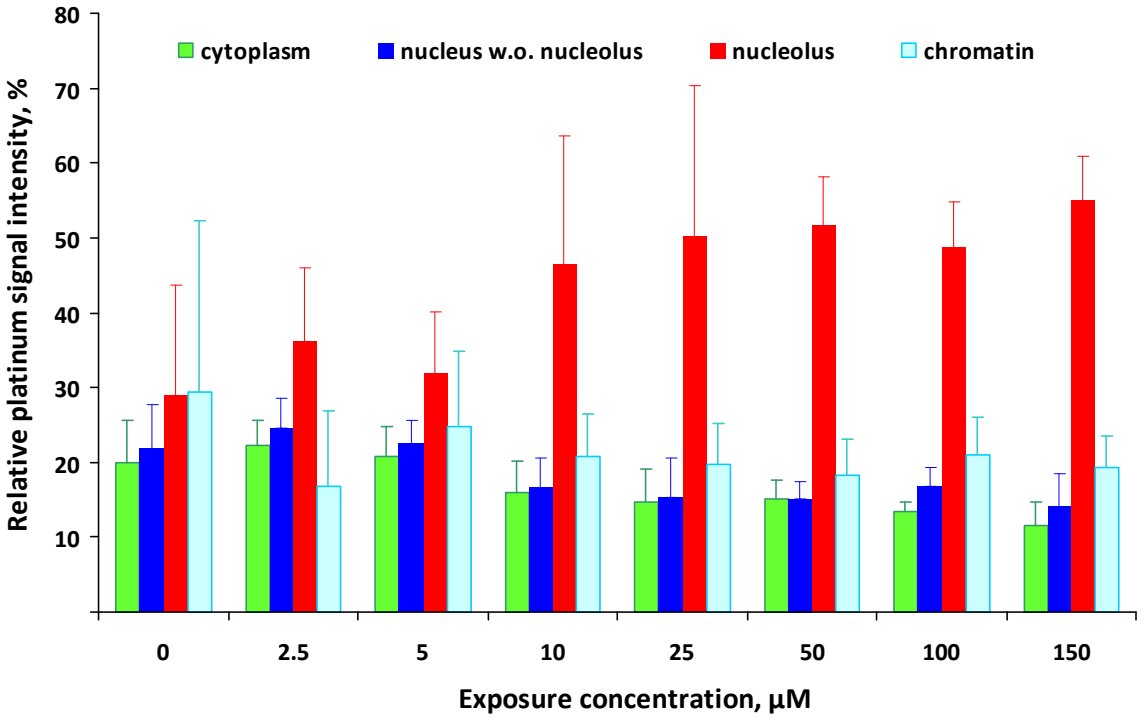

Fig. S4 Comparison of the relative platinum signal intensities ($^{194}Pt^{-}/^{12}C_2^{-}$) over the indicated compartments of SW480 cells upon 24 h CDDP exposure. 100% refers to the sum of the mean intensities for each concentration as obtained from the ROI analysis. Error bars refer to one standard deviation of the ROI values within the respective compartment.

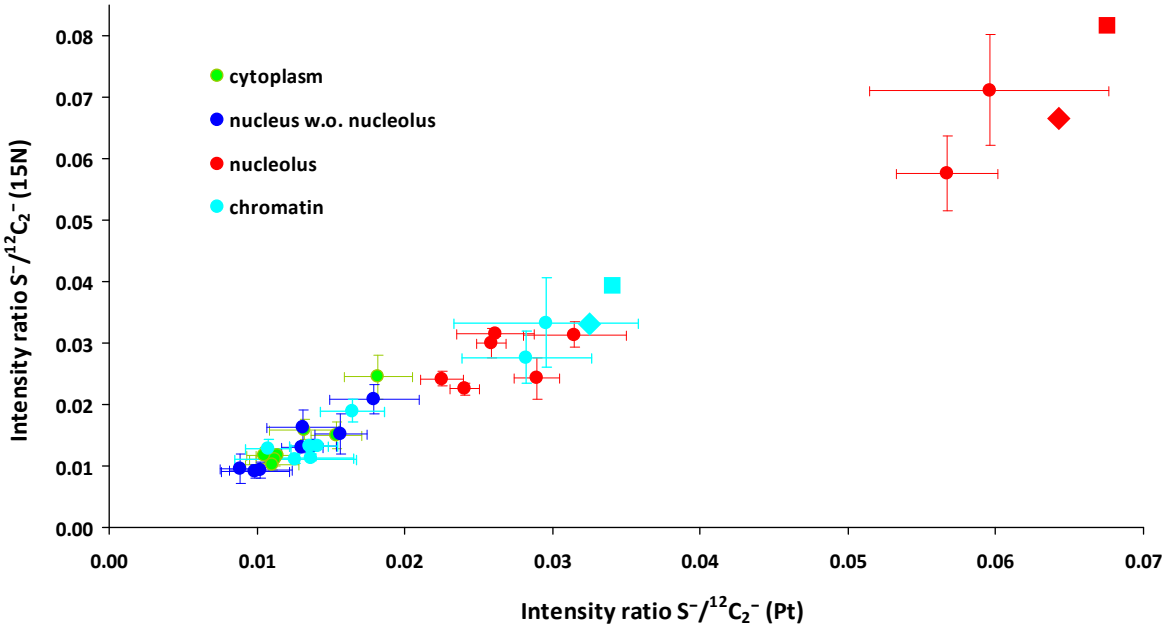

Fig. S5 Relative sulfur content of cellular compartments after 24 h exposure to eight different concentrations of cisplatin, ranging from 0 to 150 µM. as inferred from the $^{12}C_2^-$ normalised signal intensities of atomic sulfur secondary ions (S^-). Values shown on the abscissa and ordinate were acquired in the Pt and ^{15}N measurement runs, respectively. The (hypothetical) S^- signal intensities were calculated from the detected $^{32}S^-$ and $^{34}S^-$ signals by taking into account the natural abundances of the two isotopes (95.02% and 4.21%, respectively). Error bars refer to one standard deviation. Note the considerable enhancement of the sulfur content within nucleoli after treatment with 100 (squares) and 150 µM (diamonds) CDDP.

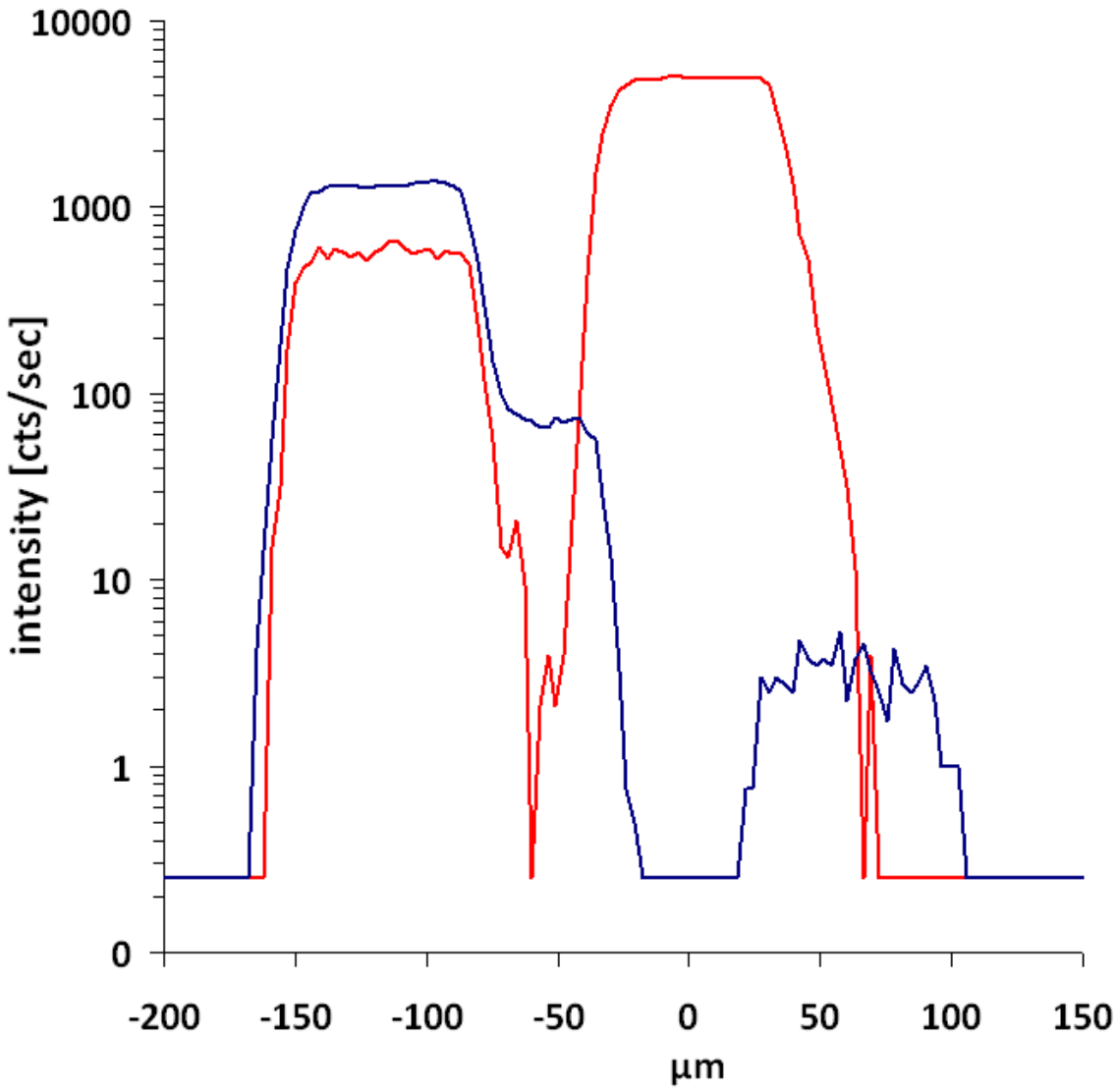

Fig. S6 NanoSIMS mass spectra at m/z = 194 u. The red curve refers to the spectrum obtained from the Pt reference sample (finely grained CDDP deposit on a semi-thin resin section of SW480 cells), the blue curve displays the spectrum of the negative control (semi-thin resin section of untreated SW480 cells).

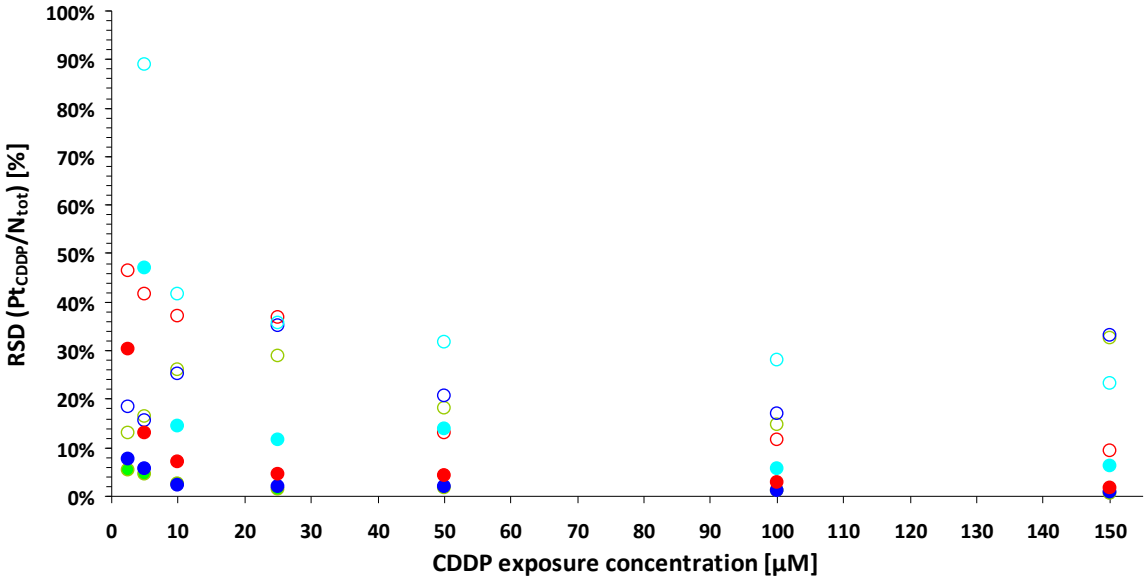

Fig. S7 Mean analytical precision (counting error, solid symbols) versus dispersion of the ROI data (open symbols) of $^{194}Pt^{-}/^{12}CN^{-}$ secondary ion signal intensities plotted on the abscissa of Fig. 3 (details are provided in the main text an in section "Stoichiometric calculations" below). Displayed values refer to one standard deviation, normalised to the mean (i.e. relative standard deviation, RSD). The different colours symbolise cytoplasmic areas (green), nuclei w.o. nucleoli (blue), nucleoli (red) and chromatin (cyan)..For further explanations see section 'Image processing, numerical data evaluation and calculations' in ESI).

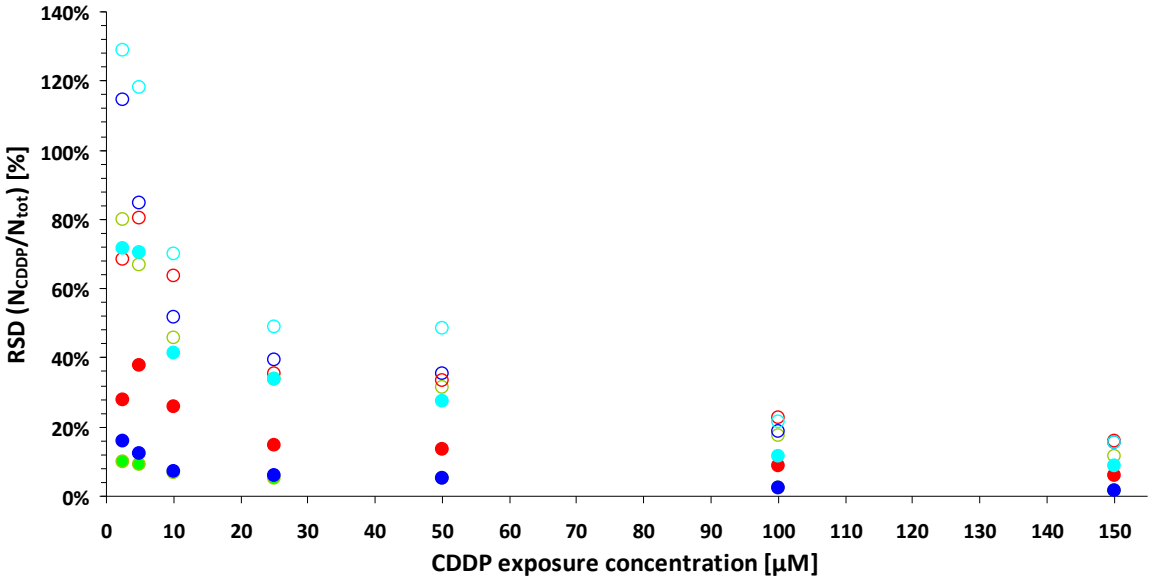

Fig. S8 Mean analytical precision (counting error, solid symbols) versus dispersion of the ROI data (open symbols) for the fraction of nitrogen atoms originating from the ammine ligands (N_{CDDP}/N_{tot}), plotted on the ordinate of Fig. 3) as inferred from the ^{15}N isotope abundance in the sample, the applied CDDP and an untreated control (see Eq. 1 in the main text, details are provided in section "Stoichiometric calculations" below). Displayed values refer to one standard deviation, normalised to the mean (i.e. relative standard deviation). The different colours symbolise cytoplasmic areas (green), nuclei w.o. nucleoli (blue), nucleoli (red) and chromatin (cyan).

Effect of cisplatin on cell viability

In order to verify that the applied CDDP concentrations are not causing cell death to a high extent within the time frame of the experiment, viability of the cells after 24 h exposure was tested with three different assays. Information about cell viability is crucial because the likelihood of cisplatin distribution artifacts will increase in dead cells due to membrane damage and breakdown of transport mechanisms.

In the MTT assay, the growth of SW480 colon carcinoma cells treated with cisplatin is not completely inhibited at concentrations lower than 100 µM (Fig. S9). The concentration of 100 µM causes total growth inhibition (complete cytostasis). The cell number is only diminished in comparison to the cell number at the beginning of exposure upon treatment with concentrations of 150 µM and higher. These observations confirm that SW480 cells are rather insensitive to cisplatin during 24 h exposure period.

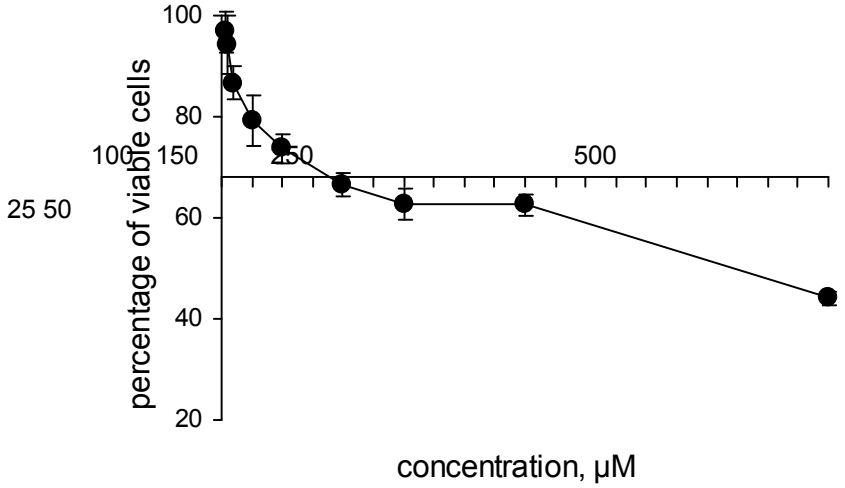

Fig. S9 Concentration-dependent effect of cisplatin on growth of SW480 cells, determined by the MTT assay (24 h exposure). The intersection of the axes corresponds to the percentage of cells already present in the beginning of drug exposure. Concentrations below 100 µM do not completely inhibit cell growth; concentrations higher than 100 µM induce a gradual cell loss.

In order to verify the low percentage of dead cells upon drug exposure in our experiments with a second method, growing SW480 cultures were treated with the CDDP in various concentrations (10–500 μM) for 24 h, then double-stained with annexin V-FITC/propidium iodide and analyzed by fluorescence-activated cell sorting (FACS). This method allows to discriminate (a) necrotic cells stained with propidium iodide (cell membrane damage is a precondition for PI penetration and intercalation into DNA, yielding red fluorescence); (b) early apoptotic cells stained with annexin V-FITC (annexin V binds to phosphatidylserine, which is a marker for early apoptosis, FITC yields green fluorescence); and (c) late apoptotic cells stained with both dies from (d) viable unstained cells. Cells treated with compound **3** (Scheme S1), which was previously shown to induce apoptosis in SW480 cells within 24 h to a higher extent, were used as a positive control. Results show that concentrations of up to 150 μM of cisplatin do not induce cell death in SW480 cells within the chosen exposure time (Fig. S10).

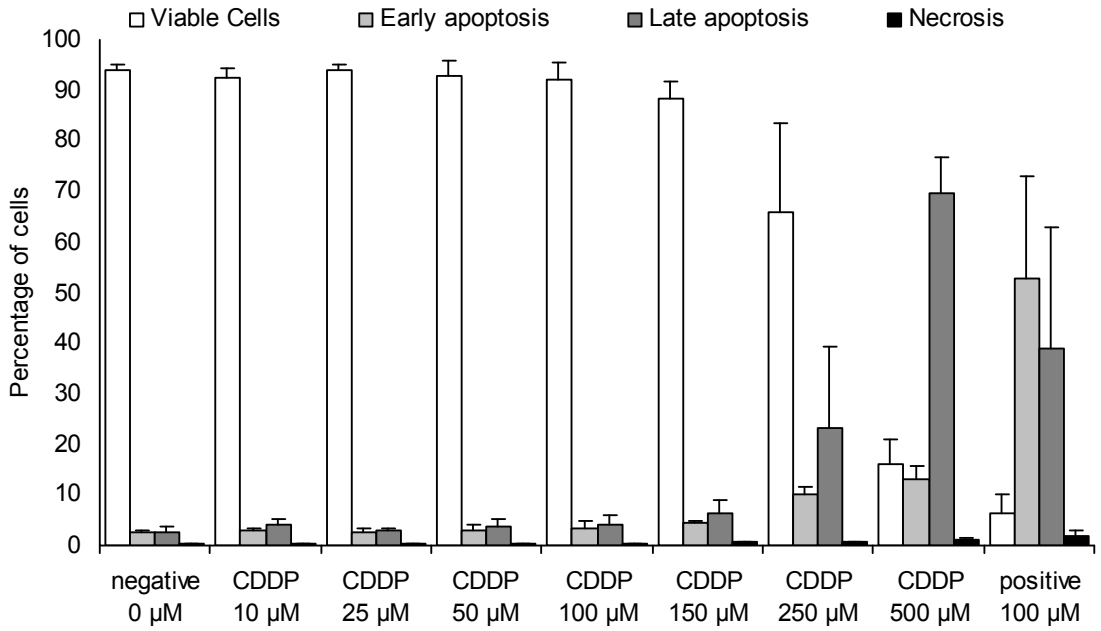

Fig. S10 Apoptosis/necrosis induction in SW480 cells after 24 h exposure to the indicated concentrations of cisplatin (CDDP), measured by FACS using annexin V-FITC/propidium iodide double-staining. Negative – untreated control, positive – cells treated with compound **3**.

In addition, mitochondrial membrane potential (MMP) was assessed by the lipophilic cationic probe JC-1, a compound selectively concentrated in intact mitochondria to form J-aggregates emitting green fluorescence, whereas depolarization of mitochondrial membranes leads to orange fluorescence of the dye, which can be measured by FACS. MMP loss is an early event in apoptotic cell death. Results confirm that cisplatin induces a marked loss of the mitochondrial transmembrane potential only in concentrations higher than 150 μM (Fig. S11).

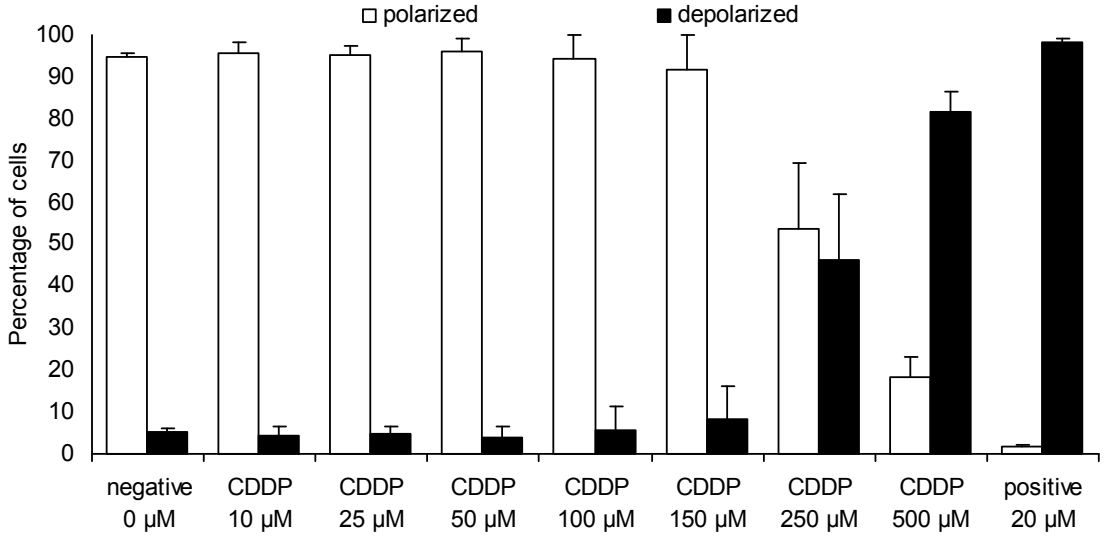

Fig. S11 Induction of mitochondrial membrane depolarization in SW480 cells after 24 h exposure to the indicated concentrations of cisplatin, measured by FACS using JC-1 staining. Negative – untreated control, positive – cells treated with CCCP (carbonyl cyanide 3-chlorophenylhydrazone).

Taken together, all three assays support the presumption that the cisplatin-treated cells that were subject to NanoSIMS measurements were neither apoptotic nor necrotic before fixation.

Materials and methods

Compounds. ^{15}N-labeled cisplatin (Scheme S1) was synthesised according to a literature procedure by using ^{15}N-labeled ammonium chloride (>98% ^{15}N enrichment level, CORTEC, USA).[1] (SP-4-1)-Dichloridobis((1*Z*)-*N*-hydroxypropane-1-imine-κ*N*)platinum(II) (complex **3**, Scheme S1) used as a positive control in the apoptosis assay was prepared according to a previously published procedure[2].

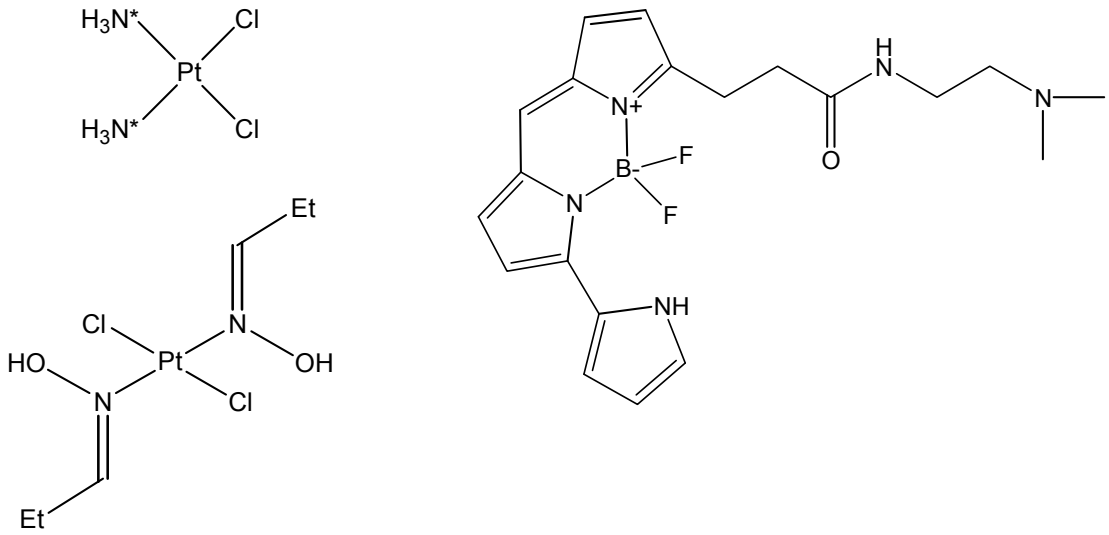

Scheme S1. Structures of cisplatin (upper left), platinum oxime complex **3** (lower left) and LysoTracker® Red DND-99 (right). ^{15}N-labeled ammine ligands are marked with asterisks.

Cell culturing. The human cancer cell line SW480 (colon carcinoma) was grown in 75 cm^2 culture flasks (Iwaki/Asahi Technoglass, Gyouda, Japan) as adherent monolayer cultures in complete medium [i.e., Minimal Essential Medium (MEM) supplemented with 10% heat-inactivated fetal bovine serum, 1 mM sodium pyruvate, 4 mM L-glutamine, and 1% nonessential amino acids solution from 100× ready-to-use stock (all purchased from Sigma-Aldrich Austria)]. Cell cultures were incubated at 37 °C in a moist atmosphere containing 5% CO_2.

Cell viability assay. The cytotoxic activity of cisplatin was determined by using the colourimetric MTT (3-(4,5-dimethyl-2-thiazolyl)-2,5-diphenyl-2*H*-tetrazolium bromide) assay to test the viability of the cells after 24 h exposure to different concentrations of the drug. SW480 cells were collected from culture flasks by trypsinization, and 1.5×10^4 cells/well were seeded in 100 µl aliquots in complete medium into 96-well microculture plates (Iwaki/Asahi Technoglass, Gyouda, Japan). The cells were allowed to settle overnight. Cisplatin was dissolved in complete medium, serially diluted, and 100 µl of the dilutions were added per well. After 24 h exposure, drug solutions were replaced with 100 µl of RPMI1640 culture medium (supplemented with 10% heat-inactivated fetal bovine serum and 2 mM L-glutamine) mixed with 20 µl MTT solution in phosphate-buffered saline (5 mg/ml). After incubation for 4 h, the RPMI/MTT mixtures were

removed, and the formazan crystals formed in viable cells were dissolved in 150 µl of DMSO per well. Optical densities were measured at 550 nm with a microplate reader (ELx808 Absorbance Microplate Reader, Bio-Tek, USA). Unspecific absorption was corrected by using a reference wavelength of 690 nm. Evaluation of growth inhibition is based on means from at least three independent experiments, each comprising six replicates per concentration level.

Apoptosis assay. In order to rule out apoptotic and necrotic cell death induction by cisplatin, cells were analyzed by fluorescence-activated cell sorting (FACS) using fluorescein isothiocyanate (FITC)-conjugated annexin V (BioVision, USA) and propidium iodide (PI; Fluka) staining. SW480 cells were seeded into 12-well plates (CytoOne, Starlab, UK) in densities of 2×10^5 cells per well in complete medium and allowed to settle for 24 h. The cells were exposed to different concentrations of cisplatin for 24 h at 37 °C. After incubation, the cells were gently trypsinised, collected in 1.5 ml tubes, washed with PBS and resuspended with FITC-conjugated annexin V (0.25 µg/ml) in binding buffer (10 mM HEPES/NaOH pH 7.4, 140 mM NaCl, 2.5 mM CaCl2) at room temperature for 15 min. PI (1 µg/ml) was added shortly before the measurement. Stained cells were analyzed with a Guava 8HT EasyCyte flow cytometer (Merck Millipore, Guava, USA) using InCyte software. Three independent experiments were conducted, and 5000 cells were analyzed in each run.

JC-1 assay. Monolayers of human SW480 colon cancer cells were seeded into 12-well plates in numbers of 1×10^5 cells/well in complete MEM. After 24 h preincubation, cells were treated with cisplatin solutions for 24 h. After exposure, the cells were trypsinised and collected in 1.5 ml tubes. The cells were washed with warm PBS before incubation with complete MEM containing 2 µM JC-1 (5,5′,6,6′-tetrachloro-1,1′,3,3′-tetraethylbenzimidazolcarbocyanine iodide, BioVision, USA) for 15 min at 37 °C. The positive control sample was incubated simultaneously with 2 µM JC-1 and 1 mM of the ionophore carbonyl cyanide 3-chlorophenylhydrazone (CCCP) for 15 min at 37 °C. Following JC-1 incubation, the cell pellets were washed with warm PBS, centrifuged and suspended in 0.5 ml PBS prior to FACS measurement (as described above).

Fluorescence Microscopy. For colocalization experiments, SW480 cells were seeded on indium tin oxide (ITO) coated glass slides (Praezisions Glas & Optik GmbH, Iserlohn, Germany) in 6-

well plates (2×10^4 cells per well in 2 ml of MEM) and allowed to attach overnight. The cells were treated with 25 µM of ^{15}N-labeled cisplatin (24 h) and stained with LysoTracker Red (5 min, 500 nM). The cells were analyzed immediately after staining under fixing solution (2.5% glutaraldehyde in 0.1 M sodium cacodylate buffer). LysoTracker Red (Life Technologies, Paisley, UK) distribution was visualised with a confocal laser scanning microscope Leica SP2 (ICS Leica Microsystems, Wetzlar, Germany) equipped with 20× and 40× dry plan apo objectives. The excitation time was kept as short as possible to minimise the bleaching effect, which gets stronger during the fixation procedure. Fluorescence was observed under blue light irradiation (488 nm) with an Ar laser. Stacks of 10 consecutive images (1 µm steps) were taken and processed with Leica Microsystems software to generate a maximum projection image. To keep the samples suitable for NanoSIMS application after microscopy, samples were washed in 0.1 M sodium cacodylate buffer to remove the fixation solution and dried on air. The dried samples were then subjected to NanoSIMS measurements. The confocal microscopy and NanoSIMS images were correlated by using GIMP software.

Preparation of semi-thin sections. In addition to dried whole cells (see above), semi-thin sections of resin embedded cells were prepared. For this purpose, SW480 cells were grown in 90 mm cell culture dishes to about 70% confluence. Cells treated with cisplatin (2.5 to 150 µM, 24 h) and untreated control cells were washed with PBS, harvested by trypsinization and pelleted in 1.5 ml tubes. Subsequently, the pellets were carefully handled through the steps of fixation with 2.5% glutaraldehyde solution for 2 h at room temperature, washing with 0.1 M sodium cacodylate buffer and dehydration in an ascending ethanol series (30%, 50%, 70%, 90% and 100% ethanol, 10 min each). 100% ethanol was then replaced with pure acetone, which was substituted gradually with low viscosity resin (100 Low Viscosity Resin, Agar Scientific, UK). Pellets in liquid resin were placed in a mold and hardened by oven heating for 18 h at 65 °C. The resin blocks were cut using a Leica microtome and freshly prepared glass knifes to obtain semi-thin sections with 300 nm thickness. For each treatment concentration, 5 to 10 sections were placed on a drop of bidistilled water on boron-doped silicon wafers (7 x 7 x 0.75 mm^3, Active Business Company GmbH, Brunnthal, Germany) and dried on a warm plate. The adherent sections were subsequently analyzed with NanoSIMS.

NanoSIMS analysis. NanoSIMS measurements were carried out on a NS 50L instrument from Cameca (Paris, France). Due to the limited length of the mass spectrometer (viz. the magnet of the double focusing electrostatic/magnetic sector field mass analyzer) and the physical width of the secondary ion detectors, the platinum distribution and the nitrogen isotope composition had to be determined in sequential analysis runs.

In the platinum measurements, the detectors of the multicollection assembly were positioned to enable parallel detection of $^{12}C_2^-$, $^{12}C^{14}N^-$, $^{31}P^-$, $^{34}S^-$ and $^{194}Pt^-$ secondary ions. With respect to sulfur it should be noted that the $^{34}S^-$ ion signal had to be chosen instead of the more intense $^{32}S^-$ signal (the natural isotopic abundance of ^{32}S and ^{34}S is 95.02% and 4.21%, respectively) since the flight path radius of $^{32}S^-$ ions was too close to the radius of $^{31}P^-$ ions for simultaneous sulfur and phosphor detection. The inner width of the selected spectrometer entrance slit was 20 µm ("ES#3") and a 200 µm aperture slit ("AS#3") was inserted in the secondary ion beam path to reduce beam divergence. The electrostatic lenses and deflectors inside the spectrometer were adjusted to achieve a mass resolving power (MRP) of 10.700 (according to Cameca`s definition) at the position of the $^{194}Pt^-$ detector. Spectrometer tuning, mass calibration and detector (electron multiplier) calibration were carried out on a semi-thin section of resin-embedded SW480 cells after precipitation of a finely grained CDDP deposit obtained from spotting and evaporation of an aqueous, 1 mM cisplatin solution on the sample surface. A 40 µm spectrometer exit slit ("ExS#2") was selected at the $^{194}Pt^-$ detector to facilitate efficient blanking of isobars, which appear both at the low and the high mass end of the peak (Fig. S6, ESI).

In the nitrogen isotope measurements, the detectors were positioned for simultaneous registration of $^{12}C_2^-$, $^{12}C^{14}N^-$, $^{12}C^{15}N^-$, $^{31}P^-$ and $^{32}S^-$ secondary ions. The spectrometer settings were analogous to the platinum measurements; however, the voltage at the quadrupole lens ("Q") that links the electrostatic with the magnetic sector of the spectrometer was slightly varied to achieve a MRP of 10.500 for detection of CN^- ions.

All data were acquired as multilayer image stacks obtained by sequential scanning of a finely focused Cs^+ primary ion beam over areas between 30×30 and $40 \times 40\ \mu m^2$ with 512×512 pixel image resolution. The physical resolution (probe size) was approx. 80 nm, accomplished through beam divergence reduction by insertion of a diaphragm with 100 µm inner diameter ("D1#3") in the primary ion beam path. The per pixel dwell time of the primary ion

beam was in the range from 7.5 to 10 ms and the number of image (scanning) cycles was chosen to achieve a total dwell time of 200 to 300 ms per pixel. Between every image cycle, secondary ion beam drift was corrected by automatic beam centering and coaxial lens ("EOS") voltage optimization - utilizing the $^{12}C2^-$ signal as reference - as well was automatic peak centering for each of the recorded secondary ion species. The total acquisition time was in the range from 15 to 20 h per measurement. Prior to data acquisition, analysis areas were pre-sputtered by scanning of an unfocused, high intensity (400 pA) Cs^+ primary ion beam over an area of 60×60 µm to remove surface adsorbates and to benefit from chemical secondary ion yield enhancement through reactive primary ion implantation. On the resin sections pre-sputtering was finished after sample irradiation with 8.3E16 ions/cm^2, which was high enough for reproducibly reaching the steady state signal intensity regime.

Image processing, numerical data evaluation. NanoSIMS image data were evaluated using the WinImage software package provided by Cameca. Prior to stack accumulation, the individual images were aligned to compensate for positional variations arising from primary ion beam and/or sample stage drift. Secondary ion signal intensities were dead time corrected on a per-pixel basis. Quasi simultaneous arrival (QSA) effects were taken into account for C_2^- and CN^- secondary ions. In contrast to dead time correction, QSA correction had to be performed manually on a per ROI basis.

Individual regions of interest (ROIs) representative for distinct cellular compartments were defined manually, based on the morphological features identifiable in the relative N, P and S elemental distribution, as inferred from the $^{12}C^{14}N^-$, $^{31}P^-$ and $^{32}S^-$ or $^{34}S^-$ signal intensity distribution maps. In the measurements on the resin sections, the raster size, pixel number and probe size were chosen to enable simultaneous analysis of several individual cells in one measurement (see e.g. Fig. 2). Nevertheless, data were only evaluated from cells containing a complete set of the considered subcellular compartments, in particular nucleoli. Results are presented as arithmetic means and standard deviations calculated from the individual ROI data for each of the defined cellular compartments. The analytical precision was estimated from the statistical error (counting error) of the secondary ion signal intensities. Based on Poisson statistics, the standard deviation of a secondary ion signal is equal to the square root of the number of detection events (counts) recorded by the detection system, which may be written as

$$\sigma_{A^{+/-}} = \sqrt{N_{A^{+/-}}}, \quad (1.1)$$

where $A^{+/-}$ designates the detected secondary ion species. Accordingly, the relative standard deviation (coefficient of variance) is given by $\frac{1}{\sqrt{N_{A^{+/-}}}}$. Counting errors were calculated for all secondary ion signals (per ROI) and propagated to the quantities applied in data representation (see also section "Stoichiometric calculations" below).

As already stated above, secondary ion signal intensities were also corrected for quasi-simultaneous arrival (QSA) of secondary ions at the detector. QSA arises from the quasi-simultaneous emission of more than one secondary ion per primary ion impact and leads to counting losses in single ion counting by electron multipliers[3, 4]. It is worthy to note that QSA events are not considered in the conventionally applied dead time correction, which takes into account counting losses due to multiple secondary ion arrivals within the detector dead time (which is electronically fixed at 44 ns for the electron multiplies of our NanoSIMS NS50L). Assuming Poisson statistics, Slodzian et al. suggested a formula for QSA correction in a first order approximation [3, 4], which reads as

$$N_{cor} = N_{exp}\left(1 + \frac{1}{2}K\right) \quad (1.2)$$

where $N_{exp.}$ and $N_{cor.}$ refer to the experimentally observed number of counts and the actual number of secondary ions arriving at the detector, respectively. K designates the number of ions arriving at the detector per impacting primary ion, which can be evaluated from the ratio of the secondary ion signal intensity over the primary ion beam intensity. Since the actual number of secondary ions that reach the multiplier is unknown, K needs to be corrected via[4]

$$K_{cor} = \frac{K_{exp}}{1 - \frac{K_{exp}}{2}} \quad (1.3)$$

It needs to be emphasised that Slodzian et al. demonstrated that the multiplication factor appearing at K in Eq.(1.2) may deviate from the theoretical value of ½ [4]. Consequently, we conducted measurements on biomass (dried yeast cells, data not shown) which yielded multiplication factors of 1,06+/-0,04 and 1,05+/-0,02 (1σ) for C_2^- and CN^- secondary ions, respectively. Using these factors, the C_2^- and CN^- secondary ion signal intensities were QSA

corrected by application of Eqs. (1.2) and (1.3). The primary ion beam intensities during the measurements were estimated from the averaged primary ion beam current measured automatically at the faraday cup in the upper part of the primary ion column ('FCp') before and after every measurement and periodical calibration of the FCp values versus the beam current measured at the faraday cup positioned behind the sample stage ('FCo').

Quantities applied in data representation, stoichiometric calculations. a_{15N} refers to the abundance of the ^{15}N isotope in a given sample. Since nitrogen comprises only two stable isotopes (i.e. ^{14}N and ^{15}N), the ^{15}N abundance corresponds to the isotope fraction $^{15}N/(^{14}N+^{15}N)$, given in at%. In SIMS, the nitrogen isotope composition is inferred from the signal intensities of CN^- ions due to the high ion yield of cyanide. In this work, the ^{15}N abundance was calculated from the (QSA corrected) $^{12}C^{14}N^-$ and $^{12}C^{15}N^-$ signal intensities by

$$a_{15N} = \frac{12C15N^-}{12C14N^- + 12C15N^-}. \tag{1.4}$$

Via error propagation of the counting error, the analytical precision (1σ) achieved in an abundance measurement can be estimated from the recorded signal intensities by

$$\sigma_{a_{15N}} = \frac{1}{\left(12C14N^- + 12C15N^-\right)^2}\sqrt{\left(12C14N^-\right)^2 12C15N^- + 12C14N^-\left(12C15N^-\right)^2}\ . \tag{1.5}$$

Note that the signal intensities have to be applied as the (absolute) number of counts registered within the considered analysis region.

$R_{15N/14N}$ refers to the ratio of $^{15}N/^{14}N$ atoms, inferred from the intensity ratio of the $^{12}C^{15}N^-$ and $^{12}C^{14}N^-$ signals. $R_{15N/14N}$ is related to the ^{15}N isotope abundance (a_{15N}) via

$$a_{15N} = \frac{R_{15N/14N}}{R_{15N/14N}+1} \text{ and } R_{15N/14N} = \frac{a_{15N}}{1-a_{15N}}. \tag{1.6}$$

By error propagation of the counting errors, the analytical precision (1σ) can be estimated from the recorded signal intensities (given in counts) as

$$\sigma_{R_{15N/14N,\,POISSON}} = \frac{1}{12C14N^-}\sqrt{12C15N^- + \frac{\left(12C15N^-\right)^2}{12C14N^-}}, \qquad (1.7)$$

N_{CDDP} / N_{tot} designates the quantity that expresses the fraction of elemental nitrogen atoms (i.e. sum over all isotopes) originating from the ligands *(N_{CDDP})* within the total number of nitrogen atoms *(N_{tot})* contained in the considered analysis region and can be calculated from the ^{15}N isotopic abundances *(a_{15N}) as*

$$\frac{N_{CDDP}}{N_{tot}} = \frac{a_{15N,tot} - a_{15N,ctr}}{a_{15N,CDDP} - a_{15N,ctr}}, \qquad (1.8)$$

where $a_{tot.}$ and a_{ctr} refer to the ^{15}N abundances measured in the sample and an untreated control, respectively. a_{CDDP} corresponds to the ^{15}N isotopic enrichment level of the cisplatin applied in the treatment experiments, which was 98%. The derivation of N_{CDDP}/N_{tot} as a function of the ^{15}N abundances is described below.

According to the error propagation theorem, the standard deviation of (N_{CDDP}/N_{tot}) is related to the standard deviations of the measured abundances by

$$\sigma_{N_{CDDP}/N_{tot}} = \sqrt{\left(\frac{\partial\frac{N_{CDDP}}{N_{tot}}}{\partial a_{15N,tot}}\right)^2 \sigma^2_{a_{15N,\,tot}} + \left(\frac{\partial\frac{N_{CDDP}}{N_{tot}}}{\partial a_{15N,ctr}}\right)^2 \sigma^2_{a_{15N,\,ctr}}}. \qquad (1.9)$$

It should be noted that the term related to the ligands had to be excluded from Eq. (1.9) since the uncertainty in the isotopic enrichment level of the applied CDDP was not specified. After calculation of the partial derivatives, Eq. (1.9) becomes

$$\sigma_{N_{CDDP}/N_{tot}} = \frac{1}{\left(a_{15N,CDDP} - a_{15N,ctr}\right)^2}\sqrt{\left(a_{15N,tot} - a_{15N,ctr}\right)^2 \sigma^2_{a_{15N,ctr}} + \left(a_{15N,CDDP} - a_{15N,ctr}\right)^2 \sigma^2_{a_{15N,tot}}}, \qquad (1.10)$$

For estimation of the analytical precision, the counting error (1σ) associated with the determination of the isotopic abundances (see Eq. (1.5) above) was inserted in Eq. (1.10).

From a more general perspective, the derivation of the algebraic function describing the relationship between the abundance of the isotopic label (here: a_{15N}) and the relative number of atoms originating from drug accumulation (here: $N_{CDDP}/N_{tot.}$) relies on the law of mass conservation, from which follows, that:

(i) For any considered element *X*, the total number of atoms contained in the analyzed region of a compartment is equal to the sum of atoms originating from the compounds in the compartment (referred to by measurement of an untreated control) and the number of atoms added through drug accumulation

$$n_{X,tot} = n_{X,ctr} + n_{X,drug}, \tag{1.11}$$

(ii) The number of label atoms $n_{^{A}X}$ contained in the considered region of the compartment is equal to the sum of label atoms originating from the compounds in the compartment and the number of label atoms added through drug accumulation

$$n_{^{A}X,tot} = n_{^{A}X,ctr} + n_{^{A}X,drug}, \tag{1.12}$$

Utilizing the isotopic abundance of the label atoms $a_{^{A}X}$, which is defined by

$$a_{^{A}X} = \frac{n_{^{A}X}}{n_{^{A}X} + n_{^{B}X} + n_{^{C}X} \ldots}, \tag{1.13}$$

where the superscripts at *X (A, B, C…)* refer to the mass number of the respective isotopes, Eq. (1.13) can also be written as

$$n_{X,tot} a_{^{A}X,tot} = n_{X,ctr} a_{^{A}X,ctr} + n_{X,drug} a_{^{A}X,drug}. \tag{1.14}$$

Rearrangement of this equation and utilizing the relationship $n_{X,ctr.} = n_{X,tot.} - n_{X,drug}$ (see Eq. (1.11)), an equation can be formulated that describes the fraction of drug atoms contained in the analyzed region

$$\frac{n_{X,drug}}{n_{X,tot.}} = \frac{a_{^{A}X,tot} - a_{^{A}X,ctr}}{a_{^{A}X,drug} - a_{^{A}X,ctr}}, \tag{1.15}$$

which is actually the relationship that we were looking for.

Pt_{CDDP} / $N_{tot.}$. As already mentioned in the main text, SIMS is only semi-quantitative in elemental analysis, which is mainly due to the fact that the product of the sputter yield and the ionization probability of sputtered particles can vary over several orders of magnitude. However, utilizing an appropriate secondary ion signal as a reference, a relationship can be established in which the normalised intensity of the secondary ion signal associated with the analyte is linearly related to the concentration of the analyte. In the measurements on the resin section we selected the $^{12}C_2^-$ signal as a reference since it showed the lowest variability over the distinct cellular compartments (in comparison to $^{12}C^-$ and $^{16}O^-$, which can also be considered as candidates for reference signals due to high concentration of carbon and oxygen in the resin, which represents the matrix in such samples). As such, the $^{194}Pt^-/^{12}C_2^-$ and $^{12}CN^-/^{12}C_2^-$ signal intensity ratios served as indicators of the local platinum and nitrogen contents. The designation $^{12}CN^-$ for the cyanide ions has deliberately been chosen to indicate that the relative ion yields of $^{12}C^{14}N^-$ and $^{12}C^{15}N^-$ also depends on the nitrogen isotopic composition. In other words, any constriction to the $^{12}C^{14}N^-$ signal leads to an underestimation of the local nitrogen content since the contribution of the highly ^{15}N enriched ammine ligands is neglected. This has to be particularly noted when the two isotopic ions cannot be detected simultaneously, which is actually the case in elemental mapping of high mass number elements, such as gold or platinum. Consequently, we first calculated the averages of the $^{12}C^{14}N^-/^{12}C_2^-$ intensity ratios determined in the platinum and nitrogen isotope measurements,

$$\left(\frac{12C14N^-}{12C_2^-}\right)_{avg} = \frac{1}{2}\left[\left(\frac{12C14N^-}{12C_2^-}\right)_{Pt} + \left(\frac{12C14N^-}{12C_2^-}\right)_{15N}\right], \qquad (1.16)$$

from which the total $^{12}CN^-$ signal intensity was calculated by consideration of the contribution of ^{15}N containing ions, which was evaluated in the nitrogen isotope measurements, i.e.

$$\left(\frac{12CN^-}{12C_2^-}\right)_{avg} = \left(\frac{12C14N^-}{12C_2^-}\right)_{avg} \times \left(1 + R_{15N/14N}\right). \qquad (1.17)$$

The local relative accumulation of platinum originating from CDDP uptake was referred to by subtraction of ROI specific $^{194}Pt^-/^{12}C_2^-$ intensity ratios measured on an untreated control *('ctr')* from the values determined on the respective samples (designated, for the sake of consistency, with the ligands, as *'total'*),

$$\left(\frac{194Pt^-}{12C_2^-}\right)_{CDDP} = \left(\frac{194Pt^-}{12C_2^-}\right)_{tot} - \left(\frac{194Pt^-}{12C_2^-}\right)_{ctr}. \quad (1.18)$$

Finally, the platinum signal intensities were normalised to the $^{12}CN^-$ signal intensities,

$$\frac{194Pt^-_{CDDP}}{12CN^-} = \left(\frac{194Pt^-}{12C_2^-}\right)_{CDDP} \times \left(\frac{12CN^-}{C_2^-}\right)^{-1}_{avg}, \quad (1.19)$$

which, by definition, is proportional to the concentration ratio of the platinum originating from CDDP to the total nitrogen content in the considered compartments,

$$\frac{Pt_{CDDP}}{N_{tot}} \propto \frac{194Pt^-_{CDDP}}{12CN^-}, \text{ presented in arbitrary units [a.u.].} \quad (1.20)$$

According to the error propagation theorem, the standard deviation of the signal intensity ratio is given by

$$\sigma_{194Pt^-_{CDDP}/12CN^-} = \left(\frac{12CN^-}{12C_2^-}\right)^{-1}_{avg} \sqrt{\sigma^2_{\left(194Pt^-_{CDDP}/12C_2^-\right)_{Pt}} + \left(\frac{194Pt^-_{CDDP}}{12C_2^-}\right)^2_{Pt} \sigma^2_{\left(12CN^-/12C_2^-\right)_{avg}}}. \quad (1.21)$$

For estimation of the analytical precision, the variances can be calculated from the measured signal intensities (in counts) as

$$\sigma^2_{194Pt^-_{CDDP}/12C_2^-} = \frac{1}{4}\left[\left(\frac{194Pt^-}{\left(12C_2^-\right)^2} + \frac{\left(194Pt^-\right)^2}{\left(12C_2^-\right)^3}\right)_{ctr} + \left(\frac{194Pt^-}{\left(12C_2^-\right)^2} + \frac{\left(194Pt^-\right)^2}{\left(12C_2^-\right)^3}\right)_{tot}\right] \quad (1.22)$$

$$\sigma^2_{12CN^-/12C_2^-} = \left(1 + R_{15N/14N}\right)^2 \sigma^2_{\left(12C14N^-/12C_2^-\right)_{avg}} + \left(\frac{12C14N^-}{12C_2^-}\right)^2_{avg} \sigma^2_{R_{15N/14N}}, \quad (1.23)$$

where

$$\sigma^2_{\left(12C14N^-/12C_2^-\right)_{avg.}} = \frac{1}{4}\left[\left(\frac{12C14N^-}{\left(12C_2^-\right)^2} + \frac{\left(12C14N^-\right)^2}{\left(12C_2^-\right)^3}\right)_{Pt} + \left(\frac{12C14N^-}{\left(12C_2^-\right)^2} + \frac{\left(12C14N^-\right)^2}{\left(12C_2^-\right)^3}\right)_{15N}\right] \quad (1.24)$$

and

$$\sigma^2_{R_{15N/14N}} = \frac{12C15N^-}{\left(12C14N^-\right)^2} + \frac{\left(12C15N^-\right)^2}{\left(12C14N^-\right)^3} \quad (1.25)$$

References

1. S. C. Dhara, *Indian. J. Chem.*, 1970, **8**, 193-194.
2. Y. Y. Scaffidi-Domianello, A. A. Legin, M. A. Jakupec, A. Roller, V. Y. Kukushkin, M. Galanski and B. K. Keppler, *Inorg. Chem.*, 2012, **51**, 7153-7163.
3. G. Slodzian, F. Hillion, F. J. Stadermann and E. Zinner, *Appl. Surf. Sci.*, 2004, **231-232**, 874-877.
4. G. Slodzian, M. Chaintreau, R. Dennebouy and A. Rousse, *Eur. Phys. J-Appl. Phys.*, 2001, **14**, 199-231.

2.2 Synthesis, characterization, and cytotoxic activity of novel potentially pH-sensitive nonclassical platinum(II) complexes featuring 1,3-dihydroxyacetone oxime ligands

Scaffidi-Domianello Yu. Yu., Legin A. A., Jakupec M. A., Arion B. V., Kukushkin V. Yu. Galanski M., Keppler B. K.

Inorganic Chemistry 2011, **50**, 10673-10681. DOI: 10.1021/ic2010612

Inorganic Chemistry

ARTICLE

pubs.acs.org/IC

Synthesis, Characterization, and Cytotoxic Activity of Novel Potentially pH-Sensitive Nonclassical Platinum(II) Complexes Featuring 1,3-Dihydroxyacetone Oxime Ligands

Yulia Yu. Scaffidi-Domianello,[†] Anton A. Legin,[†,‡] Michael A. Jakupec,[†,‡] Vladimir B. Arion,[†] Vadim Yu. Kukushkin,[§] Markus Galanski,*[,†] and Bernhard K. Keppler*[,†]

[†]Institute of Inorganic Chemistry and [‡]Research Platform "Translational Cancer Therapy Research", University of Vienna, Währinger Strasse 42, A-1090 Vienna, Austria

[§]Department of Chemistry, St. Petersburg State University, 198504 Stary Petergof, Russian Federation

Supporting Information

ABSTRACT: The reaction of 1,3-dihydroxyacetone oxime with diam(m)minediaquaplatinum(II) under basic conditions produced zwitterionic diam(m)mine(3-hydroxy-2-(oxidoimino)propan-1-olato-κ^2N,O)platinum(II) complexes featuring the *N,O*-chelating ligand. Upon reaction with hydrochloric acid, it was possible to isolate either the singly protonated species still exhibiting the intact *N,O*-chelate or the open-chain chlorido complex. All complexes were characterized in detail with multinuclear (^{1}H, ^{13}C, and ^{195}Pt) NMR spectroscopy, ESI mass spectrometry, and in one case X-ray diffraction. Cytotoxicity was investigated in three human cancer cell lines (CH1, SW480, and A549). The obtained IC_{50} values are in the medium or even low micromolar range, remarkable for platinum complexes having N_3O or N_3Cl coordination spheres. To study the solution behavior of the prepared complexes at physiologically relevant proton concentrations, time-dependent ^{1}H NMR measurements were performed for the ethane-1,2-diamine-containing series at pH values of 7.4, 6.0, and exemplarily 5.0. While the zwitterionic complex proved to be stable at both pH 7.4 and 6.0, the protonated species were deprotonated at pH 7.4, tending toward ring opening in slightly acidic environments, as characteristic for many solid tumors. Finally, the open-chain form stayed intact at pH 6.0, being completely converted into its chelated analogue at pH 7.4. A pH-dependent evaluation of antiproliferative effects of the two latter complexes at pH 7.4 and pH 6.0 revealed an activation under slightly acidic conditions, which might be of interest for further *in vivo* studies.

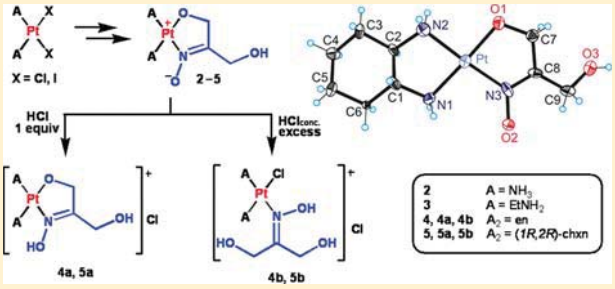

INTRODUCTION

Currently, there are three platinum-based anticancer drugs in worldwide clinical use, viz., cisplatin and carboplatin—mainly but not exclusively applied in the treatment of tumors of the urogenital tract—and oxaliplatin, which is used in colorectal cancer.[1−5] In spite of important achievements of platinum-based chemotherapy, one cannot deny a number of serious drawbacks of platinum medicines, especially severe side effects caused by their unselective reaction with biomolecules. Therefore, development of antitumor complexes attributed with an enhanced selectivity for tumor tissue or increased reactivity at the tumor site is a crucial goal of current cancer research.

Preferably, novel platinum drugs should attack exclusively cancerous cells without affecting the normal ones. However, this bar is almost certainly unreachable in the case of such a complex disease as cancer. Nevertheless, there is a possibility of approximating the ideal situation, developing platinum-based prodrugs almost innocent in the administered form and being activated under certain conditions by conversion within the tumor tissue to their cytotoxic/reactive analogues. Ideally, only the latter form destroys cancer cells.

Several strategies for the design and application of platinum-based drugs which can be activated in the tumor tissue have been developed so far (Figure 1). The first and most abundant class of platinum-based anticancer prodrugs are kinetically inert and unreactive platinum(IV) complexes, which can be converted to more reactive platinum(II) species, taking advantage of the reducing environment in solid tumors (activation by reduction).[2,6−10] The second promising platinum prodrug strategy pursues the development of platinum(IV) species which can be photoactivated, implying that they are inactive in the dark but can be photoreduced to cytotoxic platinum(II) species by visible light,[11−19] with the advantage of external initiation and control of the activation. Third, an intriguing class of platinum-based antitumor prodrugs represents platinum complexes that are inert at physiological pH but which can be activated under slightly acidic pH values, converting platinum species to their cytotoxic/activated form.[20−29]

As far as the latter strategy is concerned, it is worth mentioning that many solid tumors are characterized by a significant acidity

Received: May 19, 2011
Published: September 27, 2011

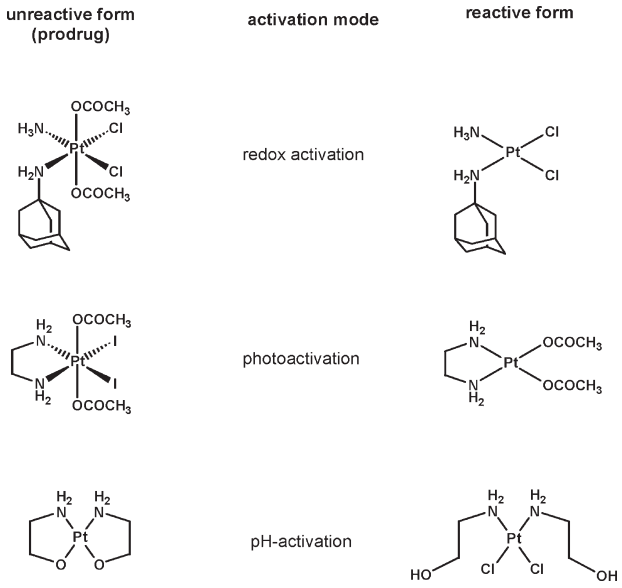

Figure 1. Strategies to activate rather unreactive platinum prodrugs in the tumor tissue.

(pH 5.6−6.8),[30] compared to the normal tissue (pH 7.4), due to their poor blood perfusion, resulting in low oxygen availability.[31] This promotes an increased metabolism of glucose and the production of metabolic acids, such as lactic acid.[32] An acidic milieu within solid tumors could be beneficially used for the application of pH sensitive anticancer platinum drugs kinetically inert and nearly inactive under physiological conditions (the unreactive or prodrug form) and displaying increased cytotoxicity under mildly acidic pH values in tumoral tissues (the activated or reactive form, Figure 1).

Up to now, only two small groups of platinum-based anticancer compounds displaying pH-dependent antitumor activity have been reported, viz., platinum(II) complexes bearing two chelating *O*-alkyldithiocarbonato[20,21] or aminoalcoholato ligands.[22−29] Both of them are, as many chelates, rather inert but can be activated under acidic conditions *via* protonation and subsequent opening of rather thermodynamically stable five-membered rings.

In view of our current interest in platinum(II) oxime complexes[33−37] and their recently reported outstanding cytotoxic properties, appreciably enhanced in the case of *trans*-geometry,[38−40] we focused our efforts on the development of novel oxime-based pH-sensitive platinum prodrugs. The scenario of this work was the following: (*i*) to synthesize and characterize kinetically inert platinum(II) complexes bearing a chelating oxime ligand; (*ii*) to study their pH-dependent behavior, especially at physiologically relevant pH values 7.4 (normal tissue) and 6.0 (tumor tissue); and (*iii*) to evaluate the cytotoxic properties of these compounds in three human tumor cell lines originating from ovarian carcinoma (CH1), colon carcinoma (SW480), and nonsmall cell lung cancer (A549), including a comparative investigation under standard pH screening conditions (pH 7.4) and in an acidified medium (pH 6.0) to figure out whether the concept of pH-dependent activation also works for this novel class of compounds.

RESULTS AND DISCUSSION

Inspired by intriguing cytotoxic properties of (oxime)Pt^{II} complexes,[38−40] we turned our attention to a commercially

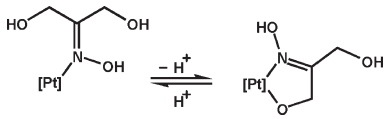

Figure 2. pH-Dependent intramolecular chelation and ring opening of the ligated 1,3-dihydroxyacetone oxime.

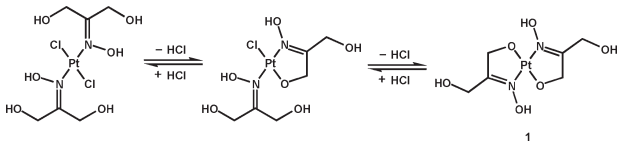

Figure 3. pH-Dependent equilibrium mixture of the opened-, mono-, and bischelated oximeplatinum species.

available 1,3-dihydroxyacetone oxime (IUPAC name:[41] 1,3-dihydroxypropan-2-one oxime) as a promising ligand for the development of novel potentially tumor-inhibiting platinum complexes that are rather inert but which can be activated at acidic pH values. Owing to the presence of three hydroxo groups, the ligand is able to form multiple hydrogen bonds, being of great importance for the binding of platinum compounds to DNA.[42] Moreover, the 1,3-dihydroxyacetone oxime ligand is particularly interesting because it is capable of a pH-dependent intramolecular chelation and ring opening (Figure 2). This reaction could be crucial in view of the lower pH value in solid tumors. Thus, the kinetically inert chelated compound might be applied as a prodrug, being converted into the more (re)active open-chain form at lower pH values in tumor tissues.

Synthesis, Characterization, and X-Ray Structure Determination of Platinum(II) Species with Chelated 1,3-Dihydroxyacetone Oxime. Synthesis of bischelate **1** proceeded in a one-step reaction through the addition of 2 equiv of 1,3-dihydroxyacetone oxime to an aqueous solution of $K_2[PtCl_4]$ at room temperature. As a consequence, an equilibrium mixture of the opened, mono-, and bischelated complexes was formed (Figure 3). The latter species, notable for the lowest solubility, precipitated from the aqueous solution and was isolated (45%) by filtration. An additional portion of the product was formed after the addition of 1M NaOH solution to the filtrate, resulting in a change of pH value from 2.0 to 5.5 and giving an overall yield of 62%.

As starting materials for the preparation of the diam(m)ineplatinum(II) compounds bearing the 3-hydroxy-2-(oxidoimino)-propan-1-olato ligand, we addressed the readily accessible complexes *cis*-$[PtX_2A_2]$, where X = chloride or iodide and A_2 = $(ammine)_2$, $(ethylamine)_2$, ethane-1,2-diamine (en), or (*R*,*R*)-cyclohexane-1,2-diamine [(1*R*,2*R*)-chxn]. The precursors of target species **2**−**5** (Scheme 1) were prepared by a one-step reaction of $K_2[PtX_4]$ with the corresponding am(m)ine or diamine by a reported method.[43,44] Further, halide abstraction using $AgNO_3$ was carried out in an aqueous solution at room temperature, whereupon one equivalent of 1,3-dihydroxyacetone oxime was slowly added in order to avoid/minimize the formation of a bis(oxime)-platinum(II) species. As a next step, the reaction mixture was treated with a basic ion exchanger, leading to deprotonation of both the side-chain and oximic hydroxo group and resulting in the formation of zwitterionic oximato species **2**−**5**. Finally, **2**−**4** were purified by semipreparative HPLC yielding 20−58% of the desired products, while **5** was isolated in 32% yield as a colorless precipitate after concentration of the reaction mixture.

Scheme 1

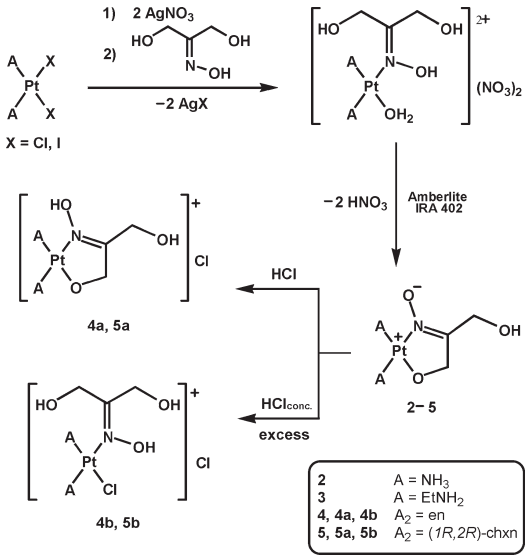

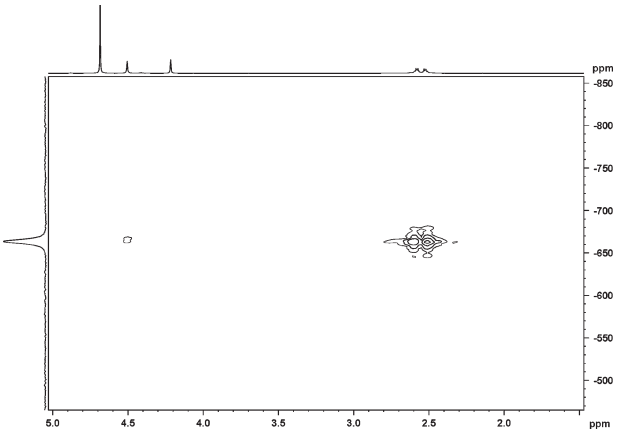

Figure 4. $^{1}H,^{195}Pt$ HMQC NMR spectrum of **4**.

Complexes **1**−**5** were characterized by elemental analyses; ^{1}H, $^{13}C\{^{1}H\}$, and ^{195}Pt NMR and IR spectroscopy; electrospray ionization mass spectrometry (ESI-MS); and also X-ray crystallography (in the case of **5**). All compounds gave satisfactory C, H, and N elemental analyses. The ESI-MS spectrum of **1** exhibited the fragment $[M - H]^-$, while in the spectra of **2**−**5**, $[M + H]^+$ and $[M + Na]^+$ peaks were found. In all cases, the observed and calculated isotopic patterns agreed well with each other.

The IR spectra of **1**−**5** displayed strong to medium ν(OH) and ν(NH) (for **2**−**5**) [2808−3474 cm^{-1}] and medium ν(C=N) [1602−1630 cm^{-1}] stretching vibrations. Chelation of the 1,3-dihydroxyacetone oxime ligand was confirmed (e.g., complex **4**) *via* acquisition of an $^{1}H,^{195}Pt$-HMQC NMR spectrum (Figure 4). Thus, for compound **4**, three correlation peaks were detected, derived from the coupling of the ^{195}Pt nucleus with the protons of the coordinated ethane-1,2-diamine as well as with one of the oxime CH_2 groups located within the chelate ring. The presence of the latter cross-peak undoubtedly proved the fact of the ring closure.

The structure of **5** was determined by X-ray diffraction (Table 1 and Figure 5). The platinum(II) atom has a slightly distorted square-planar coordination geometry. It is coordinated by two ligands, bidentate (*R*,*R*)-cyclohexane-1,2-diamine and a doubly deprotonated 1,3-dihydroxyacetone oxime ligand acting as a bidentate as well. Deviation of the platinum atom from the mean plane through N1, N2, O1, N3 is at 0.011 Å. The bond lengths Pt−N1 = 2.040(11) and Pt−N2 = 2.054(11) Å are in a good agreement with those of oxaliplatin, (SP-4−2)-((*R*,*R*)-cyclohexane-1,2-diamine)oxalato-platinum(II) [Pt−N1 = 2.06(2) Å, Pt−N2 = 2.04(2) Å].[45] The Pt−N3 distance is 1.997(13) Å and correlates well with Pt−N bond lengths in previously reported (oxime)Pt(II) complexes displaying an *N*-bound ligand in the *trans* position to an oxime [1.993−2.032 Å].[46−48] It is worth mentioning that no nitrate counteranions were detected in the structure of **5**, providing additional evidence for the double deprotonation of the 1,3-dihydroxyacetone oxime. The atoms O1 and O2 seem to be deprotonated, acting as proton acceptors in hydrogen bonding interactions with cocrystallized water molecules and the O3−H group of the oxime ligand in the adjacent molecule of **5**.

Table 1. Crystal Data and Details of Data Collection for $5\cdot 2H_2O$

	$5\cdot 2H_2O$
empirical formula	$C_9H_{23}N_3O_5Pt$
fw	448.39
space group	$P2_12_12_1$
a [Å]	7.3783(15)
b [Å]	8.3748(19)
c [Å]	22.125(5)
V [Å^3]	1367.1(5)
Z	4
λ [Å]	0.71073
ρ_{calcd} [g cm^{-3}]	2.178
cryst size [mm^3]	0.40 × 0.02 × 0.01
T [K]	100
μ [mm^{-1}]	10.281
R_1[a]	0.0556
wR_2[b]	0.1145
GOF[c]	1.009

[a] $R_1 = \Sigma||F_o| - |F_c||/\Sigma|F_o|$. [b] $wR_2 = \{\Sigma[w(F_o^2 - F_c^2)^2]/\Sigma[w(F_o^2)^2]\}^{1/2}$. [c] GOF = $\{\Sigma[w(F_o^2 - F_c^2)^2]/(n - p)\}^{1/2}$, where n is the number of reflections and p is the total number of parameters refined.

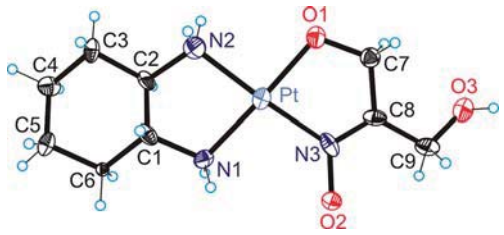

Figure 5. ORTEP view of **5** with the atom labeling scheme. The thermal ellipsoids have been drawn at the 50% probability level. Selected bond lengths (Å) and bond angles (deg): Pt−N1 = 2.040(11), Pt−N2 = 2.054(11), Pt−N3 = 1.997(13), Pt−O1 = 2.006(9); N1−Pt−N2 = 83.4(4), O1−Pt−N3 = 82.5(4).

Protonation of the Oximato Group and Opening of the Oxime Chelate Ring. Above described complexes **4** and **5** were

converted into the corresponding cationic species by the addition of an equivalent amount of hydrochloric acid (pH ≈ 2.5; Scheme 1), whereupon the reaction mixture was immediately frozen and lyophilized in order to avoid further protonation of the ligated oxime and opening of the chelate ring. The compounds **4a** and **5a** were isolated with nearly quantitative yields.

Opening of the oxime chelate ring was performed in an analogous way, adding an excess of HCl_{conc} (about 4 equivs) until a pH of 1 was reached to an aqueous solution of **4** or **5** and stirring the mixture for 24 h at room temperature for completion of the reaction (Scheme 1). Finally, products were isolated *via* lyophilization, resulting in pale-yellow hygroscopic species **4b** and **5b**, obtained in 65% and 72% yield, respectively. Unfortunately, HCl addition to complexes **1**−**3** led to the formation of highly unstable species which could not be isolated.

Complexes **4a**, **4b**, **5a**, and **5b** gave satisfactory elemental analyses and the expected molecular ion/fragmentation patterns in ESI-MS spectra. Thus, $[M - Cl]^+$ and $[M + H]^+$ peaks were detected for **4a** and **5a**, whereas the ESI-MS spectra of **4b** and **5b** exhibited $[M - HCl - Cl]^+$ and $[M - Cl]^+$ signals. The IR spectra of the complexes displayed the characteristic ν(OH) and ν(NH) [2862−3394 cm^{-1}] bands of strong intensity, as well as medium-intensive ν(C═N) [1613−1675 cm^{-1}] bands. In the ^1H NMR spectra, the downfield shifting of the oxime CH_2 group signals as a result of oximato group protonation and consequent chelate ring opening could be clearly observed. Thus, the above-mentioned proton signals appeared at 4.50 and 4.22 ppm for chelated oximato species **4** and **5**, changing to 4.60 and 4.28 ppm for protonated cationic complexes **4a** and **5a**, and finally resonating at 4.98 and 4.60 ppm for open-chain compounds **4b** and **5b**. As expected, the oximato group protonation hardly influenced the chemical shift of the platinum signal in ^{195}Pt NMR spectra (δ_{Pt} = −663 ppm for **4** vs −666 ppm for **4a**). In contrast, the oxime ring opening resulted in a significant shift of the platinum signal (δ_{Pt} = −978 ppm for **4b**) due to the change in the ligand sphere (Cl vs O). Additionally, the presence of the oxime chelate ring for complexes **4a** and **5a** was confirmed by ^1H,^{195}Pt-HMQC NMR.

Time-Dependent NMR Studies Under Physiological and Slightly Acidic Conditions. To elucidate the solution behavior of the prepared complexes at physiologically relevant proton concentrations, time-dependent ^1H NMR measurements at pH values of 7.4, 6.0, and in one case 5.0 were carried out with the most water-soluble ethane-1,2-diamine complexes **4**, **4a**, and **4b**. For that purpose, a phosphate-buffered solution (pH 7.4 and pH 6.0) or a solution of DNO_3 in D_2O (pH 5.0) was used.

The zwitterionic complex **4** proved to be stable at both pH 7.4 and 6.0. Thus, no changes in the NMR spectra were observed during a measurement time of 24 h at ambient temperature. In contrast to **4**, compound **4a**, featuring the protonated oximic group, was immediately deprotonated at pH 7.4 and stayed unchanged for the next 24 h. Expectedly, at pH 6.0, no deprotonation of **4a** took place, but a partial opening of the oximic chelate ring was observed. Hence, small signals of the open-chain form **4b** were visible already 5 min after dissolution and increased with time, 17 h later reaching an equilibrium ratio of 10 to 1 (**4a** versus **4b**), or in other words ∼9% of conversion. This different behavior of **4a** in comparison to **4** at a given pH value is at first sight astonishing but might be explainable due to the presence of chloride ions in the case of **4a**, having an influence on the ring-opening reaction. Additional time-dependent measurements were carried out also at pH 5.0, resulting in ∼12% ring opening after 8 h.

Table 2. Cytotoxicity of the (1,3-Dihydroxyacetone Oxime)Platinum(II) Complexes in CH1, SW480, and A549 Cancer Cells (Exposure Time 96 h)

	IC_{50} [μM]		
compound	CH1	SW480	A549
1	190 ± 20	571 ± 47	>640
2	3.9 ± 1.1	130 ± 23	302 ± 7
3	16 ± 5	277 ± 23	575 ± 86
4	33 ± 9	350 ± 34	>640
4a	15 ± 2	307 ± 6	>320
4b	1.0 ± 0.1	37 ± 9	63 ± 19
5	37 ± 10	33 ± 2	217 ± 36
5a	8.3 ± 3.2	12 ± 3	56 ± 13
5b	1.1 ± 0.2	0.97 ± 0.30	5.6 ± 1.6
cisplatin	0.14 ± 0.3	3.3 ± 0.4	1.3 ± 0.4
oxaliplatin[a]	0.33 ± 0.09	0.30 ± 0.08	

[a] Data taken from ref 49.

As far as complex **4b** is concerned, chelate ring closure takes place while keeping it at a pH of 7.4. Thus, the first signals of **4** appeared within 5 min after dissolution, whereas the complete conversion of **4b** into **4** occurred 25 h later, proving the reversibility of the ring-opening process. As expected, at pH 6.0, no chelation was observed, and the open-chain complex **4b** stayed intact during the measurement time (24 h).

Cytotoxic Activity at Physiologically Relevant Proton Concentrations. The *in vitro* cytotoxicity of complexes **1**−**5**, **4a**, **4b**, **5a**, and **5b** was evaluated in three human cancer cell lines (CH1, SW480, and A549), using the MTT assay (Table 2 and Figures S1−S3, Supporting Information) under standard screening conditions at a pH of 7.4. Of all compounds, the bis(1,3-dihydroxyacetone oxime) complex **1** displayed the lowest antiproliferative potency. For example, in CH1 cells, the IC_{50} value of **1** was 190 times higher compared to the most potent complex in this series. Among zwitterionic ring-closed compounds **2**−**5** (Figure S1, Supporting Information), the nonleaving am(m)ine ligands have a distinct influence on cytotoxic properties. Complexes with monodentate amine ligands (NH_3 in complex **2** or $EtNH_2$ in complex **3**) yielded lower IC_{50} values in the CH1 cell line as compared to complexes **4** or **5** featuring bidentate ethane-1,2-diamine or (*R*,*R*)-cyclohexane-1,2-diamine ligands. However, this cannot be generalized for other, inherently cisplatin-resistant cell lines (such as SW480 and A549), as the (*R*,*R*)-cyclohexane-1,2-diamine ligand (in complex **5**) results in a completely different sensitivity profile analogous to oxaliplatin.

Comparing analogues **4**, **4a**, and **4b** (Figure S2, Supporting Information) or **5**, **5a**, and **5b** (Figures S3, Supporting Information), oxidoimino complexes **4** and **5** showed the lowest cytotoxic potency. A comparable or by trend slightly improved antiproliferative behavior was found in the case of protonated counterparts **4a** and **5a**, respectively, a circumstance which is not explainable at the moment. Ring opening and formation of the chloridoplatinum(II) species **4b** and **5b** was accompanied by a noteworthy lowering of the IC_{50} values (increase in cytotoxicity) down to 1 μM in CH1 cells. The antiproliferative potency is significantly lower compared to cisplatin. However, these cytotoxicities in the low micromolar range are remarkable, taking into account that **4b** and **5b** display three coordinated nitrogen donor atoms (nonclassic platinum complexes). Similar structure−activity relationships were found in SW480 and A549 cells.

Table 3. Comparison of the Cytotoxicities of 4a and 4b in SW480 and A549 Cancer Cells at pH 7.4 and 6.0 (Drug Exposure Time 24 h)

	GI_{50} [μM]			
	SW480		A549	
compound	pH 7.4	pH 6	pH 7.4	pH 6
4a	>640	590 ± 57	>640	373 ± 103
4b	231 ± 42	127 ± 22	438 ± 51	113 ± 31

Not unexpectedly for complexes **1**−**4**, the cytotoxic potency was highest in the cisplatin sensitive cell line CH1 but decreased significantly in inherently cisplatin-resistant SW480 and A549 cells. Contrarily, IC_{50} values for the (*R*,*R*)-cyclohexane-1,2-diamine derivatives **5**, **5a**, and **5b**, were comparable in CH1 (ovarian carcinoma) and SW480 (colon carcinoma) cells. As mentioned above, this pattern is analogous to oxaliplatin, which is clinically approved for the treatment of colorectal cancer (compare with IC_{50} values of oxaliplatin, Table 2).

Protonation and/or ring opening of complexes **2**−**5** in an acidic environment (as observed in many solid tumors) should be accompanied by an enhanced cytotoxic effect. Therefore, ethane-1,2-diamine compound **4a** and its open-chain analog **4b** were exemplarily investigated in SW480 and A549 cells under standard screening conditions at a pH of 7.4 and in an acidified cell culture medium at a pH of 6.0 (Table 3). Note that the drug exposure time was only 24 h, followed by incubation in a drug-free medium at a pH of 7.4 for a further 72 h; consequently, the IC_{50} values are higher in comparison to experiments with 96 h of exposure. Expectedly, antiproliferative activity was improved under acidic conditions in both cell lines for **4a** as well as for **4b**.

Binding of Complex 5b to 5′-GMP. Monodentately bound oxime in **4b** and **5b** may act as a leaving or nonleaving group, leading to either bis- or monoadduct formation with DNA. In order to judge the reactivity, complex **5b** (0.5 mM) was incubated with a 10-fold excess of the model nucleotide 5′-guanosine monophosphate (5′-GMP, 5 mM) in a phosphate buffer (10 mM, pH 6) at 25 °C. The reaction was monitored by electrospray mass spectrometry (ESI-MS).

During the course of incubation, the intensity of the peaks corresponding to **5b** (413 $[M_{\mathbf{5b}} - HCl - Cl]^+$ and 450 $[M_{\mathbf{5b}} - Cl]^+$) was reduced with time in comparison to the peak related to 5′-GMP (408 $[M_{5'\text{-GMP}} + 2Na - H]^+$; Figure S4, Supporting Information). A total of 8 h after the experiment was started, a peak at 776 corresponding to the mono-5′-GMP adduct was detected and attributed to the positively charged species $[M_{\mathbf{5b}} - HCl - Cl + GMP]^+$ ($C_{19}H_{34}N_8O_{11}PPt$, calcd *m*/*z* 776.57; Figure S5, Supporting Information). Signals in the range where bisconjugates of **5b** with 5′-GMP would be expected were not visible in the positive ion mode. With the aim of proving that bifunctional adducts could be detected under these conditions and for reasons of comparison, an experiment was performed with [Pt(*1R*,*2R*-chxn)Cl_2] in parallel. The latter complex is an analogue to **5b**, in which the monodentate oxime ligand was exchanged for chloride, now featuring two chlorido leaving groups [Pt(*1R*,*2R*-chxn)Cl_2] was reacted with 1 equiv of $AgNO_3$ in order to increase the aqueous solubility of the complex). As could be expected, a peak related to the Pt-5′-GMP monoadduct at 708 $[M_{[Pt(1R,2R\text{-chxn})Cl_2]} - Cl + GMP]^+$ ($C_{16}H_{28}ClN_7O_8PPt$, calcd *m*/*z* 707.94) was detected 25 min after the beginning of the incubation, whereupon two peaks corresponding to Pt-5′-GMP bisadducts were observed at 1034 $[M_{[Pt(1R,2R\text{-chxn})Cl_2]} - HCl - Cl + 2GMP]^+$ ($C_{26}H_{41}N_{12}O_{16}P_2Pt$, calcd *m*/*z* 1034.70) and 1056 $[M_{[Pt(1R,2R\text{-chxn})Cl_2]} - 2HCl + 2GMP + Na]^+$ ($C_{26}H_{40}N_{12}O_{16}P_2PtNa$, calcd *m*/*z* 1056.68) after 24 h, increasing with time.

A second experiment was performed with complex **5b** and [Pt(1*R*,2*R*-chxn)Cl_2] under the same conditions, but at 37 °C and with MS detection both in the positive and in the negative ion mode (Figures S6 and S7, Supporting Information). In the positive ion mode, bisconjugates of **5b** with 5′-GMP were not visible. However, bisadduct formation of **5b** after 1 week of incubation with 5′-GMP could be proven by detection of a doubly negatively charged peak at 515.6 corresponding to $[M_{5b} - 2Cl - oxime + 2GMP - 4H]^{2-}$ $C_{26}H_{38}N_{12}O_{16}P_2Pt$, calcd *m*/*z* 515.84), although to a significantly lesser extent compared to [Pt(1*R*,2*R*-chxn)Cl_2]. On the basis of these results, the oxime group may be classified as a leaving ligand. However, whether such a ligand is easily exchangeable in a physiologically relevant time frame cannot be answered yet.

CONCLUSIONS

The results of this work may be considered from two perspectives. In a narrow sense, four novel (3-hydroxy-2-(oxidoimino)propan-1-olato-κ^2N,O)platinum(II) complexes were prepared and completely characterized, along with the protonated and open-chain species in the case of two complexes featuring a bidentate ethane-1,2-diamine or (*R*,*R*)-cyclohexane-1,2-diamine ligand. The cytotoxicity of the investigated compounds in human cancer cells was found in the medium or even low micromolar range, which is remarkable for nonclassic platinum complexes with three coordinated N donor atoms. Interestingly, similar structure−activity relationships were found for two series of complexes featuring ethane-1,2-diamine and (*R*,*R*)-cyclohexane-1,2-diamine ligands. Chelate ring opening improved the IC_{50} values 8 and 15 times, respectively, in CH1 ovarian cancer cells. Time-dependent NMR studies at physiologically relevant pH values, performed for the most water-soluble ethane-1,2-diamine-containing series, showed that zwitterionic oximato complex **4** is stable toward ring opening both at pH 7.4 and at pH 6.0. Differently, protonated form **4a** is being deprotonated to analogue **4** at pH 7.4, while tending to chelate ring-opening in an acidic medium. As discussed above, this different behavior of complex **4a** in comparison to **4** at a given pH value is most probably the result of the presence of one equivalent of chloride ions in the case of **4a**. In contrast, open-chain species **4b**, stable at pH 6.0, was completely converted into the ring-closed form **4** at pH 7.4. Comparative investigation of the cytotoxic potency of complexes **4a** and **4b** under standard cell line screening conditions (pH 7.4) and in an acidified cell culture medium (pH 6.0) showed a significant increase of antiproliferative activity under slightly acidic conditions. Whether this pH-dependent activation is of relevance for the *in vivo* situation will be the subject of our future research program.

In a wider sense, this research is an important contribution to the development of inert and unreactive complexes (prodrugs) which can be activated in the tumor tissue. From this point of view, a number of novel oxime-based pH-sensitive potential platinum prodrugs have been prepared. Moreover, in this work, we have demonstrated the possibility of reversible pH-dependent intramolecular chelation and ring-opening reaction for the novel complexes as well as an increase of their cytotoxic potency under the

slightly acidic conditions characteristic for many solid tumor tissues. However, the prepared 3-hydroxy-2-(oxidoimino)propan-1-olato species proved to be less accessible to protonation at slightly acidic pH values than, for instance, the previously reported aminoalcoholato or *O*-alkyldithiocarbonato complexes. A promising strategy to facilitate the chelate ring opening under acidic conditions could be introducing, e.g., an alkyl substituent into the 1,3-dihydroxyacetone oxime ligand, which should result in a decrease of acidity of the side-chain hydroxo group due to its positive inductive effect. As a consequence, complexes of a weaker acid are probably easier to protonate, which should favor the formation of the open-chain species. Investigation of these aspects is ongoing.

EXPERIMENTAL SECTION

General Procedures. Potassium tetrachloridoplatinate and 1,3-dihydroxyacetone oxime were supplied by Johnson Matthey and TCI, respectively. Ammonium hydroxide solution (25% in water), ethylamine solution (70% in water), and (*R*,*R*)-cyclohexane-1,2-diamine [(1*R*,2*R*)-chxn] were purchased from Fluka, while ethane-1,2-diamine (en) was obtained from Aldrich. All of these chemicals were used as received without further purification. The complexes *cis*-$[PtI_2(NH_3)_2]$, *cis*-$[PtI_2(EtNH_2)_2]$, $[PtCl_2(en)]$, and $[PtCl_2\{(1R,2R)\text{-chxn}\}]$ were prepared according to standard literature procedures starting from $K_2[PtCl_4]$.[43,44] Bidistilled water was used. The synthetic procedures were carried out in a light-protected environment due to the known photosensitivity of some platinum species.[50] For HPLC separation, a semipreparative 250 × 20 mm Kromasil 100 Å C18 10 μm column was used. C, H, and N elemental analyses were carried out by the elemental analyses laboratory of the University of Vienna using a Perkin-Elmer 2400 CHN elemental analyzer. ESI-MS spectra were obtained with a Bruker Esquire 3000 instrument. IR spectra were obtained by using an ATR unit with a Perkin-Elmer 370 FTIR 2000 instrument (4000−400 cm^{-1}). ^1H, $^{13}C\{1H\}$, ^{195}Pt, and two-dimensional NMR spectra were measured with a Bruker Avance III 500 MHz NMR spectrometer at 500.32 (^1H), 125.81 (^{13}C), and 107.55 MHz (^{195}Pt), correspondingly, at 298 K. ^{195}Pt chemical shifts are referenced relative to $K_2[PtCl_4]$, and the half-height line width is given in parentheses.

Synthesis of the Platinum(II) Complexes with Chelated 1,3-Dihydroxyacetone Oxime. (SP-4−1)-Bis(3-hydroxy-2-(hydroxyimino)propan-1-olato-κ^2N,O)platinum(II) (1). $K_2[PtCl_4]$ (121.0 mg, 0.29 mmol) was dissolved in 2.5 mL of H_2O; then 1,3-dihydroxyacetone oxime (61.0 mg, 0.58 mmol) was added. The reaction mixture was stirred at room temperature overnight. Formation of a colorless precipitate was observed, which was filtered off. Then, 1M NaOH solution (160 μL, 0.16 mmol) was added to the yellow filtrate (pH value changed from 2.0 to 5.5), and the reaction mixture was stirred at room temperature for 24 h. An additional portion of the colorless precipitate formed was filtered off, combined with the first portion, washed twice with 0.5 mL of ice-cold water, and dried *in vacuo* at room temperature. Yield: 73 mg (62%). Anal. Calcd. for $C_6H_{12}N_2O_6Pt$: C, 17.87; H, 3.00; N, 6.95. Found: C, 18.02; H, 2.82; N, 6.89%. ESI-MS^- (H_2O/MeOH), *m*/*z*: 402 $[M - H]^-$. IR in KBr (selected bands), cm^{-1}: 3474 s, 3422 s ν(OH), 1615 m ν(C═N). ^1H NMR (D_2O): δ 4.59 (s, br, OCH_2,), 4.28 (s, br, $HOCH_2$). $^{13}C\{^1H\}$ NMR (D_2O): δ 166.2 (*C*═N), 71.8 (OCH_2), 55.3 ($HOCH_2$). ^{195}Pt NMR (D_2O): δ −137 (780 Hz).

General Synthesis of (SP-4−3)-Diam(m)ine(3-hydroxy-2-(oxidoimino)propan-1-olato-κ^2N,O)platinum(II). $[PtX_2A_2]$ (0.50 mmol) and $AgNO_3$ (1.0 mmol) were mixed and suspended in 10 mL of H_2O, whereupon the mixture was stirred at room temperature overnight. The precipitate of AgX was filtered off, and a solution of 1,3-dihydroxyacetone oxime (0.50 mmol) in 2 mL of H_2O was added slowly (dropwise within 1−2 h). After the reaction mixture was stirred at the same temperature for 12 h, it was diluted with 50 mL of H_2O and subsequently mixed with approximately 3 g of a preconditioned basic anion exchange resign, Amberlite IRA 402 (the commercially available chloride form was treated with 30 mL of 2M NaOH for 30 min and washed with deionized water until a pH of 7), and the mixture was stirred for several minutes. After the ion-exchanger turned from slightly yellow to dark-gray (pH∼9−10), it was filtered off, and the fine precipitate of platinum black (formed in small amount) was removed by filtration through a Glass Microfibre 696. In the case of **2**−**4**, the resulting yellow solution was evaporated to dryness, and 15 mL of acetone was added. The yellow solid formed was filtered off, washed with acetone (2 × 1 mL), and dried *in vacuo*. After that, the crude product was purified through semipreparative HPLC (H_2O/MeOH 98/2 for **2** and **4**, H_2O/MeOH 95/5 for **3**) and lyophilized. In the case of **5**, the yellowish filtrate was reduced to 0.5 mL and placed into the fridge (+5 °C) for 2 h. The colorless precipitate formed was filtered off, washed twice with a few drops of ice-cold H_2O, and dried *in vacuo*. The yields were 25% (**2**), 20% (**3**), 58% (**4**), and 32% (**5**).

(SP-4−3)-Diammine(3-hydroxy-2-(oxidoimino)propan-1-olato-κ^2N,O)platinum(II) (2). Anal. Calcd. for $C_3H_{11}N_3O_3Pt\cdot 2H_2O$: C, 9.78; H, 4.11; N, 11.41. Found: C, 10.18; H, 3.77; N, 11.05%. ESI-MS^+ (H_2O/MeOH), *m*/*z*: 333 $[M + H]^+$, 355 $[M + Na]^+$. IR in KBr (selected bands), cm^{-1}: 3092 s, 2987 s, 2808 m ν(OH) and ν(NH), 1630 m ν(C═N). ^1H NMR (D_2O): δ 4.51 (m, 2H, OCH_2), 4.23 (m, 2H, $HOCH_2$). $^{13}C\{^1H\}$ NMR (D_2O): δ 168.1 (*C*═N), 73.6 (OCH_2), 56 ($HOCH_2$). ^{195}Pt NMR (D_2O): δ −527 (800 Hz).

(SP-4−3)-Bis(ethylamine)(3-hydroxy-2-(oxidoimino)propan-1-olato-κ^2N,O)platinum(II) (3). Anal. Calcd. for $C_7H_{19}N_3O_3Pt\cdot 1/2H_2O$: C, 21.16; H, 5.07; N, 10.58. Found: C, 20.90; H, 4.66; N, 10.21%. ESI-MS^+ (H_2O/MeOH), *m*/*z*: 344 $[M - EtNH_2 + H]^+$, 389 $[M + H]^+$, 411 $[M + Na]^+$. ESI-MS^- (H_2O/MeOH), *m*/*z*: 433 $[M - Cl]^-$. IR in KBr (selected bands), cm^{-1}: 3200 s, 3128 s, 3068 s ν(OH) and ν(NH), 1606 ν(C═N). ^1H NMR (D_2O): δ 4.57 (m, 2H, OCH_2), 4.30 (m, 2H, $HOCH_2$), 2.66 (m, 4H, $2CH_3CH_2$), 1.17 (t, 6H, $2CH_3$, $^3J_{H,H}$ = 6.9 Hz). $^{13}C\{^1H\}$ NMR (D_2O): δ 176.2 (*C*═N), 73.1 (OCH_2), 56.3 ($HOCH_2$), 41.9 (CH_3CH_2), 41.3 (CH_3CH_2), 15.6 ($2CH_3$). ^{195}Pt NMR (D_2O): δ −589 (720 Hz).

(SP-4−3)-(Ethane-1,2-diamine)(3-hydroxy-2-(oxidoimino)propan-1-olato-κ^2N,O)platinum(II) (4). Anal. Calcd. for $C_5H_{13}N_3O_3Pt\cdot H_2O$: C, 16.35; H, 3.84; N, 11.44. Found: C, 16.68; H, 3.45; N, 11.14%. ESI-MS^+ (H_2O/MeOH), *m*/*z*: 359 $[M + H]^+$. IR in KBr (selected bands), cm^{-1}: 3177 m, 2935 s, 2889 s ν(OH) and ν(NH), 1618 m ν(C═N). ^1H NMR (D_2O): δ 4.50 (m, 2H, OCH_2), 4.22 (m, 2H, $HOCH_2$), 2.55 (m, 4H, $2CH_2$). $^{13}C\{^1H\}$ NMR (D_2O): δ 168.3 (*C*═N), 73.6 (OCH_2), 55.9 ($HOCH_2$), 46.43 (CH_2), 46.36 (CH_2). ^{195}Pt NMR (D_2O): δ −663 (600 Hz).

(SP-4−3)-{(*R*,*R*)-Cyclohexane-1,2-diamine}(3-hydroxy-2-(oxidoimino)propan-1-olato-κ^2N,O)platinum(II) (5). Anal. Calcd. for $C_9H_{19}N_3O_3Pt\cdot H_2O$: C, 25.12; H, 4.92; N, 9.76. Found: C, 24.78; H, 4.71; N, 9.49%. ESI-MS^+ (H_2O/MeOH), *m*/*z*: 413 $[M + H]^+$. IR in KBr (selected bands), cm^{-1}: 3184 s, 3100 s, 2937 m ν(OH) and ν(NH), 1602 m ν(C═N). ^1H NMR (MeOD): δ 4.66 (m, 2H, OCH_2), 4.34 (m, 2H, $HOCH_2$), 2.32 (m, 2H, 2*CH*), 2.03 (m, 2H, CH_2), 1.64 (m, 2H, CH_2), 1.33 (m, 2H, CH_2), 1.23 (m, 2H, CH_2). $^{13}C\{^1H\}$ NMR (MeOD): δ 167.5 (*C*═N), 74.2 (OCH_2), 61.2 (*CH*), 60.9 (*CH*), 56.5 ($HOCH_2$), 32.7 (CH_2), 32.5 (CH_2), 24.3 (CH_2), 24.2 (CH_2). ^{195}Pt NMR (MeOD): δ −610 (630 Hz). Crystals for X-ray study were obtained by slow evaporation of a water solution at room temperature.

Protonation of the Chelated Platinum(II) Oximato Species. In a typical experiment, 1 equiv of 1.2M HCl was added to a solution/suspension of **4** or **5** (0.1 mmol) in 10 mL of H_2O, resulting in the change of the solution color from pale- to bright-yellow. The reaction mixture was immediately frozen and lyophilized. The products **4a** and **5a** were isolated as colorless solids in almost quantitative yield.

(SP-4−3)-(Ethane-1,2-diamine)(3-hydroxy-2-(hydroxyimino) propan-1-olato-κ^2N,O)platinum(II) Chloride (4a). Anal. Calcd. for $C_5H_{14}N_3O_3ClPt \cdot 1/2H_2O$: C, 14.87; H, 3.74; N, 10.41. Found: C, 15.06; H, 3.78; N, 9.98%. ESI-MS$^+$ (H_2O/MeOH), m/z: 359 $[M - Cl]^+$, 396 $[M + H]^+$. ESI-MS$^-$ (H_2O/MeOH), m/z: 394 $[M - H]^-$, 430 $[M + Cl]^-$. IR (selected bands), cm^{-1}: 3353 m, 3224 s, 3055 s, 2966 s ν(OH) and ν(NH), 1675 m ν(C═N). ^{1}H NMR (D_2O): δ 5.16 (m, 4H, 2NH_2), 4.67 (s, 2H, OCH_2), 4.33 (s, 2H, HOCH_2), 2.55 (m, 4H, 2CH_2). ^{13}C{^{1}H} NMR (D_2O): δ 160.2 (C═N), 73.8 (OCH_2), 56.2 (HOCH_2), 46.7 (CH_2), 46.5 (CH_2). ^{195}Pt NMR (D_2O): δ −666 (960 Hz).

(SP-4−3)-{(*R*,*R*)-Cyclohexane-1,2-diamine}(3-hydroxy-2-(hydroxyimino)propan-1-olato-κ^2N,O)platinum(II) Chloride (5a). Anal. Calcd. for $C_9H_{20}N_3O_3ClPt \cdot 1/2H_2O$: C, 23.61; H, 4.62; N, 9.18. Found: C, 23.57; H, 4.49; N, 8.91%. ESI-MS$^+$ (H_2O/MeOH), m/z: 413 $[M - Cl]^+$, 435 $[M - HCl + Na]^+$, 450 $[M + H]^+$. IR in KBr (selected bands), cm^{-1}: 3394 s, 3191 s, 3067 s, 2938 s ν(OH) and ν(NH), 1613 m ν(C═N). ^{1}H NMR (D_2O): δ 4.60 (s, 2H, OCH_2), 4.28 (s, 2H, HOCH_2), 2.32 (m, 2H, 2CH), 1.97 (m, 2H, CH_2), 1.51 (m, 2H, CH_2), 1.22 (m, 2H, CH_2), 1.09 (m, 2H, CH_2). ^{13}C{^{1}H} NMR (D_2O): δ 174.9 (C═N), 73.8 (OCH_2), 61.1 (CH), 61.0 (CH), 56.1 (HOCH_2), 32.3 (CH_2), 32.2 (CH_2), 24.0 (CH_2), 23.9 (CH_2). ^{195}Pt NMR (D_2O): δ −636 (870 Hz).

Oxime Chelate Ring Opening. In a typical experiment, 4 equiv of HCl_{conc} was added to a solution/suspension of **4** or **5** (0.2 mmol) in 5 mL of H_2O, and the reaction mixture was stirred for 24 h at room temperature. A small amount of a brownish-yellow solid formed was filtered off through a Glass Microfibre 696. The resulting clear yellow solution was lyophilized, giving hygroscopic pale-yellow solids of **4b** and **5b**. Yields of **4b** and **5b** were 65% and 72%, respectively.

(SP-4−3)-Chlorido(1,3-dihydroxoacetone Oxime-κN)-(Ethane-1,2-diamine)platinum(II) Chloride (4b). Anal. Calcd. for $C_5H_{15}N_3O_3Cl_2Pt \cdot H_2O$: C, 13.37; H, 3.81; N, 9.35. Found: C, 13.74; H, 3.59; N, 9.04%. ESI-MS$^+$ (H_2O/MeOH), m/z: 359 $[M - HCl - Cl]^+$, 396 $[M - Cl]^+$. IR (selected bands), cm^{-1}: 3380 s, 3249 s, 3193 s, 3094 s, 2994 m ν(OH) and ν(NH), 1647 m ν(C═N). ^{1}H NMR (D_2O): δ 5.57 (m, 2H, 2NH_2), 5.37 (m, 2H, 2NH_2), 4.97 (s, 2H, HOCH_2), 4.60 (s, 2H, HOCH_2), 2.61 (m, 4H, 2CH_2). ^{13}C{^{1}H} NMR (D_2O): δ 169.2 (C═N), 60.6 (HOCH_2), 57.3 (HOCH_2), 48.2 (CH_2), 47.7 (CH_2). ^{195}Pt NMR (D_2O): δ −978 (670 Hz).

(SP-4−3)-Chlorido{(*R*,*R*)-cyclohexane-1,2-diamine}(1,3-dihydroxyacetone Oxime-κN)platinum(II) Chloride (5b). Anal. Calcd. for $C_9H_{21}N_3Cl_2O_3Pt$: C, 22.28; H, 4.36; N, 8.66. Found: C, 22.10; H, 4.23; N, 8.26%. ESI-MS$^+$ (H_2O/MeOH), m/z: 413 $[M - HCl - Cl]^+$, 450 $[M - Cl]^+$. IR in KBr (selected bands), cm^{-1}: 3183 s, 3083 s, 2937 s, 2862 m ν(OH) and ν(NH), 1647 m ν(C═N). ^{1}H NMR (D_2O): δ 5.91 (m, 1H, NHH), 5.62 (m, 1H, NHH), 5.04 (m, 2H, 2NHH), 4.98 (s, 2H, HOCH_2), 4.60 (s, 2H, HOCH_2), 2.46 (m, 1H, CH), 2.38 (m, 1H, CH), 1.99 (m, 2H, CH_2), 1.53 (m, 2H, CH_2), 1.26 (m, 2H, CH_2), 1.09 (m, 2H, CH_2). ^{13}C{^{1}H} NMR (D_2O): δ 169.1 (C═N), 62.8 (HOCH_2), 62.2 (HOCH_2), 60.7 (CH), 57.3 (CH), 32.0 (CH_2), 31.8 (CH_2), 23.8 (CH_2), 23.7 (CH_2). ^{195}Pt NMR (D_2O): δ −945 (670 Hz).

^{1}H NMR (DMF-d_6): δ 12.44 (s, 1H, HON), 6.91 (m, 1H, NHH), 6.22 (m, 1H, NHH), 5.99 (m, 1H, NHH), 5.57 (m, 1H, NHH), 5.08 (d, 1H, HOCHH, $^3J_{H,H}$ = 12.8 Hz), 5.00 (d, 1H, HOCHH, $^3J_{H,H}$ = 12.8 Hz), 4.60 (s, 2H, HOCH_2), 2.54 (m, 2H, 2CH), 2.10 (m, 2H, CH_2), 1.57 (m, 2H, CH_2), 1.49 (m, 2H, CH_2), 1.15 (m, 2H, CH_2). ^{13}C{^{1}H} NMR (DMF-d_6): δ 170.5 (C═N), 62.8 (HOCH_2), 62.3 (HOCH_2), 60.8 (CH), 57.1 (CH), 32.3 (CH_2), 31.7 (CH_2), 24.5 (CH_2), 24.3 (CH_2). ^{15}N NMR (DMF-d_6): δ −22.6 (NH_2), −10.7 (NH_2). ^{195}Pt NMR (DMF-d_6): δ −933 (500 Hz).

Crystal Structure Determination. X-ray diffraction measurement for **5** · $2H_2O$ was performed on a Bruker X8 APEXII CCD diffractometer. A single crystal was positioned at 35 mm from the detector, and 1330 frames were measured, each for 60 s over 1° scan width. The data were processed using SAINT software.[51] Crystal data, data collection parameters, and structure refinement details are given in Table 1. The structure was solved by direct methods and refined by full-matrix least-squares techniques. Non-H atoms were refined with anisotropic displacement parameters. H atoms were inserted in calculated positions and refined with a riding model. The structure solution was achieved with *SHELXS-97*[52] and refinement with *SHELXL-97*,[53] and graphics were produced with *ORTEP-3*.[54]

Cell Lines and Culture Conditions. The human cancer cell lines CH1 (ovarian carcinoma), kindly provided by Lloyd R. Kelland (CRC Centre for Cancer Therapeutics, Institute of Cancer Research, Sutton, UK), as well as A549 (nonsmall cell lung cancer) and SW480 (colon carcinoma), both provided by Brigitte Marian (Institute of Cancer Research, Department of Medicine I, Medical University of Vienna, Austria), were used for the experiment. Cells were grown in 75 cm^2 culture flasks (Iwaki/Asahi Technoglass, Gyouda, Japan) as adherent monolayer cultures in a complete medium [i.e., Minimal Essential Medium (MEM) supplemented with 10% heat-inactivated fetal bovine serum, 1 mM sodium pyruvate, 2 mM L-glutamine, and 1% nonessential amino acids for the standard condition experiments and bicarbonate-free Dulbecco's Modified Eagles Medium (DMEM) supplemented with 10% heat-inactivated fetal bovine serum, 1 mM sodium pyruvate, 4 mM L-glutamine, 1% nonessential amino acids, and 8.8 mM (pH 6.0) or 39.6 mM (pH 7.4) sodium bicarbonate for pH-dependent experiments (all purchased from Sigma-Aldrich, Austria)]. Cell cultures were incubated at 37 °C in a moist atmosphere containing 5% CO_2 (standard conditions) or 8% CO_2 (pH-dependent experiments).

Cytotoxicity Tests in Cancer Cell Lines. The cytotoxic activity of the compounds was determined by means of a colorimetric microculture assay (MTT assay, MTT = 3-(4,5-dimethyl-2-thiazolyl)-2,5-diphenyl-2H-tetrazolium bromide). A549, CH1, and SW480 cells were harvested from culture flasks by trypsinization and seeded in 100 μL aliquots in MEM into 96-well plates (Iwaki/Asahi Technoglass, Gyouda, Japan) in cell densities of 3×10^3, 1×10^3, and 2.5×10^3 cells per well, respectively. After 24 h of preincubation of the cells, the test compounds were dissolved in a complete medium and then added in aliquots of 100 μL per well. After continuous exposure for 96 h, drug solutions were replaced with 100 μL of RPMI 1640 medium (supplemented with 10% heat-inactivated fetal bovine serum and 2 mM L-glutamine) plus 20 μL of MTT solution in phosphate-buffered saline (5 mg/mL). After incubation for 4 h, the medium/MTT mixtures were removed, and the formazan crystals formed by viable cells were dissolved in 150 μL of DMSO per well. Optical densities at 550 nm were measured with a microplate reader (Tecan Spectra Classic), using a reference wavelength of 690 nm to correct for unspecific absorption. The quantity of viable cells was expressed in terms of T/C values by comparison to untreated control microcultures, and 50% inhibitory concentrations (IC_{50}) were calculated from concentration-effect curves by interpolation. Evaluation is based on means from at least three independent experiments, each comprising three replicates per concentration level. For pH-dependent experiments, A549 and SW480 cells were harvested from culture flasks by trypsinization and seeded in 100 μL aliquots in DMEM (pH 7.4) into 96-well plates in cell densities of 3×10^3 and 4×10^3 cells per well, respectively. After 24 h, the medium from adherent microcultures was removed, and cells were exposed to the drug solutions (200 μL per well) for another 24 h in a moist atmosphere containing 8% CO_2 at 37 °C (for drugs dissolved in DMEM pH 6) and 5% CO_2 at 37 °C (for drugs dissolved in DMEM pH 7.4), followed by incubation in drug-free DMEM (pH 7.4) for a further 72 h. Further incubation and measurements were performed as described above.

Binding of Complex 5b to 5′-GMP. For investigating the time-dependent binding of 5′-GMP to complex **5b**, the complex (0.5 mM) was incubated with 5′-GMP (5 mM) in a phosphate buffer (10 mM, pH 6)

at 25 °C. In parallel, an experiment was performed with [Pt(*1R,2R*-chxn)Cl_2] under the same conditions. A second experiment was performed with complex **5b** under the same conditions, but at 37 °C. The progress of the reaction was monitored by electrospray mass spectrometry (ESI-MS) in the positive as well as in the negaive ion mode.

■ ASSOCIATED CONTENT

Supporting Information. Figures with concentration-effect curves of complexes **1**−**5**, **4a**, **4b**, **5a**, and **5b** in CH1 cells. Figures with ESI-MS spectra of **5b** incubated with 5′-GMP. X-ray crystallographic file in CIF format for **5**. This material is available free of charge via the Internet at http://pubs.acs.org.

■ AUTHOR INFORMATION

Corresponding Author

*Phone: +43-1-4277-52600. Fax: +43-1-4277-52680. E-mail: markus.galanski@univie.ac.at, bernhard.keppler@univie.ac.at.

■ ACKNOWLEDGMENT

The authors are indebted to the FFG—Austrian Research Promotion Agency, the Austrian Council for Research and Technology Development, and COST D39. V.Y.K. is grateful to RFBR for grant 11-03-90417.

■ REFERENCES

(1) Jakupec, M. A.; Galanski, M.; Keppler, B. K. *Rev. Physiol. Biochem. Pharmacol.* **2003**, *146*, 1–54.
(2) Galanski, M.; Jakupec, M. A.; Keppler, B. K. *Curr. Med. Chem.* **2005**, *12*, 2075–2094.
(3) Galanski, M.; Arion, V. B.; Jakupec, M. A.; Keppler, B. K. *Curr. Pharm. Des.* **2003**, *9*, 2078–2089.
(4) O'Dwyer, P. J.; Stevenson, J. P.; Johnson, S. W. *Drugs* **2000**, *59*, 19–27.
(5) Cvitkovic, E.; Bekradda, M. *Semin. Oncol.* **1999**, *26*, 647–662.
(6) Hall, M. D.; Mello, H. R.; Callaghan, R.; Hambley, T. W. *J. Med. Chem.* **2007**, *50*, 3403–3411.
(7) Reithofer, M. R.; Valiahdi, S. M.; Jakupec, M. A.; Arion, V. B.; Egger, A.; Galanski, M.; Keppler, B. K. *J. Med. Chem.* **2007**, *50*, 6692–6699.
(8) Reithofer, M. R.; Schwarzinger, A.; Valiahdi, S. M.; Galanski, M.; Jakupec, M. A.; Keppler, B. K. *J. Inorg. Biochem.* **2008**, *102*, 2072–2077.
(9) Reithofer, M. R.; Valiahdi, S. M.; Galanski, M.; Jakupec, M. A.; Arion, V. B.; Keppler, B. K. *Chem. Biodiv.* **2008**, *5*, 2160–2170.
(10) Reithofer, M. R.; Bytzek, A. K.; Valiahdi, S. M.; Kowol, C. R.; Groessl, M.; Hartinger, C. G.; Jakupec, M. A.; Galanski, M.; Keppler, B. K. *J. Inorg. Biochem.* **2011**, *105*, 46–51.
(11) Bednarski, P. J.; Mackay, F. S.; Sadler, P. J. *Anti-Cancer Agents Med. Chem.* **2007**, *7*, 75–93.
(12) Brunner, H.; Schellerer, K.-M. *Z. Naturforsch., B: Chem. Sci.* **2002**, *57*, 751–756.
(13) Lottner, C.; Bart, K.-C.; Bernhardt, G.; Brunner, H. *J. Med. Chem.* **2002**, *45*, 2064–2078.
(14) Lottner, C.; Bart, K.-C.; Bernhardt, G.; Brunner, H. *J. Med. Chem.* **2002**, *45*, 2079–2089.
(15) Brunner, H.; Schellerer, K.-M. *Monatsh. Chem.* **2002**, *133*, 679–705.
(16) Brunner, H.; Schellerer, K.-M. *Inorg. Chim. Acta* **2003**, *350*, 39–48.
(17) Kratochwil, N. A.; Parkinson, J. A.; Bednarski, P. J.; Sadler, P. J. *Angew. Chem., Int. Ed.* **1999**, *38*, 1460–1463.
(18) Kratochwil, N. A.; Zabel, M.; Range, K.-J.; Bednarski, P. J. *J. Med. Chem.* **1996**, *39*, 2499–2507.
(19) Muller, P.; Schroder, B.; Parkinson, J. A.; Kratochwil, N. A.; Coxall, R. A.; Parkin, A.; Parsons, S.; Sadler, P. J. *Angew. Chem., Int. Ed.* **2003**, *42*, 335–339.
(20) Friebolin, W.; Schilling, G.; Zoeller, M.; Amtmann, E. *J. Med. Chem.* **2004**, *47*, 2256–2263.
(21) Amtmann, E.; Zoller, M.; Wesch, H.; Schilling, G. *Cancer Chemother. Pharmacol.* **2001**, *47*, 461–466.
(22) Zimmermann, W.; Galanski, M.; Keppler, B. K.; Giester, G. *Inorg. Chim. Acta* **1999**, *292*, 127–130.
(23) Zimmermann, W.; Galanski, M.; Keppler, B. K.; Fiebig, H. H.; Burger, A. M. *Contr. Oncol.* **1999**, *54*, 447–450.
(24) Galanski, M.; Zimmermann, W.; Baumgartner, C.; Keppler, B. K. *Eur. J. Inorg. Chem.* **2001**, 1145–1149.
(25) Robillard, M. S.; Galanski, M.; Zimmermann, W.; Keppler, B. K.; Reedijk, J. *J. Inorg. Biochem.* **2002**, *88*, 254–259.
(26) Galanski, M.; Baumgartner, C.; Arion, V.; Keppler, B. K. *Eur. J. Inorg. Chem.* **2003**, 2619–2625.
(27) Galanski, M.; Baumgartner, C.; Meelich, K.; Arion, V. B.; Fremuth, M.; Jakupec, M. A.; Schluga, P.; Hartinger, C. G.; von Keyserlingk, N. G.; Keppler, B. K. *Inorg. Chim. Acta* **2004**, *357*, 3237–3244.
(28) Schluga, P.; Hartinger, C. G.; Galanski, M.; Meelich, K.; Timerbaev, A. R.; Keppler, B. K. *Analyst* **2005**, *130*, 1383–1389.
(29) van Zupfen, S.; Stone, E. A.; van Rijt, S.; Robillard, M. S.; Van der Marel, G. A.; Overkleeft, H. S.; Den Dulk, H.; Brouwer, J.; Reedijk, J. *J. Inorg. Biochem.* **2005**, *99*, 2032–2038.
(30) Lindner, D.; Raghavan, D. *Br. J. Cancer* **2009**, *100*, 1287–1291.
(31) Yotnda, P.; Wu, D.; Swanson, A. M. *Methods Mol. Biol.* **2010**, *651*, 1–29.
(32) Chiche, J.; Brahimi-Horn, M. C.; Pouyssegur, J. *J. Cell. Mol. Med.* **2010**, *14*, 771–794.
(33) Kukushkin, V. Yu.; Belsky, V. K.; Tudela, D. *Inorg. Chem.* **1996**, *35*, 510–513.
(34) Kukushkin, V. Yu.; Nishioka, T.; Tudela, D.; Isobe, K.; Kinoshita, I. *Inorg. Chem.* **1997**, *36*, 6157–6165.
(35) Kukushkin, V. Yu.; Belsky, V. K.; Tudela, D. *Inorg. Chem.* **1996**, *35*, 510–513.
(36) Kukushkin, V. Yu.; Pombeiro, A. J. L. *Coord. Chem. Rev.* **1999**, *181*, 147–175.
(37) Kukushkin, V. Yu.; Izotova, Y. A.; Tudela, D.; Guedes da Silva, M. F. C.; Pombeiro, A. J. L. *Inorg. Synth.* **2004**, *34*, 81–85.
(38) Scaffidi-Domianello, Yu. Yu.; Meelich, K.; Jakupec, M. A.; Arion, V. B.; Kukushkin, V. Yu.; Galanski, M.; Keppler, B. K. *Inorg. Chem.* **2010**, *49*, 5669–5678.
(39) Quiroga, A. G.; Cubo, L.; de Blas, E.; Aller, P.; Navarro-Ranninger, C. *J. Inorg. Biochem.* **2007**, *101*, 104–110.
(40) Zorbas-Seifried, S.; Jakupec, M. A.; Kukushkin, N. V.; Groessl, M.; Hartinger, C. G.; Semenova, O.; Zorbas, H.; Kukushkin, V. Yu.; Keppler, B. K. *Mol. Pharmacol.* **2007**, *71*, 357–65.
(41) IUPAC. http://www.iupac.org/nomenclature/ (accessed Sep 2011).
(42) Reedijk, J. *Inorg. Chim. Acta* **1992**, *198*−*200*, 873–881.
(43) Dhara, S. C. *Indian J. Chem.* **1970**, *8*, 193–194.
(44) Kemp, S.; Wheate, N. J.; Buck, D. P.; Nikac, M.; Collins, J. G.; Aldrich-Wright, J. R. J. *Inorg. Biochem.* **2007**, *101*, 1049–1058.
(45) Bruck, M. A.; Bau, R.; Noji, M.; Inagaki, K.; Kidani, Y. *Inorg. Chim. Acta* **1984**, *92*, 279–284.
(46) Scaffidi-Domianello, Yu. Yu.; Meelich, K.; Jakupec, M. A.; Arion, V. B.; Kukushkin, V. Yu.; Galanski, M.; Keppler, B. K. *Inorg. Chem.* **2010**, *49*, 5669–5678.
(47) Kukushkin, V. Yu.; Tudela, D.; Izotova, Y. A.; Belsky, V. K.; Stash, A. I. *Polyhedron* **1998**, *17*, 2455–2461.
(48) Kukushkin, V. Yu.; Nishioka, T.; Tudela, D.; Isobe, K.; Kinoshita, I. *Inorg. Chem.* **1997**, *36*, 6157–6165.
(49) Abramkin, S. A.; Jungwirth, U.; Valiahdi, S. M.; Dworak, C.; Habala, L.; Meelich, K.; Berger, W.; Jakupec, M. A.; Hartinger, C. G.;

Nazarov, A. A.; Galanski, M.; Keppler, B. K. *J. Med. Chem.* **2010**, *53*, 7356–7364.
(50) Perumareddi, J. R.; Adamson, A. W. *J. Phys. Chem.* **1968**, *72*, 414–420.
(51) *SAINT-Plus*, version 7.06a; *APEX2*; Bruker-Nonius AXS Inc.: Madison, WI, 2004.
(52) Sheldrick, G. M. *Acta Crystallogr.* **1990**, *A46*, 467–473.
(53) Sheldrick, G. M. *Acta Crystallogr.* **2008**, *A64*, 112–122.
(54) Johnson, G. K. Report ORNL-5138; OAK Ridge National Laboratory: Oak Ridge, TN, 1976.

2.3 Novel oximato-bridged platinum(II) di- and trimer(s): synthetic, structural, and in vitro anticancer activity studies

Scaffidi-Domianello Yu. Yu., Legin A. A., Jakupec M. A., Roller A., Kukushkin V. Yu. Galanski M., Keppler B. K.

Inorganic Chemistry 2012, **51**, 7153-7163. DOI: 0.1021/ic300148e

Inorganic Chemistry

Article

pubs.acs.org/IC

Novel Oximato-Bridged Platinum(II) Di- and Trimer(s): Synthetic, Structural, and in Vitro Anticancer Activity Studies

Yulia Yu. Scaffidi-Domianello,[†] Anton A. Legin,[†,‡] Michael A. Jakupec,[†,‡] Alexander Roller,[†] Vadim Yu. Kukushkin,[§] Markus Galanski,*[,†] and Bernhard K. Keppler*[,†]

[†]Institute of Inorganic Chemistry and [‡]Research Platform "Translational Cancer Therapy Research", University of Vienna, Währinger Strasse 42, A-1090 Vienna, Austria

[§]Department of Chemistry, St. Petersburg State University, 198504 Stary Petergof, Russian Federation

Supporting Information

ABSTRACT: Novel platinum complexes of trans geometry $[PtCl_2\{(Z)\text{-}R(H)C{=}NOH\}_2]$ [R = Me (**1**), Et (**3**)] and $[PtCl_2\{(E)\text{-}R(H)C{=}NOH\}\{(Z)\text{-}R(H)C{=}NOH\}]$ [R = Me (**2**), Et (**4**)] as well as the classic *trans*-$[PtCl_2(R_2C{=}NOH)_2]$ [R = Me, Et] were reacted with an equivalent amount of silver acetate in acetone solution at ambient temperature, resulting in formation of unprecedented head-to-tail-oriented oximato-bridged dimers $[PtCl\{\mu\text{-}(Z)\text{-}R(H)C{=}NO\}\{(Z)\text{-}R(H)C{=}NOH\}]_2$ [R = Me (**5**), Et (**7**)], $[PtCl\{\mu\text{-}(Z)\text{-}R(H)C{=}NO\}\{(E)\text{-}R(H)C{=}NOH\}]_2$ [R = Me (**6**), Et (**8**)], and $[PtCl(\mu\text{-}R_2C{=}NO)(R_2C{=}NOH)]_2$ [R = Me (**9**), Et (**10**)], correspondingly. The dimeric species feature a unique six-membered diplatinacycle and represent the first example of oxime ligands coordinated to platinum via the oxygen atom. All complexes were characterized by elemental analyses, electrospray ionization mass spectrometry, IR and multinuclear (^{1}H, ^{13}C, and ^{195}Pt) NMR spectroscopy, as well as X-ray diffraction in the cases of dimers **6** and **9**. Furthermore, the crystal and molecular structures of a trimeric oximato-bridged complex **11** comprising three platinum units connected in a chain way were established. The cytotoxicity of both dimers and the respective monomers was comparatively evaluated in three human cancer cell lines: cisplatin-sensitive CH1 cells as well as cisplatin-resistant SW480 and A549 cells, whereupon structure−activity relationships were drawn. Thus, it was found that dimerization results in a substantial (up to 7-fold) improvement of IC_{50} values of (aldoxime)Pt^{II} compounds, whereas for the analogous complexes featuring ketoxime ligands the reverse trend was observed. Remarkably, the novel dimers yielded no cross-resistance with cisplatin in SW480 cells, exhibiting up to 2-fold enhanced cytotoxicity in comparison with the CH1 cell line and thereby possessing a promising potential to overcome resistance toward platinum anticancer drugs. The latter point was also confirmed by investigating the potency of apoptosis induction in the case of one monomer as well as one dimer; the investigated complexes proved to be strong apoptotic agents which could induce cell death even in the cisplatin-resistant SW480 cell line.

INTRODUCTION

Great efforts have been undertaken to develop novel anticancer platinum-based drugs breaking the classic structure−activity relationships.[1,2] This is being done with the expectation that the novel species would be capable of forming DNA adducts completely dissimilar to those deriving from clinically approved platinum agents.[3−6] Moreover, others may show a radically different mode of action, e.g., with respect to alternative cellular targets. Among reported nonclassic platinum-based complexes exhibiting extraordinary cytotoxic properties, there are a few classes of multinuclear platinum(II) compounds, viz., (i) di- and triplatinum(II) complexes with bridging aliphatic[7−18] and aromatic[19] diamine ligands, where the platinum units are linked in a linear fashion (with trinuclear complex BBR3464[20−26] representing the most promising anticancer agent that reached phase II clinical trials); (ii) azole-bridged platinum(II) dimers, yielding high uptake levels as well as a high extent of interstrand cross-links;[27−35] (iii) dinuclear platinum(II)−bisphosphonate complexes, featuring medium cytotoxicity but capable of specific accumulation in the bone;[36,37] and (iv) a dimeric carboplatin analogue, showing greater in vitro antitumor activity and lower toxicity in mice than carboplatin.[38] All of the above listed species are able to circumvent cisplatin resistance in vitro.

Recently, some fascinating results concerning a novel class of nonclassic platinum(II) complexes, i.e., ketoxime-containing platinum(II) species, were reported. It was demonstrated that *trans*-$[PtCl_2(Me_2C{=}NOH)(NH_2CHMe_2)]$, unlike its cis analogue, causes cell death via an apoptotic mechanism.[39] Furthermore, complexes $[PtX_2(R_2C{=}NOH)_2]$ (X = Cl, Br, I; R = Me, Et) exhibiting a trans configuration were shown to possess a higher cytotoxicity,[40,41] enhanced cellular accumulation, and elevated DNA platination compared to their cis isomers.[42] Hence, (ketoxime)Pt^{II} complexes of trans geometry represent a new and promising class of platinum-based

Received: January 19, 2012
Published: June 12, 2012

antitumor agents clashing with the classic Cleare and Hoeschele's structure–activity rules.[1,2]

Conducting the project on the synthesis and antitumor activity of (oxime)Pt^{II} complexes,[40−42] we attempted to elucidate the solution behavior of these species in the course of the hydrolysis studies insofar as the displacement of the so-called leaving groups (mostly chlorido or carboxylato ligands) by water molecules is believed to be a prerequisite for anticancer activity of the platinum-based drugs. As a starting point, we determined their acidity constants by ^{1}H NMR titration. However, we were able to establish only pK_{a1} (ca. 7.2;[43] the acid–base equilibrium is reversible), whereas further titration at pH over 8 indicated a partial irreversibility of the system due to a chemical reaction. Being interested in a deep understanding of possible conversions of the oxime complexes in aqueous solutions, we carried out a synthetic experiment and isolated novel-type oximato-bridged di- and trinuclear species generated as a result of association of the oximato complexes.

Herein, we report on the synthesis and characterization of unprecedented di- and triplatinum(II) oximato-bridged species derived from classic trans-configured ketoxime platinum(II) complexes[40,41] as well as from newly prepared aldoxime analogues. Furthermore, the cytotoxicity of the novel monomeric and dimeric compounds was comparatively evaluated in three human tumor cell lines originating from cisplatin-sensitive (CH1) or -resistant (SW480 and A549) cancer cells.

RESULTS AND DISCUSSION

Recently, we reported on the promising cytotoxic properties of trans-configured platinum(II) ketoxime complexes.[40−42] In line with these results, we now focused on the development of new aldoxime analogues featuring (*E*)- or (*Z*)-R(H)C═NOH (R = Me, Et) ligands in the trans configuration. As expected, the novel agents exhibit considerably higher aqueous solubility as compared to their ketoxime congeners with ligated R_2C═NOH (R = Me, Et). As a next step of the project, we performed dimerization of both aldoxime- and ketoxime-containing complexes, yielding head-to-tail-oriented oximato-bridged dimers of general formula [PtCl(μ-RR′C═NO)(RR′C═NOH)]$_2$ (R = Me, Et; R′ = H, Me, Et) and verified their cytotoxic properties. In addition, for R = R′ = Et a novel structure consisting of three platinum units linked in a linear fashion and bridged by oximato ligands was established.

Synthesis, Characterization and X-ray Structure Determination of *trans*-Bis(aldoxime)platinum(II) Complexes. Generation of **1**−**4** (Figure 1) was carried out by a conventional route[44−46] via reaction of K_2[$PtCl_4$] with 2 equiv of *E*/*Z*-R(H)C═NOH (R = Me, Et) in an aqueous solution at room temperature followed by thermal isomerization in $MeNO_2$ and column separation of isomers (yields are 31−35%). Complexes were characterized by elemental analysis, electrospray ionization mass spectrometry (ESI-MS), IR, and ^{1}H, ^{13}C{^{1}H}, and ^{195}Pt NMR spectroscopy and also by X-ray crystallography (for **1** and **4**, Figure S1 and Table S1, Supporting Information). The trans configuration of the complexes and *E*/*Z* configuration of the ligands were established by X-ray diffraction. A detailed description of the syntheses and characterization of **1**−**4** is given in the Supporting Information, whereas synthetic experiments are reported in the Experimental Section.

Synthesis, Characterization, and X-ray Structure Determination of Oximato-Bridged Platinum(II)

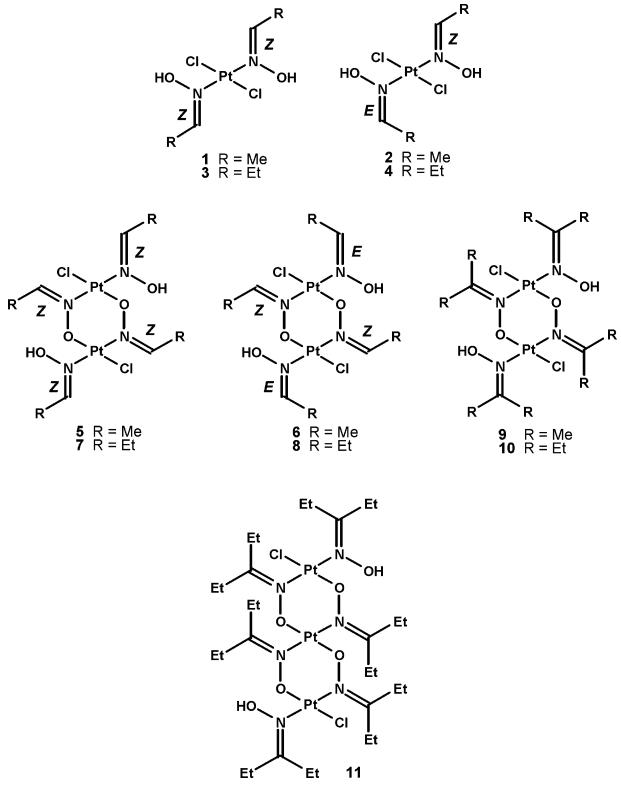

Figure 1. Platinum(II) oxime complexes used in this study.

Dimers/Trimer. The corresponding dimeric species derived from **1**−**4** which were obtained in this work as well as originated from the previously reported *trans*-[$PtCl_2$(R_2C═NOH)$_2$] (R = Me,[46] Et[41]) were prepared by abstraction of a chlorido ligand with 1 equiv of silver acetate. The reaction was carried out in acetone at room temperature for a limited time (1−3 h) in order to minimize the probability of acetato complex formation; final products **5**−**10** (Figure 1) were purified by column chromatography and isolated in moderate yields (31−36%).

Interestingly, slow evaporation of a solution of complex **10** in a mixture of undried ethanol, ethylacetate, and acetone resulted in formation of trimer **11** (Figure 1). The obtained crystals were characterized by X-ray crystallography (see below) as well as ESI-MS spectrometry ([M + Na]$^+$ and [M + K]$^+$ peaks were detected). A plausible mechanism of trimer formation could be associated with a dimer–monomer equilibrium.

Complexes **5**−**10** gave satisfactory elemental analyses and appropriate molecular ion/fragmentation patterns in the ESI-MS$^+$ spectra ([M + H]$^+$ and [M + Na]$^+$ peaks were found). Furthermore, **5**−**10** were characterized by IR spectroscopy, exhibiting characteristic strong ν(OH) [3143−3377 cm^{-1}] and ν(NO) [958−970 cm^{-1}] stretching vibrations as well as two ν(C═N) [1609−1625 and 1651−1681 cm^{-1}] bands of medium intensity. Expectedly, two sets of oxime proton signals were observed in the ^{1}H NMR spectra of all prepared dimers, corresponding to the bridging and nonbridging ligated oximes. Starting with *Z*/*E* monomeric complexes **2** and **4**, the respective dimers [PtCl{μ-(*Z*)-R(H)C═NO}{(*E*)-R(H)C═NOH}]$_2$ (R = Me (**6**), Et (**8**)), featuring bridging *Z*-oximato ligands, were formed as major products. However, traces of *Z*,*E*-(**6a**/**8a**) and *E*,*E*-oximato bridged dimers (**6b**/**8b**) were

dx.doi.org/10.1021/ic300148e | Inorg. Chem. 2012, 51, 7153−7163

detected by NMR spectroscopy. Moreover, dissolution of **6** and **8** in CD_3OD led to an increase of the signals of the latter species with time, resulting in the following equilibrium ratios: **6**:**6a**:**6b** ≈ 7:2:1 and **8**:**8a**:**8b** ≈ 3:2:1. This fact might be explained by an equilibrium possibly established between a dimer and its corresponding monomer in solution, resulting in a mixture of dimers (Figure 2).

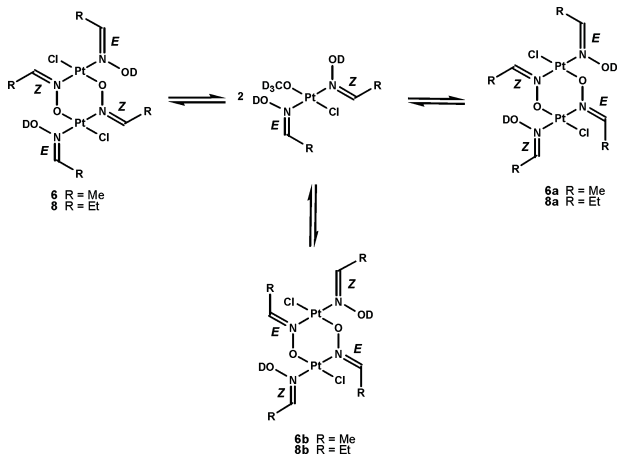

Figure 2. Equilibrium in CD_3OD solution of **6** and **8**.

In the ^{195}Pt NMR spectra, the platinum signals of aldoxime-containing dimers **5**−**8** appear in a narrow range between −208 and −251 ppm, while δ_{Pt} of the corresponding ketoxime complexes **9** and **10** resonate at a lower field (−35 and −152 ppm, respectively).

The crystal structures of dimers **6** and **9** and trimer **11** were determined by X-ray diffraction (Tables 1, 2, and 3; Figures 3 and 4). The three compounds feature pairs of head-to-tail-oriented oximato ligands, which bind the platinum centers via the oximic nitrogen and the oxygen of the deprotonated hydroxy group. In **11**, three platinum atoms are connected to each other via bridging ligands in a chain manner. Apart from the bridging ligands, the coordination sphere of each platinum center in **6** and **9** and the terminal Pts in **11** is completed by the corresponding aldoxime (**6**) or ketoxime (**9** and **11**) and a chlorido ligand.

A comparison of selected geometric features of oximato-bridged platinum complexes **6**, **9**, and **11** is presented in Table 4. Interestingly, the Pt···Pt distances in **6** and **11** (3.1872(6) and 3.2094(2) Å, respectively) are considerably longer compared to that in **9** (2.8668(5) Å), which is probably due to an increased steric effect exerted by the alkyl substituents of

Table 2. Selected Bond Lengths (Å) and Angles (deg) for Complexes 6 and 9

	6	9
Pt(1)−N(1)	1.992(9)	2.009(6)
Pt(1)−N(2)	2.032(9)	2.019(7)
Pt(1)−Cl(1)	2.282(2)	2.2962(19)
Pt(1)−O(3)	2.023(7)	2.030(5)
Pt(2)−N(3)	1.974(8)	2.012(6)
Pt(2)−N(4)	2.024(9)	2.026(6)
Pt(2)−Cl(2)	2.291(3)	2.2981(19)
Pt(2)−O(1)	2.036(8)	2.016(5)
N(1)−C(1)	1.260(14)	1.294(10)
N(2)−C(3)	1.264(14)	
N(3)−C(5)	1.278(14)	
N(4)−C(7)	1.268(15)	
N(2)−C(4)		1.273(10)
N(3)−C(7)		1.289(10)
N(4)−C(10)		1.272(10)
N(1)−Pt(1)−N(2)	176.2(3)	177.0(3)
N(1)−Pt(1)−Cl(1)	91.6(3)	90.88(19)
N(2)−Pt(1)−Cl(1)	89.8(2)	91.09(18)
N(3)−Pt(2)−N(4)	177.5(4)	176.0(3)
N(3)−Pt(2)−Cl(2)	91.0(3)	90.26(19)
N(4)−Pt(2)−Cl(2)	90.4(3)	92.04(19)

Table 1. Crystal Data and Details of Data Collection for 1, 4, 6, 9, and 11

	1	4	6	9	11
empirical formula	$C_4H_{10}Cl_2N_2O_2Pt$	$C_6H_{14}Cl_2N_2O_2Pt$	$C_8H_{18}Cl_2N_4O_4Pt_2$	$C_{12}H_{26}Cl_2N_4O_4Pt_2$	$C_{30}H_{62}Cl_2N_6O_6Pt_3$
fw	384.13	412.18	695.34	751.45	1259.03
space group	*P*-1	*Pn*	$P2_1/c$	*P*-1	*P*-1
a, Å	4.2101(3)	4.3305(3)	11.1533(6)	8.4994(8)	9.2330(3)
b, Å	6.5803(6)	10.0784(6)	10.7869(6)	9.7473(10)	9.5490(3)
c, Å	8.7596(7)	13.1600(7)	13.1609(7)	13.5101(15)	11.2825(4)
α, deg	75.388(4)			79.033(3)	85.637(3)
β, deg	82.707(5)	98.440(4)	95.596(3)	79.998(3)	82.020(2)
γ, deg	78.825(4)			67.676(2)	80.387(2)
V, Å^3	229.59(3)	568.14(6)	1575.84(15)	1010.11(18)	969.84(6)
Z	1	2	4	2	1
λ, Å	0.71073	0.71073	0.71073	0.71073	0.71073
ρ_{calcd}, g cm^{-3}	2.778	2.409	2.931	2.471	2.156
cryst size, mm	0.50 × 0.04 × 0.01	0.30 × 0.05 × 0.05	0.13 × 0.13 × 0.04	0.20 × 0.20 × 0.15	0.20 × 0.10 × 0.05
T, K	100	100	100	100	100
μ, cm^{-1}	158.16	127.92	180.90	141.21	10.976
R1[a]	0.0185	0.0336	0.0369	0.0287	0.0302
wR2[b]	0.0407	0.0659	0.0951	0.0719	0.0736
GOF[c]	1.033	1.024	1.005	1.081	1.031

[a] $R1 = \Sigma||F_o| - |F_c||/\Sigma|F_o|$. [b] $wR2 = \{\Sigma[w(F_o^2 - F_c^2)^2]/\Sigma[w(F_o^2)^2]\}^{1/2}$. [c] $GOF = \{\Sigma[w(F_o^2 - F_c^2)^2]/(n-p)\}^{1/2}$, where *n* is the number of reflections and *p* is the total number of parameters refined.

dx.doi.org/10.1021/ic300148e | Inorg. Chem. 2012, 51, 7153−7163

Table 3. Selected Bond Lengths (Å) and Angles (deg) for Complex 11

Pt(1)−N(1)	2.028(4)	Pt(2)−O(1A)	2.005(3)
Pt(1)−O(2)	2.047(3)	N(1)−C(1)	1.290(6)
Pt(2)−N(2)	1.997(4)	N(2)−C(6)	1.280(6)
Pt(2)−N(3)	2.020(4)	N(3)−C(11)	1.284(6)
Pt(2)−Cl(1)	2.3169(13)		
N(1A)−Pt(1)−N(1)	180.000(1)	N(2)−Pt(2)−N(3)	177.00(16)
N(1)−Pt(1)−O(2)	87.66(14)	N(2)−Pt(2)−Cl(1)	93.46(12)
N(1A)−Pt(1)−O(2)	92.34(14)	N(3)−Pt(2)−Cl(1)	89.46(12)

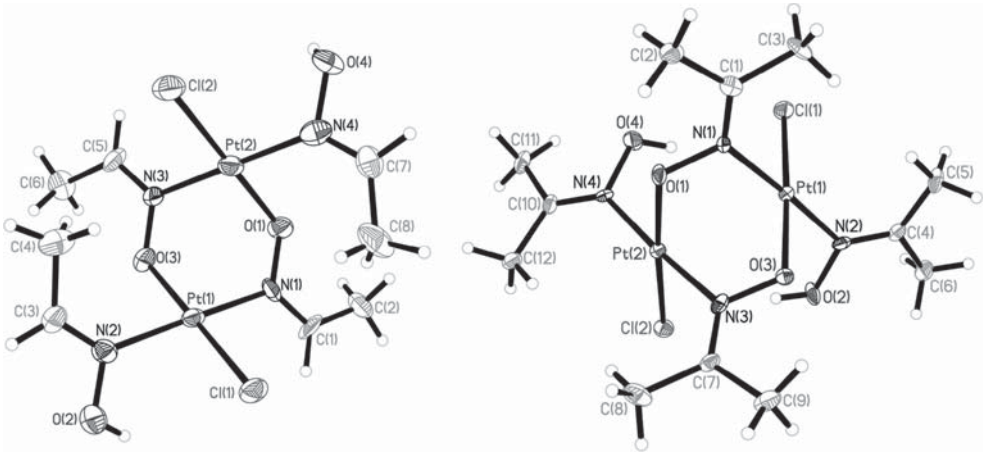

Figure 3. ORTEP view of **6** (left) and **9** (right) with atom-labeling scheme; thermal ellipsoids have been drawn at the 50% probability level.

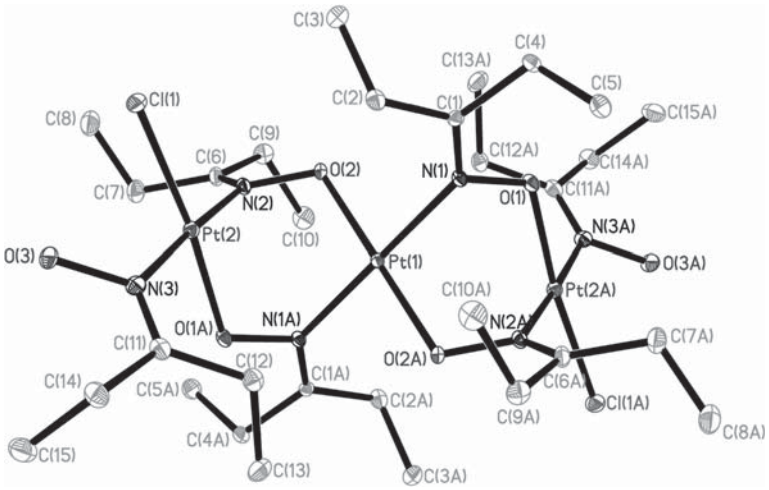

Figure 4. ORTEP view of **11** with atom-labeling scheme; thermal ellipsoids have been drawn at the 30% probability level.

Table 4. Selected Geometric Parameters of the Oximato-Bridged Platinum Complexes

	dihedral angle,[a] deg			
	Pt···Pt, Å	τ	ω	Pt···Pt···Pt angle, deg
6	3.1872(6)	81.4	9.9	
9	2.8668(5)	57.2	2.5	
11	3.2094(2)	85.3	19.2	180.0

[a] τ is the tilt angle between the adjacent platinum coordination planes, and ω is the average torsion angle about the Pt(1)···Pt(2) vector.

the nonbridging oxime ligand directed to the platinum−platinum core. Contrary to **6** and **11**, in **9** the methyl substituents of the coordinated acetoxime are turned away from the bisoximato bridge. Moreover, the two hydrogen bonds between the oximic hydroxo group of one platinum unit and the chlorido ligand of the second one could favor the approaching of two platinum centers and result in an additional stabilization of the dimeric structure of **9**. The O4···Cl1 and O2···Cl2 distances are at 3.301 and 3.303 Å, respectively. These distances fall into the range of typical O···Cl contacts when OH···Cl hydrogen bonding takes place [2.95−3.40 Å],[47] representing relatively weak interactions compared to the reported values. The angles O4−H4···Cl1 and O2−H2···Cl2 are 145.3° and 162.3°, correspondingly.

Generally, the distances between the adjacent platinum atoms in **6**, **9**, and **11** are shorter than a double van der Waals

radius for Pt [1.72 × 2 = 3.44 Å]. Compared to the reported Pt···Pt distances in the platinum(II) dimeric complexes featuring two bridging ligands, e.g., (i) α-pyridonate [2.88−2.90 Å],[48] (ii) 1-methyluracilate or 1-methylthyminate [2.927−2.986 Å],[49] (iii) amidate [2.993−3.060 Å],[50] (iv) amidinate [3.381 Å],[51] and (v) carboxylate [2.952−2.990 Å],[52] the Pt···Pt distances in **6** and **11** correspond to a rather weak nonbonded interaction between the platinum centers. On the contrary, the Pt···Pt distance in **9** is one of the shortest known for platinum(II) dimers. Being in good agreement with literature data,[53,54] the tilt angle (τ) between the neighboring platinum coordination planes is directly related to the Pt···Pt distance. Thus, the shortest Pt···Pt distance in **9** corresponds to the lowest τ value (57.2° versus 81.4° and 85.3° for **6** and **11**, respectively), additionally confirming the lowest repulsive interactions in the case of the acetone oxime-containing platinum(II) dimer. The coordination planes in **6** and **9** are twisted only slightly (ω = 9.9° and 2.5°, respectively), while in **11** the twist angle was proved to be substantially higher (ω = 19.2°), serving to minimize the steric interactions between the ethyl substituents of the bridging oximato and nonbridging oxime ligands.

The platinum ions in **6** and **9** and the terminal Pts in **11** nearly adopt a square-planar geometry, being slightly displaced out of the coordination plane by 0.02−0.06 Å, whereas Pt1 in **11** lies ideally within the corresponding N1−O2−N1′−O2′ plane. The Pt−Cl bond lengths [2.282(2)−2.3169(13) Å] correspond to previously reported distances for platinum(II) chlorido compounds.[55,56] The Pt−N and Pt−O bond lengths appear in the range normally found in related platinum(II) complexes,[51,57,58] namely, 1.974(8)−2.032(9) and 2.005(3)−2.047(3) Å, respectively. The values of C═N distances [1.260(14)−1.294(10) Å] are similar within 3σ and correspond to previously published distances of C═N double bonds in metal-bound oximes.[59−61]

Comparative Studies of the Cytotoxic Activity of Novel Platinum(II) Oxime Complexes and Corresponding Oximato-Bridged Dimers. In view of our previous findings on the cytotoxic activity of *trans*-(oxime)Pt^{II} complexes,[40,41] the cytotoxicity of **1**−**9** was evaluated in comparison with cisplatin and transplatin by means of a colorimetric microculture assay (MTT) in three human cancer cell lines: cisplatin-sensitive ovarian carcinoma (CH1) as well as intrinsically cisplatin-resistant colon carcinoma (SW480) and nonsmall cell lung cancer (A549) cell lines, yielding the IC_{50} values listed in Table 5. The cytotoxic potency of dimer **10** could not be examined because of its insufficient aqueous solubility.

Generally, CH1 and SW480 cancer cell lines showed a similar response toward both monomeric (**1**−**4**) and dimeric (**5**−**9**) complexes, as also reported for (ketoxime)Pt^{II} species.[41] However, in the case of **1** and **3** nearly 2-fold improvement of the cytotoxic potency in cisplatin-resistant SW480 cells compared to cisplatin-sensitive CH1 cells could be observed. In contrast, the A549 cell line exhibited a somewhat lower sensitivity to the novel oxime complexes, yielding IC_{50} values increased by factors of 2.2−4.0 for monomers **1**−**4** and 4.3−12 for dimers **5**−**9** in comparison with those in the CH1 cell line.

Unexpectedly, an enlargement of the alkyl chain length of the oxime ligand using propionaldehyde oxime (in **3**, **4**, **7**, and **8**) instead of acetaldehyde oxime (in **1**, **2**, **5**, and **6**) did not result in an increase of cytotoxicity in the case of monomers **1**−**4** and only slightly reduced IC_{50} values of dimers **5**−**8** (by a factor of 1.1−2.3). Interestingly, some influence of the *E*- and *Z*-configuration of the coordinated aldoximes on the IC_{50} values was observed. Thus, monomeric complexes **2** and **4** featuring both *E*-and *Z*-aldoximes proved to be by a factor of 2 more cytotoxic in CH1 cells compared to their isomers **1** and **3**, containing two *Z* ligands.

Table 5. Cytotoxicity of Monomeric (1−4) and Dimeric (5−9) (oxime)Pt^{II} Complexes in CH1, SW480, and A549 Cancer Cells (Exposure Time 96 h)

compound	IC_{50} (μM), 96 h		
	CH1	SW480	A549
1	6.6 ± 0.2	3.5 ± 0.1	14 ± 1
2	3.3 ± 0.1	3.3 ± 0.1	13 ± 1
3	6.2 ± 0.3	3.6 ± 0.1	21 ± 3
4	3.4 ± 0.2	3.3 ± 0.04	13 ± 1
5	0.95 ± 0.1	1.2 ± 0.1	12 ± 0.4
6	1.8 ± 0.2	1.9 ± 0.1	12 ± 1
7	0.94 ± 0.09	1.0 ± 0.1	5.1 ± 0.5
8	0.96 ± 0.09	1.3 ± 0.1	5.7 ± 0.3
9	2.2 ± 0.4	2.5 ± 0.3	9.5 ± 1.6
trans-[$PtCl_2(Me_2C{=}NOH)_2$][a]	0.17 ± 0.09	0.22 ± 0.05	
cisplatin	0.14 ± 0.03	3.3 ± 0.4	1.3 ± 0.4
transplatin[a]	15 ± 2	19 ± 3	

[a]Data taken from ref 40.

Comparing aldoxime-containing monomeric complexes **1**−**4** and the corresponding dimers **5**−**8** it should be pointed out that dimerization results in 1.8- to 6.7-fold enhancement of the cytotoxic potency in CH1 cells. However, dimer **9** featuring a ketoxime ligand exhibited 13 and 11 times higher IC_{50} values in CH1 and SW480 cells, respectively, as compared to the corresponding monomer *trans*-[$PtCl_2(Me_2C{=}NOH)_2$],[40] reversing the structure−activity relationships valid for (aldoxime)Pt^{II} complexes.

With respect to cisplatin, monomeric species **1**−**4** proved to be significantly less cytotoxic in CH1 (24−47 times) and A549 (10−16 times) cell lines, while in SW480 cells the IC_{50} values were similar to that of cisplatin. Remarkably, dimers **5**−**9** exhibited 1.3−3.0-fold improved cytotoxicity in SW480 cells compared to cisplatin, being however less potent both in CH1 and A549 cell lines (by factors of 3.9−13). In comparison to transplatin, novel (oxime)Pt^{II} complexes **1**−**9** were found to display up to 17 times enhanced cytotoxic potency.

Behavior of Monomer 1 and Dimer 5 in Aqueous Solution under Physiological Conditions. In order to reveal the behavior of the prepared monomeric and dimeric species in aqueous solutions under the conditions used for cell culture experiments, time-dependent ^{1}H NMR measurements of monomer **1** and the respective dimer **5** were carried out in phosphate-buffered D_2O solutions (10 mM, pH 7.4) containing NaCl (0.125 M) with concentrations of complexes being ca. 400 and 200 μM, respectively. Figure S2 (Supporting Information) shows a selected range of ^{1}H NMR spectra (6−8 ppm) where the signals of the N═C*H* protons are detected. Keeping dimer **5** or monomer **1** under these conditions over 3 days resulted in a nearly identical peak pattern (spectra 2 and 4, respectively) consisting of five N═C*H* proton signals corresponding to the dimer, monomer, hydrolyzed monomer, and an additional so far unknown species. These results are in good agreement with IC_{50} values of **1** and **5** in SW480 cell line, showing a 2-fold improvement of the cytotoxicity in the case of dimer **5** as compared to monomer **1**. However, the ratio

dx.doi.org/10.1021/ic300148e | *Inorg. Chem.* 2012, 51, 7153−7163

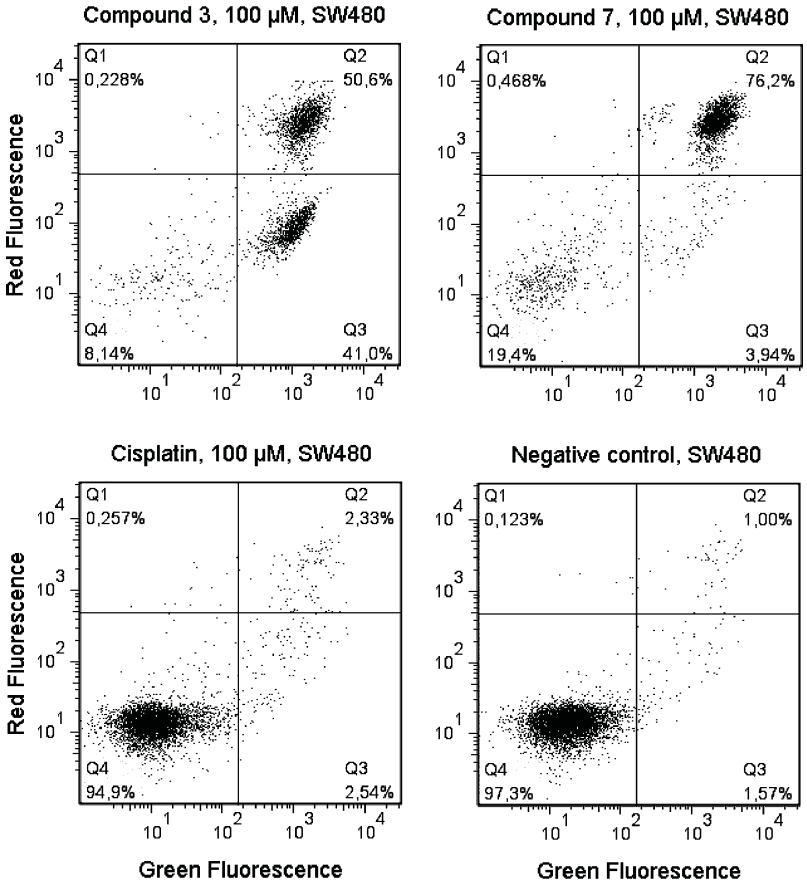

Figure 5. Apoptosis induction detected by annexin V-FITC and PI staining and FACS analysis in the cisplatin-resistant colon cancer cell line SW480 (24 h exposure with 100 μM of cisplatin, compounds **3** and **7**). Upper left quadrant (Q1) contains necrotic, lower right (Q3) early apoptotic, upper right (Q2) late apoptotic, and lower left (Q4) viable cell population.

$IC_{50}(\mathbf{1})/IC_{50}(\mathbf{5})$ in two other cell lines used in this work deviate from a factor of 2, being 6.6 in CH1 and 1.25 in A549 cells, indicating a slightly different behavior in these cell lines.

Spectra 5−7 (Figure S2, Supporting Information) additionally represent time-dependent hydrolysis studies of complex **1**. For this purpose no sodium chloride was added to the phosphate-buffered D_2O solution of **1** (pH 7.4), resulting in an enhanced aquation of the complex. Five minutes after dissolution of the compound, a peak corresponding to the N=C*H* proton of the hydrolyzed species could be observed (spectrum 5). A total of 5 h after the experiment was started the dichlorido complex was completely converted into the aqua species (spectrum 6). In addition, small signals related to the dimeric complex were detected. Finally, 3 days later, the mixture of N=C*H* proton signals turned into one single peak (spectrum 7). With the intention to elucidate which species was formed as a result of the conversions taking place in aqueous solution, a ^{195}Pt NMR spectrum was recorded. A signal at 316.7 ppm was observed, which correlates well with δ_{Pt} values for trans-configured platinum(II) species having a $[N_2O_2]$ ligand donor set reported in the literature in the range between 209 and 366 ppm.[62] Further, in the ESI-MS$^+$ spectrum a peak at *m*/*z* 956 was detected that could be attributed to a sodiated trimeric complex $[Pt_3(C_2H_4NO)_6 + Na]^+$ ($C_{12}H_{24}N_6O_6Pt_3Na$, calcd *m*/*z* 956.06). Due to the fact that only one set of N=C*H* proton signals was observed in the ^{1}H NMR spectrum 7, a ring-shaped trimeric structure containing six equivalent oximato bridges can be suggested (Figure S3, Supporting Information).

Apoptosis Assay. In order to compare the capacities of inducing apoptosis and necrosis of compounds **3**, **7**, and cisplatin, growing SW480 and HL60 cells were treated with these drugs in equal concentrations for 24 h, then stained with annexin V-FITC/propidium iodide and analyzed by fluorescence-activated cell sorting (FACS). This method allows one to discriminate necrotic (stained by propidium iodide only, red fluorescence), early apoptotic (stained by annexin V-FITC only, green fluorescence), and late apoptotic (stained by both, green and red fluorescence) from viable (unstained, only self-fluorescence) cells. From the dot plots (Figures 5 and 6) we can infer that the apoptosis-inducing potency of compound **3** is much higher than that of cisplatin in SW480 cells but decreases relative to cisplatin in HL60 cells. The apoptosis-inducing potency of compound **7** exceeds that of cisplatin in SW480 cells and is comparable in HL60 cells. A concentration of 100 μM of compounds **3** and **7** reduces the amount of viable SW480 cells to below 20% by induction of both early and late apoptosis, while the same concentration of cisplatin has insignificant effects within the chosen exposure time. Summarized data (Figure S4 and Tables S2 and S3, Supporting Information) show that compounds **3** and **7** are strong apoptotic agents which can induce cell death even in a cisplatin-resistant cell line.

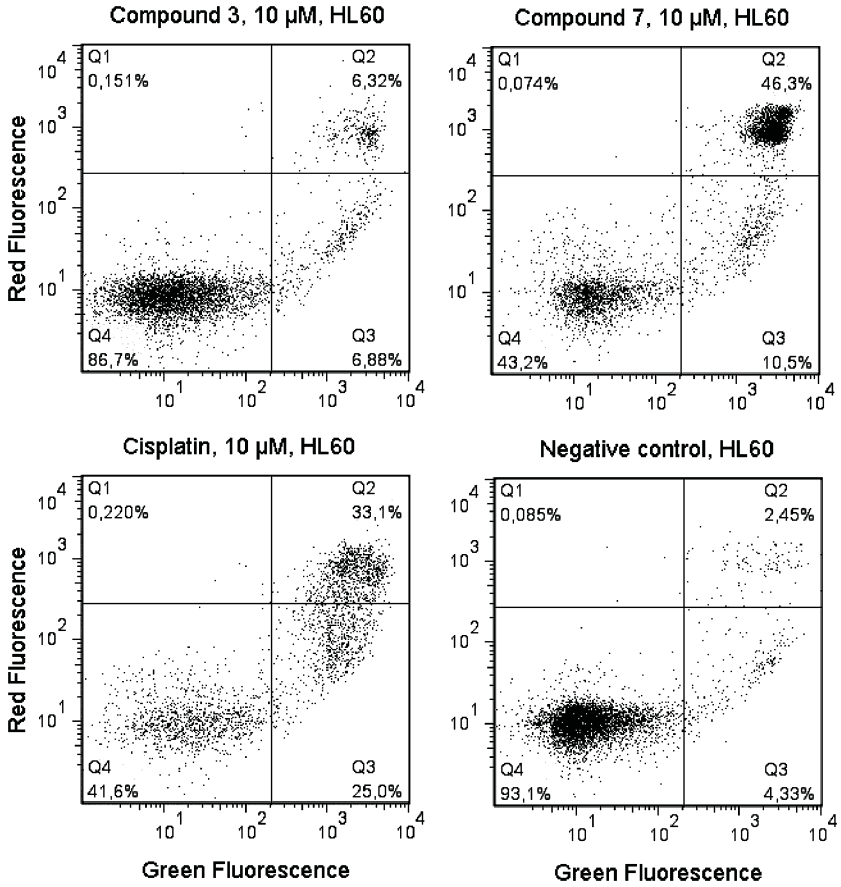

Figure 6. Apoptosis induction detected by annexin V-FITC and PI staining and FACS analysis in the cisplatin-sensitive human promyelocytic leukemia cell line HL60 (24 h exposure with 10 μM of cisplatin, compounds **3** and **7**). Upper left quadrant (Q1) contains necrotic, lower right (Q3) early apoptotic, upper right (Q2) late apoptotic, and lower left (Q4) viable cell population.

CONCLUSIONS

The possibility of di- and trimerization of (oxime)Pt^{II} complexes leading to formation of a six-membered diplatinacycle has been demonstrated. The oximato-bridged platinum(II) dimers were isolated and completely characterized, including X-ray diffraction in the case of two dimers. Additionally, the crystal structure of a novel oximato-bridged platinum(II) trimer featuring platinum units connected to each other in a chain manner was determined.

Although the bridging properties of oximic ligands have been extensively studied, e.g., nearly exhaustively in the case of group VIII metals (Fe,[63,64] Ru,[65] Os,[66] Co,[67,64] Ni,[63,64,68−70] and Pd[69]) and partially for some representatives of group I (Cu[63,68,70−84]), II (Zn[63,64,85] Cd[85]), III (Gd[64]), IV (Ti[86] and Zr[86]), VI (Cr[64]), and VII (Mn[63,64,87−89]), there are no reports on oximato-bridged platinum complexes. Moreover, to the best of our knowledge the novel di-/trimer(s) exhibit a unique six-membered diplatinacycle as well as represent the first example of oxime/oximato ligands coordinated to the platinum atom via oxygen.

In general, the di-/trimerization observed in this work at the kinetically inert platinum(II) center could give a possible rationale for various polymerizations involving oxime/oximato species based on more labile metals. Considering these results, previous work on the synthesis of polymeric oximato-bridged complexes should be thoroughly revisited and the possibility of the consecutive association of the monomeric oximato units should be taken into account in further studies.

Additionally, the cytotoxic properties of the novel dimers were examined in three human cancer cell lines (CH1, SW480, and A549) in comparison with the corresponding monomeric complexes of trans geometry and structure−activity relationships were established. It was found that dimerization improves significantly the cytotoxic potency of the aldoxime-containing complexes, whereas the dimer bearing ketoxime ligands proved to be considerably less potent than the respective monomer. Notably, the novel oximato-bridged dimers display appreciably enhanced cytotoxicity in the intrinsically cisplatin-resistant SW480 cell line as compared to cisplatin, indicating in perspective a promising potential to overcome cisplatin resistance. The latter point was confirmed by investigating the ability of induction of apoptosis, demonstrating a strong apoptotic potential even in the cisplatin-resistant cell line.

EXPERIMENTAL SECTION

General Procedures. Potassium tetrachloridoplatinate and 2-propanone oxime were supplied by Johnson Matthey and Fluka, respectively. 3-Pentanone, acetaldehyde oxime (a mixture of syn and anti forms), and propionaldehyde oxime (a mixture of syn and anti forms) were purchased from Aldrich. All chemicals were used as received without further purification. 3-Pentanone oxime was synthesized from the corresponding ketone by a standard textbook procedure.[90,91] Complexes *trans*-$[PtCl_2(Me_2C{=}NOH)_2]$[46] and *trans*-$[PtCl_2(Et_2C{=}NOH)_2]$[41] were prepared according to the previously

published methods starting from $K_2[PtCl_4]$. Synthetic procedures were carried out in a light-protected environment when platinum was involved. Fluka silica gel 60 (220−440 mesh) was used for column chromatography. C, H, and N elemental analyses were carried out by the elemental analyses laboratory of the University of Vienna using a Perkin-Elmer 2400 CHN elemental analyzer. ESI-MS spectra were measured with a Bruker Esquire 3000 instrument. IR spectra were obtained using an ATR unit with a Perkin-Elmer 370 FTIR 2000 instrument (4000−400 cm^{-1}). ^1H, $^{13}C\{^1H\}$, and ^{195}Pt NMR spectra were measured with a Bruker Avance III 500 MHz NMR spectrometer at 500.32 (^1H), 125.81 (^{13}C), and 107.55 MHz (^{195}Pt), respectively, at 298 K. ^{195}Pt chemical shifts are given relative to $K_2[PtCl_4]$, and the half-height line width is given in parentheses.

Reaction of $K_2[PtCl_4]$ with *Z*/*E*-R(H)C═NOH (R = Me, Et). $K_2[PtCl_4]$ (0.7 mmol) was dissolved in 15 mL of H_2O, and a solution of *Z*/*E*-R(H)C═NOH (1.4 mmol) in 2 mL of H_2O was added dropwise. The reaction mixture was stirred for 24 h at room temperature. A small amount of undefined reddish precipitate formed was filtered off, washed with H_2O, and dried in vacuo. The filtrate was evaporated to dryness, and 10 mL of MeOH was added. A colorless precipitate of KCl was filtered off. Then MeOH was removed on a rotary evaporator, and 5 mL of $CHCl_3$ or Et_2O (for R = Me or Et, respectively) was added, whereupon a yellow precipitate of $K[PtCl_3\{R(H)C═NOH\}]$ was filtered off, washed with $CHCl_3$ or Et_2O (2 × 2 mL), and dried in vacuo (yield was 23−26%). The filtrate was evaporated to dryness, and the crude product was stored for purification with column chromatography, see below.

To a solution ($K[PtCl_3\{R(H)C═NOH\}]$, 0.16−0.18 mmol) in 10 mL of H_2O an equivalent amount of *Z*/*E*-R(H)C═NOH was added, and the reaction mixture was stirred at room temperature for 24 h. The solvent was removed, 10 mL of MeOH was added, and a colorless precipitate of KCl was filtered off, whereupon MeOH was removed on a rotary evaporator, the solid residue was combined with the crude products synthesized previously (see above), and 15 mL of $MeNO_2$ was added, whereupon the reaction mixture was refluxed for 1 h. Afterward the solvent was removed and products **1** (first fraction) and **2** (second fraction) or **3** (first fraction) and **4** (second fraction) were separated by column chromatography ($CHCl_3$:$Me_2C═O$ 8:1 (v/v) for R = Me and 10:1 (v/v) for R = Et). Yields of **1**−**4**: 31−35%.

(SP-4-1)-Dichloridobis((1*Z*)-*N*-hydroxyethanimine-κ*N*)-platinum(II) (1). Anal. Calcd for $C_4H_{10}N_2Cl_2O_2Pt$: C, 12.51; H, 2.62; N, 7.29. Found: C, 12.90; H, 2.46; N, 7.03. ESI-MS^+ (MeOH), *m*/*z*: 407 $[M + Na]^+$, 423 $[M + K]^+$. TLC (8:1 (v/v) $CHCl_3/Me_2C═O$): R_f = 0.73. IR in KBr (selected bands), cm^{-1}: 3202 s ν(OH), 1667 m ν(C═N), 970 s ν(NO). ^1H NMR (CD_3OD), δ: 7.39 (q, 1*H*, C*H*, $^3J_{H,H}$ = 5.8 Hz), 2.05 (d, 3*H*, C*H*$_3$, $^3J_{H,H}$ = 5.7 Hz). $^{13}C\{^1H\}$ NMR (CD_3OD), δ: 156.4 (*C*═N), 12.7 (CH_3). ^{195}Pt NMR (CD_3OD), δ: −479 (500 Hz). Crystals for X-ray study were obtained by slow evaporation of an acetone/toluene solution.

(SP-4-1)-Dichlorido((1*E*)-*N*-hydroxyethanimine-κ*N*)((1*Z*)-*N*-hydroxyethanimine-κ*N*)platinum(II) (2). Anal. Calcd for $C_4H_{10}N_2Cl_2O_2Pt$: C, 12.51; H, 2.62; N, 7.29. Found: C, 12.79; H, 2.60; N, 7.22. ESI-MS^+ (MeOH), *m*/*z*: 407 $[M + Na]^+$, 466 $[M + Me(H)C═NOH + Na]^+$, 482 $[M + Me(H)C═NOH + K]^+$. ESI-MS^- (MeOH), *m*/*z*: 287 $[M - Me(H)C═NOH - HCl - H]^-$. TLC (8:1 (v/v) $CHCl_3/Me_2C═O$): R_f = 0.52. IR in KBr (selected bands), cm^{-1}: 3215 s ν(OH), 1677 m ν(C═N), 980 s ν(NO). ^1H NMR (CD_3OD), δ: 7.51 (q, 1*H*, C*H*, $^3J_{H,H}$ = 6.1 Hz), 7.50 (q, 1*H*, C*H*, $^3J_{H,H}$ = 5.7 Hz), 2.49 (d, 3*H*, C*H*$_3$, $^3J_{H,H}$ = 6.1 Hz), 2.05 (d, 3*H*, C*H*$_3$, $^3J_{H,H}$ = 5.7 Hz). $^{13}C\{^1H\}$ NMR (CD_3OD), δ: 156.0 (*C*═N), 155.4 (*C*═N), 16.1 (CH_3), 12.7 (CH_3). ^{195}Pt NMR (CD_3OD), δ: −532 (550 Hz).

(SP-4-1)-Dichloridobis((1*Z*)-*N*-hydroxypropane-1-imine-κ*N*)-platinum(II) (3). Anal. Calcd for $C_6H_{14}N_2Cl_2O_2Pt$: C, 17.48; H, 3.42; N, 6.80. Found: C, 17.77; H, 3.11; N, 6.65. ESI-MS^+ (MeOH), *m*/*z*: 435 $[M + Na]^+$, 451 $[M + K]^+$. TLC (10:1 (v/v) $CHCl_3/Me_2C═O$): R_f = 0.54. IR in KBr (selected bands), cm^{-1}: 3338 s ν(OH), 1671 m ν(C═N), 985 s ν(NO). ^1H NMR (CD_3OD), δ: 7.29 (t, 1*H*, C*H*, $^3J_{H,H}$ = 5.8 Hz), 2.52 (m, 2*H*, C*H*$_2$), 1.09 (t, 3*H*, C*H*$_3$, $^3J_{H,H}$ = 7.7 Hz). $^{13}C\{^1H\}$ NMR (CD_3OD), δ: 161.9 (*C*═N), 20.9 (CH_2), 8.6 (CH_3). ^{195}Pt NMR (CD_3OD), δ: −490 (510 Hz).

(SP-4-1)-Dichlorido((1*E*)-*N*-hydroxypropane-1-imine-κ*N*)((1*Z*)-*N*-hydroxypropane-1-imine-κ*N*)platinum(II) (4). Anal. Calcd for $C_6H_{14}N_2Cl_2O_2Pt$: C, 17.48; H, 3.42; N, 6.80. Found: C, 17.73; H, 3.13; N, 6.66. ESI-MS^+ (MeOH), *m*/*z*: 435 $[M + Na]^+$, 451 $[M + K]^+$. ESI-MS^- (MeOH), *m*/*z*: 301 $[M - Et(H)C═NOH - HCl - H]^-$. TLC (10:1 (v/v) $CHCl_3/Me_2C═O$): R_f = 0.41. IR in KBr (selected bands), cm^{-1}: 3246 s ν(OH), 3204 s ν(OH), 1676 m ν(C═N), 1666 m ν(C═N), 983 s ν(NO). ^1H NMR (CD_3OD), δ: 7.42 (t, 1*H*, C*H*, $^3J_{H,H}$ = 6.9 Hz), 7.39 (t, 1*H*, C*H*, $^3J_{H,H}$ = 5.8 Hz), 3.04 (m, 2*H*, C*H*$_2$), 2.52 (m, 2*H*, C*H*$_2$), 1.21 (t, 3*H*, C*H*$_3$, $^3J_{H,H}$ = 7.6 Hz), 1.11 (d, 3*H*, C*H*$_3$, $^3J_{H,H}$ = 7.7 Hz). $^{13}C\{^1H\}$ NMR (CD_3OD), δ: 161.5 (*C*═N), 160.0 (*C*═N), 24.6 (CH_2), 20.9 (CH_2), 9.3 (CH_3), 8.6 (CH_3). ^{195}Pt NMR (CD_3OD), δ: −529 (500 Hz). Crystals for X-ray study were obtained by slow evaporation of a methanol/toluene solution.

Dimerization of *trans*-Bis(aldoxime)- and *trans*-Bis(ketoxime)platinum(II) Complexes. Monomers **1**−**4** and *trans*-$[PtCl_2(R_2C═NOH)_2]$ (R = Me,[46] Et[41]) (0.1 mmol) were dissolved in 2−3 mL of acetone, and an equivalent amount of AgOAc (0.1 mmol) was added. The reaction mixture was stirred at room temperature for 1−3 h (followed by TLC), then the precipitate of AgCl was filtered off, and the resulting yellow solution was reduced to dryness. The product was isolated by column chromatography as the first fraction using a mixture of $CHCl_3$ and $Me_2C═O$ as mobile phase with a ratio of 20:1 for **5**, 8:1 for **6** and **9**, 30:1 for **7**, and 10:1 for **8** and **10**. Yields were 31−36%.

(SP-4-2)-Di-μ-((1*Z*)-*N*-oxyethanimine-κ*N*,κ*O*)bis[chlorido((1*Z*)-*N*-hydroxyethanimine-κ*N*)platinum(II)] (5). Anal. Calcd for $C_8H_{18}N_4Cl_2O_4Pt_2$: C, 13.82; H, 2.61; N, 8.06. Found: C, 13.87; H, 2.36; N, 7.65. ESI-MS^+ (MeOH), *m*/*z*: 542 $[M - 2\,Me(H)C═NOH - Cl]^+$, 600 $[M - 2\,Me(H)C═NOH + Na]^+$, 718 $[M + Na]^+$, 734 $[M + K]^+$. TLC (20:1 (v/v) $CHCl_3/Me_2C═O$): R_f = 0.58. IR in KBr (selected bands), cm^{-1}: 3247 s ν(OH), 1678 and 1619 m ν(C═N), 970 s ν(NO). ^1H NMR (CD_3OD), δ: 7.59 (q, 1*H*, C*H*, $^3J_{H,H}$ = 5.8 Hz), 6.99 (q, 1*H*, C*H*, $^3J_{H,H}$ = 5.8 Hz), 2.07 (d, 3*H*, C*H*$_3$, $^3J_{H,H}$ = 5.7 Hz), 1.94 (d, 3*H*, C*H*$_3$, $^3J_{H,H}$ = 5.8 Hz). $^{13}C\{^1H\}$ NMR (CD_3OD), δ: 153.8 (*C*═N), 151.3 (*C*═N), 12.3 (CH_3), 12.1 (CH_3). ^{195}Pt NMR (CD_3OD), δ: −208 (480 Hz).

(SP-4-2)-Di-μ-((1*Z*)-N-oxyethanimine-κ*N*,κ*O*)bis[chlorido((1*E*)-*N*-hydroxyethanimine-κ*N*)platinum(II)] (6). Anal. Calcd for $C_8H_{18}N_4Cl_2O_4Pt_2$: C, 13.82; H, 2.61; N, 8.06. Found: C, 14.02; H, 2.42; N, 7.72. ESI-MS^+ (MeOH), *m*/*z*: 600 $[M - Me(H)C═NOH - Cl]^+$, 676 $[M - 2\,Me(H)C═NOH + K]^+$, 718 $[M + Na]^+$, 734 $[M + K]^+$. TLC (8:1 (v/v) $CHCl_3/Me_2C═O$): R_f = 0.48. IR in KBr (selected bands), cm^{-1}: 3248 s ν(OH), 1676 and 1618 m ν(C═N), 964 s ν(NO). ^1H NMR (CD_3OD), δ: 7.78 (q, 1*H*, C*H*, $^3J_{H,H}$ = 5.8 Hz), 7.38 (q, 1*H*, C*H*, $^3J_{H,H}$ = 6.2 Hz), 2.33 (d, 3*H*, C*H*$_3$, $^3J_{H,H}$ = 6.2 Hz), 2.09 (d, 3*H*, C*H*$_3$, $^3J_{H,H}$ = 5.8 Hz). $^{13}C\{^1H\}$ NMR (CD_3OD), δ: 154.1 (*C*═N), 152.0 (*C*═N), 15.8 (CH_3), 12.4 (CH_3). ^{195}Pt NMR (CD_3OD), δ: −251 (490 Hz). Crystals for X-ray study were obtained by slow evaporation of a methanol/toluene solution at room temperature.

(SP-4-2)-Di-μ-((1*Z*)-*N*-oxypropane-1-imine-κ*N*,κ*O*)bis-[chlorido((1*Z*)-*N*-hydroxypropane-1-imine-κ*N*)platinum(II)] (7). Anal. Calcd for $C_{12}H_{26}N_4Cl_2O_4Pt_2$: C, 19.18; H, 3.49; N, 7.46. Found: C, 19.11; H, 3.25; N, 7.22. ESI-MS^+ (MeOH), *m*/*z*: 628 $[M - 2Et(H)C═NOH + Na]^+$, 716 $[M - Cl]^+$, 752 $[M + H]^+$, 774 $[M + Na]^+$. TLC ($CHCl_3$): R_f = 0.59. IR in KBr (selected bands), cm^{-1}: 3232 s ν(OH), 1660 and 1625 m ν(C═N), 961 s ν(NO). ^1H NMR (CD_3OD), δ: 7.50 (t, 1H, C*H*, $^3J_{H,H}$ = 5.7 Hz), 6.88 (t, 1*H*, C*H*, $^3J_{H,H}$ = 5.8 Hz), 2.55 (m, 2*H*, C*H*$_2$), 2.43 (m, 2*H*, C*H*$_2$), 1.13 (t, 3*H*, C*H*$_3$, $^3J_{H,H}$ = 7.6 Hz), 1.06 (t, 3*H*, C*H*$_3$, $^3J_{H,H}$ = 7.7 Hz). $^{13}C\{^1H\}$ NMR (CD_3OD), δ: 160.0 (*C*═N), 157.9 (*C*═N), 20.6 (CH_2), 20.5 (CH_2), 8.9 (CH_3), 8.7 (CH_3). ^{195}Pt NMR (CD_3OD), δ: −212 (440 Hz).

(SP-4-2)-Di-μ-((1*Z*)-*N*-oxypropane-1-imine-κ*N*,κ*O*)bis-[chlorido((1*E*)-*N*-hydroxypropane-1-imine-κ*N*)platinum(II)] (8). Anal. Calcd for $C_{12}H_{26}N_4Cl_2O_4Pt_2$: C, 19.18; H, 3.49; N, 7.46. Found: C, 19.21; H, 3.43; N, 7.16. ESI-MS^+ (MeOH), *m*/*z*: 628 $[M - 2Et(H)C═NOH + Na]^+$, 716 $[M - Cl]^+$, 752 $[M + H]^+$, 774 $[M + Na]^+$. TLC (20:1 (v/v) $CHCl_3/Me_2C═O$): R_f = 0.71. IR in KBr

(selected bands), cm^{-1}: 3250 s ν(OH), 1681 and 1624 m ν(C═N), 958 s ν(NO). ^{1}H NMR (CD_3OD), δ: 7.70 (t, 1*H*, C*H*, $^3J_{H,H}$ = 5.7 Hz), 7.31 (t, 1*H*, C*H*, $^3J_{H,H}$ = 6.8 Hz), 2.89 (m, 2*H*, CH_2), 2.58 (m, 2*H*, CH_2), 1.161 (t, 3*H*, CH_3, $^3J_{H,H}$ = 7.6 Hz), 1.160 (t, 3*H*, CH_3, $^3J_{H,H}$ = 7.7 Hz). $^{13}C\{^1H\}$ NMR (CD_3OD), δ: 159.6 (C═N), 157.2 (*C*═N), 24.2 (*C*H_3), 20.7 (*C*H_3), 9.8 (*C*H_3), 8.6 (*C*H_3). ^{195}Pt NMR (CD_3OD), δ: −243 (450 Hz).

(SP-4-2)-Di-μ-(*N*-oxypropane-2-imine-$\kappa N,\kappa O$)bis[chlorido(*N*-hydroxypropane-2-imine-κN))platinum(II)] (9). Anal. Calcd for $C_{12}H_{26}N_4Cl_2O_4Pt_2$: C, 19.36; H, 3.27; N, 7.06. Found: C, 19.54; H, 3.29; N, 7.43%. ESI-MS$^+$ (MeOH), *m*/*z*: 752 $[M + H]^+$, 774 $[M + Na]^+$. TLC (8:1 (v/v) $CHCl_3/Me_2C$═O): R_f = 0.53. IR in KBr (selected bands), cm^{-1}: 3143 s ν(OH), 1666 and 1620 m ν(C═N), 969 s ν(NO). ^{1}H NMR ($CDCl_3$), δ: 8.67 (s, 2*H*, O*H*), 2.72 (s, 6*H*, CH_3), 2.55 (s, 6*H*, CH_3), 2.29 (s, 6*H*, CH_3), 2.09 (s, 6*H*, CH_3). $^{13}C\{^1H\}$ NMR ($CDCl_3$), δ: 165.4 (*C*═N), 157.4 (*C*═N), 25.0 (CH_3), 23.7 (CH_3), 18.4 (CH_3), 17.7 (CH_3). ^{195}Pt NMR ($CDCl_3$), δ: −35 (400 Hz). Crystals for X-ray study were obtained by slow evaporation of an acetone solution at room temperature.

(SP-4-2)-Di-μ-(*N*-oxypentane-3-imine-$\kappa N,\kappa O$)bis[chlorido(*N*-hydroxypentane-3-imine-κN))platinum(II)] (10). Anal. Calcd. for $C_{20}H_{42}N_4Cl_2O_4Pt_2$: C, 27.81; H, 4.90; N, 6.49. Found: C, 27.42; H, 4.73; N, 6.27. ESI-MS$^+$ (MeOH), *m*/*z*: 828 $[M - Cl]^+$, 864 $[M + H]^+$, 886 $[M + Na]^+$. TLC (20:1 (v/v) $CHCl_3/Me_2C$═O): R_f = 0.43. IR in KBr (selected bands), cm^{-1}: 3377 s ν(OH), 1651 and 1609 m ν(C═N), 966 s ν(NO). ^{1}H NMR (CD_3OD), δ: 3.59 (m, 2*H*, 2CH*H*), 3.36 (m, 2*H*, 2CH*H*), 3.22 (m, 2*H*, 2CH*H*), 3.11 (m, 2*H*, 2CH*H*), 2.65 (m, 4*H*, 4CH*H*), 2.52 (m, 2*H*, 2CH*H*), 2.36 (m, 2*H*, 2CH*H*), 1.34 (t, 6*H*, 2CH_3, $^3J_{H,H}$ = 7.6 Hz), 1.21 (t, 6*H*, 2CH_3, $^3J_{H,H}$ = 7.6 Hz), 1.16 (t, 6*H*, 2CH_3, $^3J_{H,H}$ = 7.6 Hz), 1.00 (t, 6*H*, 2CH_3, $^3J_{H,H}$ = 7.6 Hz). $^{13}C\{^1H\}$ NMR (CD_3OD), δ: 173.2 (2*C*═N), 168.5 (2*C*═N), 29.1 (CH_2), 28.9 (CH_2), 28.3 (CH_2), 28.1 (CH_2), 22.4 (2CH_2), 22.1 (2CH_2), 10.3 (4CH_3), 9.17 (2CH_3), 9.0 (2CH_3). ^{195}Pt NMR (CD_3OD), δ: −152 (510 Hz). Crystals of the respective trimer for X-ray study were obtained by slow evaporation of an EtOH, EtOAc, and acetone mixture solution at room temperature.

Crystal Structure Determinations. X-ray diffraction measurements were performed with Bruker X8 APEX II CCD diffractometer at 100 K. Single crystals were positioned at 35 mm from the detector, and 1557, 1865, 1853, 3003, and 1194 frames were measured, each for 60, 30, 5, 20, and 50 s over 1° scan width for **1**, **4**, **6**, **9**, and **11**, respectively. Data were processed using the SAINT software package.[92] Crystal data, data collection parameters, and structure refinement details for **1**, **4**, **6**, **9**, and **11** are given in Table 1. Structures were solved by direct methods and refined by full-matrix least-squares techniques. Non-hydrogen atoms were refined with anisotropic displacement parameters. H atoms were placed at calculated positions and refined as riding atoms in the subsequent least-squares model refinements. The isotropic thermal parameters were estimated to be 1.2 times the values of the equivalent isotropic thermal parameters of the non-hydrogen atoms to which hydrogen atoms were bonded. SHELXS-97[93] was used for structure solution and SHELXL-97[94] for refinement; molecular diagrams were produced with ORTEP.[95]

Cell Lines and Culture Conditions. Human cancer cell lines: CH1 (ovarian carcinoma) kindly provided by Lloyd R. Kelland (CRC Centre for Cancer Therapeutics, Institute of Cancer Research, Sutton, U.K.) and A549 (nonsmall cell lung cancer) and SW480 (colon carcinoma), both provided by Brigitte Marian (Institute of Cancer Research, Department of Medicine I, Medical University of Vienna, Austria), were used for the experiments. Cells were grown in 75 cm^2 culture flasks (Iwaki/Asahi Technoglass, Gyouda, Japan) as adherent monolayer cultures in complete medium [i.e., Minimal Essential Medium (MEM) supplemented with 10% heat-inactivated fetal bovine serum, 1 mM sodium pyruvate, 4 mM L-glutamine, and 1% nonessential amino acids (all purchased from Sigma-Aldrich, Austria)]. Cell cultures were incubated at 37 °C in a moist atmosphere containing 5% CO_2.

Cytotoxicity in Cancer Cell Lines. The cytotoxic activity of the compounds was determined by means of a colorimetric microculture assay (MTT assay, MTT = 3-(4,5-dimethyl-2-thiazolyl)-2,5-diphenyl-2*H*-tetrazolium bromide). A549, CH1, and SW480 cells were harvested from culture flasks by trypsinization and seeded in 100 μL aliquots in MEM into 96-well plates (Iwaki/Asahi Technoglass, Gyouda, Japan) in cell densities of 3×10^3, 1×10^3, and 2.5×10^3 cells per well, respectively. After 24 h preincubation of the cells, the test compounds were dissolvedand serially diluted in MEM, and 100 μL of solution was added per well. Compounds **5**−**9**, which are insufficiently soluble in medium, were dissolved in dimethyl sulfoxide and then diluted in MEM not to exceed the concentration of 0.5% DMSO in the applied solution. After continuous exposure for 96 h, drug solutions were replaced with 100 μL of RPMI 1640 culture medium (supplemented with 10% heat-inactivated fetal bovine serum and 2 mM L-glutamine) plus 20 μL of MTT solution in phosphate-buffered saline (5 mg/mL). After incubation for 4 h, the RPMI/MTT mixtures were removed, and the formazan crystals formed in viable cells were dissolved in 150 μL of DMSO per well. Optical densities were measured at 550 nm with a microplate reader (Tecan Spectra Classic) using a reference wavelength of 690 nm to correct for unspecific absorption. The quantity of viable cells was expressed in terms of T/C values by comparison to untreated control microcultures, and 50% inhibitory concentrations (IC_{50}) were calculated from concentration−effect curves by interpolation. Evaluation is based on means from at least three independent experiments, each comprising three replicates per concentration level.

Solution Behavior. For investigation of the behavior of monomer **1** and respective dimer **5** in aqueous solution, time-dependent ^{1}H NMR measurements were carried out in a 10 mM phosphate-buffered D_2O solution at pH of 7.4 containing 0.125 M NaCl over 3 days. The concentrations of complexes were ca. 400 and 200 μM, correspondingly. Additionally, the hydrolysis experiment for **1** was performed at analogous conditions in the absence of NaCl. All NMR measurements were performed at ambient temperature.

Apoptosis Assay. Cell death induction was analyzed by fluorescence-activated cell sorting (FACS) using FITC-conjugated annexin V (BioVision, USA) and propidium iodide (PI; Fluka) staining. Colon carcinoma (SW480) and human promyelocytic leukemia (HL60) cells were seeded into 12-well plates (CytoOne, Starlab, U.K.) in amounts of 1×10^5 cells per well in complete medium (MEM) and allowed to settle for 24 h. The cells were exposed to cisplatin and compounds **3** and **7** for 24 h at 37 °C. After incubation, SW480 cells were gently trypsinized and both cell lines were collected, washed with PBS, and resuspended with FITC-conjugated annexin V (0.25 μg/mL) in binding buffer (10 mM HEPES/NaOH pH 7.4, 140 mM NaCl, 2.5 mM $CaCl_2$) at room temperature for 15 min. PI (1 μg/mL) was added shortly before measurement. Stained cells were analyzed with Guava 8HT EasyCyte Flow cytometer (Merk Milipore, Guava, USA) using InCyte software. At least three independent experiments were conducted, and 5000 cells were counted per analysis.

■ ASSOCIATED CONTENT

Supporting Information

Description of synthesis and characterization of *trans*-bis(aldoxime)platinum(II) complexes, as well as X-ray structure determination for **1** and **4**; ORTEP view of **1** and **4**; table with selected bond lengths and angles for complexes **1** and **4**; figure with ^{1}H NMR spectra of monomer **1** and corresponding dimer **5** under different conditions; geometry optimization of a ring-shaped trimer; figure with the optimized structure of the ring-shaped trimer; figure and tables with results of the induction of apoptosis in SW480 and HL60 cancer cells; X-ray crystallographic file in CIF format for **1**, **4**, **6**, **9**, and **11**. This material is available free of charge via the Internet at http://pubs.acs.org.

AUTHOR INFORMATION

Corresponding Author

*Phone: +43-1-4277-52600. Fax: +43-1-4277-52680. E-mail: markus.galanski@univie.ac.at; bernhard.keppler@univie.ac.at.

Notes

The authors declare no competing financial interest.

ACKNOWLEDGMENTS

The authors are indebted to the FFG-Austrian Research Promotion Agency, the Austrian Council for Research and Technology Development, and COST D39. V.Y.K. is grateful to RFBR for grant 11-03-90417. We are thankful to Mag. H. Varbanov for geometry optimization of the ring-shaped trimeric structure.

REFERENCES

(1) Cleare, M. J.; Hoeschele, J. D. *Platinum Met. Rev.* **1973**, *17*, 2−13.
(2) Cleare, M. J.; Hoeschele, J. D. *Bioinorg. Chem.* **1973**, *2*, 187−210.
(3) Rosenberg, B.; Van Kamp, L.; Crigas, T. *Nature* **1965**, *205*, 698−699.
(4) Jakupec, M. A.; Galanski, M.; Keppler, B. K. *Rev. Physiol. Biochem. Pharmacol.* **2003**, *146*, 1−54.
(5) Galanski, M.; Jakupec, M. A.; Keppler, B. K. *Curr. Med. Chem.* **2005**, *12*, 2075−2094.
(6) Galanski, M.; Arion, V. B.; Jakupec, M. A.; Keppler, B. K. *Curr. Pharm. Des.* **2003**, *9*, 2078−2089.
(7) Farrell, N. *PCT Int. Appl.* **1991**, 1−31.
(8) Farrell, N.; Qu, Y.; Hoeschele, J. D. *PCT Int. Appl.* **1994**, 1−36.
(9) Kraker, A. J.; Hoeschele, J. D.; Elliott, W. L.; Showalter, H. D.; Hollis, L. S.; Sercel, A. D.; Farrell, N. P. *J. Med. Chem.* **1992**, *35*, 4526−4532.
(10) Wu, P. K.; Qu, Y.; Van Houten, B.; Farrell, N. *J. Inorg. Biochem.* **1994**, *54*, 207−220.
(11) Farrell, N.; Appleton, T. G.; Qu, Y.; Roberts, J. D.; Fontes, A. P. S.; Skov, K. A.; Wu, P.; Zou, Y. *Biochemistry* **1995**, *34*, 15480−15486.
(12) Qu, Y.; Bloemink, M. J.; Reedijk, J.; Hambley, T. W.; Farrell, N. *J. Am. Chem. Soc.* **1996**, *118*, 9307−9313.
(13) Farrell, N.; Menta, E.; Valsecchi, M.; Di Domenico, R.; Da Re, G.; Manzotti, C.; Pezzoni, G.; Giuliani, F. C.; Spinelli, S *J. Inorg. Biochem.* **1997**, *67*, 173.
(14) Qu, Y.; Farrell, N.; Kasparkova, J.; Brabec, V. *J. Inorg. Biochem.* **1997**, *67*, 174.
(15) Perego, P.; Caserini, C.; Gatti, L.; Carenini, N.; Romanelli, S.; Supino, R.; Colangelo, D.; Viano, I.; Leone, R.; Spinelli, S.; Pezzoni, G.; Manzotti, C.; Farrell, N.; Zunino, F. *Mol. Pharmacol.* **1999**, *55*, 528−534.
(16) Kloster, M. B. G.; Hannis, J. C.; Muddiman, D. C.; Farrell, N. *Biochemistry* **1999**, *38*, 14731−14737.
(17) Qu, Y.; Rauter, H.; Fontes, A. P. S.; Bandarage, R.; Kelland, L. R.; Farrell, N. *J. Med. Chem.* **2000**, *43*, 3189−3192.
(18) Cox, J. W.; Berners-Price, S. J.; Davies, M. S.; Qu, Y.; Farrell, N *J. Am. Chem. Soc.* **2001**, *123*, 1316−1326.
(19) Fan, D.; Yang, X.; Wang, X.; Zhang, S.; Mao, J.; Ding, J.; Lin, L.; Guo, Z. *J. Biol. Inorg. Chem.* **2007**, *12*, 655−665.
(20) McGregor, T. D.; Hegmans, A.; Kasparkova, J.; Neplechova, K.; Novakova, O.; Penazova, H.; Vrana, O.; Brabec, V.; Farrell, N. *J. Biol. Inorg. Chem.* **2002**, *7*, 397−404.
(21) Kasparkova, J.; Zehnulova, J.; Farrell, N.; Brabec, V. *J. Biol. Chem.* **2002**, *277*, 48076−48086.
(22) Hegmans, A.; Berners-Price, S. J.; Davies, M. S.; Thomas, D. S.; Humphreys, A. S.; Farrell, N. *J. Am. Chem. Soc.* **2004**, *126*, 2166−2180.
(23) Kasparkova, J.; Vrana, O.; Farrell, N.; Brabec, V. *J. Inorg. Biochem.* **2004**, *98*, 1560−1569.
(24) Harris, A. L.; Ryan, J. J.; Farrell, N. *Mol. Pharmacol.* **2006**, *69*, 666−672.
(25) Kabolizadeh, P.; Ryan, J.; Farrell, N. *Biochem. Pharmacol.* **2007**, *73*, 1270−1279.
(26) Malina, J.; Farrell, N. P.; Brabec, V. *Chem.−Asian J.* **2011**, *6*, 1566−1574.
(27) Wheate, N. J.; Collins, J. G. *J. Inorg. Biochem.* **2000**, *78*, 313−320.
(28) Wheate, N. J.; Cutts, S. M.; Phillips, D. R.; Aldrich-Wright, J. R.; Collins, J. G. *J. Inorg. Biochem.* **2001**, *84*, 119−127.
(29) Wheate, N. J.; Evison, B. J.; Herlt, A. J.; Phillips, D. R.; Collins, J. G. *Dalton Trans.* **2003**, *18*, 3486−3492.
(30) Collins, J. G.; Wheate, N. J. *J. Inorg. Biochem.* **2004**, *98*, 1578−1584.
(31) Chikuma, M.; Hirai, M.; Komeda, S.; Kimura, Y.; Kumakura, K. *J. Inorg. Biochem.* **1997**, *67*, 348.
(32) Komeda, S.; Lutz, M.; Spek, A. L.; Chikuma, M.; Reedijk, J. *Inorg. Chem.* **2000**, *39*, 4230−4236.
(33) Komeda, S.; Lutz, M.; Spek, A. L.; Yamanaka, Y.; Sato, T.; Chikuma, M.; Reedijk, J. *J. Am. Chem. Soc.* **2002**, *124*, 4738−4746.
(34) Komeda, S.; Kalayda, G. V.; Lutz, M.; Spek, A. L.; Yamanaka, Y.; Sato, T.; Chikuma, M.; Reedijk, J. *J. Med. Chem.* **2003**, *46*, 1210−1219.
(35) Komeda, S.; Lin, Y.-L.; Chikuma, M. *Chem. Med. Chem.* **2011**, *6*, 987−990.
(36) Margiotta, N.; Ostuni, R.; Teoli, D.; Morpurgo, M.; Realdon, N.; Palazzo, B.; Natile, G. *Dalton Trans.* **2007**, *29*, 3131−3139.
(37) Margiotta, N.; Ostuni, R.; Piccinonna, S.; Natile, G.; Zanellato, I.; Boidi, C. D.; Bonarrigo, I.; Osella, D. *J. Inorg. Biochem.* **2011**, *105*, 548−557.
(38) Xie, M.; Liu, W.; Lou, L.; Chen, X.; Ye, Q.; Yu, Y.; Chang, Q.; Hou, S. *Inorg. Chem.* **2010**, *49*, 5792−5794.
(39) Quiroga, A. G.; Cubo, L.; de Blas, E.; Aller, P.; Navarro-Ranninger, C. *J. Inorg. Biochem.* **2007**, *101*, 104−110.
(40) Zorbas-Seifried, S.; Jakupec, M. A.; Kukushkin, N. V.; Groessl, M.; Hartinger, C. G.; Semenova, O.; Zorbas, H.; Kukushkin, V. Yu.; Keppler, B. K. *Mol. Pharmacol.* **2007**, *71*, 357−365.
(41) Scaffidi-Domianello, Yu. Yu.; Meelich, K.; Jakupec, M. A.; Arion, V. B.; Kukushkin, V. Yu.; Galanski, M.; Keppler, B. K. *Inorg. Chem.* **2010**, *49*, 5669−5678.
(42) Bartel, C.; Bytzek, A. K.; Scaffidi-Domianello, Yu. Yu.; Grabmann, G.; Jakupec, M. A.; Hartinger, C. G.; Galanski, M.; Keppler, B. K. *J. Biol. Inorg. Chem.* **2012**, *17*, 465−474.
(43) Grabmann, G.; Meier, S. M.; Scaffidi-Domianello, Yu. Yu.; Galanski, M.; Keppler; B. K.; Hartinger, C. G. Manuscript in preparation.
(44) Kukushkin, V. Yu.; Belsky, V. K.; Aleksandrova, E. A.; Konovalov, V. E.; Kirakosyan, G. A. *Inorg. Chem.* **1992**, *31*, 3836−3840.
(45) Kukushkin, V. Yu.; Tudela, D.; Izotova, Y. A.; Belsky, V. K.; Stash, A. I. *Polyhedron* **1998**, *17*, 2455−2461.
(46) Kukushkin, V. Yu.; Izotova, Y. A.; Tudela, D. *Inorg. Synth.* **2004**, *34*, 81−85.
(47) Wells, A. F. *Structural Inorganic Chemistry*, 5th ed.; Oxford University Press: Oxford, U.K., 1986; pp 357, 692.
(48) Hollis, L. S.; Lippard, S. J. *J. Am. Chem. Soc.* **1981**, *103*, 1230−1232.
(49) Peilert, M.; Erxleben, A.; Lippert, B. *Z. Anorg. Allg. Chem.* **1996**, *622*, 267−274.
(50) Liu, F.; Chen, W.; Wang, D. *Dalton Trans.* **2006**, 3445−3453.
(51) Cornacchia, D.; Pellicani, R. Z.; Intini, F. P.; Pacifico, C.; Natile, G. *Inorg. Chem.* **2009**, *48*, 10800−10810.
(52) Sakai, K.; Takeshita, M.; Tanaka, Y.; Ue, T.; Yanagisawa, M.; Kosaka, M.; Tsubomura, T.; Ato, M.; Nakano, T. *J. Am. Chem. Soc.* **1998**, *120*, 11353−11363.
(53) Hollis, L. S.; Lippard, S. J. *Inorg. Chem.* **1983**, *22*, 2600−2604.
(54) O'Halloran, T. V.; Roberts, M. M.; Lippard, S. J. *Inorg. Chem.* **1986**, *25*, 957−964.
(55) Crespo, M.; Font-Bardia, M.; Granell, J.; Martinez, M.; Solans, X. *Dalton Trans.* **2003**, 3763−3769.
(56) Vicente, J.; Chicote, M.-T.; Lagunas, M.-C. *Inorg. Chem.* **1995**, *34*, 5441−5445.
(57) Marino, N.; Fazen, C. H.; Blakemore, J. D.; Incarvito, C. D.; Hazari, N.; Doyle, R. P. *Inorg. Chem.* **2011**, *50*, 2507−2520.

(58) Wang, K.-W.; Chen, J.-L.; Cheng, Y.-M.; Chung, M.-W.; Hsieh, C.-C.; Lee, G.-H.; Chou, P.-T.; Chen, K.; Chi, Y. *Inorg. Chem.* **2010**, *49*, 1372−1383.
(59) Kukushkin, V. Yu.; Belsky, V. K.; Tudela, D. *Inorg. Chem.* **1996**, *35*, 510−513.
(60) Scaffidi-Domianello, Yu. Yu.; Haukka, M.; Kelly, P. F.; Galanski, M.; Keppler, B. K.; Kukushkin, V. Yu. *Z. Krystallogr. NCS* **2006**, *221*, 226−228.
(61) Kaplan, S. F.; Kukushkin, V. Yu.; Shova, S.; Suwinska, K.; Wagner, G.; Pombeiro, A. J. L. *Eur. J. Inorg. Chem.* **2001**, 1031−1038.
(62) Appleton, T. G.; Bailey, A. J.; Barnham, K. J.; Hall, J. R. *Inorg. Chem.* **1992**, *31*, 3077−3082.
(63) Biswas, B.; Salunke-Gawali, S.; Weyhermüller, T.; Bachler, V.; Bill, E.; Chaudhuri, P. *Inorg. Chem.* **2010**, *49*, 626−641.
(64) Costes, J.-P.; Dahan, F.; Dupuis, A.; Laurent, J.-P. *Inorg. Chem.* **2000**, *39*, 169−173.
(65) Langenbahn, M.; Stoeckli-Evans, H.; Suess-Fink, G. *J. Organomet. Chem.* **1990**, *397*, 347−358.
(66) Chao, M.-H.; Kumaresan, S.; Wen, Y.-S.; Lin, S.-C.; Hwu, J. R.; Lu, K.-L. *Organomet.* **2000**, *19*, 714−717.
(67) Dreos, R.; Tauzher, G.; Trendafilova, D. H.; Nardin, G.; Randaccio, L. *Inorg. Chem.* **1996**, *35*, 2715−2716.
(68) Kanderal, O. M.; Kozłowski, H.; Dobosz, A.; Swiatek-Kozlowska, J.; Meyerd, F.; Fritsky, I. O. *Dalton Trans.* **2005**, 1428−1437.
(69) Audhya, A.; Bhattacharya, K.; Maity, M.; Chaudhury, M. *Inorg. Chem.* **2010**, *49*, 5009−5015.
(70) Kanderal, O. M.; Kozłowski, H.; Dobosz, A.; Swiatek-Kozlowska, J.; Meyerd, F.; Fritsky, I. O. *Dalton Trans.* **2005**, 1428−1437.
(71) Ross, P. F.; Murmann, R. K.; Schlemper, E. O. *Acta Crystallogr.* **1974**, *B30*, 1120−1123.
(72) Bencini, A.; Costes, J.-P.; Dahan, F.; Dupuis, A.; Garcia-Tojal, J.; Gatteschi, D.; Totti, F. *Inorg. Chim. Acta* **2004**, *357*, 2150−2156.
(73) Mathrubootham, V.; Addison, A. W. K.; Holman, T.; Laurence, E. S.; Thompson, K. *Dalton Trans.* **2009**, 8111−8116.
(74) Cano, J.; Rodríguez-Fortea, A.; Alemany, P.; Alvarez, S.; Ruiz, E. *Chem.—Eur. J.* **2000**, *6*, 327−333.
(75) Liu, X.-W.; Chu, S.; Wang, X.-Q.; Zhang, Y.; Wang, R.; Shen, G.-Q.; Shen, D.-Z. *Inorg. Chem. Commun.* **2002**, *5*, 1086−1089.
(76) Dominguez-Vera, J. M.; Colacio, E.; Escuer, A.; Klinga, M.; Kivekäs, R.; Romerosa, A. *Polyhedron* **1996**, *16*, 281−289.
(77) Escuer, A.; Vlahopoulou, G.; Perlepes, S. P.; Font-Bardia, M.; Calvet, T. *Dalton Trans.* **2011**, *40*, 225−233.
(78) Datta, D.; Mascharak, P. K.; Chakravorty, A. *Inorg. Chem.* **1981**, *20*, 1673−1679.
(79) Akagi, F.; Michihiro, Y.; Nakao, Y.; Matsumoto, K.; Sato, T.; Mori, W. *Inorg. Chim. Acta* **2004**, *357*, 684−688.
(80) Koumousi, E. S.; Raptopoulou, C. P.; Perlepes, S. P.; Escuer, A.; Stamatatos, T. C. *Polyhedron* **2010**, *29*, 204−211.
(81) Ruiz, R.; Lloret, F.; Julve, M.; Faus, J. M.; Mufioz, C.; Solans, X. *Inorg. Chim. Acta* **1998**, *268*, 263−269.
(82) Maekawa, M.; Kitagawa, S.; Nakao, Y.; Sakamoto, S.; Yatani, A.; Mori, W.; Kashino, S.; Munakata, M. *Inorg. Chim. Acta* **1999**, *293*, 20−29.
(83) Cervera, B.; Ruiz, R.; Lloret, F.; Julve, M.; Cano, J.; Faus, J.; Bois, C.; Mrozinski, J. *Dalton Trans.* **1997**, 395−401.
(84) Birkelbach, F.; Winter, M.; Flöke, U.; Haupt, H.-J.; Butzlaff, C.; Lengen, M.; Bill, E.; Trautwein, A. X.; Wieghardt, K.; Chaudhuri, P. *Inorg. Chem.* **1994**, *33*, 3990−4001.
(85) Salonen, M. *J. Coord. Chem.* **2010**, *63*, 3127−3136.
(86) Buyuktas, B. S.; Aktas, O. *Transition Met. Chem.* **2006**, *31*, 56−61.
(87) Stoumpos, C. C.; Inglis, R.; Roubeau, O.; Sartzi, H.; Kitos, A. A.; Milios, C. J.; Aromi, G.; Tasiopoulos, A. J.; Nastopoulos, V.; Brechin, E. K.; Perlepes, S. P. *Inorg. Chem.* **2010**, *49*, 4388−4390.
(88) Milios, C. J.; Wood, P. A.; Parsons, S.; Foguet-Albiol, D.; Lampropoulos, C.; Christou, G.; Perlepes, S. P.; Brechin, E. K. *Inorg. Chim. Acta* **2007**, *360*, 3932−3940.
(89) Cremades, E.; Cano, J.; Ruiz, E.; Rajaraman, G.; Milios, C. J.; Brechin, E. K. *Inorg. Chem.* **2009**, *48*, 8012−8019.
(90) Portela-Cubillo, F.; Lymer, J.; Scanlan, E. M.; Scott, J. S.; Walton, J. C. *Tetrahedron* **2008**, *64*, 11908−11916.
(91) Wang, K.; Fu, X.; Liu, J.; Liang, Y.; Dong, D. *Org. Lett.* **2009**, *11*, 1015−1018.
(92) *SAINT-Plus*, version 7.06a and APEX2; Bruker-Nonius AXS Inc.: Madison, WI, 2004.
(93) Sheldrick, G. M. *Acta Crystallogr.* **1990**, *A46*, 467−473.
(94) Sheldrick, G. M. *Acta Crystallogr.* **2008**, *A64*, 112−122.
(95) Burnett, M. N.; Johnson, G. K. *ORTEP III*, Report ORNL-6895; Oak Ridge National Laboratory: Oak Ridge, TN, 1996.

2.4 Synthesis and characterization of novel bis(carboxylato)dichloridobis(ethylamine) platinum(IV) complexes with higher cytotoxicity than cisplatin

Varbanov H., Valiahdi S. M., Legin A. A., Jakupec M. A., Roller A., Galanski M., Keppler B. K.

European Journal of Medical Chemistry 2011, **46**, 5456-5464. DOI: 10.1016/j.ejmech.2011.09.006

European Journal of Medicinal Chemistry 46 (2011) 5456–5464

Contents lists available at SciVerse ScienceDirect

European Journal of Medicinal Chemistry

journal homepage: http://www.elsevier.com/locate/ejmech

Original article

Synthesis and characterization of novel bis(carboxylato)dichloridobis(ethylamine) platinum(IV) complexes with higher cytotoxicity than cisplatin

Hristo Varbanov, Seied M. Valiahdi, Anton A. Legin, Michael A. Jakupec, Alexander Roller, Markus Galanski*, Bernhard K. Keppler*

University of Vienna, Institute of Inorganic Chemistry, Währinger Strasse 42, A-1090 Vienna, Austria

ARTICLE INFO

Article history:
Received 15 April 2011
Received in revised form
22 July 2011
Accepted 4 September 2011
Available online 8 September 2011

Keywords:
Platinum complexes
Synthesis
Characterization
Lipophilicity
Cytotoxicity

ABSTRACT

A series of six novel bis(carboxylato)dichloridobis(ethylamine)platinum(IV) complexes was synthesized and characterized in detail by elemental analysis, FT-IR, ESI-MS, HPLC, multinuclear (^{1}H, ^{13}C, ^{15}N, ^{195}Pt) NMR spectroscopy and in one case by X-ray diffraction. Cytotoxic properties of the complexes were evaluated in four human tumor cell lines originating from ovarian carcinoma (CH1 and SK-OV-3), colon carcinoma (SW480) and non-small cell lung cancer (A549) by means of the MTT colorimetrical assay. In addition, their octanol/water partition coefficients (log *P* values) were determined. Remarkably the most active (and also most lipophilic) compounds, having 4-propyloxy-4-oxobutanoato and 4-(2-propyloxy)-4-oxobutanoato axial ligands, showed IC_{50} values down to the low nanomolar range.

1. Introduction

Nowadays, 35 years after the serendipitous discovery of the cytotoxic potential of *cis*-diamminedichloridoplatinum(II) [1], more than 50% of anticancer therapy is platinum based. All platinum containing drugs used in the clinics are platinum(II) compounds (cisplatin, carboplatin, oxaliplatin, nedaplatin, lobaplatin and heptaplatin) [2]. However, it was shown, that Pt(IV) complexes also exhibit strong cytotoxic activity and can have some advantages in comparison to their Pt(II) analogues [3,4]. Consequences of the higher oxidation state are the introduction of two extra ligands and the change from planar to octahedral geometry. These characteristics, together with their higher kinetic inertness compared to their platinum(II) counterparts, opens up new possibilities in the design of novel platinum-based drugs (easier modulation of the pharmacokinetic properties, more opportunities for targeted therapy, oral administration, etc.) [5]. Nevertheless, no Pt(IV) complex has gained clinical approval up to now [2]. Four Pt(IV) compounds were in clinical trials (Fig. 1): tetraplatin was rejected after phase I because of a high general toxicity [6]; iproplatin was abandoned after phase III clinical trials, because it didn't show advantages compared with carboplatin [2]; satraplatin was rejected after the SPARC (Satraplatin and Prednisone Against Refractory Cancer) phase III clinical trials [7], because it didn't show a convincing benefit in terms of overall survival [8]; currently satraplatin is in phase I and II clinical trials in combination regimens [9]; its adamantylamine analogue LA-12 has passed phase I clinical trials.

Considering the mechanism of action of Pt(IV) complexes, it is accepted that they act as prodrugs via activation by reduction to their reactive Pt(II) species [10,11]. Pt(IV) based drugs would have better activity and lower side effects, when they are reduced primarily in the cell; contrary, an extracellular reduction would lead to deactivation and general toxicity. Consequently, the drug's potential strongly correlates with the rate of reduction which depends on the respective reduction potential [12]. Depending on the nature of the axial ligands, platinum(IV) complexes are reduced more easily in the following order: $CF_3COO > Cl > CH_3COO > OH$ [13] It was found that complexes with Cl^- as axial ligands were reduced very fast and showed a high general toxicity (tetraplatin [14]), on the other hand, complexes with axial hydroxido ligands were not reduced fast enough in the body to express their antitumor activity (iproplatin [15]). In the case of axial carboxylato ligands, an intermediate and optimal redox potential was observed [16], which led to promising results, obtained in preclinical and clinical evaluation of satraplatin and its adamantylamine analogue LA-12.

* Corresponding authors. Tel.: +43 1 4277 52601; fax: +43 1 4277 52680.
E-mail addresses: markus.galanski@univie.ac.at (M. Galanski), bernhard.keppler@univie.ac.at (B.K. Keppler).

0223-5234/
doi:10.1016/j.ejmech.2011.09.006

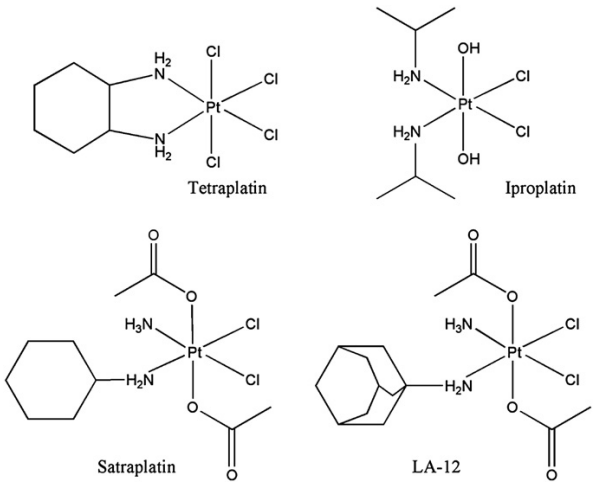

Fig. 1. Chemical structures of anticancer Pt(IV) complexes evaluated in clinical trials.

Recently, a convenient way for obtaining a series of dicarboxylatoplatinum(IV) complexes and modulation of their physicochemical properties such as solubility and lipophilicity was reported by our group [17–22]. In order to broaden the knowledge with respect to structure–activity relationships for that type of compounds and to find candidates with a promising physicochemical and pharmacological profile, we have synthesized a series of bis(carboxylato)dichloridobis(ethylamine)platinum(IV) complexes. The new compounds were fully characterized by elemental analysis, ATR IR, multinuclear NMR spectroscopy, HPLC and X-ray crystallography in one of the cases. Their cytotoxic properties were evaluated in four human tumor cell lines, originating from ovarian carcinoma (CH1 and SK-OV-3), colon carcinoma (SW480) and non-small cell lung cancer (A549), by means of the MTT colorimetrical assay. In addition, their octanol/water partition coefficients (log *P*) were determined.

2. Result and discussion

2.1. Synthesis

The new complexes were prepared according to the reaction scheme shown in Fig. 2, starting from K_2PtCl_4, which was converted to (SP-4-2)-dichloridobis(ethylamine)platinum(II) (complex **1**). Oxidation of **1** to the dihydroxido complex **2** was performed in aqueous solution, using 15% hydrogen peroxide as oxidizing agent.

Subsequent carboxylation of **2** with succinic anhydride was carried out in absolute DMF obtaining the dicarboxylato complex. The latter was used as starting material for the synthesis of complexes **4**–**8** via activation of its free carboxylic groups with CDI (1,1′-carbonyldiimidazole) in absolute DMF under argon atmosphere. To the imidazolide formed *in situ*, the respective alcoholate/alcohol mixtures or amine were added to obtain the respective esters (**4**–**6**) or amide (**8**). Purification of the crude products was performed with column chromatography and re-crystallization, when necessary.

When synthesizing complex **7** following the described procedure, a mixture of the desired diisopropylester (**7**) and asymmetric methylisopropylester (**7a**) in a ratio of 2:1 (according to ^{1}H NMR) was obtained. Unfortunately separation and isolation of compound **7** was not successful. Formation of the mixed methylisopropylester derivative **7a** was also confirmed by ESI-MS. Most likely **7a** was formed during separation via column chromatography. Apparently, reaction of **3** after CDI activation with isopropanol is not as fast as in the case of complexes **4**–**6**. As a result, the monoimidazolide platinum complex reacted with methanol, one of the constituents of the mobile phase. By increasing the reaction time from 24 to 72 h and avoiding the use of methanol in the mobile phase for purification, we were able to obtain exclusively pure **7** in satisfactory yield.

2.2. Spectroscopic characterization

Structures of the starting compounds (**1**, **2**) were proven by NMR and ATR IR spectroscopy and the new complexes (**3**–**8**) were fully characterized by elemental analysis, one- and two-dimensional

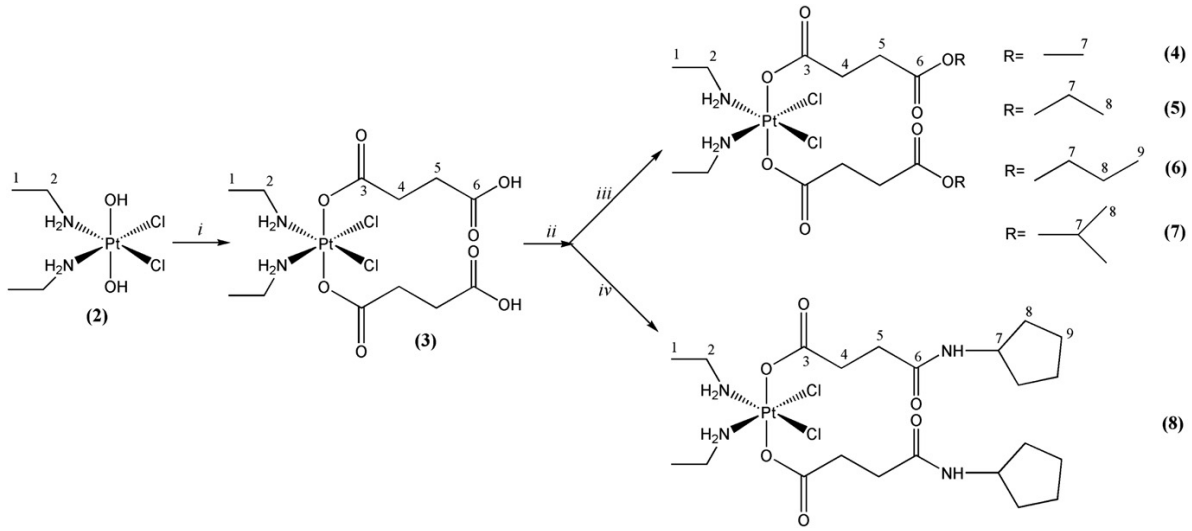

Fig. 2. Synthesis of novel bis(carboxylato)dichloridobis(ethylamine)platinum(IV) complexes with NMR numbering scheme; *i* = succinic anhydride/DMF, 70 deg., *ii* = CDI/DMF, 60 deg., *iii* = RONa/ROH, RT, *iv* = cyclopentylamine/DMF, RT.

multinuclear NMR (^{1}H, ^{13}C, ^{15}N, ^{195}Pt), ESI-MS and ATR IR spectroscopy and in the case of **4** also by X-ray diffraction.

Configuration of the novel platinum agents can best be established with the help of one- and two-dimensional multinuclear NMR spectroscopy. ^{1}H and ^{13}C chemical shifts of compounds **1**–**8** were found in the expected range, proving the supposed structure of the complexes. Correct assignment of the signals was based on ^{1}H^{1}H COSY, ^{1}H^{13}C HSQC and ^{1}H^{13}C HMBC spectra of the complexes. In ^{1}H NMR spectra, oxidation and subsequent derivatization can best be judged according to the shift of the NH_2 signal from 5.09 ppm in the Pt(II) complex **1** to 5.96 ppm in the dihydroxido complex **2**, and to 7.85–7.91 ppm in the dicarboxylato complexes **3**–**8**, respectively. Also indicative are the ^{15}N resonances, where the signal for NH_2 shifts from −40.9 ppm in complex **1** to around −21.3 ppm in compounds **3**–**8**. Additionally, successful derivatizations of complex **3** were observed in ^{13}C NMR spectra. The resonance of C-6 (uncoordinated COOH) was shifted upfield upon formation of esters **4**–**7** or amide **8** by ca. 2 ppm. ^{195}Pt NMR is very powerful technique for investigating the oxidation state and the coordination sphere of platinum complexes. ^{195}Pt signals for complexes **3**–**8** were detected in the region between 2849 and 2853 ppm, typical for compounds with *cis*,*cis*,*trans*-$Pt^{IV}Cl_2N_2O_2$ coordination [23] In comparison, the platinum(II) complex **1** resonates at −601 ppm, more than 3000 ppm upfield to the platinum(IV) analogues. As expected, derivatization of **3** had no influence on the ^{195}Pt signal, because the changes in the molecule are far away from the ^{195}Pt nucleus.

Oxidation of **1** and derivatization of **2** can also be followed in the IR spectra of the complexes. A new and intense signal at 3490 cm^{-1}, corresponding to ν_{PtO-H} can be observed in the spectrum of complex **2**, in comparison with that of **1**. After esterification with succinic anhydride this signal disappeared and in complexes **3**–**8** new strong bands in the region 1730–1630 cm^{-1} ($\nu_{C=O}$) were detected, proving the successful carboxylation. In esters **4**–**7**, bands with 10–25 higher reciprocal wavelengths were detected in comparison with the complex featuring free carboxylic groups (**3**). However, the signal around 1710 cm^{-1} is missing in compound **8**, because of amide formation and a strong band with a shoulder around 1639 cm^{-1}could be observed.

ESI-MS spectra have also confirmed the identity of the complexes. All new compounds (**3**–**8**) were measured in the positive as well as in the negative ion mode. In the positive ion mode, the peak assigned to $[M + Na^+]^+$ displayed the highest intensity, whereas in the negative ion mode the highest intensity was detected for $[M - H^+]^-$. However, a peak corresponding to $[M + Cl^-]^-$, could also be observed in the spectra of esters (complexes **4**–**7**). The detected *m*/*z* values as well as the isotopic distribution were in accordance with the expected chemical structures **3**–**8**.

2.3. Crystal structure of complex 4

The result from the X-ray diffraction analysis of **4** is shown in Fig. 3. Crystal data, data collection parameters and structure-refinement details are given in the Experimental section. Selected bond lengths and angles are listed in Table 1. The compound crystallized in the triclinic centrosymmetric space group *P*−1. The Pt(IV) atom has an octahedral coordination geometry with two ethylamine and two chlorido ligands in the equatorial plane and two 4-methoxysuccinates coordinated in axial positions. The Pt–N, Pt–Cl, and Pt–O bond lengths (Table 1) are well comparable with those, observed in structurally similar complexes [17,18]. Angles in the $PtCl_2N_2O_2$ octahedron were found between 86.26 and 92.69°, and between 172.70 and 178.18°, respectively. The torsion angles (Pt–O1–C1–O2, and Pt–O5–C6–O6) were found to be close to zero.

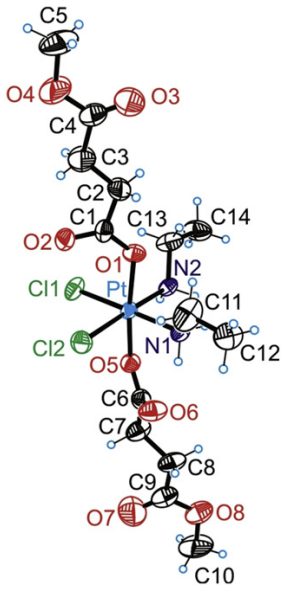

Fig. 3. ORTEP diagram of **4** displaying thermal ellipsoids at 50% probability.

2.4. Cytotoxicity in cancer cell lines

The new compounds were tested in comparison to cisplatin in four human tumor cell lines, originating from ovarian carcinoma (CH1, SK-OV-3), colon carcinoma (SW480) and non-small cell lung cancer (A549) with the help of the colorimetric microculture MTT assay. Except for CH1 cells, these cell lines are resistant to cisplatin, showing IC_{50} values about one order of magnitude higher than that in CH1 cells. The concentration-effect curves of the tested complexes are shown in Fig. 4 and the obtained IC_{50} values are summarized in Table 2.

Expectedly, the platinum(IV) precursor **3** featuring two COOH moieties showed the lowest cytotoxicity in all cell lines. In accordance with previously published data [18,19,22], lipophilicity as well as cellular accumulation are low for such types of complexes. Conversion of **3** to the corresponding ester derivatives **4**–**7** has a significant influence on antiproliferative potency. Whereas complex **4** is as cytotoxic as cisplatin in the cisplatin-sensitive CH1 cell line, complexes **5**–**7** are 3 to 17 times more cytotoxic than cisplatin in the same cell line. An analogous trend was also observed in cisplatin-resistant A549, SW480 and SK-OV-3 cells. Parallel to an increasing lipophilicity of the ester residue (Me, Et, Pr), the IC_{50} values are decreasing in all cell lines, yielding clear structure–activity relationships. The ^{i}Pr analogue **7** is similar in

Table 1
Selected bond lengths (Å) and bond angles (°) in complex **4**.

Bond lengths (Å)			
Pt–O1	2.039	Pt–N2	2.068
Pt–O5	2.039	Pt–Cl1	2.324
Pt–N1	2.063	Pt–Cl2	2.309
Bond angles (deg)			
N1–Pt1–O1	86.26	O1–Pt–O5	172.70
N1–Pt–N2	92.69	N1–Pt–Cl1	178.18
N2–Pt–Cl1	86.26	N2–Pt–Cl2	175.68
N1–Pt–Cl2	88.72	Pt–O1–C1–O2	−1.87
Cl1–Pt–Cl2	92.22	Pt–O5–C6–O6	−0.45

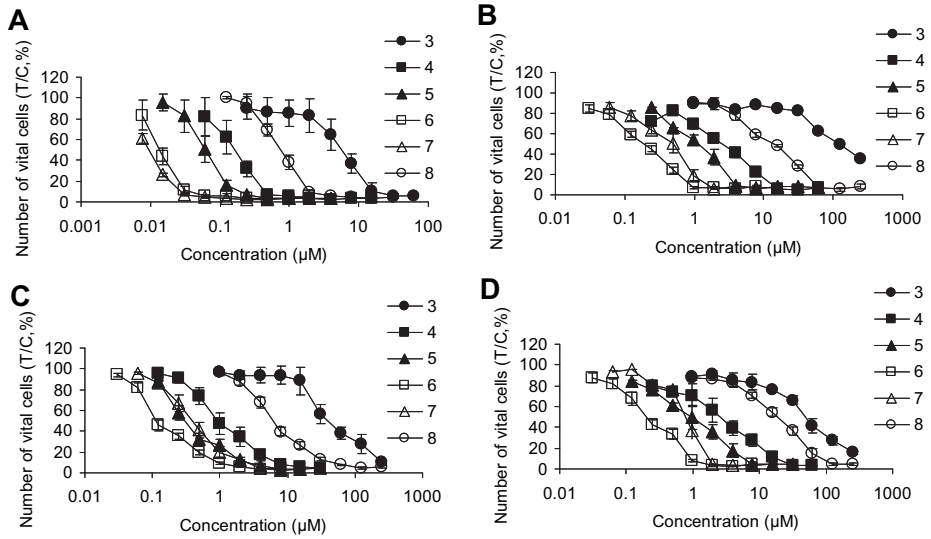

Fig. 4. Concentration-effect curves of complexes (**3**–**8**) in CH1 (A), SK-OV-3 (B), SW480 (C) and A549 (D) obtained by the MTT assay (96 h exposure).

cytotoxic potency to the Pr analogue **6** in CH1 cells, but somewhat less potent in the other cell lines. In analogy to previous observations [22], the cyclopentylamide derivative is equipped with a very low antiproliferative potency, despite its high lipophilicity (see below).

2.5. Lipophilicity vs. cytotoxicity

As an important factor for the pharmacokinetics and the cellular accumulation of the new complexes, the lipophilicity was determined by measuring octanol/water partition coefficients (log *P*) by two different methods; log *P* values, obtained by RP-HPLC and by the shake-flask method are shown in Table 3.

Complexes **4**–**8** have significantly higher log *P* values than that reported for cisplatin (−2.59) and platinum(II) complex **1** (−1.47) [24]. However, complex **3** is also more lipophilic than its Pt(II) congener (**1**), but its lipophilicity is pH-dependent, due to the presence of two underivatized carboxylic groups (lower lipophilicity under physiological conditions is expected). In Fig. 5, a semi-logarithmic graph plotting the cytotoxicity versus log *P* of the new complexes is shown. In case of compounds **3**–**7**, a linear dependency between lipophilicity and cytotoxicity could be observed – the more lipophilic a complex, the higher its cytotoxicity. The amide complex **8** does not match this trend – according to its lipophilicity, a higher cytotoxicity would be expected. The reasons for the latter finding are yet unclear.

2.6. Induction of apoptosis and necrosis

In order to compare the capacities of inducing apoptosis and necrosis of one representative, namely compound **7**, with those of cisplatin, growing SW480 cultures were treated with these compounds in various concentrations for 48 h, then double-stained with annexin V-FITC and propidium iodide and analyzed by fluorescence-activated cell sorting (FACS). This method allows to discriminate necrotic (stained by propidium iodide only), early apoptotic (stained by annexin V-FITC) and late apoptotic (stained by both) from viable (unstained) cells. From the dot plots (Fig. 6), it becomes obvious that the apoptosis-inducing potency of compound **7** is much higher than that of cisplatin. 50 μM of compound **7** reduce the amount of viable cells to 50% by induction of both apoptosis (29%) and necrosis (21%), while the same concentration of cisplatin has very little effect within the chosen exposure time in the intrinsically cisplatin-resistant SW480 (colon cancer) cells.

Table 2
Cytotoxicity of novel complexes (**3**–**8**) in comparison to cisplatin in four human cancer cell lines.

Compound	IC_{50} (μM)[a]			
	CH1	A549	SW480	SK-OV-3
3/R–COOH	5.6 ± 1.6	50 ± 8	40 ± 12	120 ± 17
4/R–COOMe	0.16 ± 0.05	2.5 ± 0.9	1.0 ± 0.3	2.4 ± 0.1
5/R–COOEt	0.061 ± 0.015	1.0 ± 0.4	0.30 ± 0.05	1.2 ± 0.3
6/R–COOPr	0.014 ± 0.002	0.20 ± 0.03	0.11 ± 0.01	0.19 ± 0.03
7/R–$COO^{i}Pr$	0.0094 ± 0.0012	0.78 ± 0.09	0.39 ± 0.07	0.49 ± 0.11
8/R–CONHR	0.75 ± 0.10	19 ± 3	6.1 ± 0.6	13 ± 1
Cisplatin	0.16 ± 0.03	1.3 ± 0.3	3.5 ± 0.3	1.9 ± 0.3

[a] 50% Inhibitory concentrations in CH1, A549, SW480 and SK-OV-3 cells in the MTT assay, 96 h exposure. Values are the means ± standard deviations obtained from three independent experiments.

Table 3
Log *P* values for complexes **3**–**8**, **R1** and **R2**, estimated by RP-HPLC and the shake-flask method.

Compound	Log *P* values, determined by RP-HPLC in different MeOH concentrations						Log *P*, determined by the shake-flask method
	0%	10%	20%	30%	40%	50%	
R1	−1.04	−1.03	−1.00	−0.95	−0.99	−0.88	−0.81
3	−0.70	−0.84	−0.79	−0.64	−1.14	−0.97	
4	0.30	0.25	0.17	0.08	0.14	−0.10	−0.12
5	0.90	0.87	0.83	0.73	0.78	0.85	0.64
6	1.38	1.41	1.44	1.49	1.47	1.48	1.44
7	1.30	1.33	1.36	1.41	1.37	1.39	
8	1.11	1.14	1.17	1.23	1.20	1.25	1.21
R2	1.39	1.41	1.44	1.48	1.44	1.46	1.69

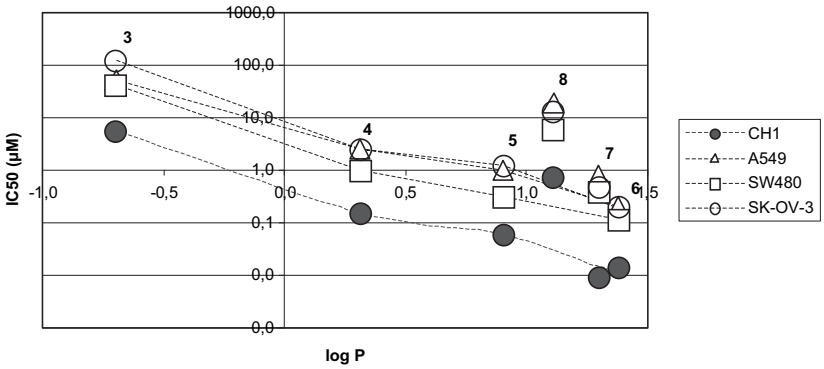

Fig. 5. Semi-logarithmic plot of lipophilicity (log *P* determined with RP-HPLC) of complexes **3**–**8** vs. cytotoxicity (IC_{50}) in CH1, A549, SW480 and SK-OV-3 cells.

A synopsis of all data (Fig. 7) further illustrates that compound **7** is a powerful apoptotic agent, which effectively causes cell death in a dose-dependent way.

3. Conclusions

Six novel bis(carboxylato)platinum(IV) complexes have been synthesized and fully characterized. The new compounds were investigated for their lipophilic properties and their in vitro cytotoxicity in four human tumor cell lines. Remarkably, IC_{50} values down to the nanomolar range, up to 32 times lower compared to cisplatin, were found. Whether the very high cytotoxicity is also accompanied by manageable systemic toxicity in vivo will be evaluated in future work.

4. Experimental protocols

4.1. Materials and methods

All reagents and solvents were obtained from commercial suppliers, and were used without further purification. Methanol and ethanol were dried, according to standard procedures. For column chromatography, silica gel 60 (Fluka) was used. (OC-6-33)-Dichloridobis(ethylamine)dihydroxidoplatinum(IV) (complex **2**, Fig. 2) was synthesized starting from K_2PtCl_4 and ethylamine, using Dhara's [25] method with some modifications. The resulting dichlorido complex **1** was oxidized with 15% H_2O_2.

^1H, ^{13}C, ^{15}N, ^{195}Pt and two-dimensional $^1H^1H$ COSY, $^1H^{13}C$ and $^1H^{15}N$ HSQC, and $^1H^{13}C$ HMBC NMR spectra were recorded with

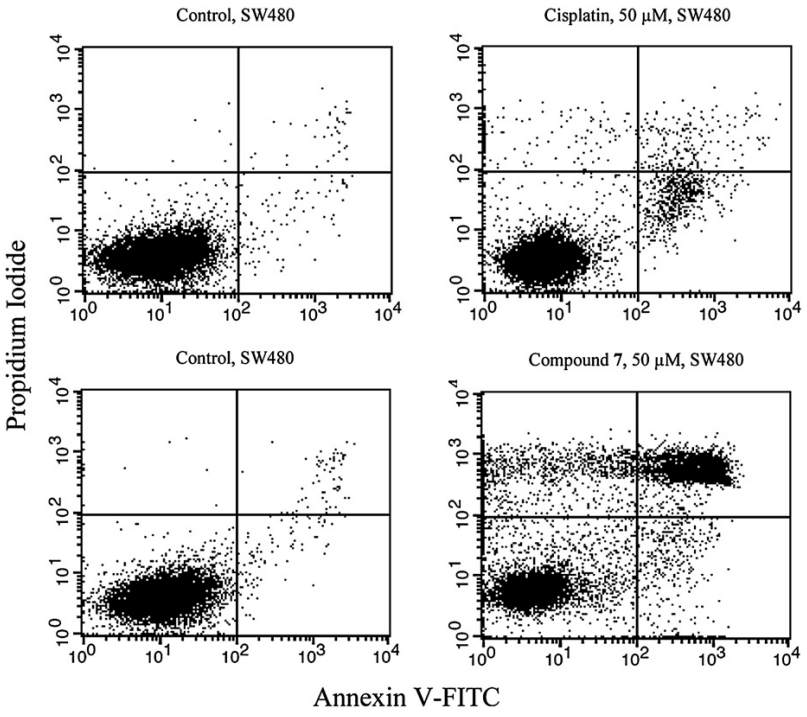

Fig. 6. FACS analysis of annexin V- and PI-stained SW480 colon cancer cells. Left column: untreated control; right column: after treatment with 50 μM cisplatin/compound **7** for 48 h. The upper left quadrant contains the necrotic (stained by PI only), the lower right early apoptotic (stained by annexin V-FITC only), the upper right late apoptotic (stained by both) and the lower left quadrant the viable (unstained) fraction of cell populations.

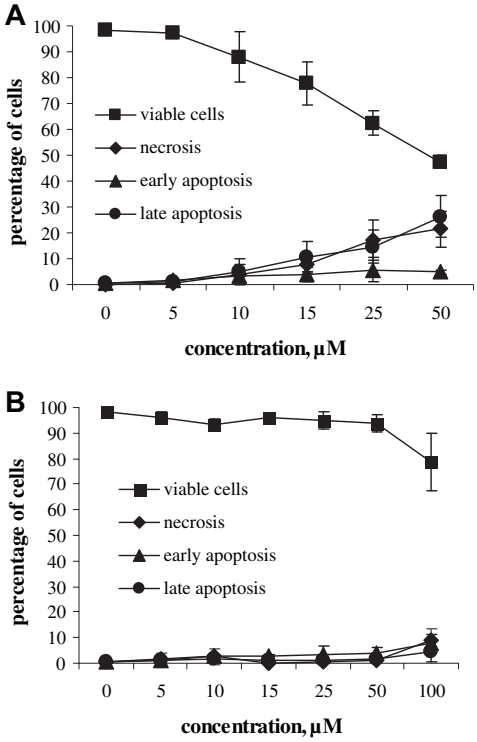

Fig. 7. Concentration-effect curves for compound **7** (A) and cisplatin (B) with regard to apoptosis and necrosis induction in SW480 cells after 48 h exposure, measured by FACS using annexin V-FITC/propidium iodide staining.

a Bruker Avance III 500 MHz NMR spectrometer at 500.32 (^{1}H), 125.81 (^{13}C), 107.55 (^{195}Pt), and 50.70 MHz (^{15}N) in DMF-d_7 at ambient temperature, using the solvent residual peak for ^{1}H and ^{13}C as internal reference. The splitting of proton resonances in the ^{1}H NMR spectra are defined as s = singlet, bs = broad singlet, d = doublet, t = triplet, and m = multiplet. ^{15}N chemical shifts were referenced relative to external NH_4Cl; whereas ^{195}Pt chemical shifts were referenced relative to external $K_2[PtCl_4]$ (see Fig. 2 for NMR numbering scheme).

IR spectra were obtained with a Perkin–Elmer 370 FT-IR 2000 instrument (4000–400 cm^{-1}) by using an ATR unit. Intensities of reported IR bands are defined as br = broad, s = strong, m = medium, and w = weak. Electrospray ionization mass spectrometry was carried out with a Bruker Esquire 3000 instrument using MeOH as solvent. Elemental analyses were performed with a Perkin–Elmer 2400 CHN-Elemental Analyzer by the Microanalytical Laboratory of the University of Vienna. Analyses indicated by the symbols of the elements or functions were within ±0.4% of the theoretical values. Purity of novel compounds was additionally proved by analytical reversed-phase HPLC.

4.2. Synthesis

4.2.1. (OC-6-33)-Bis(3-carboxypropanoato)dichloridobis(ethylamine)-platinum(IV) (**3**)

Succinic anhydride (674.3 mg, 6.738 mmol) and 653 mg (1.675 mmol) of (*OC*-6-33)-dichloridobis(ethylamine)dihydroxidoplatinum(IV) were suspended in 9 mL of absolute DMF and the reaction mixture was stirred at 65 °C for 40 min and then for 2 more hours at room temperature. During this time, the solid material dissolved to form a yellow-brown solution. DMF was removed under reduced pressure. The residue was dissolved in acetone and filtered to give a clear, yellow solution. This solution was concentrated under reduced pressure, and subsequent addition of diethyl ether led to precipitation of a pale yellow solid. The precipitate was filtrated and dried in vacuo, while heating at 40 °C. Yield: 398 mg (40%). Anal. $C_{12}H_{24}Cl_2N_2O_8Pt$ (C, H, N). ESI-MS: *m*/*z* 612.6 $[M + Na^+]^+$, 588.7 $[M - H^+]^-$. ^{1}H NMR: δ = 12.52 (bs, 2H, COOH), 7.87 (bs, 4H, NH_2), 3.10 (m, 4H, H-2), 2.75 (m, 4H, H-4), 2.68 (m, 4H, H-5), 1.44 (t, $^{3}J_{H,H}$ = 7.2 Hz, 6H, H-1) ppm. ^{13}C NMR: δ = 181.3 (C-3), 174.1 (C-6), 39.9 (C-2), 31.2 (C-4), 29.9 (C-5), 14.3 (C-1) ppm. ^{15}N NMR7: δ = −21.2 ppm. ^{195}Pt NMR: δ = 2851 ppm. IR (ATR): 3241 m, 3197 br; 2977 br; 1710 s ($\nu_{C=O}$), 1642 m ($\nu_{C=O}$); 1357 m, 1344 m; 1238 s 1216 m, 1175 m; 1081 w, 1024 w (ν_{C-N}) cm^{-1}.

4.2.2. (OC-6-33)-Dichloridobis(ethylamine)bis((4-methoxy)-4-oxobutanoato)platinum(IV) (**4**)

CDI (241.1 mg, 1.4869 mmol) in absolute DMF (10 mL) was added to a solution of **3** (433.4 mg, 0.7342 mmol) in absolute DMF (6 mL), and the mixture was heated to 60 °C. After 10 min of being stirred, the solution was cooled to room temperature and CO_2 was removed by flushing with argon. Sodium methanolate (a piece of Na in 10 mL of absolute MeOH) in absolute MeOH was added and the solution was stirred for 24 h at room temperature. Methanol and DMF were removed under reduced pressure to form a yellow oil. The crude product was purified by column chromatography (EtOAc/MeOH, 7:1) to yield a yellow solid, which was dried in vacuo. Yield: 106 mg (23%). Anal. $C_{14}H_{28}Cl_2N_2O_8Pt$ (C, H, N). ESI-MS: *m*/*z* 640.8 $[M + Na^+]^+$, 616.5 $[M - H^+]^-$, 652.8 $[M + Cl^-]^-$. ^{1}H NMR: δ = 7.85 (bs, 4H, NH_2), 3.82 (s, 6H, H-7), 3.10 (m, 4H, H-2), 2.78 (m, 4H, H-4), 2.71 (m, 4H, H-5), 1.45 (t, $^{3}J_{H,H}$ = 7.2 Hz, 6H, H-1) ppm. ^{13}C NMR: δ = 181.0 (C-3), 173.1 (C-6), 51.2 (C-7), 39.9 (C-2), 31.1 ($^{3}J_{C,Pt}$ = 38.2 Hz, C-4), 29.8 (C-5), 14.3 ($^{3}J_{C,Pt}$ = 35.0 Hz, C-1) ppm. ^{15}N NMR: δ = −21.3 ppm. ^{195}Pt NMR: δ = 2853 ppm. IR (ATR): 3221 w, 3188 m; 2894 br; 1729 s ($\nu_{C=O}$), 1647 s ($\nu_{C=O}$); 1362 m 1333s; 1259 s, 1198s, 1176 s; 1088 m, 1026 w (ν_{C-N}); 683 w cm^{-1}. Crystals, suitable for X-ray data collection, were obtained after vapor diffusion of diethyl ether into a methanol solution of **4**.

4.2.3. (OC-6-33)-Dichloridobis((4-ethoxy)-4-oxobutanoato)-bis(ethylamine)platinum(IV) (**5**)

The synthesis was carried out as described for **4**. The crude product was purified by column chromatography (EtOAc/MeOH, 9:1), then recrystallized from ethyl acetate and diethyl ether to yield a pale yellow solid. The final product was dried in vacuo. Yield: 24 mg (16%). Anal. $C_{16}H_{32}Cl_2N_2O_8Pt$ (C, H, N). ESI-MS: *m*/*z* 669.1 $[M + Na^+]^+$, 644.3 $[M - H^+]^-$, 681.0 $[M + Cl^-]^-$. ^{1}H NMR: δ = 7.86 (bs, 4H, NH_2), 4.26 (m, $^{3}J_{H,H}$ = 7.1 Hz, 4H, H-7), 3.10 (m, 4H, H-2), 2.77 (t, 4H, H-4), 2.69 (t, 4H, H-5), 1.45 (t, $^{3}J_{H,H}$ = 7.2 Hz, 6H, H-1), 1.39 (t, $^{3}J_{H,H}$ = 7.1 Hz, 6H, H-8) ppm. ^{13}C NMR: δ = 181.0 (C-3), 172.7 (C-6), 60.2 (C-7), 39.9 (C-2), 31.1 ($^{3}J_{C,Pt}$ = 37.3 Hz, C-4), 30.0 (C-5), 14.4 ($^{3}J_{C,Pt}$ = 34.5 Hz, C-1), 14.0 (C-8) ppm. ^{15}N NMR: δ = −21.3 ppm. ^{195}Pt NMR: δ = 2850 ppm. IR (ATR): 3180 w, 3153 w; 2987 w; 1727 s ($\nu_{C=O}$); 1658 m, 1631 m ($\nu_{C=O}$); 1369 m; 1260 s, 1231 s; 1163 s; 1085 w; 1039 m, 1023 s (ν_{C-N}); 857 w, 681 m cm^{-1}.

4.2.4. (OC-6-33)-Dichloridobis(ethylamine)bis((4-propyloxy)-4-oxobutanoato)platinum(IV) (**6**)

The synthesis was carried out as described for **4**. The crude product was purified by column chromatography (EtOAc/MeOH, 11:1), then recrystallized from ethyl acetate and diethyl ether to yield a pale yellow solid. The final product was dried in vacuo. Yield: 33 mg (11%). Anal. $C_{18}H_{36}Cl_2N_2O_8Pt$ (C, H, N). ESI-MS: *m*/*z* 697.1 $[M + Na^+]^+$, 672.9 $[M - H^+]^-$, 708.9 $[M + Cl^-]^-$. ^{1}H NMR:

δ = 7.86 (bs, 4H, NH_2), 4.18 (t, $^3J_{H,H}$ = 6.7 Hz, 4H, H-7), 3.10 (m, 4H, H-2), 2.78 (m, 4H, H-4), 2.71 (m, 4H, H-5), 1.80 (m, $^3J_{H,H}$ = 7.3 Hz, 4H, H-8), 1.44 (t, $^3J_{H,H}$ = 7.2 Hz, 6H, H-1), 1.09 (t, $^3J_{H,H}$ = 7.4 Hz, 6H, H-9) ppm. ^{13}C NMR: δ = 181.0 (C-3), 172.7 (C-6), 65.8 (C-7), 39.9 (C-2), 31.1 ($^3J_{C,Pt}$ = 31.1 Hz, C-4), 29.9 (C-5), 22.0 (C-8), 14.4 ($^3J_{C,Pt}$ = 34.7 Hz, C-1), 10.1 (C-9) ppm. ^{15}N NMR: δ = −21.4 ppm. ^{195}Pt NMR: δ = 2850 ppm. IR (ATR): 3222 m, 3192 m; 2970 w; 1731 s ($\nu_{C=O}$); 1671 m, 1654 s ($\nu_{C=O}$); 1370 m, 1326 m; 1164 s, 1088 w; 684 w cm^{-1}.

4.2.5. (OC-6-33)-Dichloridobis(ethylamine)bis((4-(2-propyloxy))-4-oxobutanoato)platinum(IV) (7)

CDI (184 mg, 1.135 mmol) in absolute DMF (6 mL) was added to a solution of **3** (325 mg, 0.551 mmol) in absolute DMF (5 mL), and the mixture was heated to 70 °C. After 10 min of being stirred, the solution was cooled to room temperature and CO_2 was removed by flushing with argon. 12 mL of sodium 2-propanolate (a piece of Na dissolved in 2-propanol, HPLC grade) was added to the solution and heated to 40 °C. The mixture was then stirred for 72 h at room temperature. 2-Propanol and DMF were removed under reduced pressure to form a yellow oil. The crude product was purified by column chromatography (EtOAc/2-propanol, 10:1) and then precipitated with Et_2O and cooled to 0 °C to give an almost white solid, which was dried in vacuo. Yield: 110 mg (30%). Anal. $C_{18}H_{36}Cl_2N_2O_8Pt$ (C, H, N). ESI-MS: *m/z* 696.8 $[M + Na^+]^+$, 673.4 $[M - H^+]^-$, 708.8 $[M + Cl^-]^-$. ^{1}H NMR: δ = 7.70 (bs, 4H, NH_2), 4.93 (m, $^3J_{H,H}$ = 6.3 Hz, 2H, H-7), 2.94 (m, 4H, H-2), 2.59 (m, 4H, H-4), 2.49 (m, 4H, H-5), 1.27 (t, $^3J_{H,H}$ = 7.2 Hz, 6H, H-1), 1.21 (d, $^3J_{H,H}$ = 6.3 Hz, 12H, H-8) ppm. ^{13}C NMR: δ = 180.9 (C-3), 172.0 (C-6), 67.4 (C-7), 39.8 (C-2), 30.9 ($^3J_{C,Pt}$ = 37.5 Hz, C-4), 30.1(C-5), 21.3 (C-8), 14.2 ($^3J_{C,Pt}$ = 32.9 Hz, C-1) ppm. ^{15}N NMR: δ = −21.3 ppm. ^{195}Pt NMR: δ = 2850 ppm. IR (ATR): 3282 m, 3206 m; 2981 w, 2937 w; 1722 s, 1702 s ($\nu_{C=O}$); 1668 s, 1637 s ($\nu_{C=O}$); 1375 m, 1362 m; 1304 s, 1265 s, 1239s; 1106 m, 1087 m cm^{-1}.

4.2.6. (OC-6-33)-Dichloridobis((4-cyclopentylamino)-4-oxobutanoato)bis(ethylamine)platinum(IV) (8)

CDI (106.5 mg, 0.6568 mmol) in absolute DMF (7 mL) was added to a solution of **3** (184.5 mg, 0.3126 mmol) in absolute DMF (5 mL), and the mixture was heated to 60 °C. After 10 min of being stirred, the solution was cooled to room temperature and CO_2 was removed by flushing with argon. Cyclopentylamine (75 μL, 0.7516 mmol) in 4 mL of absolute DMF was added to the solution and stirred for 30 h in the dark at room temperature. DMF was removed under reduced pressure to form a brown oil. The crude product was purified by column chromatography (EtOAc/MeOH, 4:1) and then precipitated with Et_2O (ultrasonic) and cooled to 0 °C to give an almost white solid, which was filtered off, washed with Et_2O and EtOAc and dried in vacuo. Yield: 64 mg (28%). Anal. $C_{22}H_{42}N_4O_6PtCl_2$ (C, H, N). ESI-MS: *m/z* 747.3 $[M + Na^+]^+$, 723.1 $[M - H^+]^-$. ^{1}H NMR: δ = 7.95 (d, $^3J_{H,H}$ = 6.9 Hz, 2H, NH-amide), 7.91 (bs, 4H, NH_2), 4.26 (m, $^3J_{H,H}$ = 6.8 Hz, 2H, H-7), 3.13 (m, 4H, H-2), 2.68 (m, 4H, C-4), 2.56 (m, 4H, H-5), 2.00 (m, 4H, H-8), 1.84 (m, 4H, H-9), 1.70 (m, 4H, H-9), 1.62 (m, 4H, H-8), 1.45 (t, $^3J_{H,H}$ = 7.1 Hz, 6H, H-1) ppm. ^{13}C NMR: δ = 181.8 (C-3), 171.3 (C-6), 51.0 (C-7), 40.0 (C-2), 32.7 (C-8), 32.1 (C-4), 31.8 (C-5), 23.8 (C-9), 14.4 (C-1) ppm. ^{15}N NMR: δ = 107.7 (CONH-amide), −20.3 (NH_2) ppm. ^{195}Pt NMR: δ = 2489 ppm. IR (ATR): 3352 m, 3210 br, 3073 br; 2871 w; 1639 s ($\nu_{C=O}$); 1535 s, 1356 w, 1258 m, 1246 w cm^{-1}.

4.3. Crystallographic structure determination

X-ray diffraction measurement was performed on a Bruker X8 APEXII CCD diffractometer. Single crystal of **4** was positioned at 40 mm from the detector, and 1839 frames were measured, each for 20 s over 1° scan width. The data were processed using SAINT software [26]. Crystal data, data collection parameters, and structure-refinement details are given in Table 4. The structures were solved by direct methods and refined by full-matrix least-squares techniques. Non-H atoms were refined with anisotropic displacement parameters. H atoms were inserted in calculated positions and refined with a riding model. The isotropic thermal parameters were estimated to be 1.2 times the values of the equivalent isotropic thermal parameters of the atoms to which hydrogens were bonded. Structure solution was achieved with *SHELXS-97* and refinement with *SHELXL-97* [27], and graphics were produced with *ORTEP-3* [28].

4.4. Determination of lipophilicity

Lipophilicity of new complexes was determined by the shake-flask method and by reversed-phased HPLC.

4.4.1. Shake-flask method

The log *P* determination of compounds (**4**, **5**, **6** and **8**) was carried out, according to the guidelines for the shake-flask method [29] with slight modifications [20]. Weighted amounts of platinum complexes were dissolved in HPLC-grade water, which was pre-saturated with *n*-octanol, and mixed by sonication for 5 min. Afterward, the solutions were centrifuged for 5 min and the concentration of Pt was determined by ICP-MS. Weighted amounts of that solutions were mixed with the same volume of *n*-octanol (pre-saturated with water) and shaken for 15. After phase separation, the Pt concentration in the aqueous phase was again determined by ICP-MS and the partition coefficients were calculated.

The platinum content in the aqueous phase was determined by ICP-MS (Agilent 7500ce, Waldbronn, Germany), equipped with a CETAC ASX-520 autosampler (Neuss, Germany), a Scott double pass spray chamber, and a MicroMist nebulizer. For the analysis, the samples were diluted 1:1000 with 2.5% HCl. Every sample contained 0.5 ppb In as internal standard (CPI International, Santa Rosa, CA, USA).

4.4.2. Reversed-phase HPLC method

HPLC analysis was performed on a Dionex Summit system controlled by the Dionex Chromeleon 6.60 software. The

Table 4
Crystallographic data for complex **4**.

	4
Empirical formula	$C_{14}H_{28}Cl_2N_4O_8Pt$
F_w	618.37
Space group	*P*−1
a [Å]	6.0519(3)
b [Å]	13.1190(6)
c [Å]	14.0840(5)
α [°]	79.521(2)
β [°]	83.694(2)
γ [°]	85.073(3)
V [Å^3]	1090.41(8)
Z	2
λ [Å]	0.71073
ρ_{calcd} [g cm^{-3}]	1.883
Crystal size [mm^3]	0.20 × 0.13 × 0.12
T [K]	100(2)
μ [mm^{-1}]	6.719
R_1[a]	0.0357
wR_2[b]	0.0858
GOF[c]	0.989

[a] $R_1 = \Sigma||F_o| - |F_c||/\Sigma|F_o|$.
[b] $wR_2 = \{\Sigma[w(F_o^2 - F_c^2)^2]/\Sigma[w(F_o^2)^2]\}^{1/2}$.
[c] GOF = $\{\Sigma[w(F_o^2 - F_c^2)^2]/(n - p)\}^{1/2}$, where *n* is the number of reflections and *p* is the total number of parameters refined.

experimental conditions were as follows: Agilent ZORBAX Bonus-RP column (4.6 mm × 250 mm); 0.1% TFA water/MeOH based mobile phases; UV–vis detection set up at 210 nm; temperature of the column: 25 °C; flow rate: 1 mL min^{-1}; concentration of the investigated complexes: 2.5 mM, (1 mM KI as internal standard was added); 25 μL injection volume. The capacity factors $k' = (t_R - t_0)/t_0$ (t_R is the retention time of the species analyzed and k_0 is the retention time of the unretained substance, used as a standard (here KI)) of the investigated compounds were determined at different MeOH/water ratios (from 60:40 for the most lipophilic to 10:90 for the most hydrophilic compounds). Using the linear relationship between log *k*' and the percentage of MeOH in the mobile phase: log $k' = \log k'_w - \%MeOH$. log *k*' values for all complexes were calculated for 0, 10, 20, 30, 40 and 50% of MeOH in the mobile phase. Complexes **3**–**8** and for comparison (OC-6-33)-dichlorido(ethane-1,2-diamine)-bis{(4-methoxy)-4-oxobutanoato}platinum(IV) (**R1**) and (OC-6-33)-bis{(5-butyloxy)-5-oxo-3-methylpentanoato}dichlorido(ethane-1,2-diamine)platinum(IV) (**R2**) described in Ref. [22] were investigated. Calibration curves for different MeOH concentrations were created on the basis of determined log *P* values of **4**–**6**, **8**, **R1**, and **R2**. The equations derived from the calibration curves for different percentage of MeOH together with their R^2 values, are shown in Table 5. From these equations log *P* values for all investigated complexes were calculated.

4.5. Cell lines and culture conditions

CH1 (ovarian carcinoma, human) cells were donated by Lloyd R. Kelland (CRC Center for Cancer Therapeutics, Institute of Cancer Research, Sutton, U.K.). A549 (non-small cell lung cancer, human) and SW480 (colon carcinoma, human) cells were kindly provided by Brigitte Marian (Institute of Cancer Research, Department of Medicine I, Medical University of Vienna, Austria), and SK-OV-3 (ovarian carcinoma, human) cells by Evelyn Dittrich (General Hospital, Medical University of Vienna, Austria). Cells were grown in 75 cm^2 culture flasks (Iwaki/Asahi Technoglass) as adherent monolayer cultures in Minimal Essential Medium (MEM) supplemented with 10% heat-inactivated fetal bovine serum, 1 mM sodium pyruvate, and 2 mM L-glutamine (all purchased from Sigma–Aldrich) without antibiotics. Cultures were maintained at 37 °C in a humidified atmosphere containing 5% CO_2 and 95% air.

4.6. Cytotoxicity tests in cancer cell lines

Cytotoxicity in the cell lines mentioned above was determined by the colorimetric MTT assay (MTT = 3-(4,5-dimethyl-2-thiazolyl)-2,5-diphenyl-2*H*-tetrazolium bromide, purchased from Fluka). Cells were harvested from culture flasks by trypsinization and seeded in 100 μL aliquots in MEM supplemented with 10% heat-inactivated fetal bovine serum, 1 mM sodium pyruvate, 2 mM L-glutamine, and 1% non-essential amino acids (100×) into 96-well microculture plates (Iwaki/Asahi Technoglass) in the following densities, to ensure exponential growth of untreated controls throughout the experiment: 1.5 × 10^3 (CH1), 3.5 × 10^3 (SK-OV-3), 4.0 × 10^3 (A549), and 2.5 × 10^3 (SW480) viable cells per well. Cells were allowed to settle and resume exponential growth in drug-free complete culture medium for 24 h, followed by the addition of dilutions of the test compounds in 100 μL/well of the same medium. After continuous exposure for 96 h, the medium was replaced by a 100 μL/well RPMI 1640 medium (supplemented with 10% heat-inactivated fetal bovine serum and 4 mM L-glutamine) plus 20 μL/well solution of MTT in phosphate-buffered saline (5 mg/mL) (all purchased from Sigma–Aldrich). After incubation for 4 h, medium/MTT mixtures were removed, and the formazan product formed by viable cells was dissolved in DMSO (150 μL/well). Optical densities at 550 nm were measured with a microplate reader (Tecan Spectra Classic), using a reference wavelength of 690 nm to correct for unspecific absorption. The quantity of viable cells was expressed as percentage of untreated controls, and 50% inhibitory concentrations (IC_{50}) were calculated from concentration-effect curves by interpolation. Evaluation is based on means from three independent experiments, each comprising six replicates per concentration level.

Table 5
Results from the calibration curves log $P = f(\log k')$ under different experimental conditions.

%MeOH	Equation	R^2
0	0.8842× −2.1484	0.92
10	0.9126× −1.6351	0.93
20	0.9586× −1.1251	0.95
30	0.9736× −0.4783	0.98
40	1.0174× +0.081	0.96
50	1.0063× +0.7582	0.98

Table 6
Viable, apoptotic and necrotic cell fractions (in %) of SW480 cells upon treatment with cisplatin or compound **7** for 48 h, analyzed by FACS using annexin V and PI staining.

Concentration, μM	Viable cells	Early apoptosis	Late apoptosis	Necrosis
Compound **7** (in %)				
0	98.3 ± 0.6	0.7 ± 0.3	0.8 ± 0.5	0.2 ± 0.1
5	97.2 ± 1.2	1.5 ± 0.8	1.0 ± 0.4	0.4 ± 0.3
10	87.9 ± 9.8	3.3 ± 1.9	5.1 ± 5.0	3.8 ± 3.7
15	77.7 ± 8.3	3.9 ± 2.9	10.6 ± 5.9	7.9 ± 2.6
25	62.4 ± 4.9	5.8 ± 4.9	14.7 ± 6.2	17.1 ± 7.8
50	47.5 ± 2.6	4.8 ± 0.8	26.3 ± 8.0	21.5 ± 7.0
Cisplatin (in %)				
0	98.1 ± 0.7	0.7 ± 0.6	0.5 ± 0.4	0.7 ± 0.5
5	96.1 ± 2.1	1.0 ± 0.2	1.1 ± 0.7	1.9 ± 2.2
10	93.5 ± 2.0	2.5 ± 0.8	1.5 ± 1.2	2.5 ± 3.1
15	95.9 ± 1.0	2.9 ± 0.3	1.0 ± 0.6	0.2 ± 0.1
25	94.9 ± 3.5	3.3 ± 3.4	1.3 ± 0.6	0.6 ± 0.5
50	93.8 ± 3.5	3.7 ± 2.6	1.6 ± 0.8	0.9 ± 0.7
100	78.7 ± 11.3	8.0 ± 3.5	4.6 ± 4.0	8.7 ± 4.7

4.7. Apoptosis/necrosis assay

Cell death was analyzed by fluorescence-activated cell sorting (FACS) using FITC-conjugated annexin V (BioVision, USA) and propidium iodide (PI; Fluka) staining (Table 6).

SW480 cells were seeded into 6-well plates (Iwaki/Asahi Technoglass, Gyouda, Japan) in amounts of 2 × 10^5 cells per well in complete medium (as described above) and allowed to settle for 24 h. The cells were exposed to cisplatin and compound **7** for 48 h at 37 °C. After the incubation, cells were gently trypsinized, washed with PBS, and suspended with FITC-conjugated annexin V (0.25 μg/mL) in binding buffer (10 mM HEPES/NaOH pH 7.4, 140 mM NaCl, 2.5 mM $CaCl_2$) at room temperature for 15 min. PI (1 μg/mL) was added shortly before the measurement. Stained cells were analyzed with a FACS Calibur instrument (Becton Dickinson, Franklin Lakes, NJ, USA) using Cell-QuestPro software. At least three independent experiments were conducted, and 10,000 cells were counted per analysis.

Acknowledgments

H. V. is thankful for financial support of the University of Vienna within the doctoral program "Initiativkolleg Functional Molecules" IKI041-N. The authors are indebted to the FFG – Austrian Research

Promotion Agency, the Austrian Council for Research and Technology Development, the FWF (Austrian Science Fund) and COST D39. We are thankful to Anna Bytzek for determination of log *P* values via the shake-flask method. We are indebted to Prof. Verena Dirsch and Daniel Schachner (Institute of Pharmacognosy, University of Vienna, Austria) for providing FACS equipment and technical assistance.

Appendix. Supplementary material

Supplementary data related to this article can be found online at doi:10.1016/j.ejmech.2011.09.006.

References

[1] M. Rosenberg, L. VanCamp, T. Krigas, Inhibition of cell division in *Escherichia coli* by electrolysis products from a platinum electrode, Nature 205 (1965) 698–699.
[2] N.J. Wheate, S. Walker, G.E. Craig, R. Oun, The status of platinum anticancer drugs in the clinic and in clinical trials, Dalton Trans. 39 (2010) 8113–8127.
[3] M.D. Hall, H.R. Mellor, R. Callaghan, T.W. Hambley, Basis for design and development of platinum(IV) anticancer complexes, J. Med. Chem. 50 (15) (2007) 3403–3411.
[4] M. Galanski, Recent developments in the field of anticancer platinum complexes, Recent Pat. Anticancer Drug Discov. 1 (2006) 285–295.
[5] M. Galanski, M.J. Jakupec, B.K. Keppler, Update of the preclinical situation of anticancer platinum complexes: novel design strategies and innovative analytical approaches, Curr. Med. Chem. 12 (18) (2005) 2075–2094.
[6] R.J. Schilder, F.P. LaCreta, R.P. Perez, S.W. Johnson, J.M. Brennan, A. Rogatko, S. Nash, C. McAleer, T.C. Hamilton, D. Roby, R.C. Young, R.F. Ozols, P.J. O'Dwyer, Phase I and pharmacokinetic study of ormaplatin (tetraplatin, NSC 363812) administered on a day 1 and day 8 schedule, Cancer Res. 54 (3) (1994) 709–717.
[7] G.B. Inc, Orplanta. Satraplatin Capsules, in Advisory Committee Briefing Document. USA Food and Drug Administration, 2007.
[8] European Medicines Agency, Withdrawal Assessment Report for Orplanta (2008) 1–37.
[9] http://www.clinicaltrials.gov, U.S National Library of Medicine, Bethesda, 1993.
[10] O. Novakova, O. Vrana, V.I. Kiseleva, V. Brabec, DNA interactions of antitumor platinum(IV) complexes, Eur. J. Biochem. 228 (3) (1995) 616–624.
[11] M. Galanski, B.K. Keppler, Is reduction required for antitumor activity of platinum(IV) compounds? Characterisation of a platinum(IV)-nucleotide adduct [enPt($OCOCH_3$)$_3$(5′-GMP)] by NMR spectroscopy and ESI-MS, Inorg. Chim. Acta 300–302 (2000) 783–789.
[12] L.T. Ellis, H.M. Er, T.W. Hambley, The influence of the axial ligands of a series of platinum(IV) anti-cancer complexes on their reduction to platinum(II) and reaction with DNA, Aust. J. Chem. 48 (4) (1995) 793–806.
[13] S. Choi, C. Filotto, M. Bisanzo, S. Delaney, D. Lagasee, J.L. Whitworth, A. Jusko, C. Li, N.A. Wood, J. Willingham, A. Schwenker, K. Spaulding, Reduction and anticancer activity of platinum(IV) complexes, Inorg. Chem. 37 (10) (1998) 2500–2504.
[14] S.G. Chaney, S. Wyrick, G.K. Till, In vitro biotransformations of tetrachloro(d, l-trans)-1,2-diaminocyclohexaneplatinum(IV) (tetraplatin) in rat plasma, Cancer Res. 50 (1990) 4539–4545.
[15] L. Pendyala, J.W. Cowens, G.B. Chheda, S.P. Dutta, P.J. Creaven, Identification of cis-dichloro-bis-isopropylamine platinum(II) as a major metabolite of iproplatin in humans, Cancer Res. 48 (1988) 3533–3536.
[16] R.R. Barefoot, Speciation of platinum compounds: a review of recent applications in studies of platinum anticancer drugs, J. Chromatogr. B. 751 (2001) 205–211.
[17] M. Reithofer, M. Galanski, A. Roller, B.K. Keppler, An entry to novel platinum complexes: carboxylation of dihydroxoplatinum(IV) complexes with succinic anhydride and subsequent derivatization, Eur. J. Inorg. Chem. 13 (2006) 2612–2617.
[18] M.R. Reithofer, S.M. Valiahdi, M.A. Jakupec, V.B. Arion, A. Egger, M. Galanski, B.K. Keppler, Novel di- and tetracarboxylatoplatinum(IV) complexes. Synthesis, characterization, cytotoxic activity, and DNA platination, J. Med. Chem. 50 (2007) 6692–6699.
[19] M.R. Reithofer, A. Schwarzinger, S.M. Valiahdi, M. Galanski, M.A. Jakupec, B.K. Keppler, Novel bis(carboxylato)dichlorido(ethane-1,2-diamine)platinum(IV) complexes with exceptionally high cytotoxicity, J. Inorg. Biochem. 102 (2008) 2072–2077.
[20] M.R. Reithofer, S.M. Valiahdi, M. Galanski, M.A. Jakupec, V.B. Arion, B.K. Keppler, Novel endothall containing platinum(IV) complexes – synthesis, characterization, and cytotoxic activity, Chem. Biodiv 5 (2008) 2160–2170.
[21] A. Bytzek, M. Reithofer, M. Galanski, M. Groessl, B.K. Keppler, C.G. Hartinger, The first example of MEEKC-ICP-MS coupling and its application for the analysis of anticancer platinum complexes, Electrophoresis 31 (2010) 1144–1150.
[22] M.R. Reithofer, A.K. Bytzek, S.M. Valiahdi, C.R. Kowol, M. Groessl, C.G. Hartinger, M.A. Jakupec, M. Galanski, B.K. Keppler, Tuning of lipophilicity and cytotoxic potency by structural variation of anticancer platinum(IV) complexes, J. Inorg. Biochem. 105 (2011) 46–51.
[23] W.H. Ang, S. Pilet, R. Scopelliti, F. Bussy, L. Juillerat-Jeanneret, P.J. Dyson, Synthesis and characterization of platinum(IV) anticancer drugs with functionalized aromatic carboxylate ligands: influence of the ligands on drug efficacies and uptake, J. Med. Chem. 48 (2005) 8060–8069.
[24] I.V. Tetko, I. Jaroszewicz, J.A. Platts, J. Kuduk-Jaworska, Calculation of lipophilicity for Pt(II) complexes: experimental comparison of several methods, J. Inorg. Biochem. 102 (7) (2008) 1424–1437.
[25] S. Dhara, A rapid method for the synthesis of *cis*-[Pt(NH_3)$_2$$Cl_2$], Indian J. Chem. 8 (1970) 193–194.
[26] SAINT-Plus, Version 7.06a and APEX2. Bruker-Nonius AXS Inc., Madison, WI, 2004.
[27] G.M. Sheldrick, A short history of SHELX, Acta Cryst. A64 (2008) 112–122.
[28] G.K. Johnson, Report ORNL-5138. OAK Ridge National Laboratory, Oak Ridge, TN, 1976.
[29] OECD Guidelines for Testing of Chemicals, No. 107. OECD, Paris, 1995.

2.5 Platinum(IV) Complexes Featuring One or Two Axial Ferrocene Bearing Ligands - Synthesis, Characterization, and Cytotoxicity

Banfic J., Legin A. A., Jakupec M. A., Roller A., Galanski M., Keppler B. K.

European Journal of Inorganic Chemistry 2014, **2014**, 484-492. DOI: 10.1002/ejic.201301282

EurJIC European Journal of Inorganic Chemistry

ChemPubSoc Europe

FULL PAPER

DOI:10.1002/ejic.201301282

Platinum(IV) Complexes Featuring One or Two Axial Ferrocene Bearing Ligands – Synthesis, Characterization, and Cytotoxicity

Jelena Banfić,[a] Anton A. Legin,[a] Michael A. Jakupec,[a] Markus Galanski,*[a] and Bernhard K. Keppler*[a,b]

Keywords: Platinum / Ferrocene / Antitumor agents / Cytotoxicity / Metallocenes

Ferrocenyl compounds show interesting antiproliferative properties. Consequently, ferrocene bearing moieties were prepared and coupled for the first time to anticancer platinum(IV) complexes. The compounds, featuring either one or two axially coordinated ferrocene-containing ligands, were fully characterized by ESI-MS and multinuclear (^{1}H, ^{13}C, ^{15}N, and ^{195}Pt) one- and two-dimensional NMR spectroscopy. Their cytotoxicity was investigated in three human cancer cell lines deriving from ovarian carcinoma (CH1), colon carcinoma (SW480), and non-small-cell lung carcinoma (A549) by means of the colorimetric MTT assay. Promising IC_{50} values in the low micromolar range in CH1 and SW480 human cancer cells were found.

Introduction

In 1965, Barnett Rosenberg discovered accidentally the ability of cisplatin to inhibit cell proliferation.[1] After cisplatin had been granted approval in 1978 as a chemotherapeutic,[2] many efforts have been made to develop novel platinum compounds with anti-proliferative potential. Besides cisplatin, two so-called second- and third-generation platinum drugs, namely carboplatin and oxaliplatin, gained worldwide approval as antineoplastic drugs (Figure 1). Three other platinum-based compounds, nedaplatin, lobaplatin, and heptaplatin, gained regional approval in Japan, China, and South Korea, respectively.[3] Due to severe side-effects of cisplatin and its analogues and tumor resistance, and due to the fact that platinum(II) compounds are kinetically labile agents, the investigation of platinum(IV) compounds has recently received more and more interest. Platinum(IV) agents are kinetically inert, thus opening up the possibility of being administered orally and thereby enabling chemotherapy to become a more convenient treatment. Furthermore, six instead of only four coordination sites may be varied, facilitating a better fine-tuning of the pharmacological properties of the drug. By now, four platinum(IV) compounds have found their way into clinical trials, namely tetraplatin, iproplatin, satraplatin, and LA-12.[4]

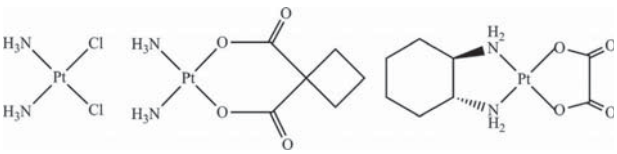

Figure 1. Worldwide approved platinum-based drugs: cisplatin (left), carboplatin (middle), and oxaliplatin (right).

Tetraplatin was abandoned due to its high toxicity in vivo, whereas iproplatin showed a lack of activity on account of its slow reduction rate.[5] Satraplatin failed to gain approval by the FDA but is still being investigated in combination therapy, while its derivative, LA-12 was in phase I clinical trials after having shown good in vivo results in mice.[4] Besides platinum-based metallodrugs, transition-metal-based complexes, such as ferrocene-bearing compounds, have shown strong antiproliferative effects in vitro as well as antitumor effects in vivo.[6,7] The most intensively investigated ferrocene-based compounds with anticancer potential are ferrocifens, prepared by replacing a phenyl group with ferrocene in tamoxifen, a selective estrogen receptor modulator (SERM) used in hormone-dependent (ER+) breast cancer treatment. In 1996, Jaouen et al. coupled ferrocene to 4-hydroxytamoxifen and modified the length of the carbon chain in order to optimize its pharmacological properties (Figure 2).[8] The hydroxyferrocifens show antiproliferative activity in hormone-dependent and in hormone-independent cells, whereas tamoxifen and hydroxytamoxifen are inactive in the latter.[9] Investigation of ferrocene-based anticancer agents ranged from design of ferrocenium salts (first investigated by Köpf-Maier et al. in

[a] Institute of Inorganic Chemistry, University of Vienna, Waehringer Strasse 42, 1090 Vienna, Austria
E-mail: markus.galanski@univie.ac.at
bernhard.keppler@univie.ac.at
http://anorg-chemie.univie.ac.at
[b] Research Platform "Translational Cancer Therapy Research", University of Vienna, Waehringer Strasse 42, 1090 Vienna, Austria

1984)[10] over combination of ferrocenyl groups with transition-metal complexes and to coupling of ferrocene moieties to drug delivery systems, such as polymers and nanoparticles.[9] During the past two decades, the synthesis of several platinum(II) compounds bearing ferrocene moieties has been accomplished.[9,11–13] Some of these compounds have shown promising IC_{50} values (Figure 3): (i) Nieto et al. recently published the successful synthesis and first cell culture tests of a *cis*-configured ferrocene-platinum derivative, which showed in vitro activity in human breast, cervix, lung and colon cancer cells in the low micromolar range (partially exceeding the antiproliferative activity of cisplatin);[11] (ii) a *trans*-dichloridoplatinum(II) complex featuring two ferrocene-bound phosphane units was designed by Schulz et al., which yielded low IC_{50} values in the micromolar range in the ovarian cancer cell line A2780.[13] A platinum(IV)-ferrocenyl system was described recently.[14] However, with the aim of combining the advantages of anticancer platinum(IV) complexes with the therapeutic potential of ferrocene-based compounds, we report here the synthesis, characterization, and antiproliferative potential of the first anticancer platinum(IV) complexes bearing ferrocene moieties as axial ligands.

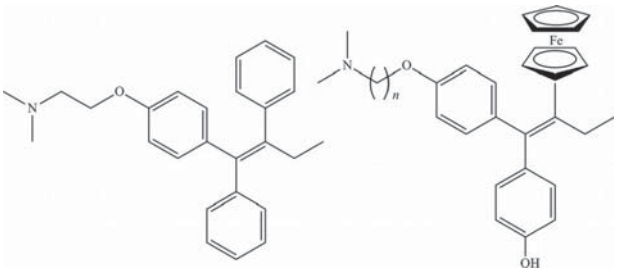

Figure 2. Molecular structures of SERM tamoxifen (left) and hydroxyferrocifens (right).

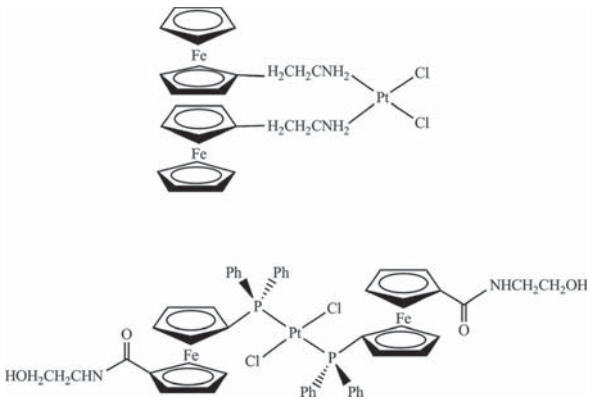

Figure 3. Cytotoxic platinum(II) complexes with ferrocene-bearing ligands.

Results and Discussion

Synthesis

For generation of ferrocene precursors **L2**–**L6**, the synthesis started with preparation of ferrocenecarboxylic acid according to literature methods (Scheme 1).[15] The acid was converted into the acyl chloride, subsequently brought to reaction with the desired diamine, *N*-*boc*-ethylenediamine, *N*-*boc*-ethanolamine or amino alcohol, and characterized by ^{1}H NMR spectroscopy. Precursors **L2**, **L4**, and **L6** could directly be used without further purification for coupling with compounds **2**, **8**, and **10** (Schemes 2 and 3), respectively. Before amidation, the *N*-*boc* protecting groups were removed from precursors of **L3** and **L5** by reaction with conc. trifluoroacetic acid (TFA).

All investigated complexes were prepared from $K_2[PtCl_4]$ according to literature methods by conversion into two different platinum(II) precursors, dichlorido(ethane-1,2-diamine) platinum(II) and (*1R*,*2R*-diaminocyclohexane)(oxalato)platinum(II). Both complexes were oxidized subsequently in the presence of hydrogen peroxide to yield dihydroxidoplatinum(IV) complexes **1** and **7** (Schemes 2 and 3). Preparation of dicarboxylic acids **2** and **8** was performed with succinic anhydride. Activation of the uncoordinated carboxylic acid groups followed by conversion into amides was accomplished by 1,1′-carbonyldiimidazole (CDI). The formed platinum(IV) imidazolides were brought to reaction in situ with ferrocene-bearing amines **L2**, **L3**, and **L5**, which resulted in amides **4**, **3**, and **11**, respectively. Synthesis of esters **5** and **12** was carried out by using the peptide coupling reagent *N*,*N*′-dicyclohexylcarbodiimide (DCC) and 4-(dimethylamino)pyridine. Since complexes **3**, **4**, **5**, **11**, and **12** show only poor solubility in water, analogous complexes with only one axial ferrocene fragment were prepared. For that purpose, (1*R*,2*R*-diaminocyclohexane)oxalatoplatinum(II) was oxidized with peracetic acid in acetic acid, which yielded acetato(1*R*,2*R*-diaminocyclohexane)hydroxido(oxalato)platinum(IV) (**9**). Thus, carboxylation with succinic anhydride of only one axial coordination site was facile, which resulted in an enhanced solubility in water of the substance when converted into esters and amides, respectively. Esterification and amidation were achieved by the same reaction pathways as described above. The final products **13**, **14**, and **15** were isolated in moderate yields of 20–41%.

Spectroscopic Characterization

The final products **3**–**5** and **11**–**15** were fully characterized by elemental analysis, ESI-MS and multinuclear (^{1}H, ^{13}C, ^{15}N, ^{195}Pt) 1D and 2D NMR spectroscopy, whereas structures of ferrocene precursors **L2**–**L6** were verified by ^{1}H NMR spectroscopy. Carboxylation and further derivatization can best be judged by NMR spectroscopy.

By analysis of the 2D NMR spectra, all protons of the final products could be assigned except for the two methylene groups in the axial position nearest to the platinum nucleus because of several overlaps. It was possible to distinguish between the three quaternary C=O carbon atoms because of the long-range shift correlation signals arising from the carbon atoms and protons of the cyclopentyl ring or protons belonging to the residue of the coupled ligand.

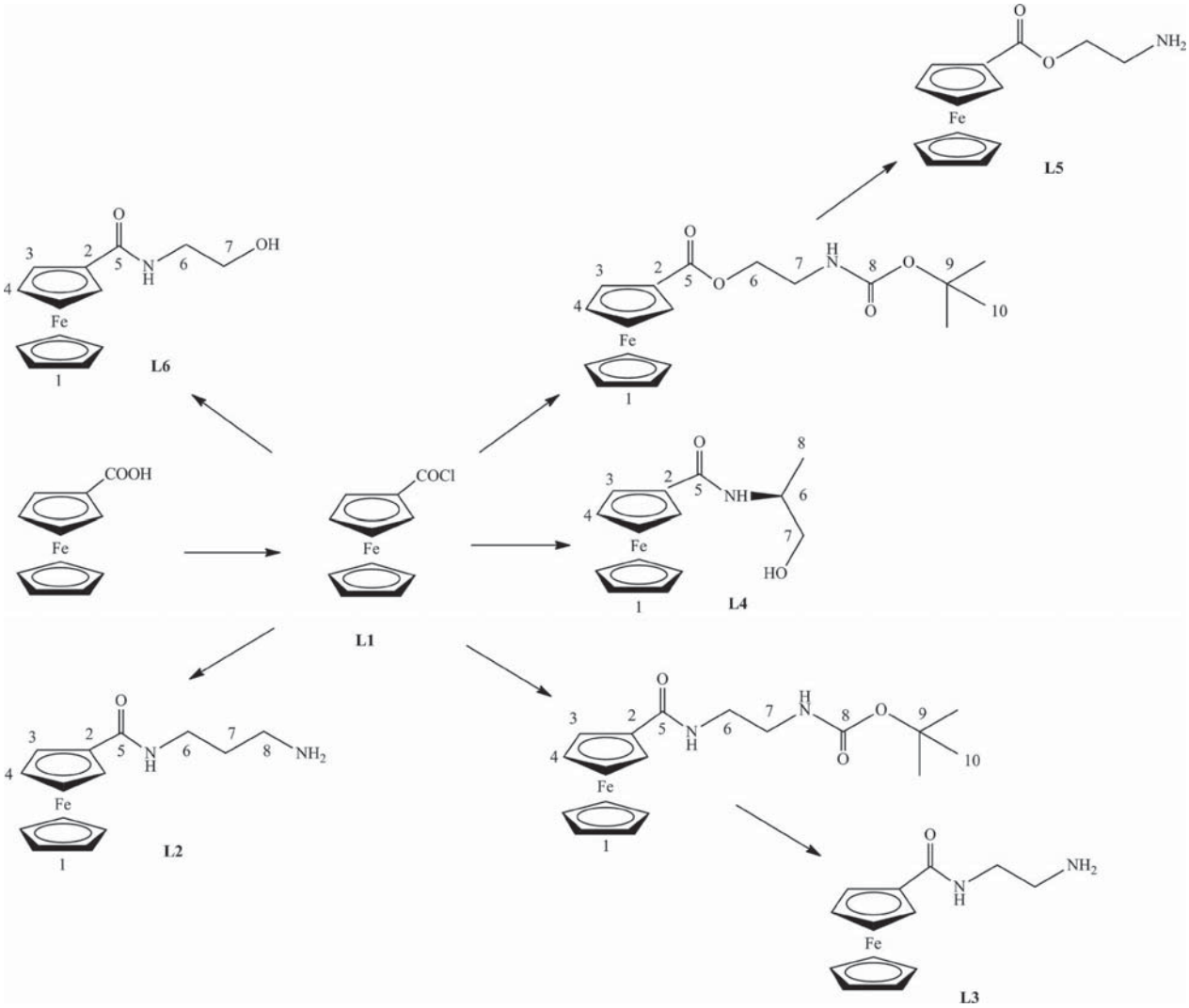

Scheme 1. Synthesis of ferrocene precursors **L2**–**L6** and NMR numbering scheme.

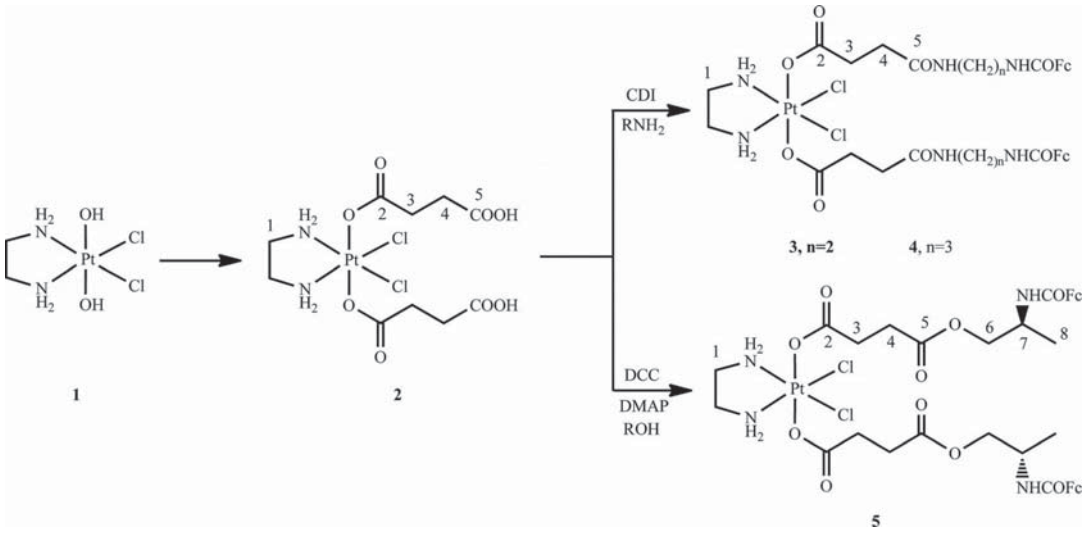

Scheme 2. Synthesis of complexes **3**–**5** and NMR numbering scheme.

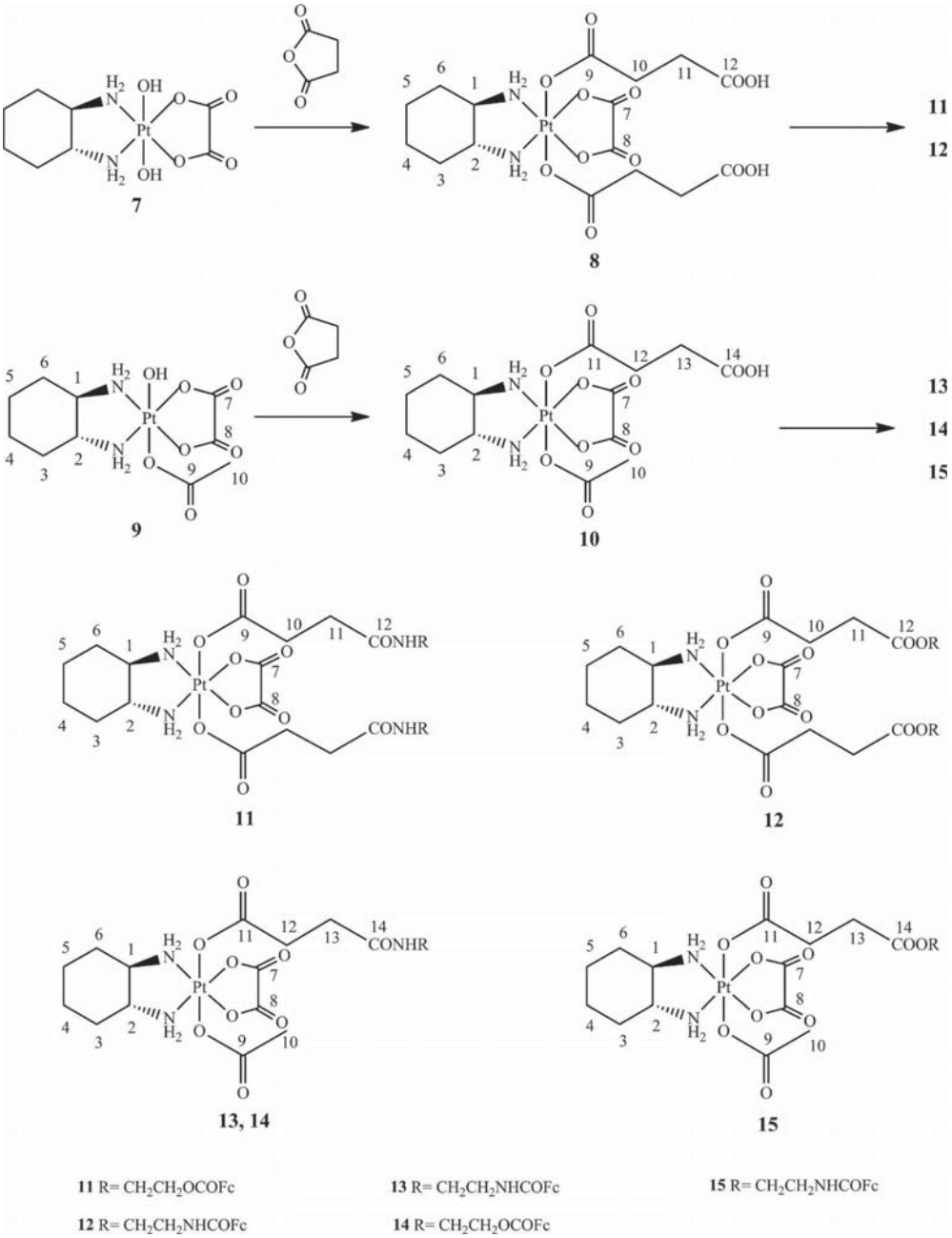

Scheme 3. Synthesis of platinum(IV) complexes **11**–**15** and NMR numbering scheme.

As described in the literature,[16] novel Pt^{IV} complexes with the $Cl_2N_2O_2$ coordination sphere show ^{195}Pt resonances in the region around 2656 ppm, whereas resonances for oxaliplatin-type platinum(IV) complexes appear in the region of 3230 ppm. As anticipated, the ^{195}Pt resonances are comparable for oxaliplatin-based Pt^{IV} complexes **13**, **14**, and **15** with one acetato and one derivatized carboxylato ligand in the axial position to those for their biscarboxylated analogues. ESI-MS spectra were measured in the positive as well as in the negative mode. The highest peak observed in each spectrum in the positive mode is $[M + Na]^+$, which is also in accordance with the calculated values.

Cytotoxicity

The cytotoxicity of dichlorido(ethane-1,2-diamine)platinum(IV) complexes **3**–**5**, as well as of the oxaliplatin derivatives **11**–**15**, was determined in cisplatin-sensitive CH1 (ovarian carcinoma) and in intrinsically cisplatin-resistant SW480 (colon carcinoma) as well as in A549 (non-small-cell lung carcinoma) cancer cells by means of the MTT colorimetric assay (Table 1). In general, the antiproliferative potency of novel ferrocene-containing complexes is highest in the ovarian carcinoma cell line CH1 with promising IC_{50} values in the low micromolar range (0.84–2.3 μM). Remark-

ably, the equatorial ligand sphere and the number of ferrocene moieties of the platinum compounds seem to have no pronounced influence on these properties. In contrast, the cytotoxicity of all tested complexes in the lung carcinoma cell line A549 is only moderate with IC_{50} values well above 20 μM. Antiproliferative potency in SW480 colon carcinoma cells was observed in an intermediate range, and a clear-cut structure–activity relationship in this cell line could be drawn. Compounds **3**–**5** featuring more cisplatin-like equatorial ligands, i.e. ethane-1,2-diamine and dichlorido, were less cytotoxic (IC_{50} = 32–46 μM) than oxaliplatin-type complexes **11**–**15** (IC_{50} = 2.7–5.6 μM).

Table 1. Cytotoxicity of complexes **3**–**5** and **11**–**15** in CH1, A549, and SW480 cancer cells.

IC_{50} [μM][a]			
Compound	CH1	SW480	A549
3	1.5 ± 0.4	43 ± 5	69 ± 15
4	1.6 ± 0.4	32 ± 11	65 ± 8
5	2.3 ± 0.5	46 ± 9	84 ± 1
11	0.86 ± 0.20	4.4 ± 1.4	>50
12	1.2 ± 0.1	3.9 ± 1.3	38 ± 4
13	0.84 ± 0.13	2.7 ± 1.0	24 ± 6
14	1.6 ± 0.1	4.8 ± 1.3	48 ± 2
15	1.3 ± 0.0	5.6 ± 0.9	49 ± 12
cisplatin[b]	0.14 ± 0.03	3.3 ± 0.4	1.3 ± 0.4
oxaliplatin	0.18 ± 0.01	0.29 ± 0.05	0.98 ± 0.21
8[c]	55 ± 28	44 ± 9	–
L6	>280	>320	>320

[a] 50% inhibitory concentrations in the MTT assay (96 h exposure). Values are means (± standard deviations) obtained from at least three independent experiments. [b] Data taken from ref.[17] [c] Data taken from ref.[18].

The latter behavior was expected, since oxaliplatin is approved for clinical treatment of metastatic colorectal carcinoma and shows above-average in vitro activity in many intrinsically cisplatin-resistant colon carcinoma cell lines such as SW480. As could be shown by evaluating monoacetato complexes **13**, **14**, and **15**, the linking fragment between the carboxylatoplatinum(IV) moiety and the ferrocene part ($NH–CH_2–CH_2–NH$ vs. $NH–CH_2–CH_2–O$ vs. $O–CH_2–CH_2–NH$) has nearly no influence on cytotoxicity. Furthermore, no substantial differences in the antiproliferative behavior of bis- and mono(ferrocene) derivatives (**11** vs. **14** and **12** vs. **15**) could be observed.

There is also no difference depending on the length of the linking methylene moiety ($NH–CH_2–CH_2–NH$ vs. $NH–CH_2–CH_2–CH_2–NH$) when comparing the cytotoxicity of compounds **3** and **4**. Generally, all complexes are less active by factors of 6–16 in the cisplatin-sensitive cell line CH1 than cisplatin. Likewise, oxaliplatin derivatives **11**–**15** are by an order of magnitude less potent than oxaliplatin in SW480 cells. All novel complexes presented in this manuscript are hence less effective than cis- and oxaliplatin, but it should be kept in mind that cis- and oxaliplatin are platinum(II) complexes, whereas the central platinum ion in complexes **3**–**5** and **11**–**15** has the oxidation state +4. This means that they act as prodrugs and, consequently, have to be activated in the organism by reduction. Therefore, their suitability according to the prodrug concept cannot be assessed based on these in vitro investigations alone. Further experiments, especially in vivo, are warranted.

Exemplarily, one of the ferrocene compounds, namely **L6**, was tested for its antiproliferative potential. IC_{50} values were mostly not reached with maximum tested concentrations of 320 μM, attesting a very low cytotoxicity. The platinum(IV) precursor **8** shows also a low antiproliferative activity (Table 1), however, when **L6** and **8** were brought to reaction resulting in ester **12**, a significant increase in cytotoxicity (one order of magnitude as compared to **8**) was observed, warranting further studies.

Conclusions

Platinum(IV) complexes featuring axially coordinated ferrocene-bearing ligands were synthesized for the first time and fully characterized by multinuclear NMR spectroscopy. Taking into account that platinum(IV) complexes act as prodrugs, which have to be activated in the organism, they show promising IC_{50} values in the low micromolar range in CH1 and SW480 human cancer cells.

Experimental Section

$K_2[PtCl_4]$ was obtained from Johnson Matthey (Switzerland), ferrocenecarboxylic acid from Alfa Aesar. All other chemicals were purchased from Aldrich, Fluka, Acros, or Fisher and used without further purification. When platinum(II) complexes were involved, syntheses were carried out under light protection; glass-coated magnetic stirring bars were used for each synthesis. For reactions in water, doubly distilled osmosis water was used.

Starting compounds **L1**–**L6** and precursors,[19–22] (SP-4–2)-(*trans*-1R,2R-diaminocyclohexane)oxalatoplatinum(II) (**6**), (*OC*-6–33)-bis(3-carboxypropanoato)dichlorido(ethane-1,2-diamine)platinum(IV) (**2**), (*OC*-6–33)-bis(3-carboxypropanoato)(*trans-1R,2R*-diaminocyclohexane)oxalatoplatinum(IV) (**8**), **9**, and **10**,[23–26] were synthesized according to literature methods.

Physical Measurements: Elemental Analysis was carried out by the Microanalytical Laboratory of the University of Vienna with a 2400 CHN Elemental Analyzer manufactured by Perkin–Elmer. For each submitted substance, the percentage of the elements carbon, hydrogen, and nitrogen was determined. Electrospray ionization mass spectra were recorded with a Bruker Esquire3000 ion trap spectrometer with MeOH as solvent, the molecular mass was determined in the positive as well as in the negative mode. NMR spectra were recorded on a Bruker FT-NMR Avance III 500 MHz instrument at 500.32 (^{1}H), 125.81 (^{13}C), 50.70 (^{15}N), and 107.55 (^{195}Pt) MHz. 2D NMR measurements were recorded by using standard pulse programs. Chemical shifts were referenced relative to the solvent signal for ^{1}H and ^{13}C spectra; for ^{15}N and ^{195}Pt spectra, the external standards $^{15}NH_4Cl$ and $K_2[PtCl_4]$ were used, respectively.

Synthesis of Ferrocene Precursors

Ferrocenyl Chloride (L1): Ferrocenecarboxylic acid was dissolved in abs. CH_2Cl_2 (typically 700 mg in 5 mL of abs. CH_2Cl_2) under an argon atmosphere, and oxalyl chloride (2 equiv.) was added. The solution was stirred for 20 min at room temperature, and the solvent was removed under reduced pressure. The obtained dark red

substance was dissolved in CH_2Cl_2 and used without purification for subsequent reactions.

***N*-3-(Aminopropyl)ferrocenecarboxamide (L2):** Compound **L1** (3.04 mmol) was dissolved in abs. CH_2Cl_2 (5 mL) and added slowly over 2 h at –23 °C to a solution of 1,3-diaminopropane (2.5 mL, 30.4 mmol) in abs. CH_2Cl_2 (50 mL). The solution was filtered (in order to get rid of the dimer) and extracted three times with water; the organic phase was dried with $MgSO_4$. After removal of the solvent under reduced pressure, the product was suspended in diethyl ether and filtered through a G-4 glass filter. The product was dried in vacuo. Yield: 235 mg, 33%. ^{1}H NMR ($CDCl_3$): δ = 6.82 (br. s, 1 H, NH), 4.69 (t, ^3J = 1.9 Hz, 2 H, H3), 4.35 (t, ^3J = 1.9 Hz, 2 H, H4), 4.22 (s, 5 H, H1), 3.53 (m, 2 H, CH_2), 2.94 (m, 2 H, CH_2), 1.76 (m, 2 H, CH_2) ppm.

***N*-2-(Aminoethyl)ferrocenecarboxamide (L3):** Compound **L1** (3.48 mmol) was dissolved in abs. CH_2Cl_2 (6 mL) and then added via a Teflon cannula to a stirred solution of *N*-*boc*-ethylenediamine (826 µL, 5.22 mmol) and triethylamine (964.7 µL 6.96 mmol) in abs. CH_2Cl_2 under an argon atmosphere and left to stir for 1 h. The solution was extracted three times with water, the organic phase was dried with $MgSO_4$, and the solvent was removed under reduced pressure. Yield: 512 mg, 33% of the *N*-*boc*-protected product. ^{1}H NMR ($CDCl_3$): δ = 6.30 (br. s, 1 H, NH), 4.67 (t, ^3J = 1.8 Hz, 2 H, H3), 4.31 (t, ^3J = 1.9 Hz, 2 H, H4), 4.18 (s, 5 H, H1), 3.42 (m, 2 H, CH_2), 2.90 (m, 2 H, CH_2), 1.63 (s, 9 H, H10) ppm. The product was dissolved in trifluoroacetic acid (4 mL) and left to stir for 5 min. Subsequently, trifluoroacetic acid was removed under reduced pressure, and the crude product was extracted three times with CH_2Cl_2 and with a saturated $NaHCO_3$ solution. The organic phase was dried again over $MgSO_4$, and the solvent was removed under reduced pressure.

(*S*)-*N*-(1-Hydroxypropan-2-yl)ferrocenecarboxamide (L4): Compound **L1** (2.17 mmol) was dissolved in abs. CH_2Cl_2 (4 mL) and then added via a teflon cannula to a stirred solution of (*S*)-2-amino-1-propanol (606 µL, 4.34 mmol) and triethylamine (604.9 µL 4.34 mmol) in abs. CH_2Cl_2 under an argon atmosphere and left to stir for 1 h. The solution was extracted three times with water, and the organic phase dried with $MgSO_4$. The solvent was removed under reduced pressure. Yield: 171 mg, 28%. ^{1}H NMR ($CDCl_3$): δ = 5.83 (m, 1 H, NH), 4.72 (m, 1 H, H3), 4.69 (m, 1 H, H3), 4.39 (s, 2 H, H4), 4.25 (s, 5 H, H1), 3.79 (m, 1 H, H6/H7), 3.65 (m, 1 H, H6/H7), 2.96 (m, 1 H, H6/H7), 1.30 (d, ^3J = 6.9 Hz, 3 H, H8) ppm.

[(2-Aminoethoxy)carbonyl]ferrocene (L5): Compound **L1** (3.04 mmol) was dissolved in abs. CH_2Cl_2 (6 mL) and then added via a teflon cannula to a stirred solution of *N*-*boc*-ethylenediamine (705.4 µL, 4.56 mmol) and triethylamine (847 µL 6.04 mmol) in abs. CH_2Cl_2 under an argon atmosphere and left to stir for 1 h. The solution was extracted three times with water, and the organic phase dried over $MgSO_4$. The solvent was removed under reduced pressure. Yield: 384 mg, 32.5% of the *N*-*boc*-protected product. ^{1}H NMR ($CDCl_3$): δ = 4.85 (t, ^3J = 1.8 Hz, 2 H, H3), 4.45 (t, ^3J = 1.8 Hz, 2 H, H4), 4.32 (m, 2 H, CH_2), 4.24 (s, 5 H, H1), 3.52 (m, 2 H, CH_2), 1.48 (s, 9 H, H10) ppm. The product was dissolved in trifluoroacetic acid (4 mL) and left to stir for 5 min. Subsequently, trifluoroacetic acid was removed under reduced pressure, and the crude product was extracted three times with CH_2Cl_2 and with a saturated $NAHCO_3$ solution. The organic phase was dried again over $MgSO_4$, and the solvent removed under reduced pressure.

{[(2-Hydroxyethyl)amino]carbonyl}ferrocene (L6): Compound **L1** (3.04 mmol) was dissolved in abs. CH_2Cl_2 (6 mL) and then added via a teflon cannula to a stirred solution of ethanolamine (550.4 µL, 9.12 mmol) and triethylamine (847 µL 6.04 mmol) in abs. CH_2Cl_2 under an argon atmosphere and left to stir for 1 h. The solution was filtered and extracted three times with water. The organic phase was dried with $MgSO_4$, and the solvent was removed under reduced pressure. Yield: 380 mg, 50%. ^{1}H NMR ($CDCl_3$): δ = 6.15 (br. s, 1 H, NH), 4.71 (t, ^3J = 1.5 Hz, 2 H, H3), 4.40 (t, ^3J = 1.6 Hz, 2 H, H4), 4.25 (s, 5 H, H1), 3.84 (t, ^3J = 4.9 Hz, 2 H, CH_2), 3.59 (m, 2 H, CH_2) ppm.

Synthesis of precursors 9 and 10

(*OC*-6–44)-Acetato(*1R*,*2R*-diaminocyclohexane)hydroxido(oxalato)platinum(IV) (9): Compound **6** (3 g, 7.6 mmol) was suspended in acetic acid (60 mL), peracetic acid (3.3 mL, 2.5 equiv.) was added, and the solution stirred for 30 min. The solution turned clear and was left to stir for 24 h. Acetic acid was removed under reduced pressure; the residue was dissolved in acetic acid (20 mL) and evaporated again. The product was suspended in ethyl acetate, methanol was added until the appearance of the suspension did not change any more, and the suspension was filtered. Solvents were removed on a rotary evaporator, and the white solid was dried in vacuo. Yield: 2.43 g, 66%. ^{1}H NMR ([D$_6$]DMSO) = 8.59 (br. m, 1 H, NH_2), 8.18 (br. m, 1 H, NH_2), 7.80 (br. m, 1 H, NH_2), 7.10 (m, 1 H, NH_2), ≈2.55 (H1/H2, underneath the DMSO peak), 2.07 (m, 2 H, H3/4/5/6), 1.92 (s, 3 H, H10), 1.54–1.29 (br. m, 4 H, H3/4/5/6); 1.13 (m, 2 H, H3/4/5/6) ppm.

(*OC*-6–44)-Acetato(3-carboxypropanoato)(*1R*,*2R*-diaminocyclohexane)oxalatoplatinum(IV) (10): Compound **9** (1 g, 2.04 mmol) and succinic anhydride (306.2 mg, 3.06 mmol) were suspended in abs. DMF (15 mL) and stirred for 24 h at 50 °C. The solvent was removed under reduced pressure, and the crude product was suspended in acetone. Methanol was added stepwise until the amount of insoluble solid did not change any more. The solution was filtered, the solvents were removed under reduced pressure, the residue was dissolved in acetone again, and ethyl acetate was added until no further precipitation was observed. The product was filtered, washed with diethyl ether, and dried in vacuo. Yield: 945 mg, 79%. ^{1}H NMR ([D$_6$]DMSO): δ = 12.13 (br. m, 1 H, OH), 8.11–8.52 (br. m, 4 H, NH_2), 2.58 (m, H1/H2), 2.40 (m, 2 H, H12/H13), 2.12 (m, 2 H, H3/H4/H5/H6), 1.97 (s, 3 H, H10), 1.51 (m, 2 H, H3/H4/H5/H6), 1.41 (m, 2 H, H3/H4/H5/H6), 1.17 (m, 2 H, H3/H4/H5/H6) ppm.

General Procedure for the Synthesis of Complexes 3, 4, 11, 13, and 14: 1,1′-Carbonyldiimidazole and the prevailing complex (**2**, **8** or **10**) were dissolved in abs. DMF stirred for 10 min at 60 °C and simultaneously flushed with argon. The solution was cooled down to room temperature, the required amine was added (**L2**, **L3** or **L5**), and the solution was left to stir for 24 h. The solvent was removed under reduced pressure; the crude product was dissolved in acetone and precipitated with diethyl ether. The product was filtered and subsequently purified by column chromatography.

General Procedure for the Synthesis of Complexes 5, 12, and 15: To a stirred solution of 4-dimethylaminopyridine, carboxylic acid (**2**, **8** or **10**), and the alcohol (**L4** or **L6**) was added *N*,*N*′-dicyclohexylcarbodiimide over 100 min. under an argon atmosphere. The solution was left to stir for 24 h at room temperature. The volume was reduced to 3 mL, and the suspension was filtered. The remaining solution was evaporated, and the crude product was purified by column chromatography.

(*OC*-6–33)-Dichlorido(ethane-1,2-diamine)bis(4-{[2-ferrocenoylamino]ethyl}amino)-4-oxobutanoatoplatin(IV) (3): 1,1′-Carbonyldiimidazole (92 mg, 0.57 mmol), **2** (144 mg, 0.26 mmol) in abs. DMF (6 mL), **L3** (175 mg, 0.64 mmol) in abs. DMF (2 mL). The

crude product was purified by column chromatography (EtOAc/MeOH, 2:1). The obtained product was dried in vacuo. Yield: 69 mg, 26%, yellow powder. $C_{36}H_{46}Cl_2Fe_2N_6O_8Pt·4H_2O$: calcd. C 37.91, H 4.77, N 7.37; found C 37.69, H 4.25, N 7.11. ^{1}H NMR ([D$_6$]DMSO): δ = 8.45 (br. s, 2 H, NH$_2$), 7.94 (br. m, 2 H, NH), 7.83 (br. m, 2 H, NH–COCp), 4.76 (br. m, 4 H, H10), 4.34 (br. m, 4 H, H11), 4.16 (s, 10 H, H12), 3.22 (m, 4 H, H7), 3.18 (m, 4 H, H6), 2.67 (br. m, 4 H, H1), ≈2.5 (H3/H4, underneath the DMSO peak), 2.32 (t, ^3J = 7.3 Hz, 4 H, H3/H4) ppm. ^{13}C NMR ([D$_6$]-DMSO): δ = 181.7 (C2), 172.0 (C5), 169.6 (C8), 77.0 (C9), 70.4 (C11), 69.9 (C12), 68.6 (C10), 49.2 (C1), 39.3 (C6/7), 39.1 (C6/7), 32.2 (C3/C4), 31.8 (C3/C4) ppm. ^{15}N NMR ([D$_6$]DMSO): δ = 91.4 (NH), 85.8 (NH–COCp), –4.4 (NH$_2$) ppm. ^{195}Pt NMR ([D$_6$]-DMSO): δ = 2655 ppm. MS (180 °C): *m*/*z* = 1091 [M + Na$^+$].

(*OC*-6–33)-Dichlorido(ethane-1,2-diamine)bis(4-{[3-ferrocenoylamino]propyl}amino)-4-oxobutanoatoplatin(IV) (4): 1,1′-Carbonyldiimidazole (109 mg, 0.67 mmol), **2** (184 mg, 0.33 mmol) in abs. DMF (7 mL), **L2** (235 mg, 0.82 mmol) in abs. DMF (2 mL). The crude product was purified by column chromatography ($CHCl_3$/MeOH, 5:1). The obtained product was dried in vacuo. Yield: 73 mg, 20%, yellow powder. $C_{38}H_{50}Cl_2Fe_2N_6O_8Pt·3H_2O$: calcd. C 39.67, H 4.91, N 7.30; found C 39.55, H 4.57, N 7.20. ^{1}H NMR ([D$_6$]DMSO): δ = 8.45 (br. s, 2 H, NH$_2$), 7.85 (br. m, 2 H, NH), 7.75 (br. m, 2 H, NH–COCp), 4.77 (br. m, 4 H, H11), 4.34 (br. m, 4 H, H12), 4.16 (s, 10 H, H13), 3.18 (m, 4 H, H8), 3.12 (m, 4 H, H6), 2.66 (br. m, 4 H, H1), ≈2.5 (H3/H4, underneath the DMSO peak), 2.31 (t, ^3J = 7.1 Hz, 4 H, H3/H4), 1.61 (m, 4 H, H7) ppm. ^{13}C NMR ([D$_6$]DMSO): δ = 181.7 (C2), 171.7 (C5), 169.3 (C9), 77.3 (C10), 70.3 (C12), 69.8 (C13), 68.5 (C11), 49.1 (C1), 36.8 (C6/C8), 36.8 (C6/C8), 32.3 (C3/C4), 31.8 (C3/C4), 30.1 (C7) ppm. ^{15}N NMR ([D$_6$]DMSO): δ = 94.1 (NH), 87.9 (NHCOCp), –4.8 (NH$_2$) ppm. ^{195}Pt NMR ([D$_6$]DMSO): δ = 2656 ppm. MS (180 °C): *m*/*z* = 1119 [M + Na$^+$], 1095 [M – H$^+$].

(*OC*-6–33)-Dichlorido(ethane-1,2-diamine)bis(4-{*S*-2-[ferrocenoylamino]propoxy})-4-oxobutanoatoplatin(IV) (5): 4-Dimethylaminopyridine (4.9 mg, 0.04 mmol), *N*,*N*′-dicyclohexylcarbodiimide (84.2 mg, 0.41 mmol) in abs. DMF (5 mL), **2** (111.4 mg, 0.20 mmol) in abs. DMF (7 mL), **L4** (171.4 mg, 0.60 mmol). The crude product was purified by column chromatography (EtOAc/MeOH, 2:1). The obtained product was dried in vacuo. Yield: 55 mg, 26%, yellow powder. $C_{38}H_{48}Cl_2Fe_2N_4O_{10}Pt·3H_2O$: calcd. C 39.60, H 4.72, N 4.86; found C 39.67, H 4.31, N 4.82. ^{1}H NMR ([D$_6$]DMSO): δ = 8.46 (br. s, 2 H, NH$_2$), 8.43 (br. s, 2 H, NH$_2$), 7.58 (d, ^3J = 8.3 Hz, 2 H, NH), 4.84 (br. m, 2 H, H11), 4.80 (br. m, 2 H, H11), 4.35 (br. m, 4 H, H12), 4.21 (m, 2 H, H7), 4.17 (s, 10 H, H13), 4.11 (m, 2 H, H6), 3.95 (m, 2 H, H6), 2.65 (br. s, 4 H, H1), 2.56 (m, 2 H, H3/H4), 2.50 (H3/H4, underneath the DMSO peak), 1.15 (d, ^3J = 6.7 Hz, 6 H, H8) ppm. ^{13}C NMR ([D$_6$]DMSO): δ = 180.0 (C2), 172.7 (C5), 169.1 (C9), 76.8 (C10), 70.5 (C12), 70.4 (C12), 69.9 (C13), 68.9 (C11), 68.5 (C11), 67.0 (C6), 49.2 (C1), 43.9 (C7), 31.3 (C3/C4), 30.1 (C3/C4), 17.7 (C8) ppm. ^{15}N NMR ([D$_6$]-DMSO): δ = 96.3 (NH), –5.1 (NH$_2$) ppm. ^{195}Pt NMR ([D$_6$]-DMSO): δ = 2658 ppm. MS (180 °C): *m*/*z* = 1121 [M + Na$^+$].

(*OC*-6–33)-(trans-*1R*,*2R*-Diaminocyclohexane)bis{4-[2-(ferrocenoyloxy)ethylamino]-4-oxobutanoato}oxalatoplatin(IV) (11): 1,1′-Carbonyldiimidazole (85.6 mg, 0.53 mmol), **8** (151.8 mg, 0.24 mmol) in abs. DMF (6 mL), **L5** (234 mg, 0.6 mmol) in abs. DMF (2 mL). The crude product was purified by column chromatography ($CHCl_3$/MeOH, 8:1). The obtained product was dried in vacuo. Yield: 112 mg, 41%, yellow powder. $PtC_{42}H_{50}Fe_2N_4O_{10}$: calcd. C 44.18, H 4.41, N 4.91; C 43.86, H 4.11, N 4.74. ^{1}H NMR ([D$_6$]-DMSO): δ = 8.36 (br. m, 2 H, NH$_2$), 8.15 (br. m, 2 H, NH$_2$), 8.07 (t, ^3J = 5.5 Hz, 2 H, NH), 4.77 (m, 4 H, H17), 4.50 (m, 4 H, H18), 4.23 (s, 10 H, H19), 4.13 (t, ^3J = 5.8 Hz, 2 H, H14), 3.37 (m, 2 H, H13), 2.69 (m, 2 H, H1/H2), ≈2.5 (H10/H11 underneath the DMSO peak), 2.35 (m, 2 H, H10/H11), 2.10 (m, 2 H, H3/H6), 1.50 (m, 2 H, H4/H5), 1.40 (m, 2 H, H3/H6), 1.18 (m, 2 H, H4/H5) ppm. ^{13}C NMR ([D$_6$]DMSO): δ = 180.7 (C9), 172.0 (C12), 171.1 (C15), 163.8 (C7/C8), 71.8 (C18), 71.1 (C16), 70.3 (C17), 70.1 (C17/C19), 62.9 (C14), 61.2 (C1/C2), 38.3 (C13), 31.6 (C3/C6/C10/C11), 31.4 (C3/C6/C10/C11), 24.0 (C4/C5) ppm. ^{15}N NMR ([D$_6$]DMSO): δ = 88.8 (NH), –6.3 (NH$_2$) ppm. ^{195}Pt NMR ([D$_6$]DMSO): δ = 3233 ppm. MS (180 °C): *m*/*z* = 1164 [M + Na$^+$], 1040 [M – H$^+$].

(*OC*-6–33)-(trans-*1R*,*2R*-Diaminocyclohexane)bis[4-(2-ferrocenoylamino)ethoxy]-4-(oxobutanoato)oxalatoplatin(IV) (12): 4-Dimethylaminopyridine (7.3 mg, 0.06 mmol), *N*,*N*′-dicyclohexylcarbodiimide (136.2 mg, 0.66 mmol) in abs. DMF (5 mL), **8** (190.4 mg, 0.30 mmol) in abs. DMF (8 mL), **L6** (247 mg, 0.90 mmol). The crude product was purified by column chromatography ($CHCl_3$/MeOH, 8:1). The obtained product was dried in vacuo. Yield: 67 mg, 20%, yellow powder. $C_{42}H_{50}Fe_2N_4O_{10}Pt·H_2O$: calcd. C 43.50, H 4.52, N 4.83; found C 43.27, H 4.21, N 4.78. ^{1}H NMR ([D$_6$]DMSO): δ = 8.35 (br. m, 2 H, NH$_2$), 8.17 (br. m, 2 H, NH$_2$), 7.89 (t, ^3J = 5.5 Hz, 2 H, NH), 4.79 (m, 4 H, H17), 4.35 (s, 4 H, H18), 4.23 (s, 10 H, H19), 4.12 (t, ^3J = 5.7 Hz, 2 H, H13), 3.42 (m, 2 H, H14), 2.69 (m, 2 H, H1/H2), ≈2.5 (H10/H11, underneath the DMSO peak), 2.15 (m, 2 H, H10/H11), 2.10 (m, 2 H, H3/H6), 1.50 (m, 2 H, H4/H5), 1.38 (m, 2 H, H3/H6), 1.13 (m, 2 H, H4/H5) ppm. ^{13}C NMR ([D$_6$]DMSO): δ = 179.9 (C9), 172.8 (C12), 169.8 (C15), 163.9 (C7/C8), 76.8 (C16), 70.5 (C18), 69.9 (C19), 68.7 (C17), 63.3 (C13), 61.3 (C1/C2), 38.2 (C14), 31.4 (C3/C6), 30.9 (C10/C11), 30.0 (C10/C11), 24.0 (C4/C5) ppm. ^{15}N NMR ([D$_6$]-DMSO): δ = 82.9 (NH), –6.4 (NH$_2$) ppm. ^{195}Pt NMR ([D$_6$]-DMSO): δ = 3238 ppm. MS (180 °C): *m*/*z* = 1164 [M + Na$^+$].

(*OC*-6–44)-Acetato(trans-*1R*,*2R*-diamminocyclohexane)[4-(2-ferrocenoylamino)ethylamino]-4-(oxobutanoato)oxalatoplatin(IV) (13): 1,1′-Carbonyldiimidazole (63.4 mg, 0.40 mmol), **10** (216.8 mg, 0.36 mmol) in abs. DMF (9 mL), **L3** (250 mg, 0.92 mmol) in abs. DMF (2 mL). The crude product was purified by column chromatography ($CHCl_3$/MeOH, 8.5:1). The obtained product was dried in vacuo. Yield: 100 mg, 34%, yellow powder. $C_{27}H_{35}Fe_2N_3O_{11}Pt·2H_2O$: calcd. C 37.55, H 4.67, N 6.49; found C 37.34, H 4.27, N 6.30. ^{1}H NMR ([D$_6$]DMSO): δ = 8.41 (br. m, 1 H, NH$_2$), 8.31 (br. m, 1 H, NH$_2$), 8.26 (m, 1 H, NH$_2$), 8.20 (m, 1 H, NH$_2$), 7.93 (br. m, 2 H, NH), 7.80 (br. m, 2 H, NH), 4.75 (br. m, 4 H, H19), 4.35 (br. m, 4 H, H20), 4.15 (s, 10 H, H21), 3.22 (br. m, 2 H, H15), 3.18 (bm, 2 H, H16), 2.67 (m, 1 H, H1/H2), 2.55 (m, H1/H2), ≈2.5 (H12/H13, underneath the DMSO peak), 2.31 (m, 2 H, H12/H13), 2.11 (m, 2 H, H3/H6), 1.96 (s, 3 H, H10), 1.50 (m, 2 H, H4/H5), 1.41 (m,2 H, H3/H6), 1.17 (m, 2 H, H4/H5) ppm. ^{13}C NMR ([D$_6$]DMSO): δ = 180.6 (C11), 179.1 (C9), 172.0 (C14), 169.6 (C17), 163.9 (C7/C8), 163.8 (C7/C8), 77.0 (C18), 70.4 (C20), 69.9 (C21), 68.6 (C19), 61.5 (C1/C2), 61.2 (C1/C2), 39.2 (C15), 39.1 (C16), 31.6 (C12/C13), 31.5 (C12/C13), 31.3 (C3/C6), 24.0 (C4/C5), 23.9 (C4/C5), 23.4 (C10) ppm. ^{15}N NMR ([D$_6$]DMSO): δ = 91.3 (NH), 85.4 (NH), –6.3 (NH$_2$) ppm. ^{195}Pt NMR ([D$_6$]DMSO): δ = 3236 ppm. MS (180 °C): *m*/*z* = 850 [M + Na$^+$].

(*OC*-6–44)-Acetato(trans-*1R*,*2R*-diaminocyclohexane)[4-(2-ferrocenoyloxy)ethylamino]-4-(oxobutanoato)oxalatoplatin(IV) (14): 1,1′-Carbonyldiimidazole (60.6 mg, 0.37 mmol), **10** (201.1 mg, 0.34 mmol) in abs. DMF (9 mL), **L5** (200 mg, 0.51 mmol) in abs. DMF (2 mL). The crude product was purified by column chromatography ($CHCl_3$/MeOH, 7:1). The obtained product was dried in vacuo. Yield: 78 mg, 28%, yellow powder.

$C_{27}H_{36}Fe_2N_4O_{10}Pt{\cdot}H_2O$: calcd. C 38.31, H 4.41, N 5.07; found C 38.41, H 4.01, N 4.95. ^{1}H NMR ([D$_6$]DMSO): δ = 8.42 (br. m, 1 H, NH_2), 8.31 (br. m, 1 H, NH_2), 8.25 (br. m, 1 H, NH_2), 8.24 (br. s, 1 H, NH_2), 8.07 (t, ^3J = 5.6 Hz, 2 H, NH), 4.77 (t, ^3J = 1.9 Hz, 2 H, H19), 4.50 (t, ^3J = 1.9 Hz, 2 H, H20), 4.23 (s, 5 H, H21), 4.13 (t, ^3J = 5.8 Hz, 2 H, H16), 3.37 (m, 2 H, H15), 2.71 (br. s, 1 H, H1/H2), ≈2.55 (m, H1/H2, underneath the DMSO peak), ≈2.50 (H12/H13, underneath the DMSO peak), 2.35 (m, 2 H, H12/H13), 2.11 (m, H3/H6), 1.96 (s, 3 H, H10), 1.50 (m, 2 H, H4/H5), 1.41 (m, 2 H, H3/H6), 1.17 (m, 2 H, H4/H5) ppm. ^{13}C NMR ([D$_6$]DMSO): δ = 180.6 (C11), 179.0 (C9), 172.0 (C14), 171.1 (C17), 163.9 (C7/C8), 163.8 (C7/C8), 71.9 (C20), 71.1 (C18), 70.3 (C19), 70.1 (C21), 62.9 (C16), 61.4 (C1/C2), 61.2 (C1/C2), 38.3 (C15), 31.5 (C3/C6/C12/C13), 31.4 (C3/C6/C12/C13), 24.1 (C4/C5), 23.9 (C4/C5), 23.4 (C10) ppm. ^{15}N NMR ([D$_6$]DMSO): δ = 87.6 (NH), –6.6 (NH_2) ppm. ^{195}Pt NMR ([D$_6$]DMSO): δ = 3236 ppm. (180 °C): *m*/*z* = 851 [M + Na$^+$], 826 [M – H$^+$].

(*OC*-6–44)-Acetato(trans-*1R*,*2R*-diaminocyclohexane)[4-(2-ferrocenoylamino)ethoxy]-4-(oxobutanoato)oxalatoplatin(IV) (15): 4-Dimethylaminopyridine (6.6 mg, 0.05 mmol), *N*,*N*′-dicyclohexylcarbodiimide (61.3 mg, 0.30 mmol) in abs. DMF (5 mL), **10** (160 mg, 0.27 mmol) in abs. DMF (8 mL), **L6** (133 mg, 0.49 mmol). The crude product was purified by column chromatography ($CHCl_3$/MeOH, 8:1). The obtained product was dried in vacuo. Yield: 67 mg, 30%, yellow powder. $C_{27}H_{35}Fe_2N_3O_{11}Pt{\cdot}1.5H_2O$: calcd. C 37.91, H 4.48, N 4.91; found C 37.73, H 4.05, N 4.82. ^{1}H NMR ([D$_6$]DMSO): δ = 8.41 (br. m, 1 H, NH_2), 8.33 (br. m, 1 H, NH_2), 8.26 (br. m, 1 H, NH_2), 8.21 (br. s, 1 H, NH_2), 7.89 (t, ^3J = 5.7 Hz, 2 H, NH), 4.79 (br. m, 2 H, H19), 4.35 (br. m, 2 H, H20), 4.16 (s, 5 H, H21), 4.11 (m, 2 H, H15), 3.41 (m, 2 H, H16), 2.57 (br. s, 2 H, H1/H2), ≈2.5 (m, H12/H13, underneath the DMSO peak), 2.10 (br. s, 2 H, H3/H6), 1.50 (m, 2 H, H4/H5), 1.40 (m, 2 H, H3/H6), 1.15 (m, 2 H, H4/H5) ppm. ^{13}C NMR ([D$_6$]DMSO): δ = 179.8 (C11), 179.0 (C9), 172.8 (C14), 169.8 (C17), 163.9 (C7/C8), 163.8 (C7/C8), 76.8 (C18), 70.5 (C20), 69.9 (C21), 68.6 (C19), 63.3 (C15), 61.4 (C1/C2), 61.2 (C1/C2), 38.2 (C16), 31.4 (C3/C6), 31.3 (C3/C6), 31.0 (C3/C6/C12/C13), 30.0 (C12/C13), 24.0 (C4/C5), 23.9 (C4/C5), 23.4 (C10) ppm. ^{15}NNMR ([D$_6$]DMSO): δ = 82.7 (NH), –6.7 (NH_2) ppm. ^{195}Pt NMR ([D$_6$]DMSO): δ = 3238 ppm. MS (180 °C): *m*/*z* = 851 [M + Na$^+$].

Evaluation of Biological Activity

Cell Lines and Cultivation Conditions: The cytotoxicity tests were performed in three cancer cell lines: CH1 (ovarian carcinoma), SW480 (colon carcinoma), and A549 (non-small cell lung cancer). Adherent cell monolayer cultures were grown in 75 cm^2 culture flasks (CytoOne, Starlab, UK) in complete medium [i.e. minimal essential medium (MEM) supplemented with 10% heat-inactivated fetal bovine serum, 1 mM sodium pyruvate, 4 mM L-glutamine, and 1% nonessential amino acids from 100× ready-to-use stock (all purchased from Sigma–Aldrich, Austria)]. Cell cultures were incubated at 37 °C in a moist atmosphere containing 5% CO_2.

Cytotoxicity Tests in Cancer Cell Lines: The cytotoxic activity of the compounds was determined by means of the MTT-based colorimetric microculture assay [MTT = 3-(4,5-dimethyl-2-thiazolyl)-2,5-diphenyl-2*H*-tetrazolium bromide]. The cells were harvested from culture flasks by trypsinization and passaged into 96-well microculture plates (CytoOne, Starlab, UK) in densities of 1×10^3 cells per well (CH1), 2×10^3 cells per well (SW480), and 3×10^3 cells per well (A549) in volumes of 100 µL per well. The cells were preincubated for 24 h before exposure to the drugs. Stock solutions of each complex were prepared in DMSO. These stock solutions were diluted in complete medium and then added in aliquots of 100 µL per well (final DMSO concentration 0.5%). After continuous exposure for 96 h, drug solutions were replaced with 100 µL of a RPMI/MTT mixture (6 parts RPMI 1640 medium supplemented with 10% heat-inactivated fetal bovine serum and 2 mM L-glutamine; 1 part MTT solution in phosphate-buffered saline [5 mg/mL]). After incubation for 4 h, the medium/MTT mixtures were removed, and the formazan crystals formed by viable cells were dissolved in 150 µL of DMSO per well. Optical densities at 550 nm were measured with a microplate reader (ELx808 Absorbance Microplate Reader, Bio-Tek, USA), by using a reference wavelength of 690 nm to correct for unspecific absorption. The quantities of viable cells were expressed in terms of T/C values by comparison to untreated control microcultures, and 50% inhibitory concentrations (IC_{50}) were calculated from concentration-effect curves by interpolation. Evaluation is based on means from at least three independent experiments, each comprising triplicates per concentration level.

Stability in DMSO/H_2O: Since the complexes had to be dissolved in DMSO and then diluted in aqueous medium for biological evaluation, stability under these conditions was addressed by NMR spectroscopy. In deuterated DMSO, all complexes were stable during the acquisition of the data (24–60 h), which is in accord with previous findings in the case of analogous platinum(IV) complexes. The stability of a representative complex (compound **3**) in a mixture of DMSO/D_2O was investigated by ^{1}H NMR spectroscopy. For this purpose, 0.5 mg of complex **3** was dissolved in 0.5 mL of DMSO mixed with 0.1 mL of D_2O. ^{1}H NMR spectra were measured from time to time. After sequential intervals of 24, 23.5, 8.5, and 14 h, 0.1 mL of D_2O was added, and the mixtures were investigated in the same way. The last mixture, consisting of 0.5 mL of DMSO and 0.5 mL of D_2O, was investigated for 48 h during which the signals broadened as a result of crystallization of **3**. However, a change in the NMR spectra could not be observed; in sum, **3** proved to be stable over 118 h under these conditions. In order to exclude precipitation of a decomposition product, 0.5 mL of the final suspension was mixed with 0.5 mL of DMSO. The clear solution was investigated by ^{1}H NMR spectroscopy, which proved the stability of **3** (significant amounts of hydrolysis products could not be detected).

Acknowledgments

The authors are indebted to the late Lloyd R. Kelland of the CRC Centre for Cancer Therapeutics, Institute of Cancer Research, Sutton, UK and Brigitte Marian (Institute of Cancer Research, Department of Medicine I, Medical University of Vienna, Austria) for providing cancer cell lines. Financial support by FWF (grant no. P20683-N19) and COST is gratefully acknowledged.

[1] B. Rosenberg, L. Van Camp, T. Krigas, *Nature* **1965**, *205*, 698–699.
[2] L. Kelland, *Nature* **2007**, 573–584.
[3] N. J. Wheate, S. Walker, G. E. Craig, R. Oun, *Dalton Trans.* **2010**, *39*, 8113–8127.
[4] M. R. Reithofer, A. K. Bytzek, S. M. Valiahdi, C. R. Kowol, M. Groessl, C. G. Hartinger, M. A. Jakupec, M. Galanski, B. K. Keppler, *J. Inorg. Biochem.* **2011**, *105*, 46–51.
[5] M. Reithofer, M. Galanski, A. Roller, B. K. Keppler, *Eur. J. Inorg. Chem.* **2006**, 2612–2617.
[6] S. Gomez-Ruiz, D. Maksimovic-Ivanic, S. Mijatovic, G. N. Kaluderovic, *Bioinorg. Chem. Appl.* **2012**, Article ID 140284.
[7] C. M. P. Pereira, D. Venzke, *Quim. Nova* **2013**, *36*, 143–152.
[8] S. Top, J. Tang, A. Vessières, D. Carrez, C. Provot, G. Jaouen, *Chem. Commun.* **1996**, 955–956.

[9] C. Ornelas, *New J. Chem.* **2011**, *35*, 1973–1985.
[10] P. Köpf-Maier, H. Köpf, E. W. Neuse, *J. Cancer Res. Clin. Oncol.* **1984**, *108*, 336–340.
[11] D. Nieto, A. M. González-Vadillo, S. Bruna, C. J. Pastor, C. Ríos-Luci, L. G. León, J. M. Padrón, C. Navarro-Ranninger, I. Cuadrado, *Dalton Trans.* **2012**, *41*, 432–441.
[12] T. A. K. Al-Allaf, L. J. Rashan, *Appl. Organomet. Chem.* **1999**, *13*, 63–68.
[13] J. Schulz, A. K. Renfrew, I. Císařová, P. J. Dyson, P. Štěpnička, *Appl. Organomet. Chem.* **2010**, *24*, 392–397.
[14] S. Jamali, S. M. Nabavizadeh, M. Rashidi, *Inorg. Chem.* **2008**, *47*, 5441–5452.
[15] C. J. Richards, A. W. Mulvaney, *Tetrahedron: Asymmetry* **1996**, *7*, 1419–1430.
[16] M. R. Reithofer, S. M. Valiahdi, M. A. Jakupec, V. B. Arion, A. Egger, M. Galanski, B. K. Keppler, *J. Med. Chem.* **2007**, *50*, 6692–6699.
[17] Y. Yu. Scaffidi-Domianello, A. A. Legin, M. A. Jakupec, V. B. Arion, V. Yu. Kukushkin, M. Galanski, B. K. Keppler, *Inorg. Chem.* **2011**, *50*, 10673–10681.
[18] M. R. Reithofer, S. M. Valiahdi, M. A. Jakupec, V. B. Arion, A. Egger, M. Galanski, B. K. Keppler, *J. Med. Chem.* **2007**, *50*, 6692–6699.
[19] J. Liu, P. He, J. Yan, X. Fang, J. Peng, K. Liu, Y. Fang, *Adv. Mater.* **2008**, *20*, 2508–2511.
[20] C. J. Richards, A. W. Mulvaney, *Tetrahedron* **1996**, *7*, 1419–1930.
[21] H. Funabashi, Y. Tanaka, Y. Amamura, M. Mie, T. Manabe, H. Tanaka, T. Takahashi, H. Handa, M. Aizawa, E. Kobatake, *Biosens. Bioelectron.* **2006**, *21*, 1675–1683.
[22] P. Steonicka, I. Cisarova, *CrystEngComm* **2005**, *7*, 37–43.
[23] E. J. Bulten, F. Verbeek, U. S. Patent 4482569, **1984**.
[24] A. R. Khokhar, S. Al-Baker, Z. H. Siddik, *J. Inorg. Biochem.* **1994**, *54*, 39–47.
[25] M. Reithofer, M. Galanski, A. Roller, B. K. Keppler, *Eur. J. Inorg. Chem.* **2006**, 2612–2617.
[26] S. Abramkin, Dissertation, University of Vienna, **2012**.

Received: October 1, 2013
Published Online: December 9, 2013

3. Conclusions and Outlook

Various side effects, acquired resistance and the limited panel of responsive tumors are the main limiting factors of classic platinum-based chemotherapeutics used in the clinic. To overcome these critical drawbacks the development of new classes of metal-based drugs that might possess a different mode of action are undertaken worldwide. In this cumulative PhD thesis, the advances in the investigation of classic and non-classic platinum-based complexes are discussed. Different bioanalytical methods (e.g. MTT assay, drug accumulation studies by means of ICP-MS, FACS-based annexin V-FITC/propidium iodide assay, as well as imaging techniques) were applied to shed some light on the activity of the complexes *in vitro* and their possible mode of action. The mechanisms underlying the efficacy, selectivity and side effects of platinum and other metal-based drugs are not sufficiently well understood. The elucidation of the cellular targets and mechanisms of different metal-based drugs should aid in the design of new classes of active antitumor agents with improved therapeutic index.

NanoSIMS is currently becoming a powerful and increasingly applied tool for subcellular mapping of target elements. In our proof-of-principle NanoSIMS project, we concentrated on developing an approach that allows the investigation of the subcellular fate of platinum-based drugs in eukaryotic cells to assess possible cellular targets. The knowledge about the subcellular drug distribution can in turn help to understand the mechanisms responsible for selectivity, cytotoxicity and side effects of Pt-based anticancer drugs. NanoSIMS technique was applied to investigate the fate of ^{15}N-isotopically labeled cisplatin in tumor cells. Due to the unknown platinum detection limits of the NanoSIMS technique, a pilot run was performed with the cells treated with a range of cisplatin concentrations. Furthermore, we optimized the conventional sample preparation method. The cells embedded into the epoxy resin blocks were cut, and subsequently the sections were analyzed by NanoSIMS. The embedding procedure was modified in order to reduce the possible wash-out effects and maintain the cellular ultrastructure. Different sectioning thickness was tried to find the optimal balance between the analyte volume and surface charging during the SIMS measurement. To establish the colocalization experiments with confocal microscopy the sample holders were specifically marked with a laser dissection microscope prior to cell seeding. The cells grown on the sample holders accumulated enough platinum for detection. We also showed the possibility to correlate the target signal with characteristic signals of carbon, nitrogen, phosphor and sulfur.

The NanoSIMS elemental imaging allowed us to obtain both qualitative and quantitative information about drug distribution. Significant implications for cisplatin stoichiometry were discovered, expanding the possibilities of quantitative SIMS application. The chemical imaging of anticancer drugs in tumor cells was brought to a new level by successful colocalization experiments conducted by

means of NanoSIMS and confocal laser scanning microscopy pointing to the accumulation of platinum within acidic organelles. The established approach will be further implemented for the investigation of drug behavior in systems of higher order of complexity such as 3D multicellular spheroids and murine tissues (e.g. organs and tumors from the treated mice). The technique proved to be a powerful tool capable of following the distribution of both metal and leaving ligands that in turn opens a new route for the investigation of the activation-by-reduction hypothesis, e.g., in the case of platinum(IV) compounds. Dissociation of platinum(IV)-based complexes can be investigated when different stable isotopes are used to label the axial and equatorial ligands. Moreover, the combination of NanoSIMS with high-resolution imaging techniques such as electron microscopy (TEM, SEM) or confocal microscopy holds much promise for resolving questions concerning the mechanisms underlying the efficacy, selectivity and side effects of platinum drugs on the ultrastructure scale. The combinatory approaches are recently being established to enable trace elemental analyses of the treated samples. Innovative techniques will allow investigation of metal-based drugs with the central atom other than platinum, and the methodology can then be expanded to ruthenium and gallium based compounds.

The activation-by-reduction hypothesis and the general idea of the local activation of prodrugs in the tumor microenvironment are the keystone questions that interconnect some of the other results presented in the dissertation. The acetoxime platinum(II) compounds and platinum(IV) are supposed to undergo the activation in the slightly acid or hypoxic milieu of solid tumors. Several approaches were used to characterize the activity of these complexes in human cancer cell lines of different origin. We reported the increased antiproliferative effects of pH-sensitive acetoxime platinum(II) complexes in slightly acidic conditions and the successful activation of the *trans*-geometry of novel oximato-bridged platinum(II) di- and trimer(s) that not only overcome the activity of the *cis*-congeners but are also capable of apoptosis induction in cisplatin-resistant cell lines. Several bis(carboxylato)dichloridobis(ethylamine)platinum(IV) complexes were proven to be strong apoptotic agents that show high levels of cytotoxicity.

4. References

1. OECD, *Health at a Glance: Europe 2012*, OECD Publishing.
2. J. Ferlay, E. Steliarova-Foucher, J. Lortet-Tieulent, S. Rosso, J. W. Coebergh, H. Comber, D. Forman and F. Bray, *Eur J Cancer*, 2013, **49**, 1374-1403.
3. Statistik Österreich., Verlag Österreich, Wien, 2013, p. v.
4. B. Rosenberg, L. Vancamp and T. Krigas, *Nature*, 1965, **205**, 698-699.
5. B. Rosenberg, L. Vancamp, J. E. Trosko and V. H. Mansour, *Nature*, 1969, **222**, 385-386.
6. L. Kelland, *Nat Rev Cancer*, 2007, **7**, 573-584.
7. L. H. Einhorn, *Clin Cancer Res*, 1997, **3**, 2630-2632.
8. T. Winton, R. Livingston, D. Johnson, J. Rigas, M. Johnston, C. Butts, Y. Cormier, G. Goss, R. Inculet, E. Vallieres, W. Fry, D. Bethune, J. Ayoub, K. Ding, L. Seymour, B. Graham, M. S. Tsao, D. Gandara, K. Kesler, T. Demmy and F. Shepherd, *N Engl J Med*, 2005, **352**, 2589-2597.
9. S. Ramalingam and C. Belani, *Oncologist*, 2008, **13 Suppl 1**, 5-13.
10. J. B. Vermorken, E. Remenar, C. van Herpen, T. Gorlia, R. Mesia, M. Degardin, J. S. Stewart, S. Jelic, J. Betka, J. H. Preiss, D. van den Weyngaert, A. Awada, D. Cupissol, H. R. Kienzer, A. Rey, I. Desaunois, J. Bernier and J. L. Lefebvre, *N Engl J Med*, 2007, **357**, 1695-1704.
11. J. Tepper, M. J. Krasna, D. Niedzwiecki, D. Hollis, C. E. Reed, R. Goldberg, K. Kiel, C. Willett, D. Sugarbaker and R. Mayer, *J Clin Oncol*, 2008, **26**, 1086-1092.
12. A. M. Florea and D. Busselberg, *Cancers (Basel)*, 2011, **3**, 1351-1371.
13. S. Quasthoff and H. P. Hartung, *J Neurol*, 2002, **249**, 9-17.
14. L. P. Rybak, C. A. Whitworth, D. Mukherjea and V. Ramkumar, *Proc Natl Acad Sci U S A*, 2007, **226**, 157-167.
15. J. Pourahmad, M. J. Hosseini, M. R. Eskandari, S. M. Shekarabi and B. Daraei, *Xenobiotica*, 2010, **40**, 763-771.
16. N. Pabla and Z. Dong, *Kidney Int*, 2008, **73**, 994-1007.
17. S. Matsumoto, T. Tanaka, H. Kurokawa, K. Matsuno, Y. Hayashida and T. Takahashi, *Anticancer Res*, 2007, **27**, 2209-2216.
18. F. Arnesano, M. Losacco and G. Natile, *Dalton Trans*, 2013, **2013**, 2701-2711.
19. G. Ciarimboli, *Anticancer Res*, 2014, **34**, 547-550.
20. J. Reedijk, *Chem Rev*, 1999, **99**, 2499-2510.
21. D. V. Deubel, *J Am Chem Soc*, 2004, **126**, 5999-6004.
22. D. Gibson, *Dalton Trans*, 2009, 10681-10689.
23. G. Chu, *J Biol Chem*, 1994, **269**, 787-790.
24. Y. Kasherman, S. Sturup and D. Gibson, *J Med Chem*, 2009, **52**, 4319-4328.
25. M. Knipp, *Curr Med Chem*, 2009, **16**, 522-537.

26. D. Wang and Z. Guo, *Anticancer Agents Med Chem*, 2007, **7**, 19-34.
27. S. E. Crider, R. J. Holbrook and K. J. Franz, *Metallomics*, 2010, **2**, 74-83.
28. D. J. Smith, M. Jaggi, W. Zhang, A. Galich, C. Du, S. P. Sterrett, L. M. Smith and K. C. Balaji, *Urology*, 2006, **67**, 1341-1347.
29. S. J. Berners-Price, L. Ronconi and P. J. Sadler, *Prog Nucl Magn Reson Spectrosc*, 2006, **49**, 65-98.
30. D. Wang and S. J. Lippard, *Nat Rev Drug Discov*, 2005, **4**, 307-320.
31. E. R. Jamieson and S. J. Lippard, *Chem Rev*, 1999, **99**, 2467-2498.
32. T. Boulikas, A. Pantos, E. Bellis and P. Christofis, *Cancer Therapy*, 2007, **5**, 537-583.
33. Y. W. Jung and S. J. Lippard, *Chem Rev*, 2007, **107**, 1387-1407.
34. M. A. Fuertes, J. Castilla, C. Alonso and J. M. Perez, *Curr Med Chem*, 2003, **10**, 257-266.
35. E. G. Chapman and V. J. DeRose, *J Am Chem Soc*, 2010, **132**, 1946-1952.
36. Z. Yang, L. M. Schumaker, M. J. Egorin, E. G. Zuhowski, Z. Guo and K. J. Cullen, *Clin Cancer Res*, 2006, **12**, 5817-5825.
37. P. J. Morin, *Drug Resist Updat*, 2003, **6**, 169-172.
38. Z. H. Siddik, *Oncogene*, 2003, **22**, 7265-7279.
39. M. A. Jakupec, M. Galanski and B. K. Keppler, *Rev Physiol Biochem Pharmacol*, 2003, **146**, 1-54.
40. I. Ali, W. A. Wani, K. Saleem and A. Haque, *Anticancer Agents Med Chem*, 2013, **13**, 296-306.
41. D. Lebwohl and R. Canetta, *Eur J Cancer*, 1998, **34**, 1522-1534.
42. N. J. Wheate, S. Walker, G. E. Craig and R. Oun, *Dalton Trans*, 2010, **39**, 8113-8127.
43. V. Brabec and J. Kasparkova, *Drug Resist Updat*, 2005, **8**, 131-146.
44. F. Yu, J. Megyesi and P. M. Price, *Am J Physiol-Renal*, 2008, **295**, F44-F52.
45. A. Mandic, J. Hansson, S. Linder and M. C. Shoshan, *J Biol Chem*, 2003, **278**, 9100-9106.
46. G. Natile and M. Coluccia, *Coord Chem Rev*, 2001, **216**, 383-410.
47. M. J. Cleare and J. D. Hoeschele, *Platinum Metals Rev.*, 1973, **17**, 2-13.
48. J. Kasparkova, O. Novakova, N. Farrell and V. Brabec, *Biochemistry*, 2003, **42**, 792-800.
49. J. M. Perez, M. A. Fuertes, C. Alonso and C. Navarro-Ranninger, *Crit Rev Oncol Hematol*, 2000, **35**, 109-120.
50. S. M. Aris and N. P. Farrell, *Eur J Inorg Chem*, 2009, **2009**, 1293.
51. U. Kalinowska-Lis, J. Ochocki and K. Matlawska-Wasowska, *Coord Chem Rev*, 2008, **252**, 1328-1345.
52. Y. Najajreh, Y. Ardeli-Tzaraf, J. Kasparkova, P. Heringova, D. Prilutski, L. Balter, S. Jawbry, E. Khazanov, J. M. Perez, Y. Barenholz, V. Brabec and D. Gibson, *J Med Chem*, 2006, **49**, 4674-4683.

53. J. M. Perez, L. R. Kelland, E. I. Montero, F. E. Boxall, M. A. Fuertes, C. Alonso and C. Navarro-Ranninger, *Mol Pharmacol*, 2003, **63**, 933-944.
54. R. Prokop, J. Kasparkova, O. Novakova, V. Marini, A. M. Pizarro, C. Navarro-Ranninger and V. Brabec, *Biochem Pharmacol*, 2004, **67**, 1097-1109.
55. P. A. Nguewa, M. A. Fuertes, S. Iborra, Y. Najajreh, D. Gibson, E. Martinez, C. Alonso and J. M. Perez, *J Inorg Biochem*, 2005, **99**, 727-736.
56. M. Coluccia, A. Nassi, A. Boccarelli, D. Giordano, N. Cardellicchio, D. Locker, M. Leng, M. Sivo, F. P. Intini and G. Natile, *J Inorg Biochem*, 1999, **77**, 31-35.
57. A. Boccarelli, F. P. Intini, R. Sasanelli, M. F. Sivo, M. Coluccia and G. Natile, *J Med Chem*, 2006, **49**, 829-837.
58. A. G. Quiroga, L. Cubo, E. de Blas, P. Aller and C. Navarro-Ranninger, *J Inorg Biochem*, 2007, **101**, 104-110.
59. S. Zorbas-Seifried, M. A. Jakupec, N. V. Kukushkin, M. Groessl, C. G. Hartinger, O. Semenova, H. Zorbas, V. Y. Kukushkin and B. K. Keppler, *Mol Pharmacol*, 2007, **71**, 357-365.
60. M. Leng, D. Locker, M. J. Giraud-Panis, A. Schwartz, F. P. Intini, G. Natile, C. Pisano, A. Boccarelli, D. Giordano and M. Coluccia, *Mol Pharmacol*, 2000, **58**, 1525-1535.
61. Y. Y. Scaffidi-Domianello, A. A. Legin, M. A. Jakupec, V. B. Arion, V. Y. Kukushkin, M. Galanski and B. K. Keppler, *Inorg Chem*, 2011, **50**, 10673-10681.
62. W. Friebolin, G. Schilling, M. Zoller and E. Amtmann, *J Med Chem*, 2004, **47**, 2256-2263.
63. M. Galanski, C. Baumgartner, V. Arion and Bernhard K. Keppler, *Eur J Inorg Chem*, 2003, **2003**, 2619-2625.
64. S. M. Valiahdi, A. E. Egger, W. Miklos, U. Jungwirth, K. Meelich, P. Nock, W. Berger, C. G. Hartinger, M. Galanski, M. A. Jakupec and B. K. Keppler, *J Biol Inorg Chem*, 2013, **18**, 249-260.
65. O. Warburg, *Science*, 1956, **124**, 269-270.
66. O. Warburg, *Science*, 1956, **123**, 309-314.
67. J. Chiche, M. C. Brahimi-Horn and J. Pouyssegur, *J Cell Mol Med*, 2010, **14**, 771-794.
68. P. Yotnda, D. Wu and A. M. Swanson, *Methods Mol Biol*, 2010, **651**, 1-29.
69. D. Hanahan and R. A. Weinberg, *Cell*, 2011, **144**, 646-674.
70. M. Galanski and B. K. Keppler, *Anticancer Agents Med Chem*, 2007, **7**, 55-73.
71. T. J. O'Rourke, G. R. Weiss, P. New, H. A. Burris, 3rd, G. Rodriguez, J. Eckhardt, J. Hardy, J. G. Kuhn, S. Fields, G. M. Clark and et al., *Anticancer Drugs*, 1994, **5**, 520-526.
72. C. Trask, A. Silverstone, C. M. Ash, H. Earl, C. Irwin, A. Bakker, J. S. Tobias and R. L. Souhami, *J Clin Oncol*, 1991, **9**, 1131-1137.
73. T. Latif, L. Wood, C. Connell, D. C. Smith, D. Vaughn, D. Lebwohl and D. Peereboom, *Invest New Drugs*, 2005, **23**, 79-84.

74. G. P. Amorino, P. J. Mohr, S. K. Hercules, H. Pyo and H. Choy, *Cancer Chemother Pharmacol*, 2000, **46**, 423-426.
75. K. Lemma, J. Berglund, N. Farrell and L. I. Elding, *J Biol Inorg Chem*, 2000, **5**, 300-306.
76. V. Pichler, P. Heffeter, S. M. Valiahdi, C. R. Kowol, A. Egger, W. Berger, M. A. Jakupec, M. Galanski and B. K. Keppler, *J Med Chem*, 2012, **55**, 11052-11061.
77. A. M. Fichtinger-Schepman, J. L. van der Veer, J. H. den Hartog, P. H. Lohman and J. Reedijk, *Biochemistry*, 1985, **24**, 707-713.
78. M. Galanski and B. K. Keppler, *Inorg Chim Acta*, 2000, **300**, 783-789.
79. M. D. Hall, S. Amjadi, M. Zhang, P. J. Beale and T. W. Hambley, *J Inorg Biochem*, 2004, **98**, 1614-1624.
80. R. P. Sharma and I. R. Edwards, *Biochem Pharmacol*, 1983, **32**, 2665-2669.
81. M. Groessl, O. Zava and P. J. Dyson, *Metallomics*, 2011, **3**, 591-599.
82. D. Esteban-Fernandez, J. M. Verdaguer, R. Ramirez-Camacho, M. A. Palacios and M. M. Gomez-Gomez, *J Anal Toxicol*, 2008, **32**, 140-146.
83. J. H. Beumer, J. H. Beijnen and J. H. Schellens, *Clin Pharmacokinet*, 2006, **45**, 33-58.
84. N. Penner, L. J. Klunk and C. Prakash, *Biopharm Drug Dispos*, 2009, **30**, 185-203.
85. J. J. Wilson and S. J. Lippard, *Inorg Chim Acta*, 2012, **389**, 77-84.
86. J. Gao, Y. G. Liu and R. A. Zingaro, *Chem Res Toxicol*, 2009, **22**, 1705-1712.
87. S. Wu, C. Zhu, C. Zhang, Z. Yu, W. He, Y. He, Y. Li, J. Wang and Z. Guo, *Inorg Chem*, 2011, **50**, 11847-11849.
88. G. V. Kalayda, B. A. Jansen, P. Wielaard, H. J. Tanke and J. Reedijk, *J Biol Inorg Chem*, 2005, **10**, 305-315.
89. S. Vogt and M. Ralle, *Anal Bioanal Chem*, 2012.
90. Z. Qin, J. A. Caruso, B. Lai, A. Matusch and J. S. Becker, *Metallomics*, 2011, **3**, 28-37.
91. K. L. Moore, E. Lombi, F. J. Zhao and C. R. Grovenor, *Anal Bioanal Chem*, 2012, **402**, 3263-3273.
92. A. Carmona, P. Cloetens, G. Devès, S. Bohic and R. Ortega, *J Anal Atom Spectrom*, 2008, **23**, 1083.
93. S. Matsuyama, M. Shimura, H. Mimura, M. Fujii, H. Yumoto, Y. Sano, M. Yabashi, Y. Nishino, K. Tamasaku, T. Ishikawa and K. Yamauchi, *X Ray Spectrom*, 2009, **38**, 89-94.
94. M. D. Hall, C. T. Dillon, M. Zhang, P. Beale, Z. Cai, B. Lai, A. P. Stampfl and T. W. Hambley, *J Biol Inorg Chem*, 2003, **8**, 726-732.
95. K. G. Chen, J. C. Valencia, B. Lai, G. Zhang, J. K. Paterson, F. Rouzaud, W. Berens, S. M. Wincovitch, S. H. Garfield, R. D. Leapman, V. J. Hearing and M. M. Gottesman, *Proc Natl Acad Sci U S A*, 2006, **103**, 9903-9907.
96. L. E. Wedlock, M. R. Kilburn, J. B. Cliff, L. Filgueira, M. Saunders and S. J. Berners-Price, *Metallomics*, 2011, **3**, 917-925.

97. M. L. Steinhauser and C. P. Lechene, *Semin Cell Dev Biol*, 2013, **24**, 661-667.
98. M. Wagner, *Annu Rev Microbiol*, 2009, **63**, 411-429.
99. P. L. Clode, M. R. Kilburn, D. L. Jones, E. A. Stockdale, J. B. Cliff, 3rd, A. M. Herrmann and D. V. Murphy, *Plant Physiol*, 2009, **151**, 1751-1757.
100. L. E. Wedlock, M. R. Kilburn, R. Liu, J. A. Shaw, S. J. Berners-Price and N. P. Farrell, *Chem Commun*, 2013, **49**, 6944-6946.
101. S. Chandra, *Methods Mol Biol*, 2010, **656**, 113-130.
102. T. Eybe, J. N. Audinot, T. Udelhoven, E. Lentzen, B. El Adib, J. Ziebel, L. Hoffmann and T. Bohn, *Chemosphere*, 2013, **90**, 1829-1838.
103. P. Hoppe, S. Cohen and A. Meibom, *Geostand Geoanal Res*, 2013, **37**, 111-154.
104. M. L. Pacholski and N. Winograd, *Chem Rev*, 1999, **99**, 2977-3006.
105. M. R. Kilburn and P. L. Clode, *Methods Mol Biol*, 2014, **1117**, 733-755.
106. A. Georgantzopoulou, Y. L. Balachandran, P. Rosenkranz, M. Dusinska, A. Lankoff, M. Wojewodzka, M. Kruszewski, C. Guignard, J. N. Audinot, S. Girija, L. Hoffmann and A. C. Gutleb, *Nanotoxicology*, 2013, **7**, 1168-1178.
107. A. A. Legin, A. Schintlmeister, M. A. Jakupec, M. Galanski, I. Lichtscheidl, M. Wagner and B. K. Keppler, *Chem Sci*, 2014, **5**, 3135-3143.
108. D. Berry, B. Stecher, A. Schintlmeister, J. Reichert, S. Brugiroux, B. Wild, W. Wanek, A. Richter, I. Rauch, T. Decker, A. Loy and M. Wagner, *Proc Natl Acad Sci U S A*, 2013, **110**, 4720-4725.
109. M. Tourna, M. Stieglmeier, A. Spang, M. Konneke, A. Schintlmeister, T. Urich, M. Engel, M. Schloter, M. Wagner, A. Richter and C. Schleper, *Proc Natl Acad Sci U S A*, 2011, **108**, 8420-8425.
110. C. Lechene, F. Hillion, G. McMahon, D. Benson, A. M. Kleinfeld, J. P. Kampf, D. Distel, Y. Luyten, J. Bonventre, D. Hentschel, K. M. Park, S. Ito, M. Schwartz, G. Benichou and G. Slodzian, *J Biol*, 2006, **5**, 20.
111. G. McMahon, B. J. Glassner and C. P. Lechene, *Appl Surf Sci*, 2006, **252**, 6895-6906.
112. S. E. Senyo, M. L. Steinhauser, C. L. Pizzimenti, V. K. Yang, L. Cai, M. Wang, T. D. Wu, J. L. Guerquin-Kern, C. P. Lechene and R. T. Lee, *Nature*, 2013, **493**, 433-436.
113. J. Pett-Ridge and P. K. Weber, *Methods Mol Biol*, 2012, **881**, 375-408.
114. T. Li, T. D. Wu, L. Mazeas, L. Toffin, J. L. Guerquin-Kern, G. Leblon and T. Bouchez, *Environ Microbiol*, 2008, **10**, 580-588.
115. D. A. Fike, C. L. Gammon, W. Ziebis and V. J. Orphan, *ISME J*, 2008, **2**, 749-759.
116. S. K. Saka, A. Vogts, K. Krohnert, F. Hillion, S. O. Rizzoli and J. T. Wessels, *Nat Commun*, 2014, **5**, 3664.
117. A. Gouzy, G. Larrouy-Maumus, D. Bottai, F. Levillain, A. Dumas, J. B. Wallach, I. Caire-Brandli, C. de Chastellier, T. D. Wu, R. Poincloux, R. Brosch, J. L. Guerquin-Kern, D.

Schnappinger, L. P. Sorio de Carvalho, Y. Poquet and O. Neyrolles, *PLoS Pathog*, 2014, **10**, e1003928.

118. K. H. Lau, M. Christlieb, M. Schroder, H. Sheldon, A. L. Harris and C. R. Grovenor, *J Microsc*, 2010, **240**, 21-31.
119. K. J. Carpenter, P. K. Weber, M. L. Davisson, J. Pett-Ridge, M. I. Haverty and P. J. Keeling, *Microsc Microanal*, 2013, 1-12.
120. J. A. Finzi-Hart, J. Pett-Ridge, P. K. Weber, R. Popa, S. J. Fallon, T. Gunderson, I. D. Hutcheon, K. H. Nealson and D. G. Capone, *Proc Natl Acad Sci U S A*, 2009, **106**, 6345-6350.
121. P. L. Clode and A. T. Marshall, *Protoplasma*, 2003, **220**, 153-161.
122. I. Lozic, C. A. Bartlett, J. A. Shaw, K. S. Iyer, S. A. Dunlop, M. R. Kilburn and M. Fitzgerald, *Metallomics*, 2014.
123. J. L. Guerquin-Kern, T. D. Wu, C. Quintana and A. Croisy, *Biochim Biophys Acta*, 2005, **1724**, 228-238.
124. S. Chandra, D. R. Smith and G. H. Morrison, *Anal Chem*, 2000, **72**, 104A-114A.
125. S. Chandra, *J Microsc*, 2008, **232**, 27-35.

5. Abbreviation List

AAS – atomic absorption spectroscopy

ATP7A, ATP7B – P-type copper-transporting ATPases A and B

BER – base excision repair

CLSM – confocal laser-scanning microscopy

Ctr1, Ctr2 - copper transporters 1 and 2

DOI – digital object identifier

EA-IRMS – and elemental analyzer–isotope ratio mass spectrometry

EDX spectroscopy – energy dispersive X-ray spectroscopy

EFTEM – energy filtering transmission electron microscopy

EM – electron microscopy

EPR – enhanced permeability and retention effect

ER – endoplasmic reticulum

ESI-MS – electrospray ionization mass spectrometry

FACS – fluorescence activated cell sorting

FELASA – Federation of European Laboratory Animal Science Associations

FISH – fluorescence *in-situ* hybridization

FITC – fluorescein isothiocyanate

FT-IR – Fourier transform infrared spectroscopy

HPLC – high-performance liquid chromatography

HRR – homologous recombinational repair

HSA – human serum albumin

ICP-MS – inductively coupled plasma mass spectrometry

MATE1 – multidrug and toxin extrusion transporter-1

MIMS – multi-isotope mass spectrometry

mtDNA – mitochondrial DNA

MTT – 3-(4,5-dimethyl-2-thiazolyl)-2,5-diphenyl-2*H*-tetrazolium bromide

NanoSIMS – nano-scale secondary ion mass spectrometry

NER – nucleotide excision repair

NMR – nuclear magnetic resonance

OCT2 – organic cation transporter-2

QSAR – quantitative structure–activity relationship

SEM – scanning electron microscopy

TEM – transmission electron microscopy

6. Curriculum Vitae

Anton A. Legin, MSc

Born	January 24th, 1987
Place of birth	Saint-Petersburg (Leningrad, USSR)
Nationality	Russian
Mail, skype	anton.legin@univie.ac.at, anton.legin
Publications	9 (co-)authored scientific articles and 9 (co-)authored conference contributions
Languages	Russian, English, German, French

Education

2010 – up to date	Ph.D. student, Department of Chemistry, Institute of Inorganic Chemistry, University of Vienna, Austria
July 2010	Master Degree with Honours, Department of Chemistry, University of Vienna, Austria
2009 – 2010	Master Student of the Department of Molecular Biology, University of Vienna, Austria
June 2010	Magister Degree with Honours, Department of Chemistry, St. Petersburg State University, Russia
2008 – 2010	Magister Student of the Department of Chemistry, St. Petersburg State University, Russia
June 2008	Bachelor Degree with Honours, Department of Biology, St. Petersburg State University, Russia
2004 – 2008	Undergraduate Student of the Department of Biology, specialization Biochemistry, St. Petersburg State University, Russia
1994 – 2004	Student, primary, secondary and high school №639 (with an intensive learning of foreign languages; supervised by UNESCO), St. Petersburg, Russia

Research experience

2009 – 2010	Master Thesis «Synthesis, in vitro antitumor activity and DNA interactions of guanidine platinum(II) complexes», under supervision of Prof. Bernhard K. Keppler and Dr. Michael Jakupec, Institute of Inorganic Chemistry,

	University of Vienna, Austria
2008 – 2010	Magister Thesis «Metal-mediated cyanamide-amine coupling and the study of antitumor activity of the resulting guanidine platinum(II) complexes» under supervision of PhD Nadezda A. Bokach, Department of Chemistry, St. Petersburg State University, Russia
2005 – 2008	Bachelor Graduation Work «The assembly of «expression cassette», consisting of *NEO* gene, under control of gene's *ACT* promoter and gene's *FLD1* terminator in yeast *Pichia Pastoris*» under supervision of Dr. Marina V. Padkina, Department of Biology, St. Petersburg State University, Russia

Additional training

2008	Summer Research Work «The functioning mechanism of antitumour drugs based on platinum complexes» under supervision of Prof. Bernhard K. Keppler and Dr. Michael Jakupec, Institute of Inorganic Chemistry, University of Vienna, Austria
2003	In the framework of international school exchange participated in English language refinement programme, Worcestershire, England
2002 – 2003	Student, School №171, French language courses, St. Petersburg, Russia
2000	Student, The Institute of Foreign Languages, French language courses, St. Petersburg, Russia

Conferences

July 2014	Oral presentation at the « 7th International Symposium on Bioorganometallic Chemistry» Vienna, Austria
March 2013	Poster presentation at the «17th International AEK Cancer Congress» Heidelberg, Germany
September 2012	Poster presentation at the «11th European Biological Inorganic Chemistry Conference » Granada, Spain
September 2012	Poster presentation at the «1st International conference on Imaging Mass Spectrometry» Ourense, Spain
July 2009	Poster presentation at the «XXIV International Chugaev Conference on Coordination Chemistry» St. Petersburg, Russia

Honors and Awards

2012	Best poster award for the poster presentation at the «11th European Biological Inorganic Chemistry Conference » Granada, Spain

2010	Awarded Magister Degree Diploma with Honours as the Highest Ranking Student, Department of Chemistry, St. Petersburg State University, Russia
2008	Awarded Bachelor Degree Diploma with Honours as the Highest Ranking Student, Department of Biology, St. Petersburg State University, Russia
2008	The Highest Record in the State Graduation Examination, Department of Biology and Pedology, St. Petersburg State University, Russia
2004	The State Certificate of Honour for Excellence in Studying: English, French, Biology and Chemistry, St. Petersburg, Russia

Skills and Interests

Biology	*Cancer research, molecular biology, biochemistry, cell biology*: cell culture; biological studies of active compounds: MTT assay, FACS analysis (ROS, cell cycle, apoptosis assay), comet assay, gradient PAAG electrophoresis; agarose electrophoresis; western blotting; DNA extraction and purification; PCR, real-time PCR (qPCR); DNA sequencing, bacterial and yeast cloning (e.g. transformation, ligation, restriction etc.); complementary sample preparation: cell culture and tissue fixation, dehydration and embedding (cryo-based and RT methods), microtome cutting (semi- and ultra-thin); immunohystochemistry (for purpose of immunofluorescent microscopy).
Chemistry	Inorganic synthesis, purification and characterization techniques, NMR techniques, IR spectroscopy, mass spectrometry (ESI-MS, ICP-MS).
Imaging	Light microscopy, laser dissection microscopy, confocal laser scanning microscopy, transmission and scanning electron microscopy, nano-scale secondary ion mass spectrometry (NanoSIMS, elemental imaging).
Languages	Russian (Mother language), English (Advanced, fluent), German (Intermediate), French (Basic skills).
Computer	Microsoft Office, OpenOffice, ChemDraw, Graph Pad Prism, ImageJ, GIMP, EndNote, Web applications (SciFinder, NCBI, Scopus) and other resources.
Hobby	Web design, web programming, active sports (ice hockey, mountain skiing, badminton, hiking) and traveling.
Driving license	B category.
Teaching 2010 – up to date	Experience with supervision of apprentices and diploma students. Teaching in undergraduate inorganic chemistry lab courses.

Publications

1. Legin, A.A., Schintlmeister, A., Jakupec, M.A., Galanski, M., Lichtscheidl, I., Wagner, M.,

Keppler, B.K. NanoSIMS combined with fluorescence microscopy as a tool for subcellular imaging of isotopically labeled platinum-based anticancer drugs (2014) Chemical Science, 5 (8), pp. 3135-3143.

2. Legin, A.A., Jakupec, M.A., Bokach, N.A., Tyan, M.R., Kukushkin, V.Y., Keppler, B.K. Guanidine platinum(II) complexes: Synthesis, in vitro antitumor activity, and DNA interactions (2014) Journal of Inorganic Biochemistry, 133, pp. 33-39.
3. Banfic, J., Legin, A.A., Jakupec, M.A., Galanski, M., Keppler, B.K.Platinum(IV) complexes featuring one or two axial ferrocene bearing ligands - Synthesis, characterization, and cytotoxicity (2014) European Journal of Inorganic Chemistry, (3), pp. 484-492.
4. Babak, M.V., Meier, S.M., Legin, A.A., Adib Razavi, M.S., Roller, A., Jakupec, M.A., Keppler, B.K., Hartinger, C.G. Am(m)ines make the difference: Organoruthenium Am(m)ine complexes and their chemistry in anticancer drug development (2013) Chemistry - A European Journal, 19 (13), pp. 4308-4318.
5. Scaffidi-Domianello, Y.Y., Legin, A.A., Jakupec, M.A., Roller, A., Kukushkin, V.Y., Galanski, M., Keppler, B.K. Novel oximato-bridged platinum(II) Di- and trimer(s): Synthetic, structural, and in vitro anticancer activity studies (2012) Inorganic Chemistry, 51 (13), pp. 7153-7163.
6. Hanif, M., Nazarov, A.A., Legin, A. A., Groessl, M., Arion, V.B., Jakupec, M.A., Tsybin, Y.O., Dyson, P.J., Keppler, B.K., Hartinger, C.G. Maleimide-functionalised organoruthenium anticancer agents and their binding to thiol-containing biomolecules (2012) Chemical Communications, 48 (10), pp. 1475-1477.
7. Scaffidi-Domianello, Y.Y., Legin, A.A., Jakupec, M.A., Arion, V.B., Kukushkin, V.Y., Galanski, M., Keppler, B.K. Synthesis, characterization, and cytotoxic activity of novel potentially pH-sensitive nonclassical platinum(II) complexes featuring 1,3-dihydroxyacetone oxime ligands (2011) Inorganic Chemistry, 50 (21), pp. 10673-10681.
8. Varbanov, H., Valiahdi, S.M., Legin, A.A., Jakupec, M.A., Roller, A., Galanski, M., Keppler, B.K. Synthesis and characterization of novel bis(carboxylato) dichloridobis(ethylamine)-platinum(IV) complexes with higher cytotoxicity than cisplatin (2011) European Journal of Medicinal Chemistry, 46 (11), pp. 5456-5464.
9. Hanif M., Meier S.M., Nazarov A.A, Risse J., Legin A.A., Casini A., Jakupec M.A., Keppler B.K., Hartinger C.G. Influence of the π-coordinated arene on the anticancer activity of ruthenium(II) carbohydrate organometallic complexes (2013) Frontiers in Chemistry, 1:27, pp. 1-7.